UNIWERSYTET MEDYCZNY
IM. PIASTÓW ŚLĄSKICH WE WROCŁAWIU

Łukasz Szczukowski

Synteza i aktywność biologiczna nowych pochodnych pirolo[3,4-*d*]pirydazynonu

Rozprawa doktorska w oparciu o monotematyczny cykl publikacji
w dziedzinie nauk medycznych i nauk o zdrowiu
w dyscyplinie nauki farmaceutyczne

Promotor: dr hab. Piotr Świątek, prof. uczelni

Katedra i Zakład Chemii Leków

Wrocław 2022

~ Człowiek ma w życiu albo wymówki, albo wyniki ~

Promotorowi mojej rozprawy doktorskiej,

Panu dr hab. Piotrowi Świątkowi, prof. UMW

składam gorące podziękowania za wsparcie, cenne wskazówki, cierpliwość i wyrozumiałość oraz zaangażowanie i nieocenioną pomoc okazane podczas realizacji niniejszej pracy

Koleżankom i Kolegom z Katedry i Zakładu Chemii Leków dziękuję za serdeczność i wsparcie w pracy naukowej oraz dydaktycznej

Współautorom publikacji – moim Koleżankom i Kolegom, z którymi wspólnie realizowaliśmy nasze projekty i badania naukowe – za życzliwość, zaufanie i owocną współpracę, dzięki której mogła powstać ta rozprawa

Żonie i Rodzicom za ich obecność

~ Tymkowi i Nikodemowi ~

SPIS TREŚCI

THE LIST OF CONTENT

WYKAZ PUBLIKACJI WCHODZĄCYCH W SKŁAD CYKLU BĘDĄCEGO PRZEDMIOTEM ROZPRAWY

THE LIST OF MANUSCRIPTS INCLUDED IN THIS DISSERTATION

W skład cyklu publikacji stanowiących podstawę do ubiegania się o nadanie stopnia doktora wchodzą trzy oryginalne artykuły opublikowane w czasopismach o zasięgu międzynarodowym w latach 2020-2021.

The series of manuscripts constituting the basis for applying for the PhD consists of three original articles published in international journals in the years 2020-2021.

❖ PUBLIKACJA 1 (P1)

Łukasz Szczukowski*, Aleksandra Redzicka, Benita Wiatrak, Edward Krzyżak, Aleksandra Marciniak, Katarzyna Gębczak, Tomasz Gębarowski, Piotr Świątek;

Design, synthesis, biological evaluation and *in silico* studies of novel pyrrolo[3,4-*d*]pyridazinone derivatives with promising anti-inflammatory and antioxidant activity

BIOORGANIC CHEMISTRY, 102 (**2020**), 104035

DOI: 10.1016/j.bioorg.2020.104035

*Autor korespondencyjny/corresponding author

Journal IF (2020): **5.275** Punkty MNiSW: **100**

❖ PUBLIKACJA 2 (P2)

Łukasz Szczukowski*, Edward Krzyżak, Adrianna Zborowska, Patrycja Zając, Katarzyna Potyrak, Krzysztof Peregrym, Benita Wiatrak, Aleksandra Marciniak, Piotr Świątek;

Design, synthesis and comprehensive investigations of pyrrolo[3,4-*d*]pyridazinone-based 1,3,4-oxadiazole as new class of selective COX-2 inhibitors

INTERNATIONAL JOURNAL OF MOLECULAR SCIENCES, **2020**, 21(24), 9623

DOI: 10.3390/ijms21249623

*Autor korespondencyjny/corresponding author

Journal IF (2020): **5.924** Punkty MNiSW: **140**

❖ PUBLIKACJA 3 (P3)

Łukasz Szczukowski*, Edward Krzyżak, Benita Wiatrak, Paulina Jawień, Aleksandra Marciniak, Aleksandra Kotynia, Piotr Świątek*;

New *N*-substituted-1,2,4-triazole derivatives of pyrrolo[3,4-*d*]pyridazinone with significant anti-inflammatory activity – design, synthesis and complementary *in vitro*, computational and spectroscopic studies

INTERNATIONAL JOURNAL OF MOLECULAR SCIENCES, **2021**, 22(20), 11235

DOI: 10.3390/ijms222011235

*Autor korespondencyjny/corresponding author

Journal IF (2020): **5.924** Punkty MNiSW: **140**

- Łączna wartość współczynnika IF: **17.123**
- Łączna wartość 5-cio letniego współczynnika IF: **17.516**
- Łączna wartość punktacji MNiSW: **380**

WYKAZ STOSOWANYCH SKRÓTÓW

THE LIST OF ABBREVIATIONS

BSA *bovine serum albumin;* bydlęca osoczowa albumina

CD *circular dichroism;* dichroizm kołowy

CMC *carboxymethylcellulosum*; karboksymetyloceluloza

CNS *central nervous system;* ośrodkowy układ nerwowy

COX *cyclooxygenase;* cyklooksygenaza

DC-FDA *2',7'-dichlorofluorescein diacetate;* dioctan 2',7'-dichlorofluoresceiny

ELISA *the enzyme-linked immunosorbent assay;* test immunoenzymosorpcyjny

ESI *electrospray ionization*

FHA *fast halo assay;* test "halo"

FTIR *Fourier-transform infrared spectroscopy;* spektroskopia w podczerwieni z transformacją Fouriera

HSA *human serum albumin;* ludzka osoczowa albumina

IC_{50} *the half maximal inhibitory concentration;* połowa wartości maksymalnego stężenia hamującego

i.g. *intragastrically;* dożołądkowo

IR *infrared;* podczerwień

LPS *lipopolysaccharide;* lipopolisacharyd

MCDA *multi-criteria decision analysis;* analiza multikryterialna

MPO *myeloperoxidase;* mieloperoksydaza

MS *mass spectrometry;* spektrometria mas

MTT *3-(4,5-dimethylthiazol-2-yl)-2,5-diphenyltetrazolium bromide;* formazan błękitu triazolowego

NHDF *normal human dermal fibroblasts;* normalne ludzkie skórne fibroblasty

NLPZ niesteroidowe leki przeciwzapalne

NMR *nuclear magnetic resonance;* jądrowy rezonans magnetyczny

NO *nitric oxide;* tlenek azotu

NSAIDs *Non-Steroidal Anti-Inflammatory Drugs;* niesteroidowe leki przeciwzapalne

OUN ośrodkowy układ nerwowy

PG *prostaglandin;* prostaglandyna

PGE_2 *prostaglandin E_2*; prostaglandyna E_2

PGI_2 *prostaglandin I_2*; prostaglandyna I_2

ppm *parts per million*

RNS *reactive nitrogen species;* reaktywne formy azotu

ROS *reactive oxygen species;* reaktywne formy tlenu

SAR *structure-activity relationships;* zależności struktura-aktywność

s.pl. *subplantarly;* podpowięziowo

SRB *sulforhodamine B;* sulforodamina B

TLC *thin layer chromatography;* chromatografia cienkowarstwowa

TMPD *N,N,N′,N′-tetramethyl-p-phenylenediamine; N,N,N′,N′*-tetrametylo-*p*-fenylenodiamina

TMS *tetramethylsilane;* tetrametylosilan

TNF-α *tumor necrosis factor α;* czynnik martwicy nowotworów α

TPSA *topological polar surface area;* topologiczne pole powierzchni polarnej

TXA_2 *tromboxane A_2*; tromboksan A_2

STRESZCZENIE

W JĘZYKU POLSKIM

1 WPROWADZENIE

Reakcja zapalna jest procesem, którego celem jest przywrócenie w organizmie stanu homeostazy. Stan zapalny mogą wywołać rozmaite egzo- i endogenne czynniki takie jak kontuzja, infekcja, przerwanie ciągłości tkanek czy też zaburzenie ich prawidłowego funkcjonowania. Przebieg oraz następstwa zapalenia są zależne od bodźca, który je zainicjował. Najczęstsze objawy jakie występują w zmienionym zapalnie obszarze organizmu to obrzęk, zaczerwienienie, nadwrażliwość oraz często ból, który odgrywa istotną rolę ostrzegawczą i ochronną. Ból wyzwala właściwą reakcję organizmu oraz kieruje jego odpowiednim zachowaniem w celu złagodzenia następstw spowodowanych uszkodzeniem tkanki[1–5].

Zapalenie jest bardzo złożonym zjawiskiem kontrolowanym przez wiele różnych mediatorów, których ekspresja oraz skomplikowana sieć wzajemnych powiązań nie została do tej pory w pełni wyjaśniona. Rozmaite czynniki prozapalne różnego pochodzenia możemy podzielić na 7 następujących grup: wazoaktywne aminy, wazoaktywne peptydy, fragmenty układu dopełniacza, mediatory lipidowe takie jak np. eikozanoidy, cytokiny, chemokiny oraz enzymy proteolityczne. Wymienione substancje nie tylko stymulują odpowiednią odpowiedź na poziomie komórkowym, ale także mogą wzajemnie modulować swoją aktywność. Dlatego też, możliwie jak najlepsze poznanie mechanizmów odpowiedzialnych za ekspresję mediatorów stanu zapalnego oraz ich wzajemnych zależności jest kluczowe w kontekście skutecznego leczenia rozmaitych chorób, u podłoża których leży zapalenie. Efektywna farmakoterapia oraz naturalne procesy naprawcze zachodzące w tkankach pozwalają wyeliminować ostry stan zapalny w ciągu zaledwie kilku dni. Z drugiej strony, brak odpowiedniej reakcji organizmu oraz stosownego postępowania farmakologicznego może doprowadzić do zmian patologicznych, których skutkiem będzie rozwój przewlekłego bólu i zapalenia[1–6].

Znakomita większość farmaceutyków stosowanych obecnie w terapii schorzeń zapalnych i dolegliwości bólowych należy do obszernej i strukturalnie zróżnicowanej grupy tzw. niesteroidowych leków przeciwzapalnych (NLPZ). Ich mechanizm działania, który został po raz pierwszy opisany przez Vane'a w 1971r. polega na hamowaniu – głównie w sposób nieselektywny – syntazy cyklicznego nadtlenku prostaglandynowego, która powszechnie znana jest jako cyklooksygenaza (COX)[7–9]. Jest to enzym związany z błoną komórkową katalizujący przekształcenie kwasu arachidonowego do bioaktywnych lipidów

takich jak prostaglandyny (PG), czy tromboksan A_2 (TXA_2). Mediatory te są istotne nie tylko dla utrzymania stanu homeostazy, ale pełnią także kluczową rolę w przekazywaniu sygnałów związanych bezpośrednio z powstałym stanem zapalnym oraz towarzyszącym mu bólem[7–10].

Biorąc pod uwagę różnice strukturalne oraz funkcjonalne, wyodrębniono trzy izoformy cyklooksygenazy. Konstytutywny wariant enzymu, nazwany cyklooksygenazą 1 (COX-1), ulega ekspresji w komórkach w warunkach fizjologicznych i jest odpowiedzialny za syntezę prostaglandyn zaangażowanych w prawidłowe funkcjonowanie przewodu pokarmowego, a także układu sercowo-naczyniowego[9,10]. Dla przykładu, prostaglandyna I_2 (PGI_2), zwana prostacykliną, wykazuje działanie cytoprotekcyjne w błonie śluzowej żołądka – zwiększa produkcję śluzu i wodorowęglanu oraz usprawnia przepływ krwi. Prostacyklina produkowana z kolei w obrębie śródbłonka naczyniowego zmniejsza agregację płytek krwi oraz działa wazodilatacyjnie[7–10]. Aktywność cyklooksygenazy 2 (COX-2), która jest w głównej mierze formą indukowaną, w warunkach fizjologicznych jest znikoma. Wzrasta natomiast w przypadku pojawienia się np. stanu zapalnego lub innych zmian patologicznych. Czynnikami, które zwiększają syntezę COX-2 są np. cytokiny czy mitogeny. Dlatego też, zwiększoną ekspresję COX-2 obserwujemy w tkankach objętych zapaleniem, infekcją lub też procesem onkogenezy[10–14]. Trzecia izoforma cyklooksygenazy, która jest wariantem COX-1, związana jest głównie z ośrodkowym układem nerwowym (OUN). Enzym ten występuje zarówno w mózgu jak i w rdzeniu kręgowym i jest celem molekularnym dla leków antynocyceptywnych o ośrodkowym mechanizmie działania[9,10].

Nieselektywne blokowanie obu obwodowych form cyklooksygenazy prowadzi nie tylko do złagodzenia stanu zapalnego i bólu, ale może także niestety skutkować, zwłaszcza podczas przewlekłej terapii, wystąpieniem groźnych działań niepożądanych, którymi charakteryzują się niesteroidowe leki przeciwzapalne[9,11,15–18]. Na pierwszy plan wysuwają się problemy gastroenterologiczne takie jak zgaga i ból żołądka, zapalenie, nadżerki i w konsekwencji owrzodzenia błony śluzowej żołądka i dwunastnicy, a nawet krwawienia z przewodu pokarmowego[15–18]. Przyczynia się do tego nie tylko zmniejszenie stężenia PGI_2, ale również natura chemiczna większości NLPZ, w których strukturze występuje wolna grupa karboksylowa. W konsekwencji, leki te działają bezpośrednio drażniąco na śluzówkę żołądka i dwunastnicy. Ponadto, z uwagi ma swój kwasowy charakter, klasyczne niesteroidowe leki przeciwzapalne ulegają w cytozolu komórek błony śluzowej efektowi pułapki jonowej. To prowadzi do ich kumulacji, co w rezultacie jeszcze bardziej nasila uszkodzenia wartwy ochronnej układu trawiennego[15–18]. Spore nadzieje były związane z wprowadzeniem do

lecznictwa selektywnych inhibitorów COX-2, czyli koksybów. Faktycznie, są one skuteczne w terapii różnych schorzeń zapalnych, a ich działanie gastrotoksyczne jest istotnie mniejsze niż w przypadku tradycyjnych NLPZ[12,17,18]. Nie oznacza to jednak, że pacjenci przyjmujący koksyby nie skarżą się na żadne dolegliwości ze strony przewodu pokarmowego. Jak się bowiem okazuje, COX-2 jest również, w pewnym stopniu, zaangażowana w działanie cytoprotekcyjne[12]. Co więcej, stosowanie koksybów niesie ze sobą ryzyko wystąpienia poważnych działań niepożądanych ze strony układu sercowo-naczyniowego, co może prowadzić nawet do śmierci pacjenta spowodowanej różnego rodzaju incydentami zakrzepowo-zatorowymi. Dlatego też, część z tych leków została wycofana z lecznictwa, a przypadek rofekoksybu jest prawdopodobnie najbardziej znanym i niechlubnym[13,14].

Niebezpieczne działania niepożądane, które towarzyszą przyjmowaniu zarówno nieselektywnych jak i selektywnych niesteroidowych leków przeciwzapalnych są czynnikiem, który w znacznej mierze ogranicza ich przewlekłe stosowanie[13–15,18]. Z tej przyczyny cały czas wysoce uzasadnione oraz konieczne jest poszukiwanie nowych, skutecznych i bezpiecznych substancji o działaniu przeciwzapalnym i przeciwbólowym.

Analizując wiodące trendy obowiązujące we współczesnej chemii medycznej, można zauważyć, że nowe substancje o potencjalnym zastosowaniu w terapii bólu i różnych schorzeń zapalnych można otrzymać opierając się na dwóch różnych ścieżkach. Pierwsza z nich polega na modyfikacji już zarejestrowanych, a w związku z tym gruntownie przebadanych, leków z grupy NLPZ takich jak np. diklofenak[19], ibuprofen[20], celekoksyb[21] czy naproksen[22]. Optymalizacja struktury znanych substancji może zaowocować otrzymaniem nowych pochodnych o zwiększonej aktywności oraz mniejszej toksyczności w porównaniu do ich prekursorów. Druga z kolei droga zakłada zaprojektowanie zupełnie innowacyjnej klasy cząsteczek pod kątem wybranego celu molekularnego. Tym sposobem możliwe jest uzyskanie grupy związków łagodzących stan zapalny poprzez np. hamowanie wspomnianego wcześniej enzymu cyklooksygenazy[23–30].

Na podstawie dokonanego przeglądu literatury, której tematyka obejmowała wątek związków o działaniu przeciwzapalnym i przeciwbólowym projektowanych i syntetyzowanych *de novo*, można zauważyć, że wiele publikacji opisuje badania skoncentrowane wokół obszernej i zróżnicowanej grupy pochodnych pirydazynonu[31–39]. Warto podkreślić, że pierwsze wzmianki na temat tego typu związków o aktywności antynocyceptywnej zaczęły pojawiać się już przeszło sześćdziesiąt lat temu. Jednakże

jedynym dotychczas zarejestrowanym lekiem przeciwbólowym, będącym pochodną pirydazynonu, jest emorfazon (**1**). Jego wzór strukturalny przedstawia **Rysunek 1**[40,41].

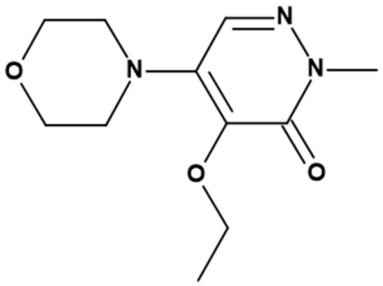

1

Rys. 1. Emorfazon (**1**) – dopuszczona do lecznictwa pochodna pirydazynonu o aktywności przeciwbólowej.

Na przestrzeni wielu lat opisano szeroką gamę cząsteczek o aktywności przeciwzapalnej i przeciwbólowej, w których strukturze występował podstawiony na różne sposoby pierścień pirydazynonu. Intensywne prace prowadzone w obrębie tego typu pochodnych pozwoliły udowodnić, że układ pirydazynonu może służyć jako doskonały szkielet służący do syntezy nowych, efektywnych inhibitorów cyklooksygenazy, cechujących się znacznym powinowactwem do indukowanej formy COX-2. Co więcej, dowiedziono, że interesujący profil aktywności farmakologicznej wykazują także połączenia biheterocykliczne, których rdzeń stanowi pierścień pirydazynonu skondensowany np. z pirazolem, izoksazolem czy pirydyną. Na **Rysunku 2** zaprezentowano struktury wybranych pochodnych pirydazynonu (**2-7**). Wyróżniały się one istotnym działaniem przeciwzapalnym, które wynikało w głównej mierze z silnego hamowania COX-2 przez te cząsteczki. Dodatkowo należy podkreślić, że w przypadku tych związków, nie obserwowano negatywnego wpływu na błonę śluzową żołądka i dwunastnicy w przeprowadzonych testach *in vivo*[32,33,38–40].

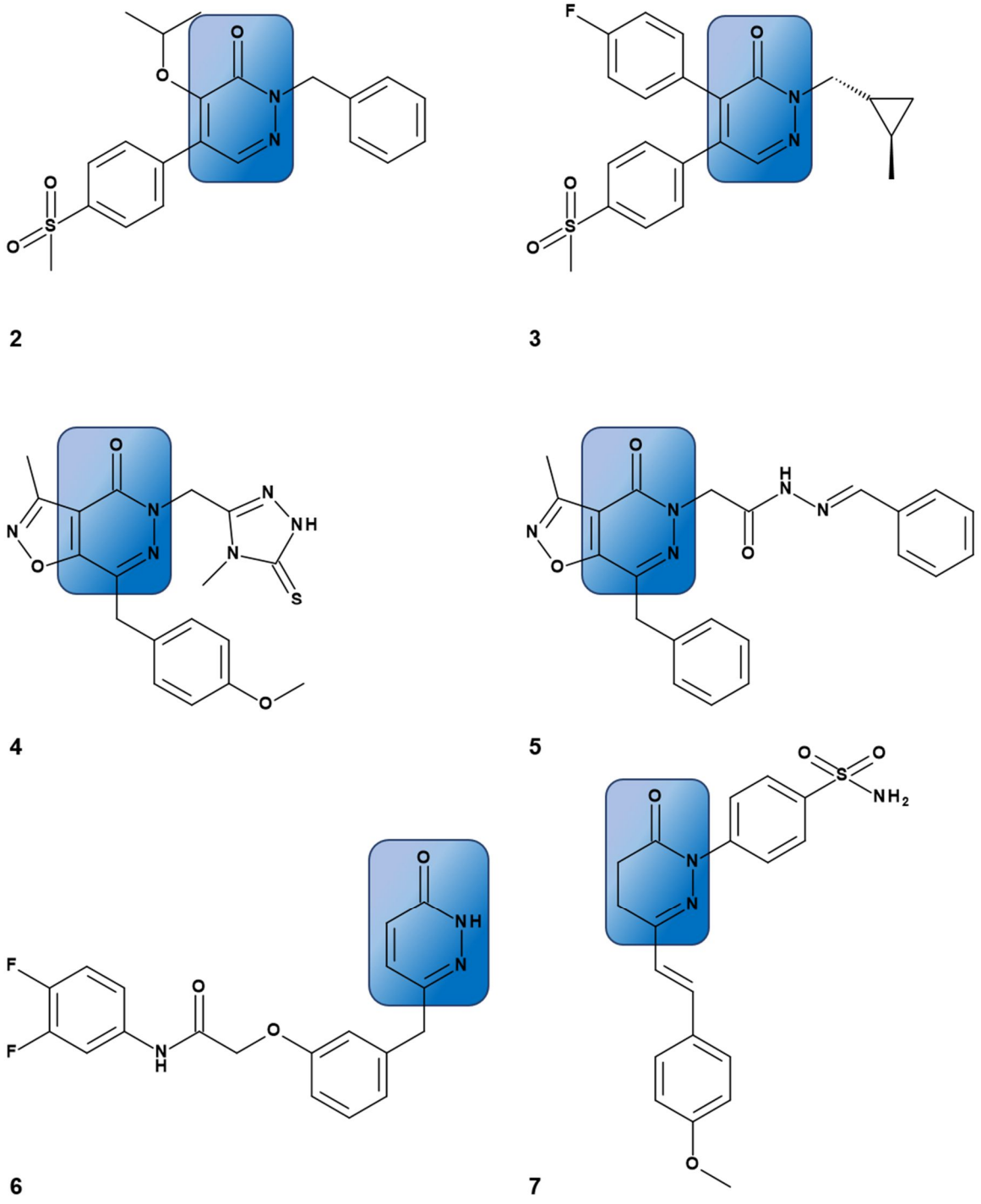

Rys. 2. Przykłady inhibitorów COX zawierających w swej strukturze pierścień pirydazynonu [32,33,38–40].

W Katedrze i Zakładzie Chemii Leków Uniwersytetu Medycznego we Wrocławiu od wielu lat prowadzone są intensywne badania polegające na projektowaniu oraz syntezie nowych, biologicznie aktywnych pochodnych różnych układów mono- oraz biheterocyklicznych. Na szczególną uwagę zasługują niewątpliwie prace mające na celu poszukiwanie związków o działaniu przeciwzapalnym i przeciwbólowym w obrębie

pochodnych pirolo[3,4-*d*]pirydazyno-1,4-dionu[36,37]. Otrzymane dotychczas i przebadane związki cechowały się znacznym działaniem analgetycznym w testach *in vitro* a także *in vivo*. Na **Rysunku 3** zostały przedstawione wzory dwóch najbardziej obiecujących pochodnych **8a** i **8b**. W teście „wicia się" wykazały one aktywność znacznie wyższą niż kwas acetylosalicylowy. Natomiast w teście „gorącej płytki" działały przeciwbólowo w dawkach zaledwie 3-5 razy mniejszych niż morfina. Ustalono ponadto, że efekt przeciwzapalny wspomnianych struktur opiera się na aktywności obwodowej, jednak dokładny mechanizm ich działania nie został poznany[37].

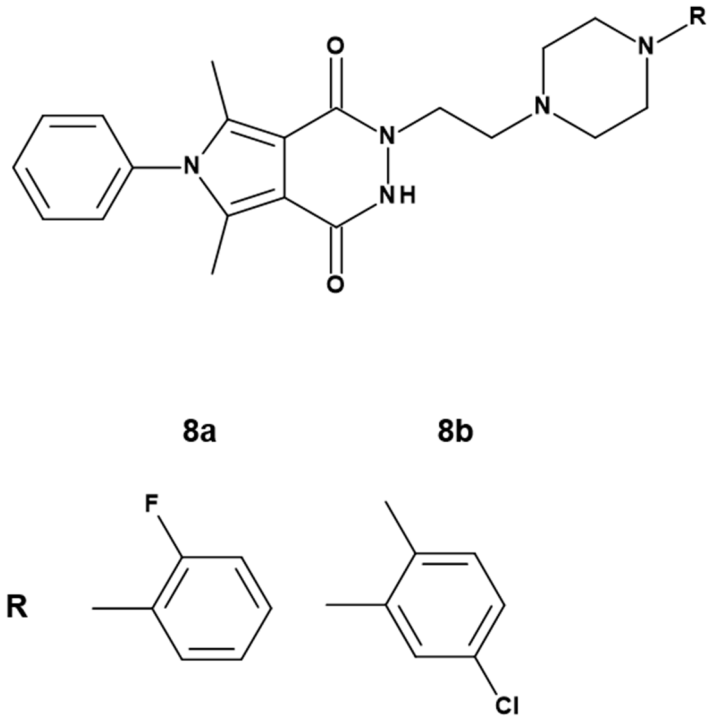

Rys. 3. Wzory aktywnych farmakologicznie pochodnych pirolo[3,4-*d*]pirydazyno-1,4-dionu [37].

Biorąc pod rozwagę pozycje piśmiennictwa, które opisują silnie działające przeciwzapalnie pochodne pirydazynonu, a także uwzględniając obiecującą aktywność związków **8a** oraz **8b**, wydaje się, że dalsze poszukiwania kandydatów na nowe leki przeciwzapalne i przeciwbólowe w obrębie analogów pirolo[3,4-*d*]pirydazyno-1,4-dionu są zdecydowanie uzasadnione. Z tego względu, projektując nowe serie związków zdecydowano się wprowadzić do struktury pirolo[3,4-*d*]pirydazyno-1,4-dionu takie ugrupowania, które pozwoliłyby na otrzymanie pochodnych charakteryzujących się dobrym powinowactwem do indukowanej formy cyklooksygenazy oraz jednocześnie niską toksycznością i brakiem działań niepożądanych na przewód pokarmowy. W strukturze

tytułowych związków można wyróżnić więc, oprócz ugrupowania pirolo[3,4-*d*]pirydazynonu, pięcioczłonowy pierścień heterocykliczny 1,3,4-oksadiazolu albo 1,2,4-triazolu, a także farmakofor arylopiperazynylowy/piperydynylowy, charakterystyczny dla związków **8a** i **8b**. Tego typu projekt jest spójny z ideą molekularnej hybrydyzacji, która opiera się łączeniu różnych struktur czy układów farmakoforowych o udowodnionej aktywności, celem otrzymania cząsteczek cechujących się wyższą skutecznością przy jednocześnie zmniejszonej ilości niebezpiecznych efektów ubocznych.

Z danych literaturowych wynika, że zastąpienie wolnej grupy karboksylowej klasycznych niesteroidowych leków przeciwzapalnych ugrupowaniem bioizosterycznym o podobnej wielkości i mniejszej kwasowości takim jak np.: 1,3,4-oksadiazol[19,20,23], 1,2,4-triazol[21,22,29,30], pirazol[24,42] czy 1,3-tiazol[43–45], pozwala istotnie zredukować ich gastrotoksyczność, przy jednoczesnym wzroście powinowactwa do COX-2. Ponadto, należy podkreślić, że wymienione wyżej pięcioczłonowe pierścienie heterocykliczne są istotnym elementem strukturalnym wielu cząsteczek o znacznej aktywności biologicznej. Do tego grona należą oczywiście także związki, które działają silnie przeciwzapalnie i przeciwbólowo [19–24]. Wystarczy nadmienić, że tego typu ugrupowania heterocykliczne stanowią rdzeń opisanych już wcześniej selektywnych inhibitorów COX-2 – koksybów[14,21,23].

Dodatkowo, należy uwzględnić fakt, że w strukturze związków **8a**, **8b** oraz ich analogów, występowała charakterystyczna reszta arylopiperazynylowa/piperydynylowa, która miała znaczący wpływ na zwiększenie ich aktywności biologicznej. Dlatego też, wprowadzenie takiego ugrupowania do struktury nowych pochodnych pirolo[3,4-*d*]pirydazynonu, będących przedmiotem niniejszej rozprawy, wydaje się być wysoce zasadne i racjonalne. Podczas syntezy serii tytułowych struktur wykorzystano komercyjnie dostępne, różnie podstawione w pierścieniu fenylowym, pochodne arylopiperazyny oraz arylopiperydyny. Miało to na celu możliwie jak najlepszą ocenę wpływu tego ugrupowania na toksyczność oraz aktywność farmakologiczną związków finalnych.

Podsumowując, nadrzędnym celem przeprowadzonych prac eksperymentalnych było stworzenie nowej klasy efektywnych inhibitorów COX, które miałyby znaczne powinowactwo do indukowanego izoenzymu COX-2 oraz jednocześnie były bezpieczne i nie wykazywały szkodliwego wpływu na układ pokarmowy. Projekt oraz koncepcja budowy nowych, 1,3,4-oksadiazolowych oraz 1,2,4-triazolowych pochodnych pirolo[3,4-*d*]pirydazynonu zostały schematycznie przedstawione na **Rysunku 4**.

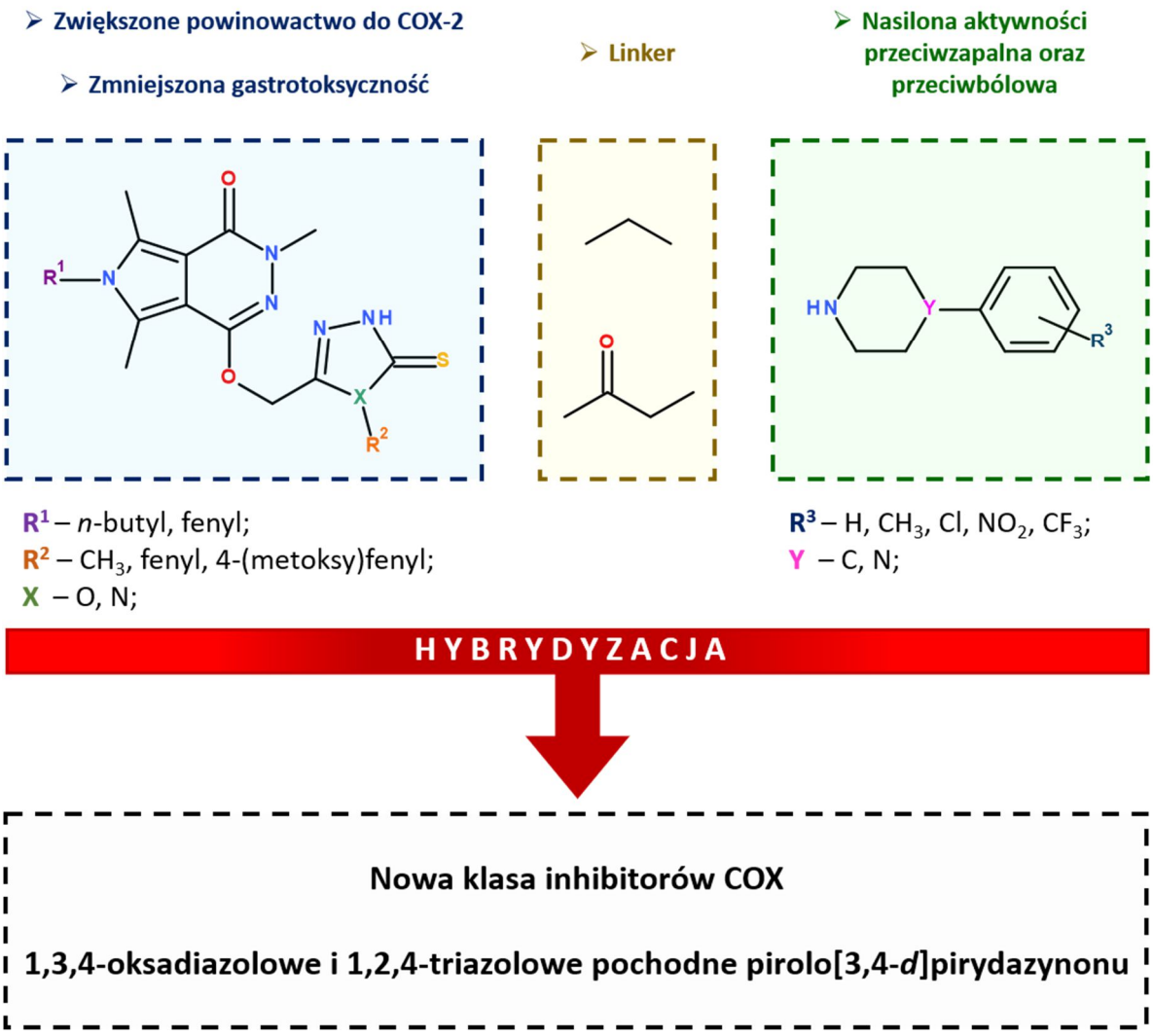

Rys. 4. Koncepcja struktury nowych pochodnych pirolo[3,4-*d*]pirydazynonu oparta o ideę molekularnej hybrydyzacji.

Zaprezentowane w dalszej części niniejszej dysertacji wyniki zrealizowanych dotychczas prac badawczych pozwoliły na wstępną ocenę potencjału nowych związków w kontekście ich możliwego wykorzystania jako bezpiecznych i efektywnych substancji o działaniu przeciwbólowym i przeciwzapalnym.

2 CELE PRACY

2.1 Cel główny

- Racjonalny projekt oraz synteza nowych pochodnych pirolo[3,4-*d*]pirydazynonu o istotnej aktywności przeciwzapalnej i przeciwbólowej

2.2 Cele szczegółowe

- Otrzymanie serii 1,3,4-oksadiazolowych oraz 1,2,4-triazolowych pochodnych pirolo[3,4-*d*]pirydazynonu, które efektywnie hamują cyklooksygenazę i nie działają gastrotoksycznie
- Ocena zdolności hamowania oraz powinowactwa nowych związków do obu obwodowych izoform cyklooksygenazy (COX-1 i COX-2) z użyciem testów enzymatycznych oraz technik dokowania molekularnego
- Ocena aktywności antyoksydacyjnej tytułowych związków
- Określenie modelu wiązania się otrzymanych pochodnych z osoczową albuminą
- Opisanie zależności struktura-aktywność w grupie nowych pochodnych pirolo[3,4-*d*]pirydazynonu w oparciu o uzyskane wyniki toksyczności oraz aktywności biologicznej
- Ocena aktywności przeciwzapalnej oraz przeciwbólowej nowych związków oraz ich wpływu na błonę śluzową przewodu pokarmowego w testach wykonanych w modelu zwierzęcym

3 METODYKA BADAŃ

3.1 Synteza nowych pochodnych pirolo[3,4-*d*]pirydazynonu

Wszystkie odczynniki, katalizatory i rozpuszczalniki użyte podczas syntezy, a także oczyszczania półproduktów oraz związków finalnych zostały zakupione od komercyjnych dostawców (Alchem, Wrocław, Polska; Chemat, Gdańsk, Polska; Archem, Łany, Polska). Jeśli było to konieczne, suche rozpuszczalniki jak np. bezwodny etanol, osuszony ksylen czy eter dietylowy, otrzymywano według standardowych procedur.

Postęp reakcji był kontrolowany dzięki użyciu techniki chromatografii cienkowarstwowej (*thin layer chromatography*, TLC) . Wykorzystywano płytki pokryte żelem krzemionkowym 60-F_{254} (Fluka Chemie GmbH, Niemcy). Były one rozwijane w komorze szklanej z zastosowaniem takich eluentów jak octan etylu i jego mieszaniny z innymi rozpuszczalnikami organicznymi takimi jak: metanol, chloroform czy cykloheksan, w różnych stosunkach objętościowych. Płytki analizowano w świetle UV przy długości fali 254 albo 366 nm.

Temperatury topnienia nowych związków zostały oznaczone techniką kapilarną przy użyciu aparatu Electro-Thermal Mel-Temp 1101D (Cole-Parmer, Vernon Hills, IL, USA). Oczyszczanie związków z użyciem techniki chromatografii kolumnowej przeprowadzono wykorzystując żel krzemionkowy 60-F_{254} (Merck, Darmstadt, Niemcy). Analiza elementarna dla atomów węgla, azotu oraz wodoru została wykonana przy użyciu aparatu Carlo Erba NA-1500 (Thermo Fisher Scientific, Waltham, MA, USA). Uzyskane wyniki nie różniły się o więcej niż ± 0.4% od wartości wyznaczonych teoretycznie.

Widma magnetycznego rezonansu jądrowego (*nuclear magnetic resonance*, NMR) ^{1}H NMR (300 MHz) oraz ^{13}C NMR (75 MHz) zostały zarejestrowane na spektrometrze NMR Bruker 300 MHz (Bruker Analytische Messtechnik GmbH, Rheinstetten, Niemcy). Badane próbki były rozpuszczane w komercyjnie dostępnych rozpuszczalnikach deuterowanych – $CDCl_3$ albo DMSO-d_6. Tetrametylosilan (TMS) był wykorzystany jako odnośnik przy wyznaczaniu przesunięć chemicznych (δ), które zostały podane w ppm (*parts per milion*). Widma w podczerwieni (*infrared*, IR) zostały wykonane na aparacie Nicolet iS50 FT-IR Spectrometer (Thermo Fisher Scientific, Waltham, MA, USA). Pomiaru dokonano na próbkach w formie stałej, częstotliwości podano w cm^{-1}. Widma masowe (*mass spectrometry*, MS) zostały zarejestrowane w jonizacji dodatniej z wykorzystaniem techniki elektrorozpylania (*electrospray ionization*, ESI) na aparacie Bruker Daltonics Compact ESI-Mass Spectrometer

(Bruker Daltonik, GmbH, Brema, Niemcy). Próbki były rozpuszczane w mieszaninie metanolu i chloroformu.

Na podstawie uzyskanych rezultatów badań analitycznych i spektralnych uznano, że wszystkie otrzymane związki, cechowały się czystością na poziomie >95%.

3.2 Ocena toksyczności, aktywności biologicznej oraz parametrów farmakokinetycznych tytułowych związków

Szczegółowe opisy procedur zastosowanych podczas badań biologicznych i spektralnych nowych związków, metodyka przeprowadzonego dokowania molekularnego i innych użytych technik *in silico*, służących ocenie właściwości badanych pochodnych, a także opisy wykorzystanych metod statystycznych zostały zamieszczone w części eksperymentalnej publikacji **P1**-**P3**.

4 PREZENTACJA I OMÓWIENIE WYNIKÓW BADAŃ

4.1 Pochodne 1,3,4-oksadiazolowe pirolo[3,4-*d*]pirydazynonu

4.1.1 Projekt oraz synteza

Zgodnie z koncepcją zaprezentowaną na **Rysunku 4** zaplanowano syntezę serii nowych pochodnych, w których strukturze można wyróżnić pierścień 1,3,4-oksadiazolo-2-tionu połączony z biheterocyklicznym układem pirolo[3,4-*d*]pirydazynonu oraz ugrupowanie arylopiperazynylowe/piperydynylowe. Tytułowe związki zostały otrzymane z dobrą wydajnością z wykorzystaniem klasycznych technik syntezy organicznej, przy użyciu komercyjnie dostępnych reagentów oraz rozpuszczalników.

Na **Rysunku 5** przedstawiono dwie kluczowe struktury, które stały się punktem wyjścia przy projektowaniu i syntezie związków finalnych. Były to: 6-butylo-3,5,7-trimetylo-2*H*-pirolo[3,4-*d*]pirydazyno-1,4-dion **9** oraz 6-fenylo-3,5,7-trimetylo-2*H*-pirolo[3,4-*d*]pirydazyno-1,4-dion **10**[36].

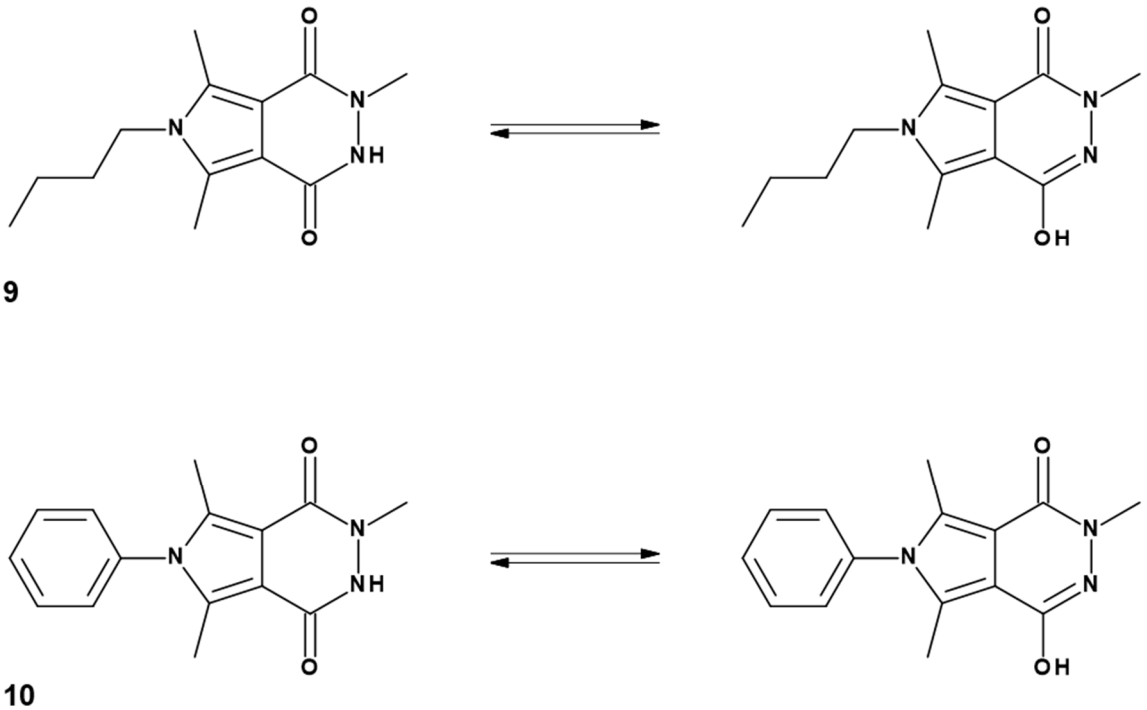

Rys. 5. Wzory wyjściowych pochodnych pirolo[3,4-*d*]pirydazyno-1,4-dionu.

Pierwszy etap zaplanowanej syntezy polegał na alkilowaniu pochodnych **9** i **10** chlorooctanem metylu w acetonitrylu w obecności K_2CO_3. W rezultacie otrzymano odpowiednie pochodne estrowe. Z uwagi na zjawisko tautomerii keto-enolowej podstawieniu

ulegał zarówno atom azotu *N*2 jak i atom tlenu grupy hydroksylowej. W zastosowanych warunkach syntezy w zdecydowanej przewadze otrzymywano *O*-izomer. Rozdziału uzyskanej mieszaniny izomerów dokonywano na kolumnie chromatograficznej. Z uwagi na niską wydajność z jaką powstawał *N*-izomer, zdecydowano, że kolejne modyfikacje strukturalne będą realizowane wyłącznie na *O*-podstawionych analogach.

Ogrzewanie pochodnych estrowych w etanolu z nadmiarem wodzianu hydrazyny pozwoliło na otrzymanie, z doskonałą wydajnością (~90%), odpowiednich hydrazydów. Te z kolei, były poddawane wewnątrzcząsteczkowej cyklizacji w środowisku zasadowym w obecności disiarczku węgla. W efekcie uzyskano kluczowe 1,3,4-oksadiazolowe pochodne pirolo[3,4-*d*]pirydazynonu.

Ostatni etap syntezy polegał na otrzymaniu związków o budowie zasad Mannicha w reakcji odpowiedniej 1,3,4-oksadiazolowej pochodnej z dodatkiem roztworu formaliny oraz wybranej aminy drugorzędowej w etanolu. Pozwoliło to na otrzymanie zaplanowanych produktów finalnych.

W wyniku przeprowadzonej kilkuetapowej syntezy otrzymano w sumie 20 nowych, nieopisanych dotąd w literaturze związków, w tym 14 finalnych pochodnych o budowie zasad Mannicha, stanowiących pierwszą serię (seria **I**) 1,3,4-oksadiazolowych pochodnych pirolo[3,4-*d*]pirydazynonu. Ich wzór ogólny został przedstawiony na **Rysunku 6**. Szczegóły dotyczące zrealizowanych na tym etapie prac syntetycznych są przedstawione na *Schematach 1* i *2* oraz opisane w *Rozdziale 2.1* publikacji **P1**.

Struktura każdego otrzymanego związku została potwierdzona dzięki wykorzystaniu technik spektralnych oraz metody analizy elementarnej. Dane analityczne, właściwości fizykochemiczne oraz widma nowych struktur są zebrane i opisane w części eksperymentalnej publikacji **P1** oraz w załączonym do niej suplemencie.

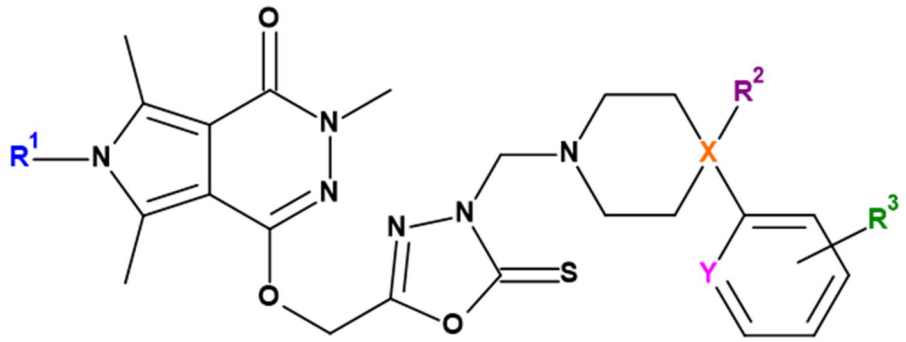

I

R^1 – *n*-butyl, fenyl;

R^2 – OH, —;

R^3 – H, CH_3, Cl, NO_2;

X – N, C, O;

Y – C, N;

Rys. 6. Ogólny wzór serii **I** pochodnych pirolo[3,4-*d*]pirydazynonu o budowie zasad Mannicha.

W kolejnym etapie prac syntetycznych, zdecydowano się otrzymać struktury, które zostały zaprojektowane w myśl teorii farmakoforowej przedstawionej przez Dogruera. Idea ta zakłada, że połączenie pochodnej arylopiperazyny z głównym szkieletem za pośrednictwem co najmniej dwuwęglowego, elastycznego łącznika z ugrupowaniem karbonylowym, może istotnie nasilać działanie antynocyceptywne związków finalnych[46,47]. Schematyczna budowa takiego ugrupowania jest przedstawiona na **Rysunku 7**.

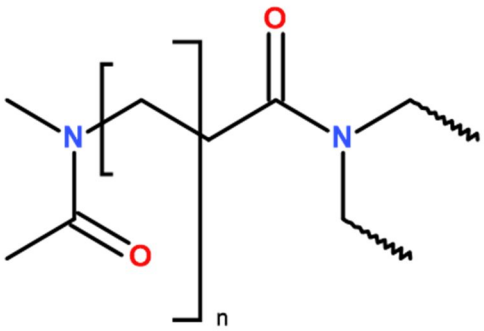

Rys. 7. Ogólny wzór farmakoforu zaproponowanego przez Dogruera.

Dlatego też, zaprojektowano oraz otrzymano grupę czterech pilotowych pochodnych pirolo[3,4-*d*]pirydazynonu, w których ugrupowanie arylopierazynylowe połączone jest z atomem siarki pierścienia 1,3,4-oksadiazolo-2-tiolu przez łącznik 2-oksoetylowy. Wzór ogólny drugiej serii związków (seria **II**) przedstawiony jest na **Rysunku 8**.

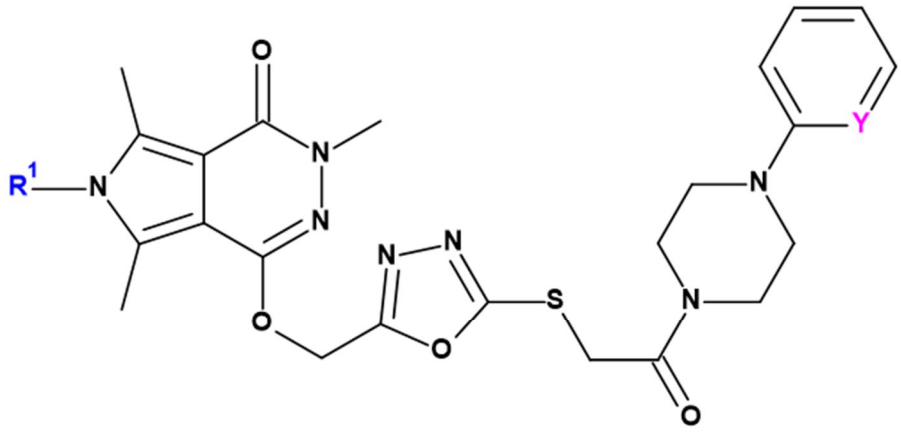

II

R^1 – *n*-butyl, fenyl; **Y – C, N;**

Rys. 8. Ogólny wzór serii **II** pochodnych pirolo[3,4-*d*]pirydazynonu z mostkiem 2-oksoetylowym.

Koncepcja oraz synteza *S*-podstawionych 1,3,4-oksadiazolowych pochodnych pirolo[3,4-*d*]pirydazynonu (seria **II)** zostały szczegółowo przedstawione na *Schemacie 1* oraz w *Rozdziałach 1* i *2.1* publikacji **P2**. Ponadto, w części chemicznej oraz eksperymentalnej tej pracy oraz w suplemencie znajdują się wyczerpujące informacje dotyczące właściwości fizykochemicznych oraz widma NMR, MS oraz IR wszystkich nowych struktur.

4.1.2 Badania *in vitro* oraz *in silico*

Wstępne badania oceny toksyczności oraz aktywności biologicznej tytułowych 1,3,4-oksadiazolowych pochodnych pirolo[3,4-*d*]pirydazynonu zostały przeprowadzone we współpracy z Panią dr inż. Benitą Wiatrak (Katedra i Zakład Podstaw Nauk Medycznych; Katedra i Zakład Farmakologii Uniwersytetu Medycznego we Wrocławiu). Dokowanie molekularne oraz badania spektralne zostały wykonane przez Pana dr Edwarda Krzyżaka oraz Panią dr inż. Aleksandrę Marciniak z Katedry i Zakładu Chemii Nieorganicznej Uniwersytetu Medycznego we Wrocławiu.

Ocena toksyczności związków o budowie zasad Mannicha, czyli pochodnych należących do serii **I**, została wykonana z użyciem testu wykorzystującego barwnik sulforodaminę B (*sulforhodamine B*, SRB) na linii komórkowej normalnych ludzkich skórnych fibroblastów (*normal human dermal fibroblasts*, NHDF). Żaden z badanych związków nie wykazał w przeprowadzonym eksperymencie potencjału cytotoksycznego (*Tabela 1*, **P1**). Z tego względu wszystkie 14 związków zostało zakwalifikowanych do dalszych badań.

Głównym celem przeprowadzonych prac badawczych było określenie zdolności hamowania cyklooksygenanazy przez otrzymane pochodne oraz ustalenie sposobu ich wiązania się z centrum aktywnym enzymu. W związku z tym, w pierwszym etapie badań biologicznych użyto dostępny komercyjnie enzymatyczny test płytkowy Cayman's COX Colorimetric Inhibitor Screening Assay (cat. no. 701050), który pozwala określić aktywność cyklooksygenazy poprzez kolorymetryczne wyznaczenie stężenia barwnej, utlenionej formy *N*,*N*,*N*′,*N*′-tetrametylo-*p*-fenylenodiaminy (*N,N,N′,N′-tetramethyl-p-phenylenediamine*, TMPD) będącej substratem enzymu. Uzyskane wyniki są przedstawione w *Rozdziale 2.2.1* oraz w *Tabeli 1* publikacji **P1**.

Wszystkie badane związki wykazały zdolność hamowania izoenzymu COX-2. Większość z nich działała preferencyjnie na COX-2, natomiast 5 z nich selektywnie blokowało formę indukowaną cyklooksygenazy. Jako referencji użyto leku o potwierdzonym działaniu przeciwzapalnym oraz znacznym powinowactwie do COX-2, a mianowicie meloksykamu. Warto podkreślić, że wszystkie analizowane pochodne pirolo[3,4-*d*]pirydazynonu serii **I** skuteczniej hamowały COX-2, niż lek odniesienia. Co więcej, również współczynnik selektywności COX-2/COX-1 obliczony dla każdego z testowanych związków był lepszy, niż w przypadku meloksykamu (*Tabela 1*, **P1**).

Te rezultaty znalazły potwierdzenie w przeprowadzonych badaniach dokowania molekularnego, które wykazały, że omawiane związki cechują się większym powinowactwem do COX-2, niż do COX-1. Można to wytłumaczyć faktem, że kieszeń wiążąca indukowanej formy COX-2, która różni się budową od miejsca aktywnego COX-1, umożliwia wiązanie większych i bardziej rozbudowanych cząsteczek[7–10]. Udowodniono, że badane związki łączą się głównie z subdomeną B (będącą miejscem wiązania meloksykamu oraz piroksykamu) oraz C, centrum aktywnego enzymu. Co więcej, nowe pochodne pirolo[3,4-*d*]pirydazynonu zajmują w kieszeni wiążącej cyklooksygenazy pozycję analogiczną do meloksykamu. Na **Rysunku 9** zaprezentowano sposób dokowania się do COX-2 dwóch najbardziej aktywnych związków **8a(P1)**, **8b(P1)** oraz meloksykamu. Szczegółowy opis wyników dokowania molekularnego znajduje się w *Rozdziale 2.2.2*, *Tabeli 2* publikacji **P1** oraz w danych uzupełniających tej pracy.

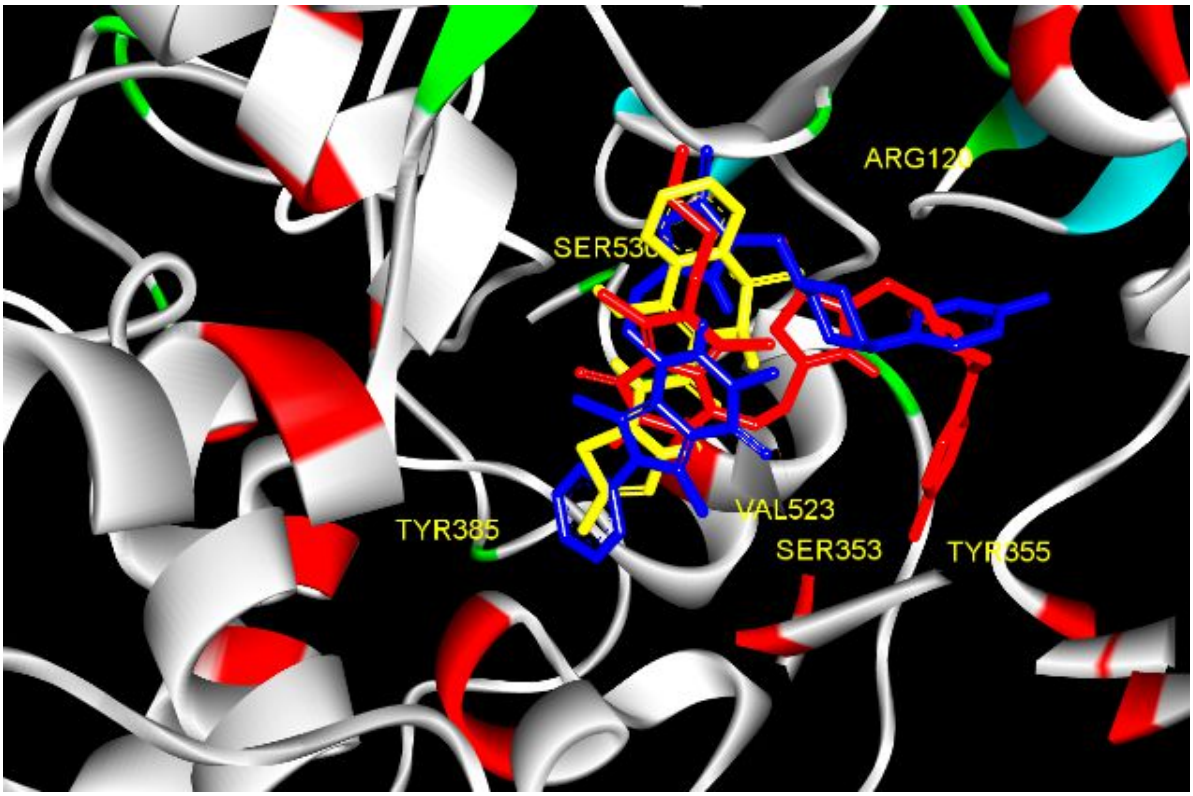

Rys. 9. Położenie w domenie wiążącej COX-2 pochodnych **8a(P1)** (niebieski), **8b(P1)** (czerwony) oraz meloksykamu (żółty).

Kolejny etap zaplanowanych badań *in vitro* zakładał ocenę potencjału antyoksydacyjnego nowych związków. Należy mieć na uwadze, że wzrost stężenia reaktywnych form tlenu czy azotu, który skutkuje zwiększonym stresem oksydacyjnym, może być spowodowany takimi czynnikami jak niedotlenienie czy stan zapalny. Z drugiej strony, wolne rodniki są silnymi czynnikami prozapalnymi, które m.in. nasilają ekspresję cyklooksygenazy. W efekcie, stres oksydacyjny oraz zapalenie są zjawiskami, które często współistnieją w uszkodzonej tkance i mogą się wzajemnie nasilać[48–50]. Dlatego też, przeprowadzono eksperymenty, które pozwoliły określić zdolność tytułowych związków do hamowania indukowanego stresu oksydacyjnego oraz nitrozacyjnego.

Wykonano test z wykorzystaniem fluorescencyjnego barwnika – dioctanu 2',7'-dichlorofluoresceiny (*2',7'-dichlorofluorescein diacetate*, DCF-DA) aby ocenić zdolność nowych pochodnych do zmniejszania poziomu reaktywnych form tlenu. Z kolei skuteczność zmiatania rodników azotowych określono testem Griess'a. W obu przypadkach badania przeprowadzono na linii komórkowej NHDF.

Związki **9a(P1)-13a(P1)** zmniejszały stężenie reaktywnych form tlenu w całym zakresie testowanych stężeń. Z kolei pochodne **7a(P1)** i **8a(P1)** były efektywne w koncentracji 10μM i 50μM. Pochodne z podstawnikiem *n*-butylowym, czyli **7b(P1)-13b(P1)**, cechowała niższa aktywność antyoksydacyjna, a w przypadku niektórych z nich obserwowano wręcz wzrost poziomu wolnych rodników tlenowych (*reactive oxygen species*, ROS). Z kolei rezultaty testu Griess'a wskazują, że praktycznie wszystkie badane związki zmniejszają stężenie reaktywnych form azotu (*reactive nitrogen species*, RNS), w tym tlenku azotu (*nitric oxide*, NO). Jedynie pochodne **7b(P1)**, **10a(P1)** oraz **10b(P1)** powodowały nieznaczny, statystycznie nieistotny, wzrost stężenia rodników azotowych. Uzyskane wyniki są dokładnie przedstawione w *Rozdziale 2.4* oraz *Tabeli 3* w publikacji **P1**.

Obiecujące wyniki testów DCF-DA oraz Griess'a stały się pretekstem do przeprowadzenia dodatkowego eksperymentu oceniającego działanie antyoksydacyjne oraz potencjał ochronny pochodnych pirolo[3,4-*d*]pirydazynonu przed szkodliwym działaniem wolnych rodników. W tym celu przeprowadzono test halo (*fast halo assay*, FHA), który pozwala oszacować efekt protekcyjny badanych związków na jądro komórkowe. Objawiaja się on ochroną chromatyny przed uszkodzeniami i pęknięciami DNA spowodowanymi zwiększonym stresem oksydacyjnym. Działanie ochronne określa się przez wyznaczenie poziomu uszkodzenia chromatyny w stosunku do próby kontrolnej. Uzyskane wyniki wskazują, że związki **7b(P1)**, **8a(P1)** (cały zakres stężęń) oraz **7a(P1)** (stężenie 10μM i 50μM), w sposób istotny statystycznie chronią DNA przed uszkodzeniami spowodowanymi podwyższonym stężeniem wolnych rodników. Na **Rysunku 10** przedstawiono wybrane mikrofotografie komórek, które były badane w teście FHA. Na fotografii **B** widoczny jest charakterystyczny efekt tzw. halo jądrowego spowodowany relaksacją chromatyny, co jest rezultatem pęknięć DNA (**Rys. 10 B**). Im większe halo, tym większe uszkodzenia chromatyny obserwujemy. W przypadku komórki inkubowanej ze związkiem **7b(P1)** efekt halo praktycznie nie występuje. Wyniki badań aktywności antyoksydacyjnej nowych pochodnych pirolo[3,4-*d*]pirydazynonu zostały szerzej opisane i przedstawione w *Rozdziale 2.4* i *2.5* a także w *Tabeli 3* publikacji **P1**.

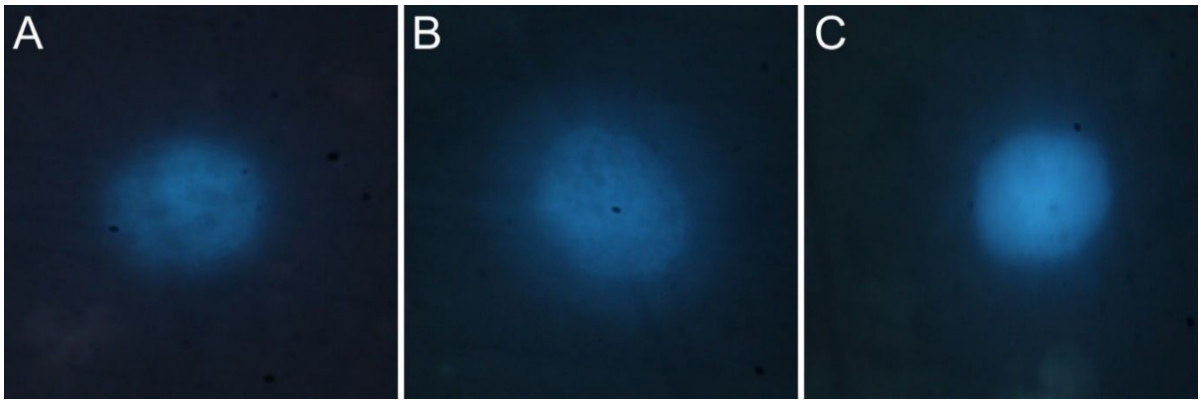

Rys. 10. Mikrofotografie (60x) komórek ukazujące relaksację chromatyny i efekt halo. **A**) komórki inkubowane w czystym medium; **B**) komórki inkubowane z 100µM H_2O_2 przez 1h; **C**) komórki inkubowane ze związkiem **7b(P1)** 10µM przez 24h i następnie z 100µM H_2O_2 przez 1h; Mikrofotografia **B** ukazuje znacznie większy efekt halo w porównaniu ze zdjęciem **A**; im większy rozmiar halo jądrowego, tym większa relaksacja chromatyny, co wskazuje na większe uszkodzenie DNA.

Uzupełnieniem eksperymentów, określających aktywność biologiczną nowych związków były badania, które pozwoliły ocenić sposób ich interakcji z albuminą, która jest najbardziej powszechnym białkiem osocza. Wiązanie się leków z białkami krwi w istotny sposób wpływa na ich farmakokinetykę, między innymi na czas półtrwania, czy dystrybucję. Dlatego też, przeprowadzono wstępne eksperymenty, które umożliwiły opis sposobu interakcji pochodnych pirolo[3,4-*d*]pirydazynonu z osoczową albuminą. Ze względu na dużo niższe koszty, użyte zostało białko bydlęce (*bovine serum albumin*, BSA). Jego struktura jest bardzo zbliżona do albuminy ludzkiej (*human serum albumin*, HSA), dlatego może być ono z powodzeniem używane w jej zastępstwie[51,52]. Celem opisania molekularnych oddziaływań między nowymi związkami a BSA wykorzystano metody spektralne takie jak dichroizm kołowy (*circular dichroism*, CD), fluorescencja oraz dokowanie molekularne.

Wyniki pomiarów spektroskopowych (wygaszanie fluorescencji, CD) wykazały, że w obecności badanych związków zachodzą zmiany w strukturze drugorzędowej BSA. Potwierdza to, że wchodzą one w interakcję z osoczową albuminą. Oddziaływanie to nie ma charakteru przypadkowych zderzeń cząsteczek, ale raczej polega na tworzeniu się kompleksów ligand-BSA w przybliżonym stosunku 1:1. Na podstawie przeprowadzonego dokowania molekularnego ustalono, że uprzywilejowanym miejscem wiązania nowych pochodnych pirolo[3,4-*d*]pirydazynonu przez BSA jest hydrofobowa kieszeń II(m).

Szczegóły wszystkich badań opisujących interakcje tytułowych związków z BSA, oraz wszelkie tabele oraz widma spektroskopowe i wykresy zostały zamieszczone w *Rozdziale 2.6* publikacji **P1** oraz w danych uzupełniających.

Po zebraniu rezultatów wszystkich eksperymentów przeprowadzono analizę multikryterialną (*multi – criteria decison analysis*, MCDA) dla badanych związków. Na podstawie jej wyników można stwierdzić, że w serii **I** 1,3,4-oksadiazolowych pochodnych pirolo[3,4-*d*]pirydazynonu, związkiem o najlepszym profilu aktywności biologicznej była cząsteczka **7b(P1)**, której strukturę przedstawiono na **Rysunku 11**. Na uwagę zasługują także pochodne **7a(P1)**, **10a(P1)**, **10b(P1)**, **13a(P1)** oraz **13b(P1)**. Kompletne wyniki analizy MCDA są przedstawione na *Rysunku 10* publikacji **P1**.

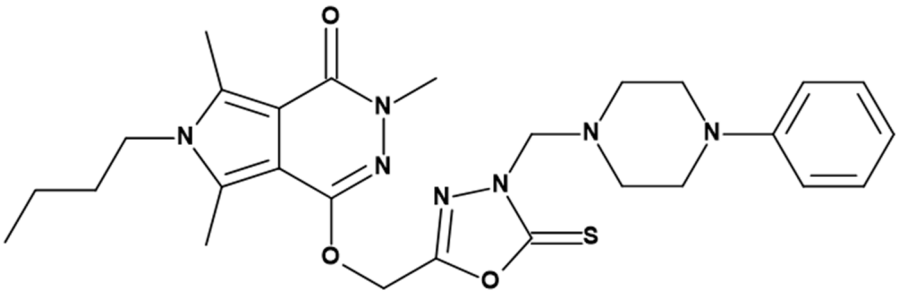

7b(P1)

Rys. 11. Związek **7b(P1)** – 1,3,4-oksadiazolowa pochodna pirolo[3,4-*d*]pirydazynonu o najbardziej obiecującym profilu aktywności biologicznej.

Analogiczne badania *in vitro* oraz *in silico* przeprowadzono także w przypadku serii **II** 1,3,4-oksadiazolowych pochodnych pirolo[3,4-*d*]pirydazynonu. Projekt, synteza, ocena aktywności biologicznej i właściwości fizykochemicznych tych związków stały się przedmiotem publikacji **P2**.

Badania toksyczności przeprowadzone na linii komórkowej NHDF wykonano z wykorzystaniem testu oceniającego aktywność mitochondrialnej dehydrogenazy bursztynianowej, której produktem widocznym w żywych komórkach jest formazan błękitu triazolowego (*3-(4,5-dimethylthiazol-2-yl)-2,5-diphenyltetrazolium bromide* MTT). Rezultaty testu MTT zostały szczegółowo opisane w *Rozdziale 2.3* publikacji **P2**.

Żaden z analizowanych związków nie zmniejszył przeżywalności komórek poniżej 30% dlatego też można stwierdzić, że nowe pochodne serii **II** nie wykazują potencjału cytotoksycznego i zostały przekazane na dalsze badania.

Aby ocenić zdolność hamowania cyklooksygenazy przez nowe związki użyty został, tak jak poprzednio, test enzymatyczny firmy Cayman (Cayman's COX Colorimetric Inhibitor Screening Assay cat. no. 701050). Wyniki przeprowadzonego eksperymentu (*Rozdział 2.2.1*, *Tabela 1* publikacja **P2**) jednoznacznie wskazują, że wszystkie analizowane pochodne wykazują aktywność tylko wobec indukowanej formy COX-2. Niestety, na podstawie uzyskanych rezultatów należy stwierdzić, że modyfikacja, polegająca na wprowadzeniu dłuższego łącznika z ugrupowaniem karbonylowym nie przyniosła spodziewanych efektów. Co prawda, otrzymano grupę selektywnych inhibitorów COX-2, ale związki serii **II** hamują ten enzym istotnie słabiej aniżeli pochodne o budowie zasad Mannicha (seria **I**) oraz meloksykam. Najbardziej aktywny okazał się związek **6a(P2)**.

Należy natomiast podkreślić, że wyniki badań dokowania molekularnego w pełni korelują z rezultatami testu enzymatycznego. W przypadku związków **5a**, **b(P2)** – **6a**, **b(P2)** wartości wolnej energii wiązania (ΔG°) podczas prób dokowania do COX-1 były dodatnie. Nowe pochodne wykazują natomiast powinowactwo do indukowanej formy COX-2 i zajmują w kieszeni wiążącej enzymu pozycję analogiczną do meloksykamu, co zostało pokazane na **Rysunku 12**. Wartości energii wiązań są nieco wyższe, ale porównywalne do tych wyznaczonych dla leku odniesienia. Szczegółowy opis badania dokowania molekularnego znajduje się w *Rozdziale 2.2.2* publikacji **P2**.

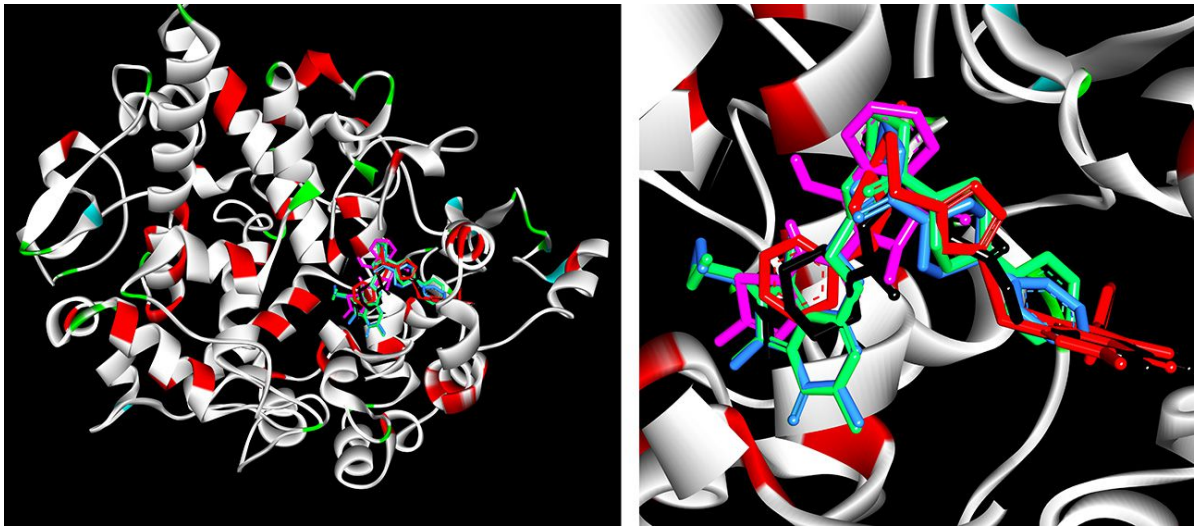

Rys. 12. Położenie w domenie wiążącej COX-2 pochodnych **5a**, **b(P2)** – **6a**, **b(P2)** oraz meloksykamu (różowy).

W kolejnym etapie badań biologicznych oceniono potencjał antyoksydacyjny nowych pochodnych pirolo[3,4-*d*]pirydazynonu serii **II** oraz ich zdolność do ochrony DNA przed uszkodzeniami wywołanymi wolnymi rodnikami. W tym celu przeprowadzono testy DCF-DA,

Griess'a oraz FHA. Szczegółowy opis wyników tych eksperymentów zamieszczono w *Rozdziale 2.4* publikacji **P2**.

Stwierdzono, że w komórkach inkubowanych ze związkami **5a(P2)**, **5b(P2)** oraz **6b(P2)** następowało zmniejszenie ilości wolnych rodników tlenowych poniżej wartości kontrolnej w całym zakresie testowanych stężeń. W przypadku związku **6a(P2)** miało to miejsce jedynie przy najniższej jego wartości tj. 10µM. Wyniki testu Griess'a wskazują, że wszystkie związki w zastosowanym najniższym stężeniu 10µM zmniejszają stężenie NO, natomiast pochodna **6a(P2)** była efektywna w całym spektrum użytych stężeń. (*Tabela 3*, publikacja **P2**).

Te rezultaty doskonale korespondują z wynikami uzyskanymi podczas testu FHA. Wykazano, że wszystkie badane pochodne zmniejszają ilość uszkodzeń chromatyny wywołanych stresem oksydacyjnym przynajmniej w jednym użytym stężeniu (*Tabela 3*, publikacja **P2**). Co więcej, udowodniono, że istnieje korelacja pomiędzy działaniem antyoksydacyjnym nowych pochodnych a ich zdolnościami naprawczymi DNA w stanie podwyższonego stresu oksydacyjnego (*Tabela 4*, publikacja **P2**).

Dodatkowo, wykonano badania spektralne oraz dokowanie molekularne, które pozwoliły na ocenę modelu interakcji z osoczową albuminą 1,3,4-oksadiazolowych pochodnych należących do serii **II**. Szczegółowe informacje dotyczące tych eksperymentów oraz ich wyniki są zawarte w *Rozdziałach 2.5-2.7* publikacji **P2** oraz w suplemencie tej pracy. Udowodniono, że badane związki oddziałują z BSA na zasadzie tworzenia kompleksów w przybliżonym stosunku 1:1. Uprzywilejowanym miejscem wiązania jest hydrofobowa kieszeń II, subdomena IIIA. Na podstawie wyników spektroskopii CD możemy przypuszczać, że związki **5a-b(P2)** wiążą się z BSA silniej niż pochodne **6a-b(P2)**.

Ze względu na zbliżone wyniki poszczególnych badań oraz stosunkowo mało liczną grupę analizowanych związków, trudno byłoby wskazać najbardziej obiecującą strukturę w obrębie pochodnych serii **II**. Niewątpliwie należy podkreślić fakt, że zamiana łącznika metylenowego na 2-oksoetylowy nie przyczyniła się do nasilenia aktywności farmakologicznej a jedynie do zwiększenia selektywności związków w stosunku do COX-2.

4.1.3 Badania *in vivo*

W związku z tym, że 1,3,4-oksadiazolowe pochodne pirolo[3,4-*d*]pirydazynonu serii **I** wykazały obiecujący profil aktywności farmakologicznej w eksperymentach *in vitro*, zdecydowano się na przekazanie wybranych związków na testy w modelu zwierzęcym. Do testów *in vivo* zostały zakwalifikowane dwie pochodne – **10b(P1)** oraz **13b(P1)**, których struktury zostały przedstawione na **Rysunku 13**. Ich wybór został dokonany głównie na podstawie wyników zdolności blokowania COX w teście enzymatycznym. Pochodna **10b(P1)** cechowała się najlepszym współczynnikiem hamowania COX-2/COX-1 spośród wszystkich badanych związków, natomiast cząsteczka o analogicznej budowie - **13b(P1)** była selektywna w stosunku do COX-2**.** Ponadto, zarówno **10b(P1)** jak i **13b(P1)** w przeprowadzonym teście SRB cechowały się jednymi z najwyższych wartości IC_{50} spośród wszystkich pochodnych pirolo[3,4-*d*]pirydazynonu serii **I**[26].

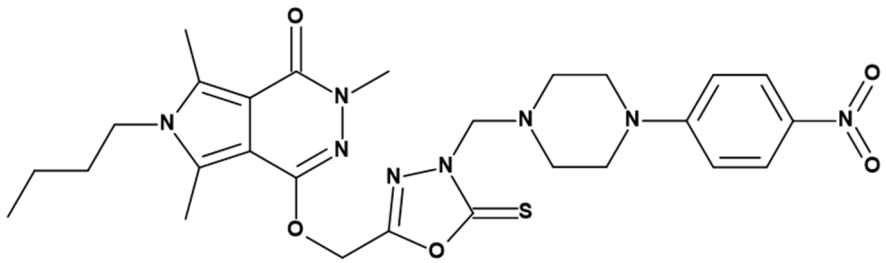

10b(P1)

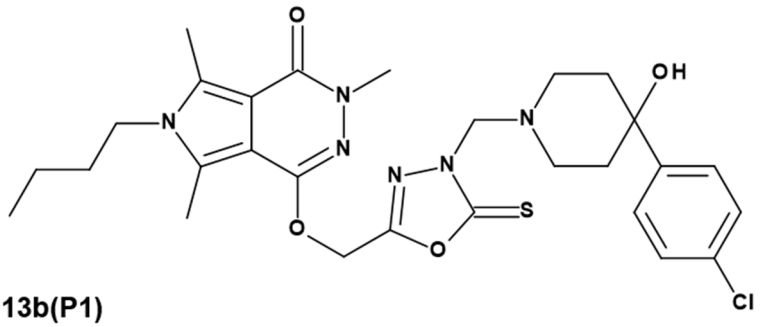

13b(P1)

Rys. 13. Wzory pochodnych pirolo[3,4-*d*]pirydazynonu, które zostały przekazane na badania *in vivo*.

Badania w modelu zwierzęcym zostały wykonane we współpracy z Katedrą i Zakładem Farmakologii Uniwersytetu Medycznego we Wrocławiu przez zespół kierowany przez Panią dr Martę Szandruk-Bender. Przeprowadzone eksperymenty miały na celu ocenę aktywności przeciwbólowej i przeciwzapalnej badanych związków, ich wpływu na kondycję błony śluzowej żołądka oraz ekspresję mediatorów stanu zapalnego.

Pierwszy etap zaplanowanych badań pozwolił określić profil działania przeciwbólowego pochodnych **10b(P1)** oraz **13b(P1)** w eksperymentalnych modelach bólu indukowanego szkodliwymi bodźcami, takich jak test odsunięcia ogona (*tail-flick test*) oraz test formalinowy (*formalin test*).

Test odsunięcia ogona pozwolił oszacować aktywność przeciwbólową związaną z mechanizmami ośrodkowymi poprzez pomiar czasu, po jakim następuje odpowiedź na stymulację termiczną wywołaną emitującym ciepło strumieniem światła. Nowe pochodne pirolo[3,4-*d*]pirydazynonu wykazały statystycznie istotną oraz dawko-zależną aktywność analgetyczną w porównaniu z kontrolą. Jednocześnie ich aktywność była istotnie niższa od morfiny. Uzyskane wyniki przedstawiono w formie wykresu na **Rysunku 14**.

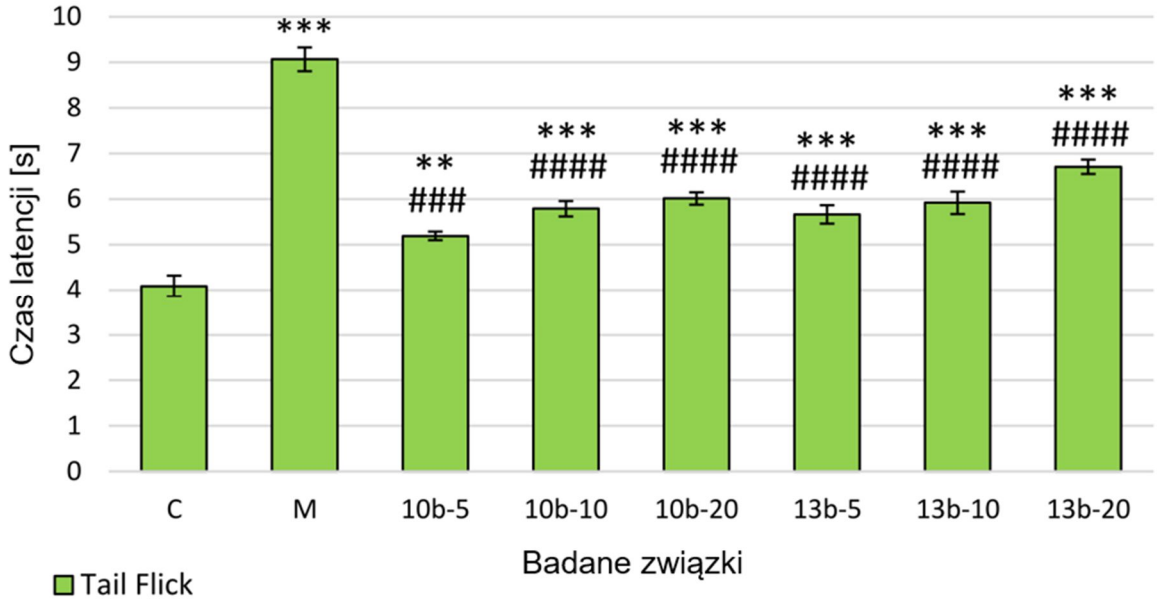

Rys. 14. Wpływ badanych związków **10b** i **13b** na czas latencji w teście odsunięcia ogona (*tail flick*). Grupa eksperymentalna *n*=12; wszystkie związki zostały podane dożołądkowo; C – grupa kontrolna; M – grupa, która otrzymała morfinę w dawce 10mg/kg; **10b**-5, **10b**-10, **10b**-20 – grupy, które otrzymały odpowiednio 5, 10, 20mg/kg związku **10b**; **13b**-5, **13b**-10, **13b**-20 – grupy, które otrzymały odpowiednio 5, 10, 20mg/kg związku **13b**; dane przedstawiono jako średnią ± SEM; różnice **p<0.01 vs. grupa kontrolna; ***p<0.001 vs. grupa kontrolna; ###p<0.001 vs. grupa morfiny; ####p<0.0001 vs. grupa morfiny uznano za statystycznie istotne. *tłumaczenie na język polski na potrzeby rozprawy wykonano na podstawie publikacji źródłowej*[53]

Uzyskane wyniki jednoznacznie wskazują, że oba badane związki **10b(P1)** oraz **13b(P1)** wykazują aktywność analgetyczną, ponieważ w porównaniu z kontrolą istotnie wydłużyły czas, po jakim nastąpiła reakcja na szkodliwy bodziec (odsunięcie ogona przez zwierzę). Może to sugerować, że pochodne **10b(P1)** i **13b(P1)** modulują centralne mechanizmy związane w nocycepcją.

Aby określić wpływ nowych związków na zarówno ośrodkowe, jak i obwodowe mechanizmy reakcji bólowej, wykonano drugi eksperyment, którym był test formalinowy. W tym modelu podskórna iniekcja roztworu formaliny do tylnej łapy wyzwala dwufazową odpowiedź nocyceptywną. Wczesna, neurogeniczna, jest rezultatem bezpośredniego pobudzenia włókien aferentnych oraz uwolnienia neuropeptydów takich jak substancja P. Faza późna wynika z rozwoju stanu zapalnego w tkance i w konsekwencji zwiększenia syntezy i uwalniania prostaglandyn. W związku z powyższym, test formalinowy pozwala określić nie tylko wpływ badanych substancji na mechanizmy nocycepcji nie związane z zapaleniem (faza wczesna), ale również na reakcję nocyceptywną o podłożu zapalnym (faza późna)[3,54,55].

Testowane pochodne **10b(P1)** i **13b(P1)** oraz leki referencyjne spowodowały, proporcjonalne do podanej dawki, skrócenie reakcji bólowej, sprowokowanej iniekcją formaliny (czasu lizania łapy), zarówno w fazie wczesnej jak i w późnej. W porównaniu do grupy kontrolnej, najbardziej efektywna w fazie wczesnej okazała się być morfina oraz związek **13b(P1)** w dawce 20mg/kg, którego siła działania była porównywalna z morfiną. Co więcej, efekt antynocyceptywny pochodnej **13b(P1)** w dawce 20mg/kg był istotnie statystycznie większy niż indometacyny. Dobra aktywność, jaką związek **13b(P1)** w najwyższej zastosowanej dawce wykazał we wczesnej fazie testu może świadczyć o tym, że jego mechanizm działania wynika także z wpływu na inne, nie związane z blokowaniem COX, szlaki i przekaźniki. Ta przesłanka wymaga dalszych, bardziej wnikliwych badań. W fazie późnej najlepsze i statystycznie istotne w porównaniu z kontrolą działanie wykazała morfina oraz oba badane związki **10b(P1)** i **13b(P1)** w dawkach 10 i 20mg/kg. Uzyskane rezultaty, które zaprezentowano na **Rysunku 15**, sugerują, że badane związki wykazują zarówno centralną jak i obwodową aktywność analgetyczną.

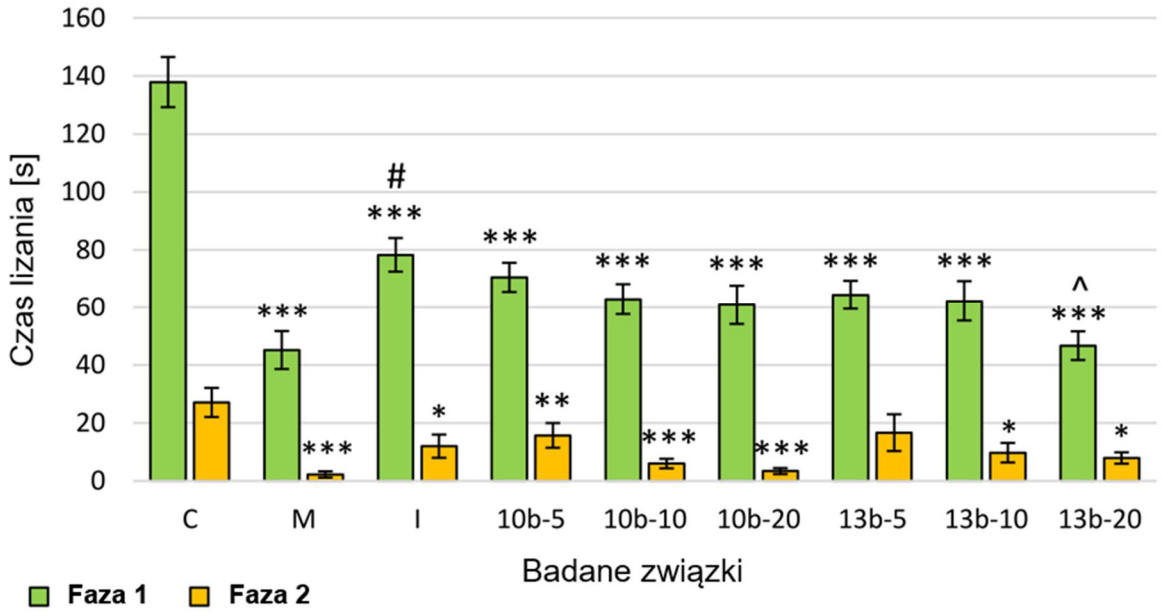

Rys. 15. Wpływ związków **10b** i **13b** na czas lizania we wczesnej (0–5 min) oraz późnej (25–30 min) fazie testu formalinowego. Morfina oraz indometacyna zostały użyte jako leki odniesienia. Wszystkie badane substancje podano dożołądkowo. Grupy badane (n = 12): C – grupa kontrolna; M – grupa, która otrzymała morfinę w dawce 10mg/kg; I – grupa, która otrzymała indometacynę w dawce 10mg/k; **10b**-5, **10b**-10, **10b**-20 – grupy otrzymujące odpowiednio 5, 10, 20 mg/kg związku **10b**; **13b**-5, **13b**-10, **13b**-20 – grupy otrzymujące odpowiednio 5, 10, 20 mg/kg związku **13b**; dane przedstawiono jako średnią ± SEM; różnice * $p < 0.05$ vs. grupa kontrolna; ** p <0.01 vs. grupa kontrolna; *** $p < 0.001$ vs. grupa kontrolna; # $p < 0.05$ vs. grupa morfiny; ^ $p < 0.05$ vs. grupa indometacyny uznano za statystycznie istotne.
tłumaczenie na język polski na potrzeby rozprawy wykonano na podstawie publikacji źródłowej [53]

Jak już zostało wcześniej nadmienione, w późnej fazie testu formalinowego dochodzi do zwiększonej syntezy i uwalniania prostaglandyn, które są jednymi z najlepiej poznanych i opisanych mediatorów prozapalnych[6]. Działają one, zwłaszcza prostaglandyna E_2 (PGE_2), uwrażliwiająco, a dodatkowo modulują reakcję bólową zarówno obwodowo jak i ośrodkowo. PGE_2 nasila także aktywność innych mediatorów prozapalnych. Dlatego zmniejszenie zależnej od COX produkcji PGE_2 powinno skutkować załagodzeniem reakcji nocyceptywnej[6,56,57]. Inną substancją, która również pełni ważną rolę w mediacji nocycepcji o podłożu zapalnym oraz wpływa na zwiększone uwalnianie PGE_2 jest mieloperoksydaza (*myeloperoxidase*, MPO). Jest ona produkowana przez neutrofile, które infiltrują tkankę objętą stanem zapalnym. Aktywacja obojętnochłonnych granulocytów w obszarze dotkniętym przez zapalenie prowadzi do wzrostu stężenia MPO, która z kolei nasila produkcję reaktywnych form tlenu i azotu[58,59]. Z tego względu substancje, które wykazują aktywność antyoksydacyjną, w sposób niejako pośredni, mogą uśmierzać stan zapalny oraz łagodzić reakcję bólową, u podłoża której leży zapalenie[48,60].

W związku z powyższym, wykonano oznaczenie poziomu PGE_2 oraz MPO w mysim osoczu testem immunoenzymosorpcyjnym (*the enzyme-linked immunosorbent assay*, ELISA). Wyniki przeprowadzonego eksperymentu zaprezentowane są w formie wykresu na **Rysunku 16**. Najniższy poziom PGE_2 został zarejestrowany w grupach, które otrzymały związek **13b(P1)** w dawce 20mg/kg lub indometacynę. Statystycznie istotnie mniejsze stężenie MPO w porównaniu z kontrolą zostało oznaczone w grupach, którym podano pochodną **13b(P1)** w dawce 10 i 20mg/kg albo indometacynę. Spadek stężenia MPO w osoczu zwierząt, które otrzymywały związek **13b(P1)** można tłumaczyć tym, że wykazywał on, w przeciwieństwie do pochodnej **10b(P1)**, działanie antyrodnikowe w testach *in vitro* (*Rozdział 2.4*, publikacja **P1**). Ponadto, warto zaznaczyć, że w przypadku obu badanych związków **10b(P1)** i **13b(P1)**, ich wpływ na stężenie PGE_2 i MPO w osoczu był zależny od zastosowanej dawki (**Rys. 16**).

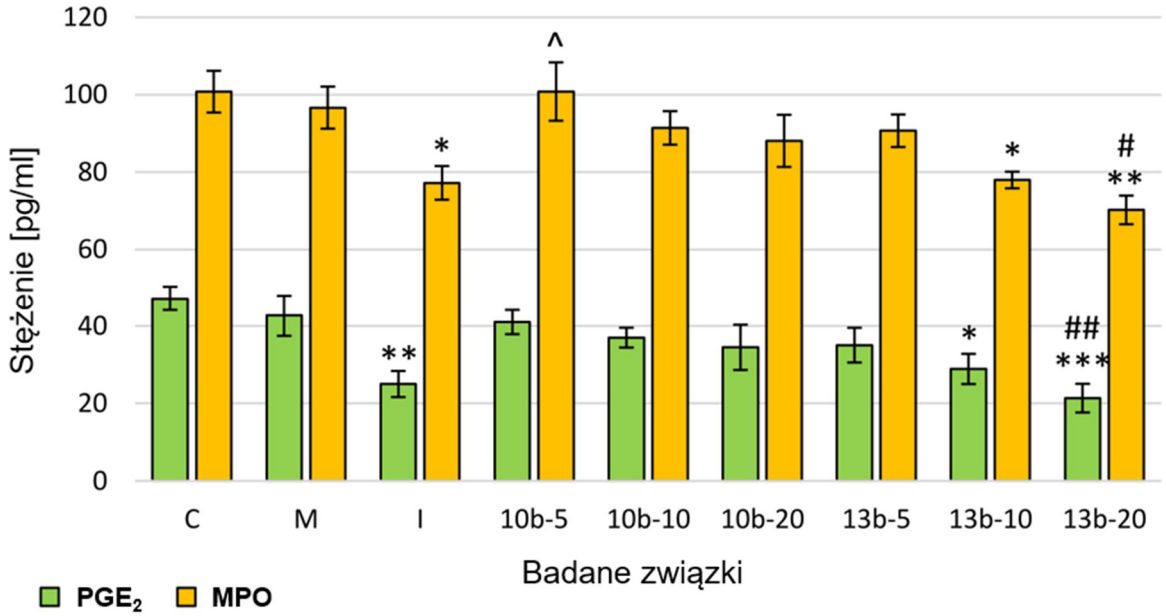

Rys. 16. Wpływ związków **10b** i **13b** na poziom stężenia prostaglandyny E2 (PGE_2) oraz mieloperoksydazy (MPO) w mysim osoczu. Próbki krwi zostały pobrane przed dokonaniem eutanazji. Lekami odniesienia były morfina oraz indometacyna. Grupy badane (n = 12): C – grupa kontrolna; M – grupa, która otrzymała morfinę w dawce 10 mg/kg; I – grupa, która otrzymała indometacynę w dawce 10 mg/kg; **10b**-5, **10b**-10, **10b**-20 – grupy otrzymujące odpowiednio 5, 10, 20 mg/kg związku **10b**; **13b**-5, **13b**-10, **13b**-20 – grupy otrzymujące odpowiednio 5, 10, 20 mg/kg związku **13b**; dane przedstawiono jako średnią ± SEM; różnice * $p < 0.05$ vs. grupa kontrolna; ** $p < 0.01$ vs. grupa kontrolna; *** $p < 0.001$ vs. grupa kontrolna; # $p < 0.05$ vs. grupa morfiny; ## $p < 0.01$ vs. grupa morfiny; ^ $p < 0.05$ vs. grupa indometacyny uznano za statystycznie istotne.
tłumaczenie na język polski na potrzeby rozprawy wykonano na podstawie publikacji źródłowej [53]

Celem przeprowadzonych badań w modelu zwierzęcym było nie tylko określenie aktywności analgetycznej badanych związków, ale także zbadanie ich wpływu na kondycję błony śluzowej żołądka. Uzyskanie związków, które nie wykazywałyby niebezpiecznych działań niepożądanych na przewód pokarmowy, charakterystycznych dla klasycznych NLZP [15–18], było jednym z podstawowych założeń niniejszej pracy. Z tego powodu dokonano makro- oraz mikroskopowej oceny stanu śluzówki żołądków pobranych od zwierząt uczestniczących w badaniu. Obecność zmian widocznych makroskopowo, takich jak wybroczyny, nadżerki czy krwawienia świadczyła o aktywności gastrotoksycznej. Uzyskane wyniki jednoznacznie wskazują, że obie pochodne **10b(P1)** i **13b(P1)**, we wszystkich użytych dawkach (5, 10, 20mg/kg) nie powodowały istotnych zmian w obrazie śluzówki żołądka. Z kolei w grupie, której podano indometacynę (10mg/kg) zaobserwowano znaczne uszkodzenia błony śluzowej żołądka. Wyniki oceny makroskopowej znalazły potwierdzenie badaniami mikroskopowymi, których rezultaty zostały przedstawione na **Rysunku 17**.

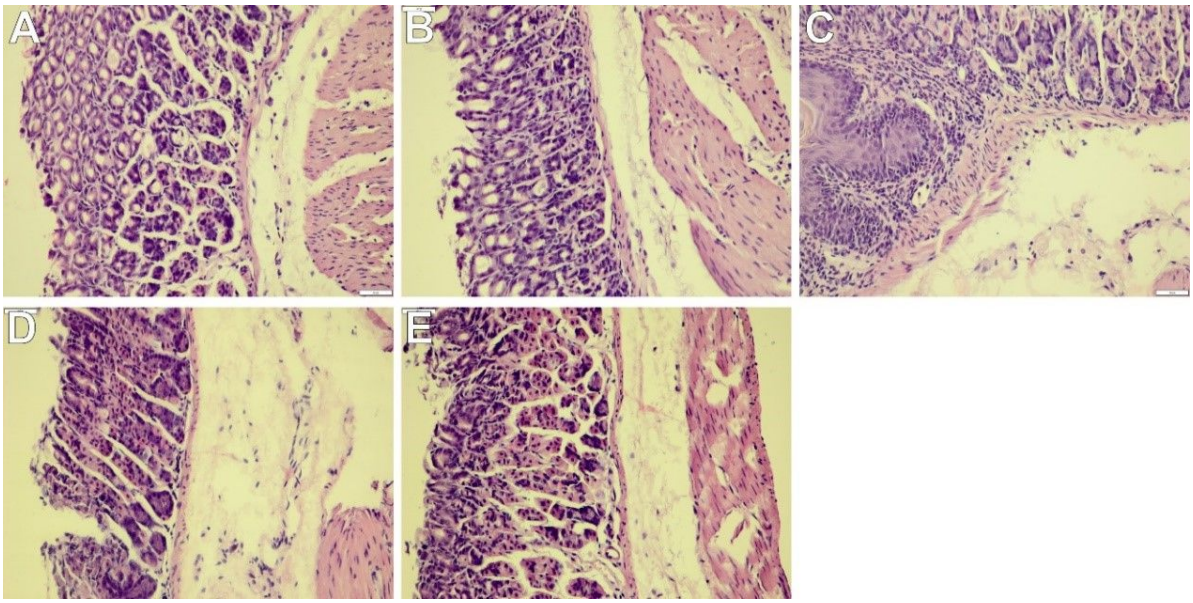

Rys. 17. Obraz mikroskopowy tkanki żołądka po barwieniu hematoksyliną-eozyną (H&E). Badane związki nie zmieniały naturalnej budowy komórek błony śluzowej żoładka, oraz nie powodowały owrzodzeń. Morfina oraz indometacyna zostały użyte jako leki odniesienia. Grupy badane (n = 12): Grupa kontrolna (**A**); grupa, która otrzymała morfinę w dawce 10 mg/kg (**B**); grupa, która otrzymała indometacynę w dawce 10 mg/kg (**C**); grupa, która otrzymała 20 mg/kg związku **10b** (**D**); grupa, która otrzymała 20 mg/kg związku **13b** (**E**); powiększenie – 200x. *tłumaczenie na język polski na potrzeby rozprawy wykonano na podstawie publikacji źródłowej* [53]

W obrazie mikroskopowym błony śluzowej żołądków zwierząt, należących zarówno do grupy kontrolnej jak i do grup otrzymujących badane pochodne **10b(P1)** oraz **13b(P1)** nie odnotowanych żadnych zmian patologicznych (**Rys. 17A**, **17D**, **17E**). Z drugiej strony, podczas

analizy histopatologicznej tkanki błony śluzowej żołądka zwierząt, którym podano indometacynę w dawce 10mg/kg, zaobserwowano liczne uszkodzenia komórek jej warstwy ochronnej. Odnotowano ogniska martwicze, obrzęk podśluzówkowy oraz przekrwienie zarówno śluzówkowych jak i podśluzówkowych naczyń krwionośnych. (**Rys. 17C**). Morfina (10mg/kg) nie spowodowała istotnych zmian w obrazie zarówno makro- jak i mikroskopowym śluzówki żołądka (**Rys. 17B**).

Reasumując, związki **10b(P1)** oraz **13b(P1)** wykazały lepszą aktywność antynocyceptywną *in vivo* niż indometacyna, przy jednocześnie znacznie obniżonej gastrotoksyczności, co najprawdopodobniej jest związane z obecnością w ich strukturze pierścienia 1,3,4-oksadiazolo-2-tionu.

Biorąc pod uwagę fakt, że badane pochodne **10b(P1)** i **13b(P1)** okazały się skuteczne w łagodzeniu nocycepcji zapalnej w późnej fazie testu formalinowego, zdecydowano się wykonać eksperyment, który pozwoliłby ocenić również ich obwodową aktywność przeciwzapalną. Dlatego przeprowadzono test karageninowy, dzięki któremu możliwe było określeniu wpływu związków **10b(P1)** i **13b(P1)** na przebieg ostrego zapalenia wywołanego iniekcją 1% roztworu karageniny w obszar rozcięgna podpodeszwowego tylnej łapy szczura. Przy użyciu pletyzmometru dokonywano pomiaru bezwzględnej objętości łapy oraz obliczono przyrosty jej objętości po 1, 2, 3 oraz 6 godzinach po wstrzyknięciu roztworu karageniny lub soli fizjologicznej (grupa kontrolna, C). Dodatkowo, oznaczono stężenie, w tkance objętej zapaleniem, mediatorów takich jak PGE_2, MPO czy czynnik martwicy nowotworów (*tumor necrosis factor* α, TNF-α) oraz zbadano wpływ nowych pochodnych pirolo[3,4-*d*]pirydazynonu na kondycję błony śluzowej żołądka.

W przeprowadzonym eksperymencie nie odnotowano żadnych istotnych statystycznie różnic w objętości łapy w grupie kontrolnej oraz w grupach badanych przed iniekcją karageniny. Natomiast wstrzyknięcie 0.1mL 1% roztworu karageniny do tylnej łapy zwierząt należących do grup badanych wywołała silną reakcję zapalną oraz znaczny wzrost objętości łapy spowodowany obrzękiem. Zmiany w wyglądzie i wielkości łap zwierząt są widoczne na fotografiach zebranych przedstawionych na **Rysunku 18**.

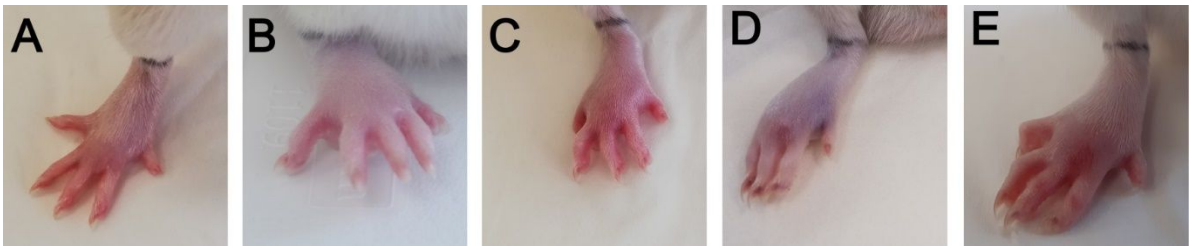

Rys. 18. Wpływ związków **10b** oraz **13b** na obrzęk łapy indukowany karageniną. Indometacyna została użyta jako lek odniesienia. Grupy badane: grupa kontrolna (**A**); grupa karageninowa (**B**); grupa otrzymująca 10mg/kg indometacyny (**C**); grupa otrzymująca 20mg/kg związku **10b** (**D**); grupa otrzymująca 20mg/kg związku **13b** (**E**). *tłumaczenie na język polski na potrzeby rozprawy wykonano na podstawie publikacji źródłowej* [61]

Największy obrzęk łapy został odnotowany w każdej grupie 6h po wykonaniu iniekcji z karageniną. W grupach zwierząt, które otrzymały pochodne **10b(P1)** i **13b(P1)**, po 2h od wstrzyknięcia roztworu karageniny zaobserwowano zahamowanie tempa narastania obrzęku (**Rys**. **18D**, **18E**). Związek **10b(P1)** zastosowany w dawkach 10 i 20mg/kg był w stanie częściowo odwrócić postępujące narastanie obrzęku po 2, 3 i 6h od iniekcji karageniny. Podobny efekt cofnięcia, do pewnego stopnia, obrzmienia odnotowano także 2, 3 oraz 6h po wstrzyknięciu roztworu karageniny we wszystkich grupach, które otrzymały pochodną **13b(P1)** (dawka 5, 10 i 20mg/kg). Co więcej, w przypadku związku **13b(P1)**, we wszystkich użytych dawkach odnotowano statystycznie istotne różnice w objętości łapy, w porównaniu z grupą kontrolną, po 2, 3 oraz 6h od indukcji zapalenia. Podobnie, stopień zahamowania wzrostu obrzęku zaobserwowany w grupie, której podano indometacynę (**Rys**. **18C**), był również statystycznie istotny. Maksymalny efekt zmniejszenia obrzmienia łapy w porównaniu z grupą karageninową zaobserwowano 3h po indukcji stanu zapalnego w grupach, które otrzymały indometacynę (obrzęk zahamowany w 71.2%) oraz związki **10b(P1)** (obrzęk zahamowany w 57.5%) i **13b(P1)** (obrzęk zahamowany w 62.3%) w najwyższych dawkach 20mg/kg. Ponadto, aktywność pochodnych **10b(P1)** i **13b(P1)** podanych w najwyższej dawce była porównywalna z aktywnością indometacyny.

Następnie, w supernatantach otrzymanych w wyniku homogenizacji tkanek łap, w których wywołano stan zapalny oznaczono, przy użyciu testów ELISA, stężenie mediatorów takich jak PGE_2, MPO oraz TNF-α, których zwiększona ekspresja towarzyszy zapaleniu[1–5]. Uzyskane wyniki zostały przedstawione w formie wykresów na **Rysunku 19**.

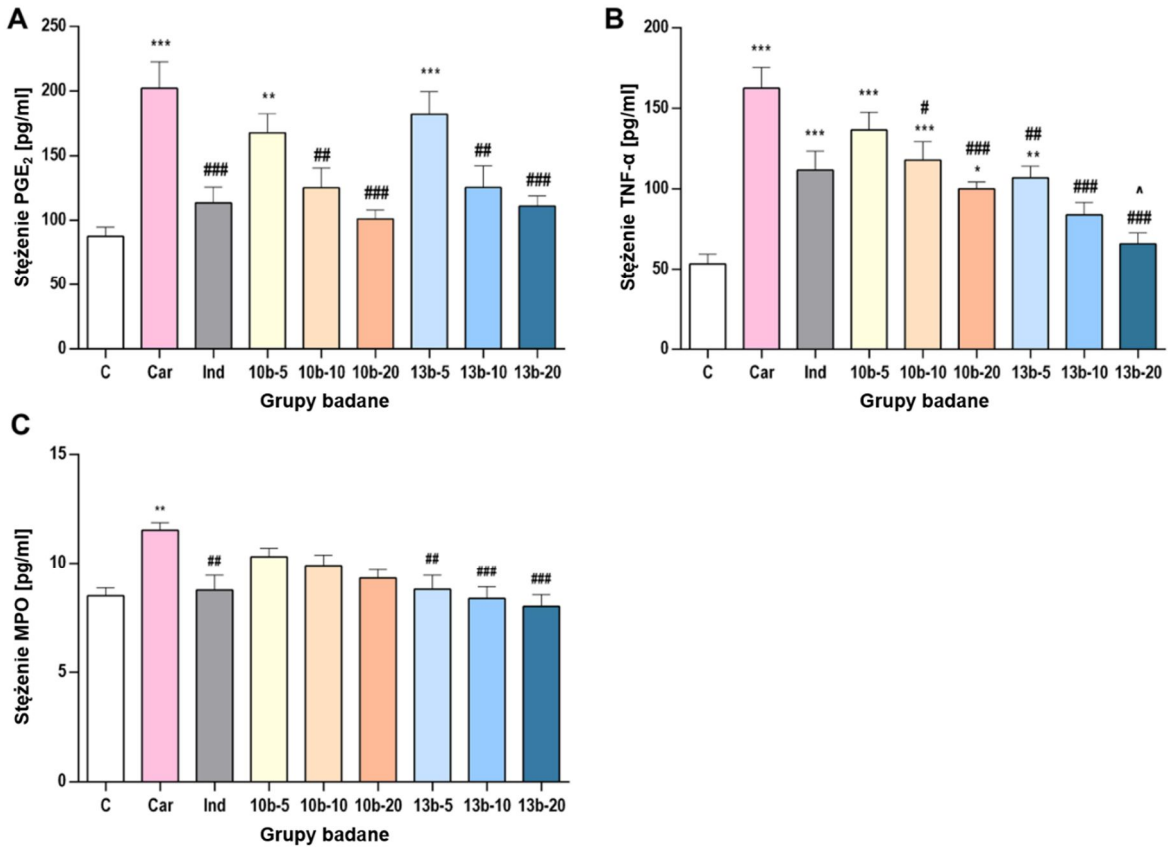

Rys. 19. Wpływ związków **10b** oraz **13b** na stężenie PGE_2 (**A**), TNF-α (**B**) i MPO (**C**) tkance łapy. Indometacyna została użyta jako lek odniesienia. Grupy badane: C – grupa kontrolna otrzymująca 0.5% roztwór karboksymetylocelulozy (carboxymethylcellulosum, CMC) dożołądkowo (*intragastrically*, i.g.) oraz sól fizjologiczną podpowięziowo (*subplantarly*, s.pl.); Car – grupa karageninowa otrzymująca 0.5% CMC i.g. i 1% roztwór karageniny s.pl.; Ind – grupa indometacyny otrzymująca 10mg/kg indometacyny i.g. i 1% roztwór karageniny s.pl.; **10b-**5, **10b-**10 i **10b-**20 – grupy otrzymujące odpowiednio 5, 10 albo 20mg/kg badanego związku **10b** i.g. i 1% roztwór karageniny s.pl.; **13b-**5, **13b-**10 i **13b-**20 – grupy otrzymujące odpowiednio 5, 10 albo 20mg/kg badanego związku **13b** i.g. i 1% roztwór karageniny s.pl. Dane zaprezentowane są jako wartości średnie ± SEM (n=12). Różnice $^{*}p<0.05$ vs grupa kontrolna; $^{**}p<0.01$ vs grupa kontrolna; $^{***}p<0.001$ vs grupa kontrolna; $^{\#}p<0.05$ vs grupa karageninowa; $^{\#\#}p<0.01$ vs grupa karageninowa; $^{\#\#\#}p<0.001$ vs grupa karageninowa; $^{\wedge}p<0.05$ vs grupa indometacyny zostały oznaczone jako istotne statystycznie.

tłumaczenie na język polski na potrzeby rozprawy wykonano na podstawie publikacji źródłowej [61]

Największy wzrost stężenia oznaczanych mediatorów stanu zapalnego wystąpił, zgodnie z przewidywaniami, w „grupie karageninowej". W tkance zwierząt, którym podano związek **10b(P1)** w dawce 10 oraz 20mg/kg poziom PGE_2 był niższy niż w „grupie karageninowej" i nie różnił się istotnie statystycznie od kontroli. Jednocześnie, w tych grupach (**10b-**10; **10-**20) odnotowano również częściowy spadek poziomu TNF-α. Pochodna **10b(P1)** w całym zakresie testowanych dawek nie wpłynęła istotnie na koncentrację MPO. Wyznaczone stężenia

mieloperoksydazy w grupach otrzymujących związek **10b(P1)** nie różniły się w sposób istotny statystycznie od tych, które oznaczono w grupie kontrolnej oraz karageninowej (**Rys. 19C**). Stężenie PGE_2, MPO oraz TNF-α w grupach, którym podano pochodną **13b(P1)** w dawkach 10 i 20mg/kg było statystycznie istotnie niższe w porównaniu z „grupą karageninową". Warto zwrócić uwagę, że ilość PGE_2 oznaczona w tkance zwierząt, którym aplikowano związek **10b(P1)** oraz **13b(P1)** w dawce 10 i 20mg/kg była porównywalna z wartościami odnotowanymi w grupie indometacyny. Ponadto, podobną zależność zaobserwowano w kontekście stężeń MPO oraz TNF-α jakie zarejestrowano w grupach, którym podano pochodne **10b(P1)** i **13b(P1)** w całym zakresie testowanych dawek (**Rys. 19B** i **19C**). Warto nadmienić, że związek **13b(P1)** w najwyższej dawce efektywniej obniżał stężenie TNF-α w objętej zapaleniem tkance, niż lek odniesienia.

Aby ocenić wpływ badanych związków na kondycję błony śluzowej żołądka wykonano analizę makro- oraz mikroskopową narządów pobranych od zwierząt uczestniczących w badaniu. Wskaźnikiem potencjalnego działania wrzodotwórczego była obecność oraz nasilenie takich zmian w obrazie śluzówki żołądka takich jak np. wybroczyny czy nadżerki. Na **Rysunku 20** przedstawiono fotografię wybranych żołądków, które były poddane analizie makroskopowej.

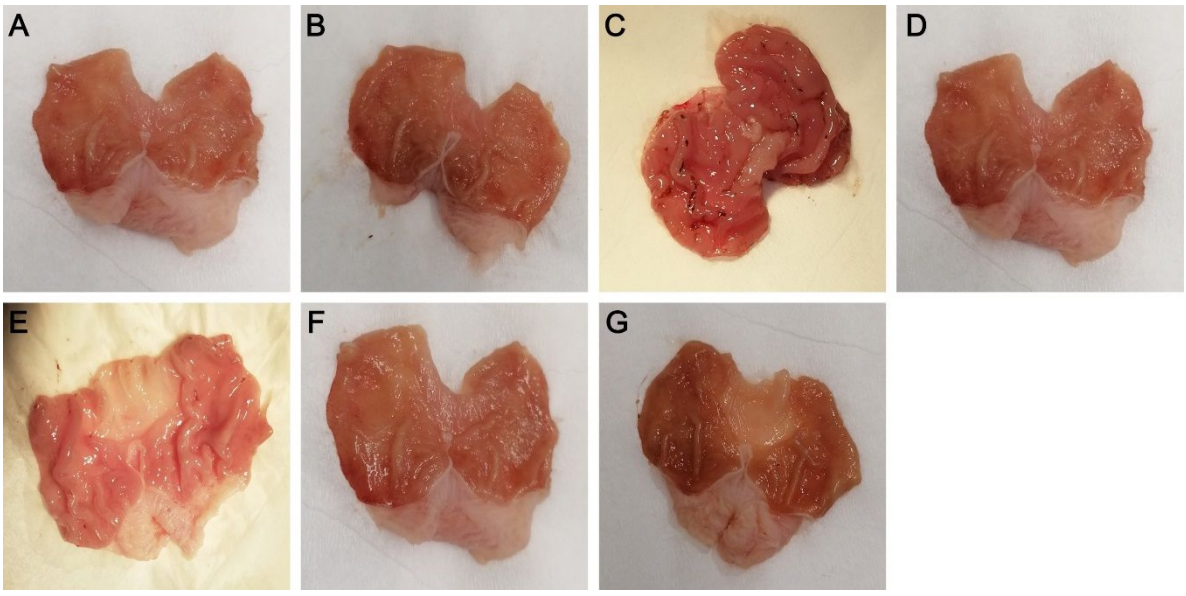

Rys. 20. Obraz makroskopowy błony śluzowej żołądków wskazuje, że badane związki nie powodują istotnych zmian w jej obrębie. Indometacyna została użyta jako lek odniesienia. Grupy badane: grupa kontrolna (**A**); grupa karageninowa (**B**); grupa otrzymująca 10mg/kg indometacyny (**C**); grupa otrzymująca 10mg/kg związku **10b** (**D**); grupa otrzymująca 20mg/kg związku **10b** (**E**); grupa otrzymująca 10mg/kg związku **13b** (**F**); grupa otrzymująca 20mg/kg związku **13b** (**G**).

tłumaczenie na język polski na potrzeby rozprawy wykonano na podstawie publikacji źródłowej [61]

W trakcie przeprowadzonego badania nie zaobserwowano uszkodzeń śluzówki żołądka w grupie kontrolnej oraz karageninowej (**Rys**. **20A**, **20B**). W przypadku żołądków pobranych od zwierząt, którym podano związki **10b(P1)** i **13b(P1)** również nie stwierdzono istotnych, w porównaniu z kontrolą, zmian patologicznych w obrębie błony śluzowej (**Rys**. **20D-G**). Z kolei w grupie otrzymującej indometacynę wystąpiły znaczne urazy śluzówki żołądka. Miały one zróżnicowany stopień nasilenia, od przekrwień po zmiany krwotoczne pokryte zakrzepłą krwią (**Rys**. **20C**).

Zaobserwowane zmiany makroskopowe zostały potwierdzone badaniami mikroskopowymi. W przypadku grupy kontrolnej i karageninowej oraz grup otrzymujących badane pochodne **10b(P1)** oraz **13b(P1)** nie odnotowano żadnych istotnych zmian w tkance śluzówki żołądka w obrazie mikroskopowym. Natomiast w przypadku grupy karageninowej stwierdzono uszkodzenie warstwy ochronnej błony śluzowej z jej miejscowym ścieńczeniem. Ponadto, zaobserwowano ubytki kraterowe, lokalne ogniska martwicze oraz obrzęk i przekrwienie podśluzówkowe.

Podsumowując wyniki, które uzyskane zostały podczas testu karageninowego możemy z pełnym przekonaniem powiedzieć, że nowe pochodne pirolo[3,4-*d*]pirydazynonu **10b(P1)** oraz **13b(P1)** wykazują aktywność przeciwzapalną, a ich mechanizm działania może polegać na obniżaniu stężenia takich mediatorów jak PGE_2, MPO czy TNF-α oraz na redukcji nacieku tkanki objętej zapaleniem. Co prawda, ich aktywność była nieco niższa niż indometacyny, jednakże w przeciwieństwie do leku odniesienia, nie powodowały one uszkodzeń błony śluzowej żołądka, co jest ich niewątpliwą zaletą.

Na podstawie przeprowadzonych badań *in vivo* możemy więc z pełnym przekonaniem stwierdzić, że 1,3,4-oksadiazolowe pochodne pirolo[3,4-*d*]pirydazynonu wykazują dobry stosunek korzyści do ryzyka. Tym samym czyni je to atrakcyjnymi i obiecującymi strukturami w kontekście dalszych badań i rozwoju oraz potencjalnego zastosowania w terapii różnych schorzeń zapalnych.

4.2 Pochodne 1,2,4-triazolowe pirolo[3,4-*d*]pirydazynonu

4.2.1 Projekt oraz synteza

Biorąc pod uwagę obiecujący profil aktywności przeciwzapalnej 1,3,4-oksadiazolowych pochodnych pirolo[3,4-*d*]pirydazynonu oraz ich niską gastrotoksyczność potwierdzoną w badaniach *in vivo*, zdecydowano się podjąć próbę dalszych modyfikacji oraz optymalizacji struktury związków opisanych w publikacjach **P1**-**P2**.

Wnikliwie analizując rezultaty dotychczas przeprowadzonych eksperymentów, oraz inspirując się doniesieniami piśmiennictwa naukowego, zdecydowano się na otrzymanie nowej serii pochodnych, w których strukturze występowałby *N*-podstawiony heterocykliczny pierścień 1,2,4-triazolu. Taka modyfikacja była podyktowana dwiema ważnymi przesłankami.

Po pierwsze, pierścień 1,2,4-triazolu może być rozpatrywany, z uwagi na zmniejszony charakter kwasowy, ale jednocześnie podobną wielkość cząsteczki, jako bioizoster wolnej grupy karboksylowej. Dlatego też, układ 1,2,4-triazolu stanowi istotny element strukturalny wielu związków szeroko opisanych w literaturze, wykazujących znaczną aktywność przeciwzapalną i przeciwbólową, przy jednocześnie niskiej gastrotoksyczności [21,22,29,30].

Po drugie, uwzględniając fakt, że kieszeń wiążąca izoenzymu COX-2 jest większa niż COX-1[7–10], oczekiwano, że synteza związków o bardziej rozbudowanej strukturze, z dodatkowym podstawnikiem w pozycji 4 pierścienia 1,2,4-triazolu, pozwoli istotnie poprawić ich współczynnik selektywności COX-2/COX-1.

Kierując się uzyskanymi dotąd wynikami, a w szczególności faktem, że w poprzedniej serii najbardziej aktywny okazał się związek **7b(P1)**, zdecydowano się skupić na syntezie oraz badaniach biologicznych 6-*n*-butylowych pochodnych pirolo[3,4-*d*]pirydazynonu.

Na **Rysunku 21** przedstawiono wzory ogólne dwóch serii nowych *N*-podstawionych 1,2,4-triazolowych pochodnych pirolo[3,4-*d*]pirydazynonu. Związki należące do pierwszej z zaplanowanych serii miały budowę zasad Mannicha (**I**). Z kolei drugą serię stanowiły pochodne, zaprojektowane w myśl wspomnianej już wcześniej teorii farmakoforowej zaproponowanej przez Dogruera (**II**)[46,47].

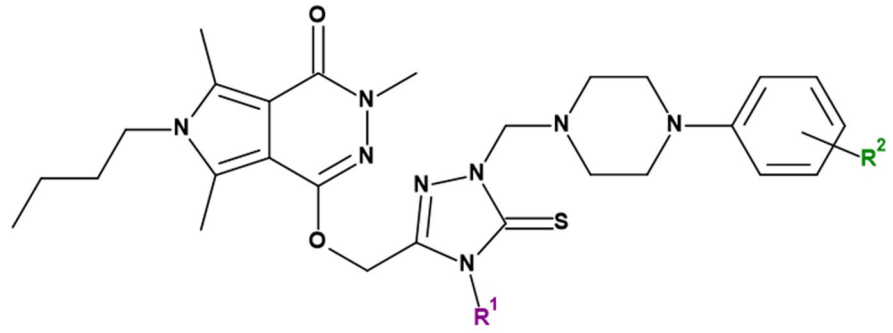

I

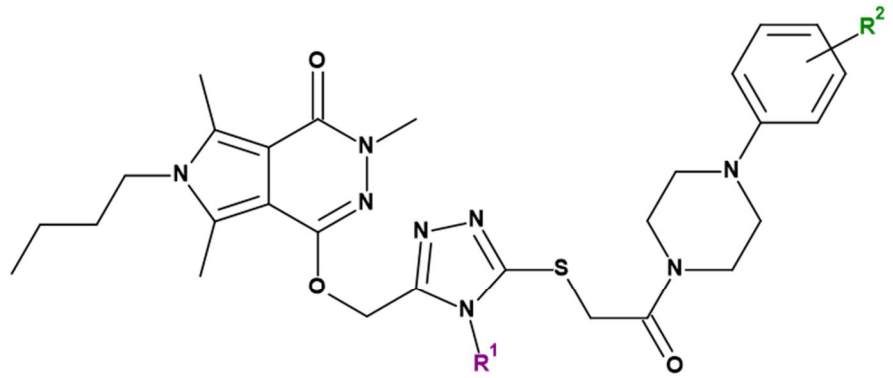

II

R^1 – CH_3, fenyl, 4-(metoksy)fenyl;

R^2 – H, CF_3, CH_3;

Rys. 21. Ogólny wzór serii **I** oraz **II** 1,2,4-triazolowych pochodnych pirolo[3,4-*d*]pirydazynonu.

Tym samym, zaprojektowano cząsteczki, które można rozpatrywać jako analogi strukturalne pochodnych 1,3,4-oksadiazolowych będących przedmiotem publikacji **P1** i **P2**. Punktem wyjścia podczas syntezy tej grupy związków był opisany w publikacji **P1** hydrazyd kwasu 2-(6-butylo-3,5,7-trimetylo-4-okso-pirolo[3,4-*d*]pirydazyn-1-yloksy)octowego **5b(P1)**. Kondensacja hydrazydu z odpowiednimi *N*-podstawionymi izotiocyjanianami pozwoliła uzyskać pochodne o budowie tiosemikarbazydu, które następnie poddawane były wewnątrzcząsteczkowej cyklizacji, w środowisku zasadowym, z utworzeniem pierścienia 1,2,4-triazolu. Ostatni etap syntezy zakładał uzyskanie grupy finalnych związków o budowie, którą przedstawiono schematycznie na **Rysunku 21**.

Pierwsza seria zaplanowanych cząsteczek miała budowę zasad Mannicha i została otrzymana w wyniku kondensacji triazolowych analogów **3a-c(P3)** z właściwymi pochodnymi arylopiperazyny, w obecności formaldehydu (**Rys**. **21 I**). Z kolei serię drugą otrzymano poprzez alkilowanie, w środowisku etanolanu sodu, związków **3a-c(P3)** odpowiednią, zsyntetyzowaną wcześniej, 1-(2-chloro-1-okso)-etylową pochodną arylopiperazyny (**Rys**. **21 II**).

W wyniku przeprowadzonych prac syntetycznych otrzymano w sumie 24 nowe, niepublikowane dotąd związki, w tym 18 pochodnych finalnych (**Rys. 21 I, II**). Struktura wszystkich nieopisanych dotąd cząsteczek została potwierdzona technikami spektralnymi. Nowe związki, po odpowiednim oczyszczeniu, zostały przekazane na badania biologiczne.

Koncepcja budowy, przeprowadzone modyfikacje strukturalne oraz sposób otrzymania nowych 1,2,4-triazolowych pochodnych pirolo[3,4-*d*]pirydazynonu zostały szczegółowo przedstawione oraz opisane na *Schemacie 1* oraz w *Rozdziałach 1*, *2.1* publikacji **P3**. Natomiast w części eksperymentalnej tejże pracy oraz w suplemencie zamieszczono dane analityczne, właściwości fizykochemiczne oraz widma (NMR, MS, IR) wszystkich nowych związków.

4.2.2 Badania *in vitro* oraz *in silico*

Wstępne badania, których celem była ocena toksyczności oraz aktywności biologicznej *N*-podstawionych 1,2,4-triazolowych pochodnych pirolo[3,4-*d*]pirydazynonu zostały przeprowadzone we współpracy z jednostkami Uniwersytetu Medycznego we Wrocławiu. W Katedrze i Zakładzie Farmakologii testy enzymatyczne oraz wszelkie eksperymenty *in vitro* wykonał zespół Pani dr inż. Benity Wiatrak. W Katedrze i Zakładzie Chemii Nieorganicznej badania spektralne oraz dokowania molekularnego wykonali Pan dr Edward Krzyżak, Pani dr inż. Aleksandra Marciniak oraz Pani dr Aleksandra Kotynia.

Pierwszy etap badań biologicznych polegał na ocenie cytotoksyczności nowych związków. Tak jak poprzednio wykonano test MTT na liniach komórkowych NHDF. Zgodnie ze standardową procedurą, za nietoksyczne uznano te pochodne, które po 24-godzinnej inkubacji nie zmniejszały przeżywalności komórek o więcej niż 30%. Ten warunek został spełniony dla 9 zbadanych pochodnych: **4a-c(P3)**, **7a-c(P3)** a także **5a(P3)**, **6a(P3)** oraz **9a(P3)**. Natomiast w przypadku 5 związków: **8a-c(P3)**, **9b-c(P3)** zaobserwowano obkurczone komórki, liczne ziarnistości i lizę na poziomie powyżej 50%. W związku z powyższym zostały one wykluczone z dalszych badań. Obserwując komórki, które były inkubowane z pochodnymi **5b(P3)**, **5c(P3)**, **6b(P3)** oraz **6c(P3)**, zauważono w ich obrazie mikroskopowym pojedyncze ziarnistości, ale przy zachowanym, wydłużonym kształcie charakterystycznym dla

fibroblastów. Dla tych pochodnych obliczone wartości IC_{50} nie były mniejsze niż graniczna wartość 100µM (*Tabela 1*, publikacja **P3**). Z tego względu podjęto decyzję o zakwalifikowaniu także tych związków to dalszego etapu badań. Podsumowując więc – na podstawie testu MTT za cytotoksyczne uznano 5 związków, pozostałych 13 zostało przekazanych na eksperymenty oceniające aktywność biologiczną. Analiza cytotoksyczności 1,2,4-triazolowych pochodnych pirolo[3,4-*d*]pirydazynonu została szczegółowo przedstawiona w *Rozdziale 2.2* publikacji **P3**.

Zdolność nowych związków do hamowania obu izoform cyklooksygenazy została wyznaczona z wykorzystaniem komercyjnego testu Cayman's COX Colorimetric Inhibitor Screening Assay (cat. no. 701050). Aby precyzyjnie ocenić zdolność blokowania cyklooksygenazy przez nowe pochodne, jako leków odniesienia użyto, oprócz meloksykamu, także diklofenaku sodowego oraz celekoksybu. Dokładny opis badań oraz uzyskane rezultaty są zamieszczone w *Rozdziale 2.3.1* publikacji **P3**.

Spośród 13 analizowanych związków, cztery blokowały preferencyjnie COX-2, a kolejne 4 okazały się selektywne w stosunku do tej indukowanej izoformy. Natomiast w przypadku 5-ciu z nich w ogóle nie odnotowano zdolności do hamowania cyklooksygenazy. Warto zauważyć, że wśród wszystkich 8 związków, które działały na COX-2 wyznaczone wartości IC_{50} były niższe niż te, oznaczone dla meloksykamu. Co więcej, współczynnik hamowania COX-2/COX-1 pochodnych preferencyjnie blokujących COX-2 był korzystniejszy niż ten wyliczony dla meloksykamu. Porównując aktywność nowych struktur do celekoksybu należy jednak stwierdzić, że lek ten przewyższa badane cząsteczki zarówno pod względem selektywności jak i siły hamowania COX-2 (*Tabela 2*, publikacja **P3**). Warto też zauważyć, że powinowactwo do cyklooksygenazy wykazały przede wszystkim te pochodne, w których pierścień 1,2,4-triazolu był podstawiony małym podstawnikiem metylowym. Natomiast najmniej efektywne okazały się związki z ugrupowaniem 4-metoksyfenylowym.

Powinowactwo nowych związków do cyklooksygenazy oceniono również wykorzystując technikę dokowania molekularnego. Uzyskane wyniki korelują w znacznym, ale nie w pełnym stopniu z rezultatami testu *in vitro*. Podczas prób dokowania 1,2,4-triazolowych pochodnych do COX-1 uzyskano dodatnie wartości wolnej energii wiązania (ΔG°). Powinowactwem do COX-2 cechowało się 8 spośród badanych struktur, przy czym podobnie jak w teście *in vitro* najlepsze wyniki uzyskano w przypadku związków z małym podstawnikiem metylowym w pierścieniu 1,2,4,-triazolu. Ponownie, 5 związków (te same, co w teście enzymatycznym) nie wykazało powinowactwa w stosunku do żadnej z form cyklooksygenazy. Sposób interakcji z COX-2

najbardziej efektywnych pochodnych pokazano na **Rysunku 22**.Szczegółowy opis dokowania molekularnego do COX znajduje się w *Rozdziale 2.3.2* publikacji **P3**.

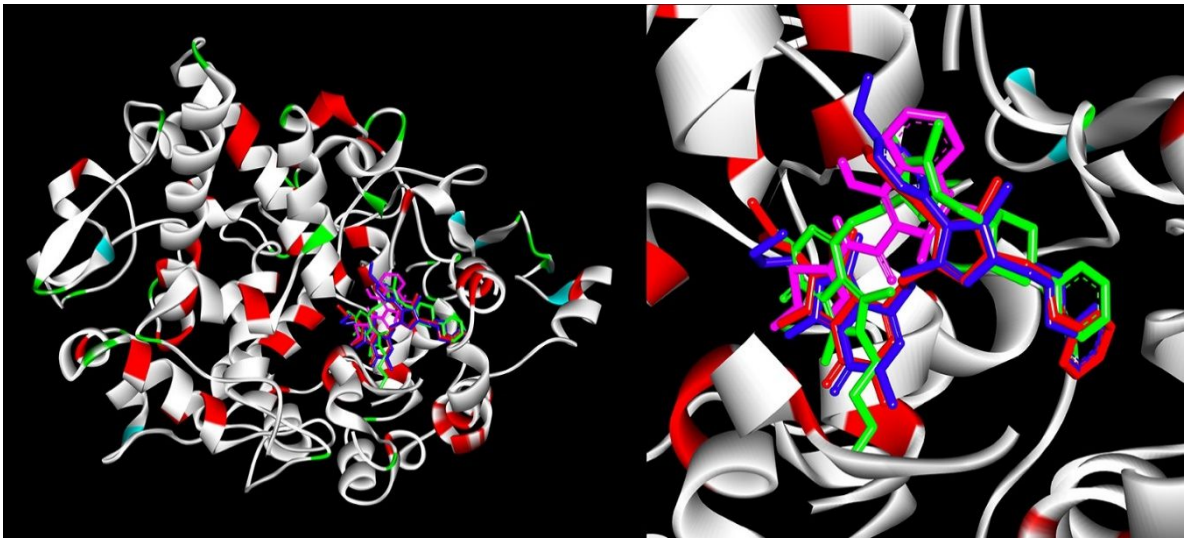

Rys. 22. Położenie związków **4a(P3)** (zielony), **4b(P3)** (czerwony), **4c(P3)** (niebieski) oraz meloksykamu (różowy) w kieszeni COX-2.

Aktywność przeciwzapalna tytułowych pochodnych została też oceniona w zmodyfikowanym eksperymencie MTT na linii komórkowej NHDF, w modelu zapalenia wywołanym przez dodanie lipopolisacharydu (*lipopolysaccharide*, LPS). Komórki były najpierw inkubowane 24h z dodatkiem LPS, który jest znanym czynnikiem prozapalnym[1,4], a następnie przez kolejną dobę z testowanymi związkami w różnych stężeniach. Na podstawie uzyskanych wyników możemy stwierdzić, że wszystkie pochodne (oprócz **5c(P3)** i **6c(P3)** w stężeniach 50 i 100μM) zwiększały przeżywalność komórek w stosunku do kontroli pozytywnej, co sugeruje ich potencjalnie dobrą aktywność przeciwzapalną. Dodatkowo, dla związków **6a(P3)** oraz **9a(P3)** zaobserwowano statystycznie istotny wzrost aktywności mitochondrialnej w odniesieniu do kontroli negatywnej.

Kolejnymi przeprowadzonymi eksperymentami *in vitro* były testy DCF-DA oraz Griess'a. Wszystkie pochodne, w całym zakresie badanych stężeń obniżały poziom wolnych rodników tlenowych w porównaniu z kontrolą pozytywną. Co więcej, w przypadku związków **6a(P3)** oraz **9a(P3)** zaobserwowano spadek stężenia reaktywnych form tlenu do poziomu kontroli negatywnej. Również w teście Griess'a odnotowano istotne statystycznie zmniejszenie ilości NO dla każdego związku w całym zakresie testowanych stężeń. Najlepszą aktywność w tym teście wykazała pochodna **9a(P3) –** w jej przypadku po okresie inkubacji stężenie NO było na poziomie zbliżonym do kontroli negatywnej.

Dokładne omówienie eksperymentów *in vitro* oceniających aktywność przeciwzapalną oraz antyoksydacyjną nowych pochodnych wraz z niezbędnymi tabelami zostało zamieszczone w *Rozdziale 2.4* publikacji **P3**.

Uzupełnieniem opisanych powyżej testów enzymatycznych i komórkowych były badania, które pozwoliły oszacować właściwości farmakokinetyczne tytułowych związków. Wykorzystując metody spektroskopowe tj. wygaszanie fluorescencji, CD, FTIR oraz technikę dokowania molekularnego podjęto próbę opisania modelu interakcji 1,2,4-triazolowych pochodnych pirolo[3,4-*d*]pirydazynonu z osoczową albuminą. Na podstawie pomiarów zarówno CD jak i FTIR stwierdzono, że w obecności badanych związków zachodzą zmiany w drugorzędowej strukturze BSA, co świadczy o interakcji białka z ligandem. Wnioski te są spójne z wynikami spektroskopii fluorescencyjnej, na podstawie których można powiedzieć, że interakcja nowych pochodnych z BSA polega na tworzeniu kompleksów w przybliżonym stosunku 1:1. Według danych uzyskanych podczas dokowania molekularnego miejscem wiązania 1,2,4-triazolowych pochodnych pirolo[3,4-*d*]pirydazynonu jest subdomena IIIA w hydrofobowej kieszeni domeny II(m) osoczowej albuminy. Dokładne omówienie tych wyników wraz z niezbędnymi tabelami, wzorami i widmami spektroskopowymi znajduje się *Rozdziale 2.6* publikacji **P3** oraz w danych uzupełniających tej pracy.

Dodatkowo, wykonano podstawowe badania *in silico* dzięki użyciu programów dostępnych *on-line*. Korzystając z tego typu narzędzi możliwe było wyznaczenie dla badanych związków takich parametrów fizykochemicznych jak np. topologiczne pole powierzchni polarnej (*topological polar surface area*, TPSA), LOG *P* i inne. Te dane były niezbędne przy szacunkowej ocenie potencjalnych parametrów farmakokinetycznych w oparciu o różne modele obliczeniowe jak np. reguła pięciu Lipińskiego. Szczegóły zamieszczono w *Rozdziale 2.7* publikacji **P3**.

Biorąc pod uwagę interesujące oraz dosyć zróżnicowane wyniki badań uzyskane w obrębie stosunkowo licznego grona związków, możliwe było, po wnikliwej analizie rezultatów, przedstawienie pewnych zależności struktura-aktywność (*structure-activity relationships*, SAR) w grupie 1,2,4-triazolowych pochodnych pirolo[3,4-*d*]pirydazynonu. Zależności te zostały precyzyjnie omówione w *Rozdziale 2.5* publikacji **P3**, natomiast na **Rysunku 23** przedstawiono schematycznie najistotniejsze wnioski.

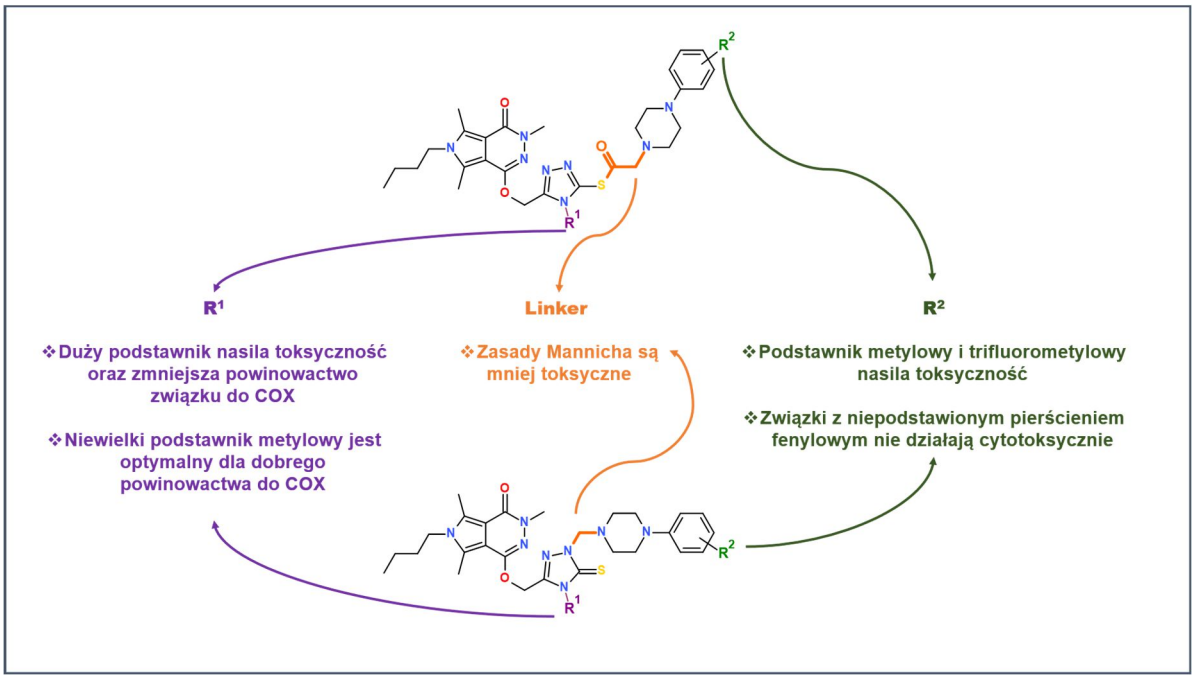

Rys. 23. Schematyczny opis zależności struktura-aktywność w grupie *N*-podstawionych 1,2,4-triazolowych pochodnych pirolo[3,4-*d*]pirydazynonu.

5 PODSUMOWANIE I WNIOSKI

W ramach zrealizowanych badań, będących przedmiotem niniejszej rozprawy, otrzymano w sumie 48 nowych, nieopisanych dotąd pochodnych pirolo[3,4-*d*]pirydazynonu. Struktura każdego związku została opisana i potwierdzona w oparciu o zaawansowane techniki spektralne.

Prace syntetyczne składały się z kilku etapów. Pierwszy z nich polegał na otrzymaniu estrowych pochodnych macierzystych układów pirolo[3,4-*d*]pirydazynonu (**Rys. 5**). W kolejnym kroku uzyskane estry w reakcji z wodzianem hydrazyny dawały odpowiednie hydrazydy. Następnie, otrzymano cykliczne (1,3,4-oksadiazolowe i 1,2,4-triazolowe) pochodne wspomnianych hydrazydów. Tym samym, uzyskano 12 nowych pochodnych stanowiących półprodukty niezbędne do otrzymania tytułowych związków o spodziewanej aktywności przeciwbólowej i przeciwzapalnej oraz niskiej gastrotoksyczności (**Rys. 4**). W wyniku przeprowadzonych prac uzyskano trzy serie związków finalnych. Do serii **I** oraz **II** należą 1,3,4-oksadiazolowe pochodne pirolo[3,4-*d*]pirydazynonu, natomiast serię **III** stanowią ich 1,2,4-triazolowe analogi. W strukturze tych związków można ponadto wyróżnić ugrupowanie arylopiperazynylowe/piperydynylowe. Po dokonaniu odpowiedniego oczyszczenia oraz potwierdzeniu ich struktury, przeprowadzono badania biologiczne, spektralne oraz dokowania molekularnego celem oceny toksyczności oraz aktywności biologicznej tytułowych pochodnych.

Zgodnie z założoną koncepcją, udało się uzyskać związki w znakomitej większości nietoksyczne, które wykazały obiecującą aktywność przeciwbólową i przeciwzapalną. Wyniki przeprowadzonych badań potwierdziły, że wprowadzenie do struktury związku pierścienia 1,3,4-oksadiazolu lub 1,2,4-triazolu pozwala uzyskać cząsteczki o dobrym powinowactwie do cyklooksygenazy, zwłaszcza do jej indukowanej izoformy COX-2. Udowodniono, za pomocą eksperymentów enzymatycznych oraz dokowania molekularnego, że większość z otrzymanych pochodnych pirolo[3,4-*d*]pirydazynonu efektywnie hamuje cykloksygenazę w sposób preferencyjny lub selektywny w stosunku do COX-2. Co więcej, część z nich przewyższa swoją aktywnością meloksykam, który został użyty jako lek odniesienia.

Ponadto wykazano, że niektóre z otrzymanych pochodnych działają antyoksydacyjnie – zmniejszają stężenie wolnych rodników w indukowanym stresie oksydacyjnym oraz wywierają efekt protekcyjny na chromatynę. To natomiast, w sposób niejako pośredni, potwierdza ich potencjalnie dobrą aktywność przeciwzapalną.

Obiecująca aktywność biologiczna, jaką nowe związki wykazały w testach *in vitro* znalazła potwierdzenie w rezultatach badań przeprowadzonych w eksperymentalnych modelach *in vivo*, które zostały wykonane dla dwóch wybranych pochodnych. Siła ich działania analgetycznego i przeciwzapalnego, w wykonanych badaniach w modelu zwierzęcym, była porównywalna z indometacyną. Co istotne, dzięki zrealizowanym testom dowiedziono, że nowe pochodne pirolo[3,4-*d*]pirydazynonu zmniejszają stężenie mediatorów stanu zapalnego takich jak MPO, TNF-α, czy przede wszystkim PGE_2, co może potwierdzać, że ich mechanizm działania związany jest z hamowaniem COX.

Warto podkreślić, że badane pochodne nie powodowały, charakterystycznych dla klasycznych NLPZ, uszkodzeń oraz zmian patologicznych w obrębie błony śluzowej żołądka. Zostało to potwierdzone analizą makro- oraz mikroskopową śluzówki żołądków zwierząt uczestniczących w badaniach. Te wyniki udowodniły słuszność przeprowadzonych modyfikacji polegających na wprowadzeniu do tytułowych cząsteczek pierścienia 1,3,4-oksadiazolu. Dowiedziono, że obecność w strukturze finalnych związków tego bioizosterycznego dla grupy karboksylowej ugrupowania skutkuje niemal całkowitym brakiem działań niepożądanych na przewód pokarmowy.

Biorąc pod uwagę wyniki wszystkich przeprowadzonych badań należy z pełnym przekonaniem stwierdzić, że wypełnione zostały cele i założenia jakie przyjęto podczas planowania i realizacji niniejszej pracy. Bez wątpienia udowodniono, że 1,3,4-oksadiazolowe oraz 1,2,4-triazolowe pochodne pirolo[3,4-*d*]pirydazynonu są interesującymi i obiecującymi związkami o korzystnym profilu farmakologicznym. Wykazują dobrą aktywność przeciwzapalną i przeciwbólową oraz, co bardzo istotne, nie działają gastrotoksycznie. Z tego względu, pochodne te mogą mieć istotne znaczenie w kontekście poszukiwań nowych związków, które mogłyby być z powodzeniem wykorzystywane w przyszłości w efektywnej, a przede wszystkim bezpiecznej terapii różnych schorzeń, u podłoża których leży ból i zapalenie.

THE SUMMARY

IN ENGLISH

1 INTRODUCTION

The inflammatory response is the process that leads to the body's homeostasis restoration. Inflammation can be triggered by a variety of exogenous and endogenous noxious stimuli such as injury, infection, disruption of tissue, or tissue malfunction. Its course and consequences depend on the trigger. The most common symptoms that occur in an inflamed area of the body are swelling, redness, hypersensitivity, and often pain, which plays an important warning and protective role. Pain stimulates the proper response and behaviour of the body to alleviate the aftermath of tissue damage[1–5].

Inflammation is a very complicated process controlled by many different mediators whose expression and complex web of relationships have not been fully understood yet. Numerous pro-inflammatory factors of different origins can be divided into the following seven groups: vasoactive amines, vasoactive peptides, fragments of the complement components, lipid mediators, e.g. eicosanoids, cytokines, chemokines, and proteolytic enzymes. These substances trigger an appropriate response at the cellular level and can also modulate each other's activity. Therefore, the best possible understanding of the mechanisms responsible for the expression of inflammatory mediators and their interrelationships is essential for the effective treatment of a variety of inflammatory diseases. Effective pharmacotherapy and natural repair processes taking place in the tissues allow eliminating acute inflammation in just a few days. On the other hand, the lack of an appropriate response of the body and suitable pharmacological treatment may lead to pathological changes, which will result in the development of chronic pain and inflammation[1–6].

The vast majority of pharmaceuticals currently used in the treatment of pain and inflammatory disorders belong to a large and structurally diverse group of the so-called Non-Steroidal Anti-Inflammatory Drugs (NSAIDs). Their mechanism of action was first described by Vane in 1971. It is based on the inhibition - mainly in a non-selective manner - of cyclic prostaglandin peroxide synthase, commonly known as cyclooxygenase (COX)[7–9]. It is a membrane-bound enzyme that catalyzes the conversion of arachidonic acid to bioactive lipids such as prostaglandins (PG) and thromboxane A_2 (TXA_2). These mediators are important for maintaining homeostasis, but also play a key role in transmitting signals directly related to the resulting inflammation and the accompanying pain[7–10].

Based on the structural and functional differences, three isoforms of the cyclooxygenase are distinguished. A constitutive variant of the enzyme called cyclooxygenase 1 (COX 1), is expressed in cells under physiological conditions and is responsible for the synthesis of prostaglandins involved in the proper functioning of the gastrointestinal tract and the cardiovascular system as well[9,10]. For example, prostaglandin I_2 (PGI_2), called prostacyclin, exhibits a cytoprotective effect in the gastric mucosa. PGI_2 increases the production of mucus and bicarbonate and improves blood flow. Prostacyclin produced within the vascular endothelium reduces platelet aggregation and has a vasodilating effect[7–10]. The activity of cyclooxygenase 2 (COX 2), which is mainly an inducible form, is negligible under physiological conditions. However, it increases in the case of e.g. inflammation or other pathological changes. Factors that stimulate the COX 2 synthesis are, for example, cytokines and mitogens. Therefore, we observe increased COX 2 expression in tissues affected by inflammation, infection, or the process of oncogenesis[10–14]. The third cyclooxygenase isoform, a variant of COX 1, is mainly associated with the central nervous system (CNS). This enzyme is present in both the brain and spinal cord and is a molecular target for centrally acting antinociceptive drugs[9,10].

Non-selective inhibition of both peripheral forms of cyclooxygenase leads not only to the relief of inflammation and pain, but may also result, especially during chronic therapy, in the occurrence of serious side effects that characterize NSAIDs[9,11,15–18]. The most important of them are gastroenterological problems such as heartburn and stomach pain, inflammation, erosions and, consequently, ulceration of the gastric and duodenal mucosa, and even gastrointestinal bleeding. This is caused not only by the reduced PGI_2 concentration but also by the chemical nature of most NSAIDs which have a free carboxyl group in their structure. As a consequence, these drugs are irritating directly to the gastric and duodenal mucosa. Moreover, the ion trap effect that occurs further intensifies its damage[15–18]. High hopes were associated with the admission of selective COX-2 inhibitors, i.e. coxibs, into the treatment. They are effective in the therapy of various inflammatory diseases, and their gastrotoxic effects are significantly lower than that of traditional NSAIDs[12,17,18]. However, patients taking coxibs also complain sometimes about gastrointestinal side effects. As it turns out, COX 2 is also involved to some extent in cytoprotective activity[12]. Moreover, the use of coxibs carries the risk of serious adverse effects on the cardiovascular system, which can even lead to the death of the patient due to various types of thromboembolic events. Therefore, some of these drugs have been withdrawn from the market, and the rofecoxib case is perhaps the most famous and shameful[13,14].

Dangerous side effects that accompany the therapy by both non-selective and selective non-steroidal anti-inflammatory drugs are a factor that strongly limits their chronic usage[13–15,18]. For this reason, it is still highly justified and necessary to search for new, effective, and safe substances with anti-inflammatory and analgesic properties.

When analyzing the leading trends in modern medical chemistry, it can be seen that new substances with potential application in the treatment of pain and various inflammatory disorders can be gained by the two following paths. The first one involves the modification of well-described and registered NSAIDs such as, for example, diclofenac[19], ibuprofen[20], celecoxib[21], or naproxen[22]. Optimization of the structure of known drugs may result in obtaining new derivatives with increased activity and lower toxicity compared to their precursors. On the other hand, the second path involves the design of a completely new class of molecules operating on a selected molecular target. In this way, it is possible to obtain a new group of compounds soothing inflammation by, for example, inhibiting the cyclooxygenase[23–30].

Based on the review of the literature on the topic of *de novo* designed and synthesized anti-inflammatory and analgesic agents, it can be noted that many publications describe research focused on a large and diverse group of pyridazinone derivatives[31–39]. It is worth emphasizing that such compounds with antinociceptive activity were firstly reported even more than sixty years ago. The only pyridazone analogue that has been approved in the market to date is emorfazone. Its structural formula is presented in **Figure 1**[40,41].

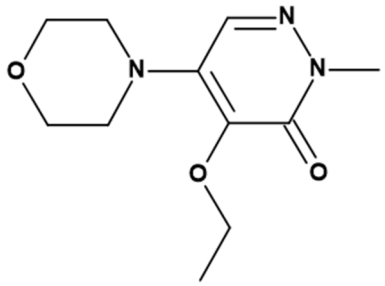

1

Fig. 1. Emorfazone (**1**) – an analgesic derivative of pyridazinone introduced in the market.

Over the years, a great variety of molecules based on diversely substituted pyridazinone ring with anti-inflammatory and analgesic activity have been described. Extensive investigations on this type of scaffold have proved, that the pyridazinone can serve as an excellent core for the synthesis of new, effective cyclooxygenase inhibitors, especially those with a high affinity to the

induced form to COX-2. Moreover, it has been reported as well, that an interesting profile of pharmacological activity is also shown by biheterocyclic derivatives, in which a pyridazinone ring is fused with, for example, pyrazole, isoxazole, or pyridine. **Figure 2** presents the structures of exemplary compounds with significant anti-inflammatory activity, which mainly relied upon their effective inhibition of COX-2 isoenzyme. Additionally, it should be emphasized that in the case of these compounds, no negative influence on the gastric and duodenal mucosa was observed in performed *in vivo* experiments[32,33,38–40].

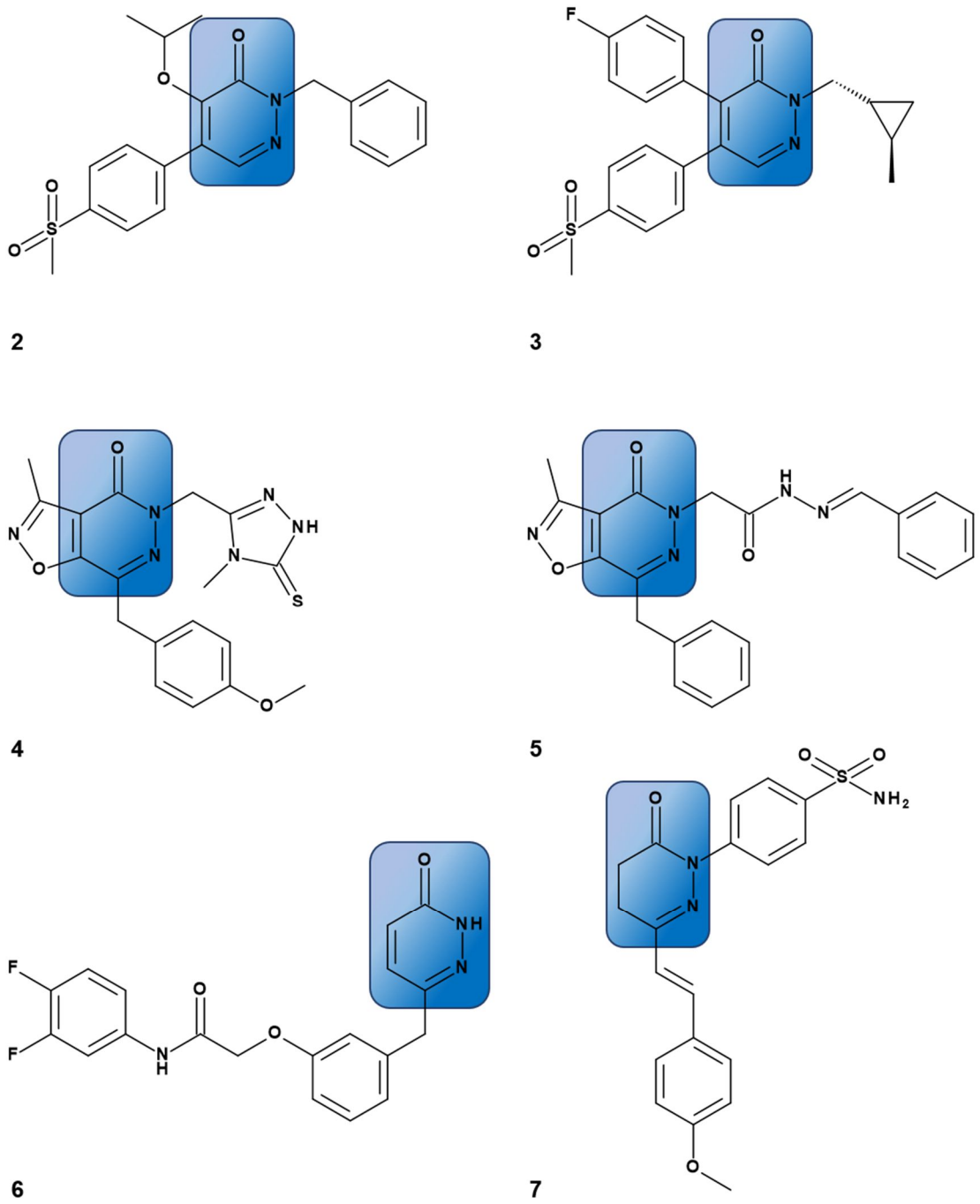

Fig. 2. The examples of COX inhibitors bearing the pyridazinone core in their structure[32,33,38–40].

At the Department of Medicinal Chemistry of the Medical University in Wrocław, intensive research consisting of the design and synthesis of new biologically active derivatives of various mono- and biheterocyclic systems, have been carried out for decades. Particularly noteworthy are investigations concerning the anti-inflammatory and analgesic derivatives of pyrrolo[3,4-*d*]pyridazine-1,4-dione[36,37]. The compounds received and examined so far exerted significant analgesic activity in *in vitro* and *in vivo* tests. **Figure 3** shows the formulas of the two most promising derivatives **8a** and **8b**, which in the "writhing" test showed activity significantly higher than acetylsalicylic acid, while in the "hot plate" test, they had an analgesic effect in doses only 3-5 times lower than morphine. Moreover, it was proved that the anti-inflammatory effect of these structures is based on peripheral activity. Nevertheless, the exact mechanism of their action has not been solved already[37].

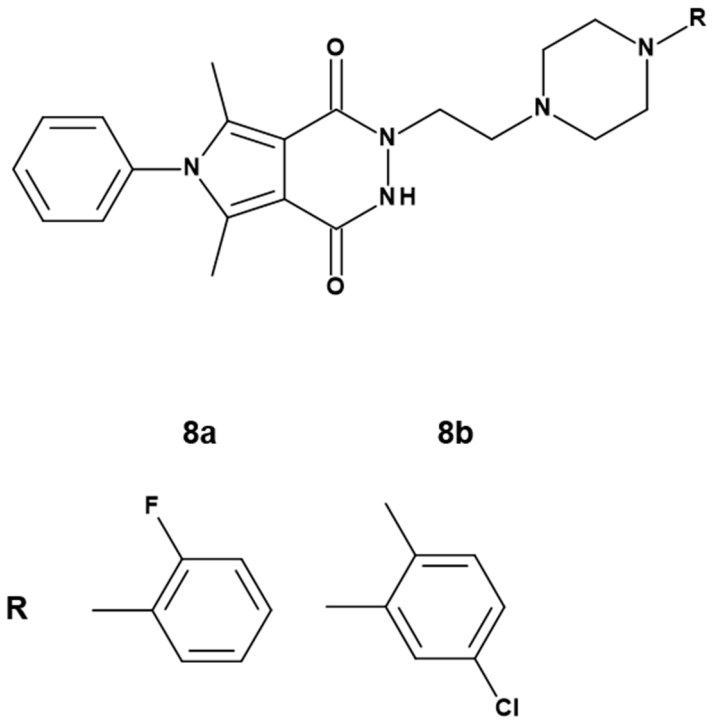

Fig. 3. The structures of the pharmacologically active derivatives of pyrrolo[3,4-*d*]pyridazine-1,4-dione.

Considering the literature reports describing potent anti-inflammatory pyridazinone derivatives alongside with the promising activity of the abovementioned compounds **8a** and **8b**, we can assume, that further search for new anti-inflammatory and analgesic drugs-candidates among the pyrrolo[3,4-*d*]-pyridazine1,4-dione analogues seems to be firmly justified. During the design of new series of compounds, we decided to introduce into the structure of pyrrolo[3,4-*d*]pyridazine-1,4-dione such groups and moieties that would allow us to receive

derivatives with good affinity to the induced form of COX and, at the same time, low toxicity and the lack of gastrointestinal adverse effects. In the structure of the title compounds, besides the pyrrolo[3,4-*d*]pyridazinone core, a 5-membered heterocyclic ring of 1,3,4-oxadiazole or 1,2,4-triazole, as well as the arylpiperazinyl/piperidinyl pharmacophore, characteristic for compounds **8a** and **8b**, could be distinguished. This type of design is consistent with the idea of molecular hybridization, which relies on the combination of various moieties and pharmacophore systems with proven activity, in order to obtain molecules characterized by higher efficiency and reduced side effects.

Literature data show that replacing the free carboxyl group of classic non-steroidal anti-inflammatory drugs with a bioisosteric group of similar size and lower acidity, such as a five-membered heterocyclic ring of 1,3,4-oxadiazole[19,20,23], 1,2,4-triazole[21,22,29,30], pyrazole[24,42], or 1,3-thiazole[43–45], allows reducing meaningly gastrotoxicity with simultaneous increase of the affinity to COX-2. Moreover, these five-membered heterocycles are an important structural element of many molecules with significant biological activity, including potent anti-inflammatory and analgesic ones[19–24]. Needless to say, they serve as the core of the previously described selective COX 2 inhibitors – coxibs[14,21,23].

Additionally, it should be taken into account, that in the structure of compounds **8a**, **8b** and their analogues, there was a characteristic arylpiperazinyl/piperidinyl residue, which had a significant effect on their increased biological activity. Therefore, the introduction of this type of moiety into the structure of the new pyrrolo[3,4-*d*]pyridazinone derivatives, which are the subject of this dissertation, seems to be highly justified and rational. During the synthesis of a series of new structures, commercially available arylpiperazine and arylpiperidine derivatives were used, which differed in the nature of the substituent on the phenyl ring and its position. It was aimed at the best possible evaluation of the influence of this moiety on the toxicity and pharmacological activity of the title compounds.

In summary, the overriding goal of the present experimental work was to create a new class of effective COX inhibitors, which would have a significant affinity to the inducible COX-2 isoenzyme and, at the same time, were safe and had no harmful impact on the digestive system. The idea and the concept of the structure of new 1,3,4 oxadiazole and 1,2,4 triazole derivatives of pyrrolo[3,4-*d*]pyridazinone is generally presented in **Figure 4**.

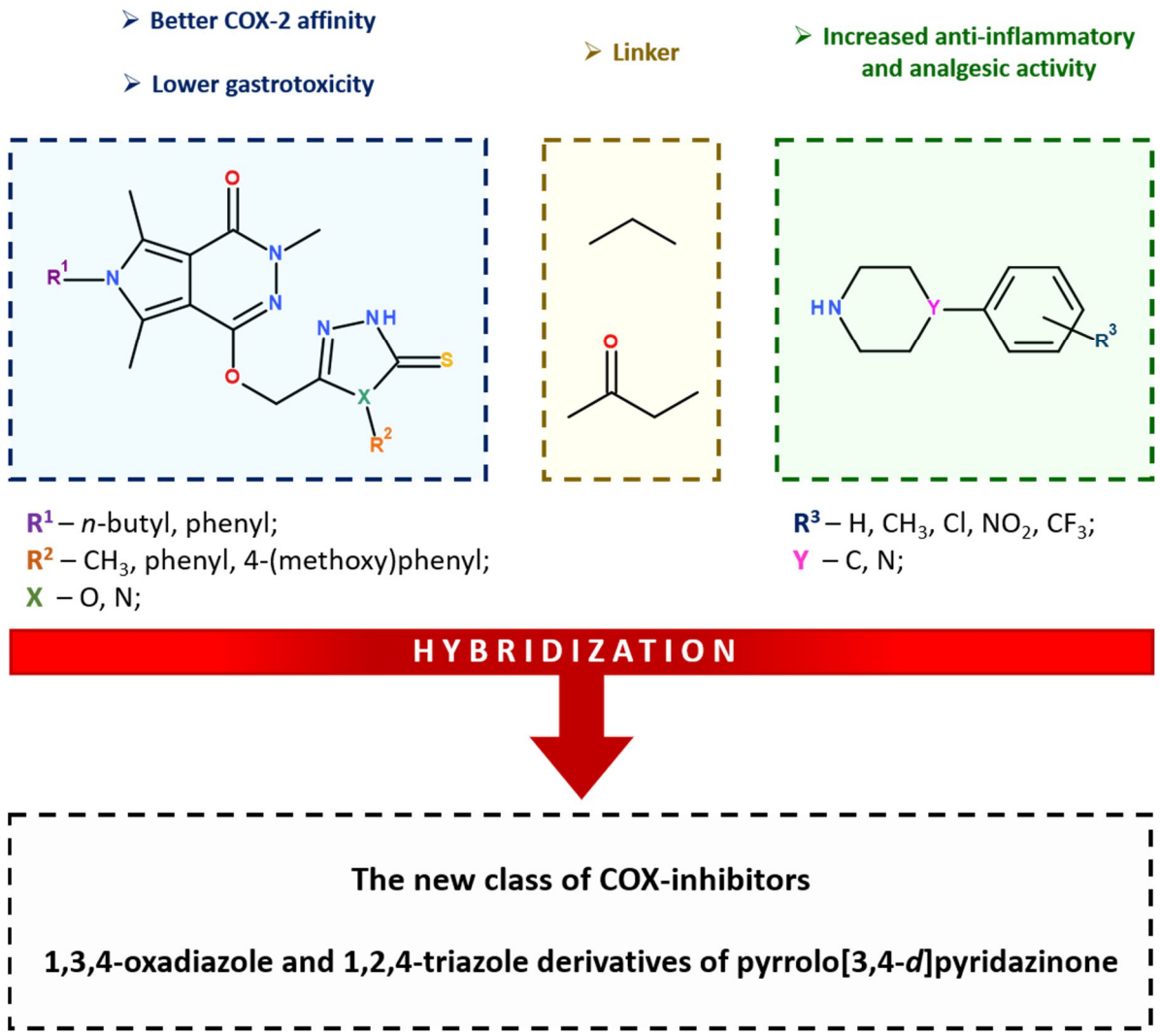

Fig. 4. The concept of the structure of new derivatives of pyrrolo[3,4-*d*]pyridazinone based on the idea of molecular hybridization.

The results of the research work carried out so far, presented later in this dissertation, allowed for a preliminary assessment of the potential of new compounds in the context of their possible use as safe and effective anti-inflammatory substances.

2 THE OBJECTIVES OF STUDY

2.1 The main objective

- The rational design and synthesis of new derivatives of pyrrolo[3,4-*d*]pyridazinone which signifacant anti-inflammatory and analgesic activity

2.2 The specific objectives

- Obtainment of a series of new 1,3,4-oxadiazole and 1,2,4-triazole derivatives of pyrrolo[3,4-*d*]pyridazinone which effectively inhibit cyclooxygenase and do not show gastrotoxicity
- Assessment of the inhibitory activity and affinity of new compounds to both peripheral cyclooxygenase isoforms (COX-1 and COX-2) by the use of enzymatic assays and molecular docking techniques
- Evaluation of the antioxidant activity of title compounds
- Determination of the model of binding of the obtained derivatives to plasma albumin
- Description of the structure-activity relationships (SAR) in the group of new pyrrolo[3,4-*d*]pyridazinone derivatives based on the obtained results of toxicity and biological activity
- The study of the anti-inflammatory and analgesic activity of new compounds and their effect on the gastrointestinal mucosa in tests performed in an animal model

3 MATERIALS AND METHODS

3.1 The synthesis of pyrrolo[3,4-*d*]pyridazinone derivatives

All of the chemicals, solvents and reagents used during chemical synthesis, purification and other experiments were delivered by commercially available suppliers (Alchem, Wrocław, Poland; Chemat, Gdańsk, Poland; Archem, Łany, Poland) and were used without further purification. Dry solvents, such as ethanol, methanol, xylene or diethyl ether were received according to the standard procedures.

The reaction progress was monitored using the thin-layer chromatography (TLC) technique on silica-gel-60-F_{254}-coated TLC plates (Fluka Chemie GmbH, Germany). They were developed in a glass chamber using such eluents as ethyl acetate or its mixtures with such solvents as methanol, chloroform or cyclohexane in a different ratio. TLC plates were observed in UV light at 254 or 366 nm.

The melting points of all of the new compounds were determined on the Electrothermal Mel-Temp 1101D apparatus (Cole-Parmer, Vernon Hills, IL, USA) using the open capillary method and were uncorrected. The column chromatography was performed using silica gel 60-F_{254} (Merck, Darmstadt, Germany). Elemental analyses for carbon, nitrogen and hydrogen were run on a Carlo Erba NA-1500 analyser, and obtained results were within ± 0.4% of the theoretical values calculated for corresponding formulas.

The ^{1}H NMR (300 MHz) and ^{13}C NMR (75 MHz) spectra were recorder on the Bruker 300 MHz NMR spectrometer (Bruker Analytische Messtechnik GmbH, Rheinstetten, Germany). The samples were dissolved in $CDCL_3$ or DMSO-d6, and tetramethylsilane (TMS) was used as an internal reference. Chemical shifts (δ) were reported in ppm. The infrared (IR) spectra were determined on the Nicolet iS50 FT-IR Spectrometer (Thermo Fisher Scientific, Waltham, MA, USA). The samples were applied as solids, and the frequencies were reported in cm^{-1}. Mass spectra (MS) were recorded using the Bruker Daltonics Compact ESI-Mass Spectrometer (Bruker Daltonik, GmbH, Bremen, Germany), operating in the positive ion mode. The analyzed compounds were dissolved in a methanol–chloroform mixture. All of the newly reported derivatives were determined to have purities of >95% by the above-mentioned methods unless stated otherwise

3.2 Evaluation of the toxicity, biological activity and pharmacokinetic parameters of the title compounds

Detailed descriptions of the procedures used during biological and spectral tests of new compounds, the methodology of the molecular docking and other *in silico* techniques used to assess the properties of the tested derivatives, as well as the descriptions of the statistical methods used, are included in the experimental part of the publication **P1**-**P3**.

4 RESULTS AND DISCUSSION

4.1 The 1,3,4-oxadiazole derivatives of pyrrolo[3,4-*d*]pyridazinone

4.1.1 The design and synthesis

According to the concept presented in **Fig. 4**, we have designed and synthesised a series of new pyrrolo[3,4-*d*]pyridazinone derivatives. In its structure, a five-membered ring of 1,3,4-oxadiazole-2-thione and an aryl piperazinyl/piperidinyl moiety could be distinguished. The title compounds were obtained in good yield using classical techniques of organic synthesis and commercially available reagents and solvents.

In **Figure 5** the structure of two substantial pyrrolo[3,4-*d*]pyridazinone derivatives, which became the starting point for the synthesis of final compounds, are presented. They are, as follows: 6-butyl-3,5-7-trimethyl-2*H*-pyrrolo[3,4-*d*]pyridazine-1,4-dione **9** and 6-phenyl-3,5-7-trimethyl-2*H*-pyrrolo[3,4-*d*]pyridazine-1,4-dione **10**[36].

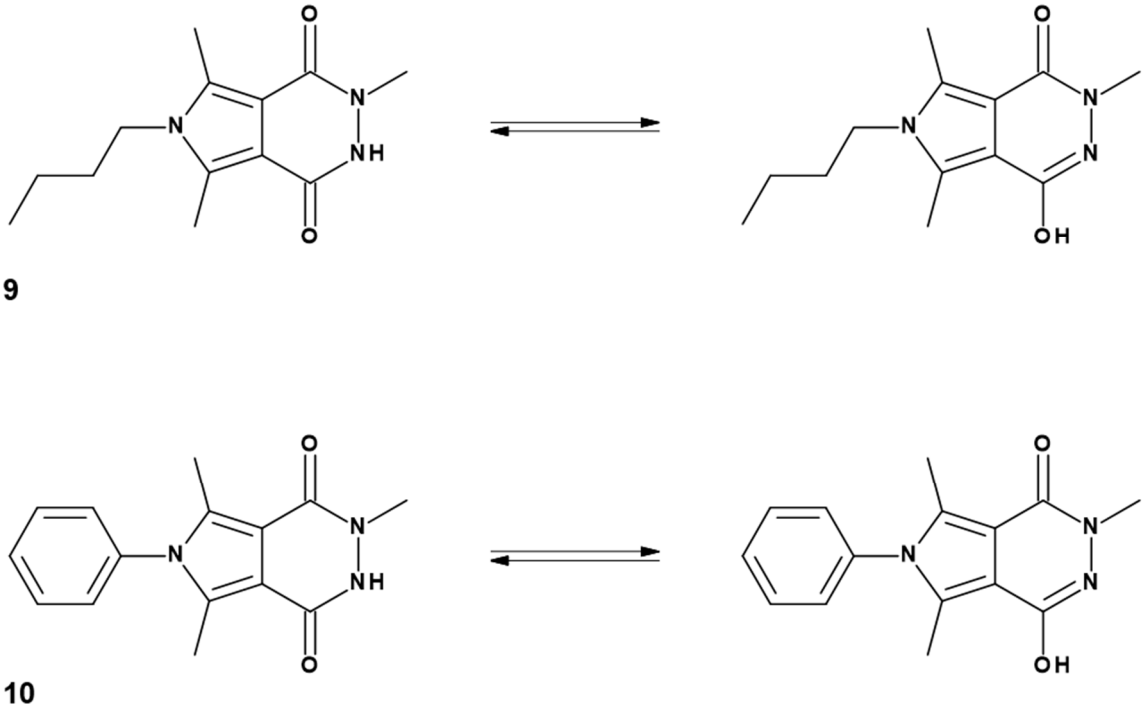

Fig 5. The structures of initial pyrrolo[3,4-*d*]pyridazine-1,4-dione derivatives.

The first stage of the intended synthesis consisted of the alkylation of derivatives **9** and **10** with methyl chloroacetate in acetonitrile in the presence of K_2CO_3. As a result, the corresponding ester derivatives were obtained. Because of the phenomenon of keto-enol tautomerism, both the nitrogen atom *N*3 and the oxygen atom of the hydroxyl group could be

substituted. Under the synthetic conditions used, the *O*-isomer was obtained predominantly. The separation of the obtained mixture of isomers was carried out on a chromatographic column. Due to the low yield in which the *N*-isomer was formed, we decided, that further structural modifications will be made only on the *O*-substituted derivatives.

Refluxing the appropriate ester in ethanol with the excess of hydrazine hydrate allowed the proper hydrazide to be received in excellent yield (~ 90%). Subsequently, an intramolecular cyclization in an alkaline environment in the presence of carbon disulfide has been performed. As a result, we have obtained the key 1,3,4-oxadiazole derivatives of pyrrolo[3,4-*d*]pyridazinone.

The last stage of the planned synthesis consisted in obtaining the Mannich bases. For this purpose, the corresponding 1,3,4-oxadiazole derivative was suspended in ethanol with the addition of a formalin. After some time, the appropriate secondary amine was added to the reaction mixture, and the mixture was stirred for several hours at room temperature. Finally, the title products have been received.

As a result of the multi-stage synthesis, 20 new compounds were obtained. Among them, the 14 were final Mannich bases. Their general formula is presented in **Figure 6**. Details of the synthesis performer at this stage are shown in *Schemes 1* and *2* and are described in *Chapter 2.1* of publication **P1**.

The structure of each obtained compound was confirmed by the use of advanced spectra techniques and the method of elemental analysis. Analytical data, physicochemical properties and spectra of the new structures are collected and described in the experimental part of the publication **P1** and at the supplementary data.

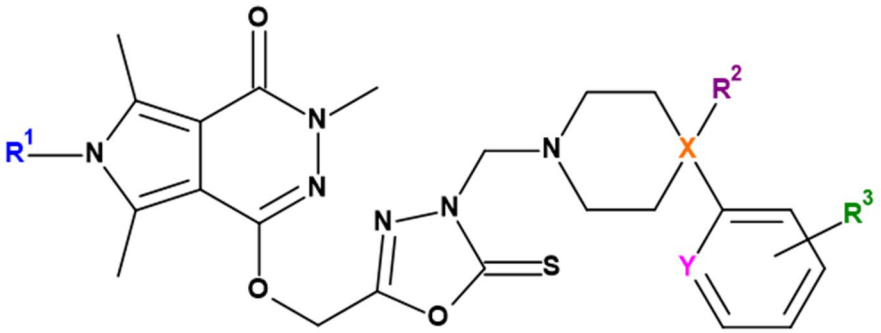

I

R^1 – *n*-butyl, phenyl;

R^2 – OH, —;

R^3 – H, CH_3, Cl, NO_2;

X – N, C, O;

Y – C, N;

Fig. 6. The general structure of pyrrolo[3,4-*d*]pyridazinone Mannich base type derivatives of series **I**.

In the next stage of intended synthetic work, we decided to obtain structures that refer to Dogruer's pharmacophoric theory. This idea assumes that the connection of an arylpiperazine derivative with the main scaffold *via* at least a two-carbon, flexible linker possessing a carbonyl residue can significantly enhance the antinociceptive effect of the final compounds[46,47]. **Figure 7** present a schematic structure of such a moiety.

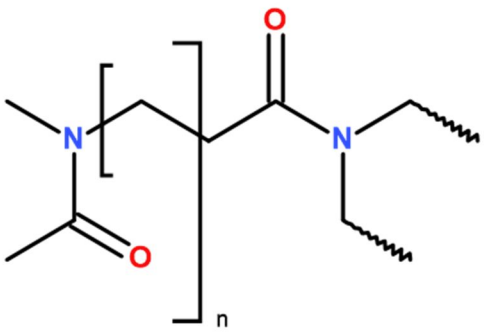

Fig. 7. The general structure of pharmacophore proposed by Dogruer.

Therefore, a group of four pyrrolo[3,4-*d*]pyridazinone derivatives were designed and obtained. In their structure, the arylpyrazinyl moiety linked to the sulfur atom of the

1,3,4-oxadiazole-2-thiol ring *via* a 2-oxoethyl linker can be distinguished. The general formula of this series of compounds is shown in **Figure 8**.

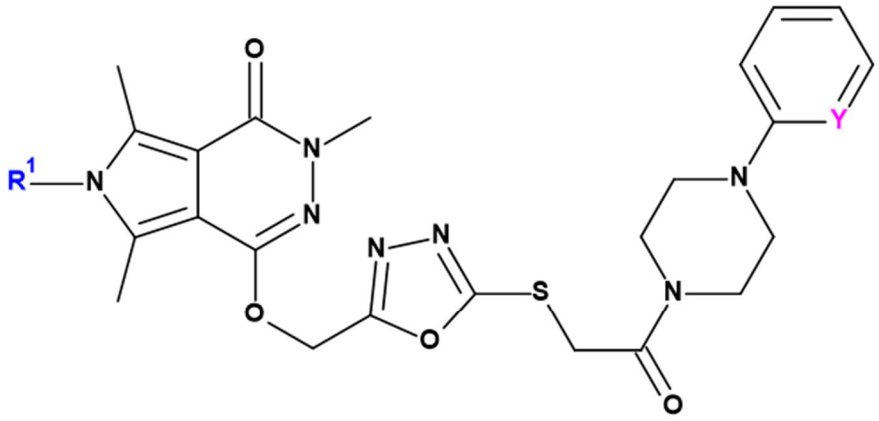

II

R^1 – *n*-butyl, phenyl; **Y – C, N;**

Fig. 8. The general structure of pyrrolo[3,4-*d*]pyridazinone derivatives with a 2-oxoethyl linker of series **II**.

The concept and synthesis of *S*-substituted 1,3,4-oxadiazole derivatives of pyrrolo[3,4-*d*]pyridazinone (series **II**) are detailed in *Scheme 1* and *Chapters 1* and *2.1* in the publication **P2**. Moreover, the chemical and experimental part of this manuscript and the supplementary data contain comprehensive information on the physicochemical properties and NMR, MS and IR spectra of all new structures.

4.1.2 *In vitro* and *in silico* investigations

The evaluation of the toxicity and biological activity of the title 1,3,4-oxadiazole derivatives of pyrrolo[3,4-*d*]pyridazinone were carried out by dr inż. Benita Wiatrak (Department Basic Medical Sciences; Department of Pharmacology, Wrocław Medical University). Molecular docking and spectral studies were performed by dr Edward Krzyżak and dr inż Aleksandra Marciniak from the Department of Inorganic Chemistry, Wrocław Medical University.

The evaluation of toxicity of compounds of series **I** was performed with the sulforhodamine B test (SRB) on the normal human dermal fibroblasts (NHDF) cell line. None of the examined compounds was cytotoxic. (*Table 1*, **P1**). Therefore, all 14 derivatives were qualified for further research.

The main aim of the conducted study was to determine the ability of obtained derivatives to inhibit cyclooxygenase. Moreover, their manner of binding with the active centre of the enzyme was determined. Therefore, in the first stage of biological research, we used the commercially available Cayman's COX Colorimetric Inhibitor Screening Assay (cat.no. cat. no. 701050) in which the concentration of N, N, N′, N′-tetramethyl-p-phenylenediamine (TMPD) which is the substrate of the enzyme, is measured. The results gained in this assay are presented in *Chapter 2.2.1* and *Table 1* of publication **P1**.

All tested compounds showed satisfactory ability to inhibit the COX-2 isoenzyme. Most of them had a preferential effect on COX-2, while 5 of them acted as selective blockers of the induced form of cyclooxygenase (COX-2). A drug with a proven anti-inflammatory effect, low gastrotoxicity and high affinity for COX-2, that is meloxicam, was used as a reference. It is worth emphasizing that all analyzed pyrrolo[3,4-*d*]pyridazinone derivatives of series **I** inhibited COX-2 stronger than the reference drug. Moreover, the COX 2 / COX 1 selectivity ratio calculated for each of the examined compounds was better than that of the reference drug (*Table 1*, **P1**).

These results are supported by the molecular docking studies, which revealed that the examined compounds show a greater affinity for COX-2 rather than for COX-1. It can be explained by the fact that the active site of the induced form of COX, due to its structure, allows the binding of larger and more complex molecules[7–10]. It has been proved that the tested compounds bind mainly to the B subdomain (which is the binding site of meloxicam and piroxicam) and the C active site of the enzyme. Moreover, the new pyrrolo[3,4-*d*]pyridazinone derivatives occupy a position analogous to that of meloxicam in the cyclooxygenase binding pocket. **Figure 9** shows how the two most active compounds **8a (P1)**, **8b (P1)** and meloxicam dock to COX-2. A detailed description of the results of molecular docking is provided in *Chapter 2.2.2*, *Table 2* of the publication **P1** and in the supplementary data.

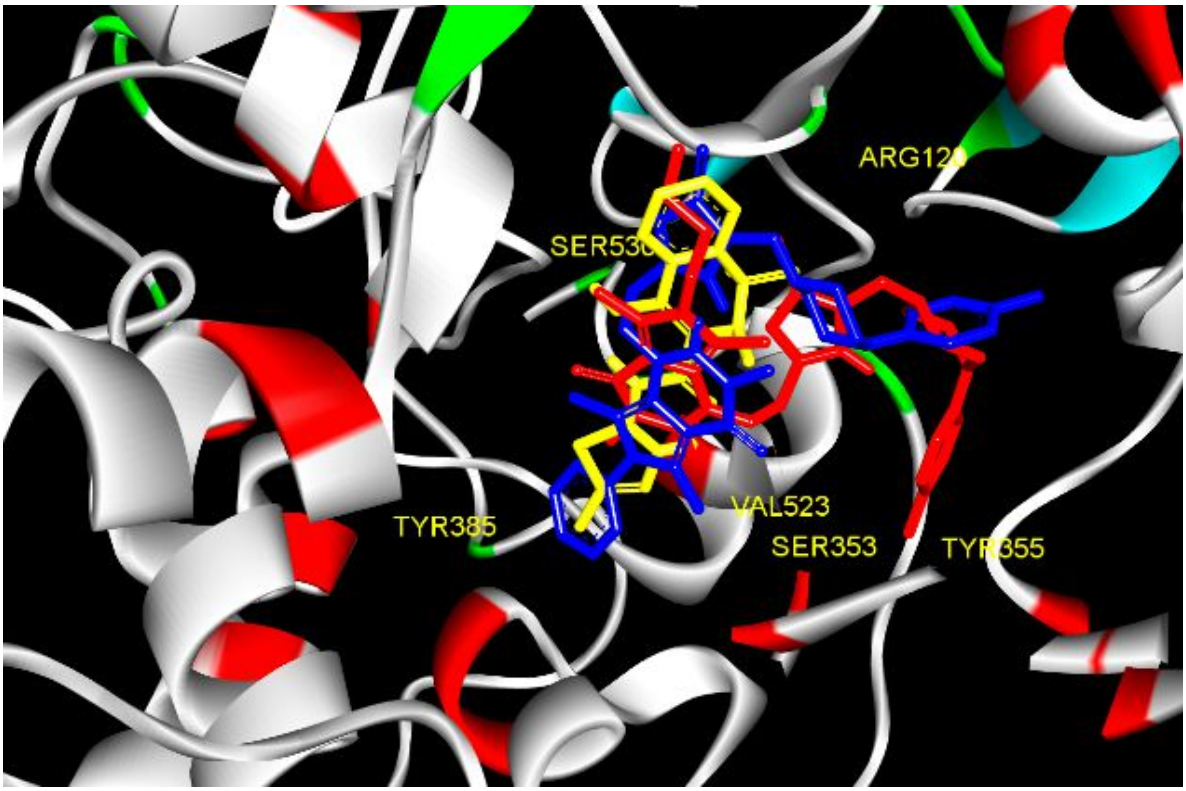

Fig. 9. The docking poses of **8a(P1)** (blue), **8b(P1)** (red) and meloxicam (yellow) in the active site of COX-2.

The next stage of the planned tests assumed the evaluation of the antioxidant potential of new compounds. It should be borne in mind that the increase in the concentration of reactive oxygen species (ROS) or reactive nitrogen species (RNS), which results in the growth of oxidative stress, may be caused by factors such as hypoxia or inflammation. On the other hand, free radicals, which are powerful pro-inflammatory agents, enhance the expression of cyclooxygenase. As a result, oxidative stress and inflammation are the phenomena often coexisting in damaged tissue, which can potentiate each other[48–50]. Therefore, we conducted experiments that determined the antioxidative activity of the title compounds.

A test using the fluorescent dye - 2', 7'-dichlorofluorescein diacetate (DCF-DA) was performed to assess the ability of new derivatives to reduce the level of ROS, while the effectiveness of scavenging nitrogen radicals was determined by the Griess assay. In both cases, the studies were performed on the NHDF cell line.

Compounds **9a(P1) - 13a(P1)** reduced the concentration of reactive oxygen species over the entire range of tested concentrations. In turn, the derivatives **7a(P1)** and **8a(P1)** were effective only at lower concentrations, i.e. 10 µM and 50 µM. Derivatives with an *n*-butyl substituent, i.e. **7b(P1) - 13b(P1)**, showed minor antioxidant activity, and in some of them, an increase in the

level of ROS was observed. In turn, the results of the Griess test show that all tested compounds reduce the concentration of RNS, including nitric oxide (NO) The derivatives **7b(P1)**, **10a(P1)** and **10b(P1)** caused a slight, statistically insignificant increase in the concentration of nitrogen radicals. The obtained results are detailed presented in *Chapter 2.4* and *Table 3* in publication **P1**.

The promising results of the DCF-DA and Griess tests forced us to conduct an additional experiment to assess the antioxidant effect of pyrrolo[3,4-*d*]pyridazinone derivatives. For this purpose, the fast halo assay (FHA) was carried out. It allowed us to estimate the protective effect of the tested compounds, which was manifested in the protection of chromatin against DNA damage and cracks caused by increased oxidative stress. The protective effect is determined by the evaluation of the level of chromatin damage to the control. The obtained results indicate that compounds **7b(P1), 8a(P1)** (the entire concentration range) and **7a(P1)** (concentration 10µM and 50µM) statistically significantly protect DNA against damage caused by increased concentration of free radicals. **Figure 10** shows selected micrographs of cells that were tested in the FHA. Photo B shows the characteristic effect of the nuclear halo caused by chromatin relaxation, which is the result of DNA breaks (**Fig**. **10B**). The larger the „halo", the greater the chromatin damage we observe. The halo effect is practically non-existent in the case of the cell incubated with compound **7b(P1)**. The results of this research are described in more detail in *Chapters 2.4* and *2.5* as well as in *Table 3* of the publication **P1**.

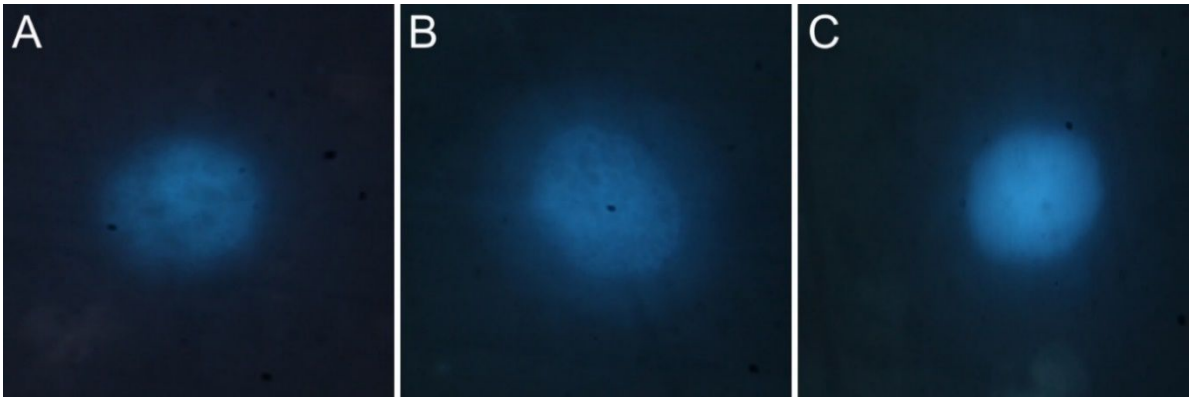

Fig. 10. Micrographs (60x) of cells showing chromatin relaxation: **A**) cell incubated in the complete medium; **B**) cell incubated with 100 µM H_2O_2 for 1h; **C**) cell incubated with compound **7b(P1)** at 10 µM for 24h and then for 1h with 100 µM H_2O_2. Micrograph **B** shows a much larger nuclear halo compared to **A**; the larger the halo size, the greater the relaxation of chromatin, which means a higher level of DNA damage.

The experiments determining the biological activity of the newly obtained compounds were complemented by studies assessing the way of their interaction with albumin, which is the

most abundant plasma protein. The binding of drugs to blood proteins significantly affects their pharmacokinetics, including half-life and distribution. Therefore, preliminary experiments were carried out, enabling the description of the interaction of pyrrolo[3,4-*d*]pyridazinone derivatives with serum albumin. Due to much lower costs, bovine serum albumin (BSA) was used. Its structure is very similar to that of human serum albumin (HSA), so it can successfully serve as a substitute[51,52]. To describe the molecular interactions between new compounds and BSA, spectral methods such as circular dichroism (CD), fluorescence and molecular docking were engaged.

Spectroscopic techniques (fluorescence quenching, CD) confirmed that changes in the secondary structure of BSA occur in the presence of the tested compounds. It confirms that they interact with plasma albumin. This interaction is not a random collision of molecules, but rather the formation of BSA ligand complexes in an approximate ratio of 1:1. Based on the performed molecular docking, it was found that the preferred binding site for new pyrrolo[3,4-*d*]pyridazinone derivatives by BSA is hydrophobic pocket II(m).

Details of all studies describing the interactions of the title compounds with BSA, as well as all tables, spectra and graphs are included in *Chapter 2.6* of the publication **P1** and in the supplementary data.

After collecting the results of all experiments, multi-criteria decision analysis (MCDA) was performed. Based on its results, it can be concluded that in series **I** of pyrrolo[3,4-*d*]pyridazinone derivatives, the compound with the best biological activity profile was the **7b(P1)**. Its structure is shown in **Figure 11**. Derivatives **7a(P1)**, **10a(P1)**, **10b(P1)**, **13a(P1)** and **13b(P1)** also appeared to be very promising. The complete results of the MCDA analysis are presented in *Figure 10* of publication **P1**.

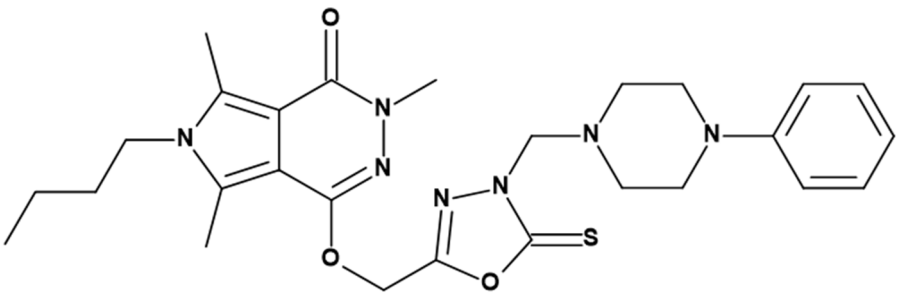

7b(P1)

Fig. 11. Compound **7b(P1)** – 1,3,4-oxadiazole derivative of pyrrolo[3,4-*d*]pyridazinone with the most promising biological activity.

Similar *in vitro* and *in silico* experiments were carried out for series **II** of 1,3,4-oxadiazole derivatives of pyrrolo[3,4-*d*]pyridazinone. The design, synthesis, evaluation of biological activity and physicochemical properties of these compounds became the subject of publication **P2**.

Evaluation of toxicity was carried out on the NHDF cell line with the use of a test assessing the activity of mitochondrial succinate dehydrogenase. Its product named triazole blue formazan (3-(4,5-dimethylthiazol-2-yl) -2,5-diphenyltetrazolium bromide, MTT) is visible in living cells. The results of the MTT assay are detailed in *Chapter 2.3* of the publication **P2**.

None of the compounds decreased the cell viability below 30%. Therefore we can conclude that the new derivatives of series **II** did not show any cytotoxic potential and were submitted for further research.

To assess the ability of the new compounds to inhibit cyclooxygenase, Cayman's COX Colorimetric Inhibitor Screening Assay (cat. No. 701050) was used, as previously. The results of the experiment (*Chapter 2.2.1*, *Table 1*, publication **P2**) indicate that all four analyzed derivatives show activity against the induced form COX-2 only. Unfortunately, based on the obtained results, it should be stated that the modification consisting of the introduction of a longer linker with the carbonyl residue did not bring the expected results. In fact, a group of selective COX 2 inhibitors was obtained, but the compounds of series **II** inhibit this enzyme significantly lower than the derivatives of series **I** and meloxicam. The compound **6a(P2)** turned out to be the most potent.

It should be noted, however, that the results of molecular docking studies fully correlate with the score of the enzyme assay. For compounds **5a,b(P2)** - **6a,b(P2)**, free binding energy (ΔG◦) values were positive during the COX-1 docking trials. On the other hand, the new derivatives show an affinity for the induced form COX-2 and occupy a position similar to that of meloxicam in the enzyme binding pocket what was shown in **Figure 12**. The binding energies are slightly higher but comparable to those determined for the reference drug. A detailed description of the molecular docking study can be found in *Chapter 2.2.2* of publication **P2**.

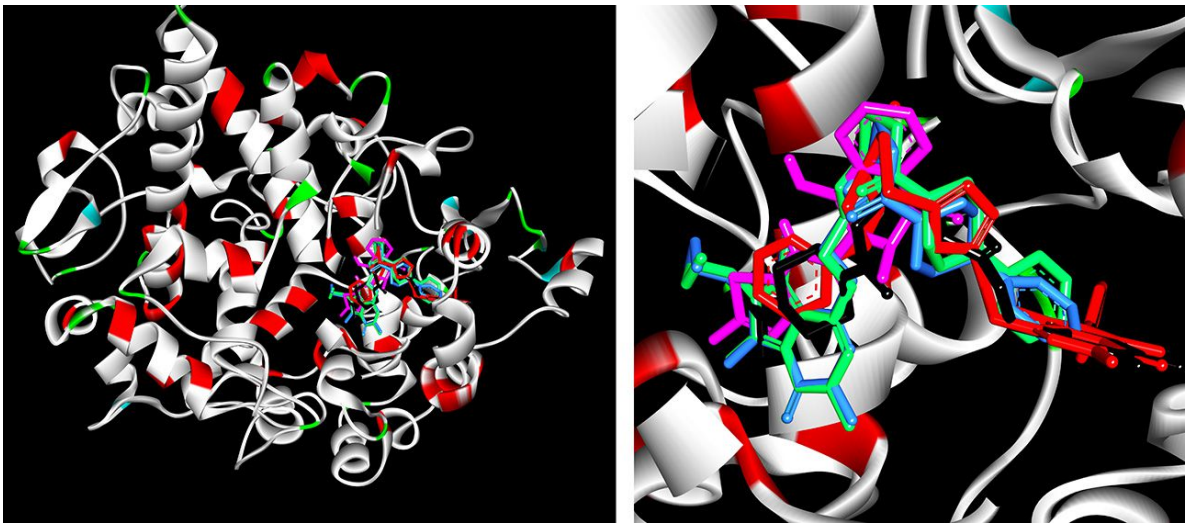

Fig. 12. The binding poses of **5a**, **b(P2)** – **6a**, **b(P2)** and meloxicam (pink) in the active site of COX-2.

In the next stage of biological research, the antioxidant potential of the new pyrrolo[3,4-d]pyridazinone derivatives and their ability to protect DNA against damage caused by free radicals were assessed. For this purpose, DCF-DA, Griess and FHA tests were performed. A detailed description of the results of these experiments is provided in *Chapter 2.4* of the publication **P2**.

It was found that in cells incubated with compounds **5a(P2)**, **5b(P2)** and **6b(P2)**, the concentration of free oxygen radicals decreased below the control value in the whole range of tested concentrations. Derivative **6a(P2)** was effective only at the lowest concentration, i.e. 10 μM. The results of the Griess assay show that all compounds at the lowest concentration (10 μM) were able to reduce the amount of NO, while the derivative **6a(P2)** was effective across the whole spectrum of the concentrations used (*Table 3*, publication **P2**).

These results correspond perfectly with the results obtained in the FHA. All tested derivatives reduce the amount of chromatin damage induced by oxidative stress in at least one concentration used (*Table 3*, publication **P2**). Moreover, it has been proved that there is a correlation between the antioxidant activity of the new derivatives and their DNA repair capacity in a state of increased oxidative stress (*Table 4*, publication **P2**).

Additionally, spectral studies and molecular docking were performed, to evaluate the interaction mode of 1,3,4-oxadiazole derivatives of series **II** with plasma albumin. Detailed information on these experiments and their results are in *Chapters 2.5-2.7* of publication **P2** and in the supplement. The tested compounds interact with BSA by forming complexes in an approximate ratio of 1:1. A privileged binding site is the hydrophobic pocket II, subdomain IIIA.

Based on the results of CD spectroscopy, we can assume that the compounds **5a-b(P2)** are bound stronger by BSA than the derivatives **6a-b(P2)**.

Due to the similar results of performed studies and the relatively small group of analyzed compounds, it would be difficult to indicate the most promising structure within derivatives of the series II. Undoubtedly, it should be emphasized, that the replacement of the methylene linker with the 2-oxoethyl linker did not contribute to the intensification of pharmacological activity, but only to the increase of the selectivity of the compounds to COX-2.

4.1.3 *In vivo* studies

Since the 1,3,4-oxadiazole derivatives of pyrrolo[3,4-d]pyridazinone of series **I** showed satisfactory pharmacological activity in performed *in vitro* experiments, we selected the most promising compounds for in *vivo tests*. Two derivatives were qualified for such evaluation - **10b(P1)** and **13b(P1)**, the structures of which are shown in **Figure 13**. Their selection was made mainly based on the results of the COX inhibitory assay. The derivative **10b(P1)** was characterized by the best COX-2/COX-1 inhibitory ratio among all the tested compounds. On the other hand, the compound with a similar structure **13b(P1)** acted as a selective COX-2 inhibitor. Moreover, compounds **10b(P1)** and **13b(P1)** were one of the least toxic among all 1,3,4-oxadiazole derivatives of series **I**[26].

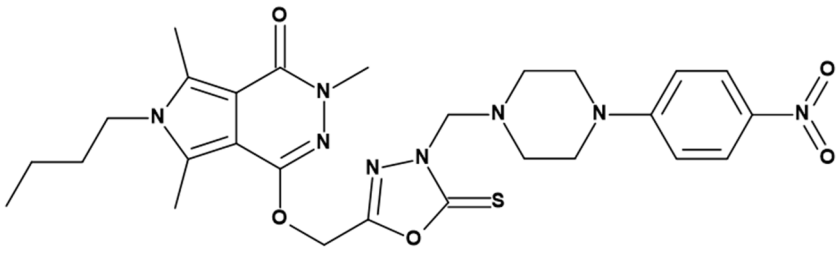

10b(P1)

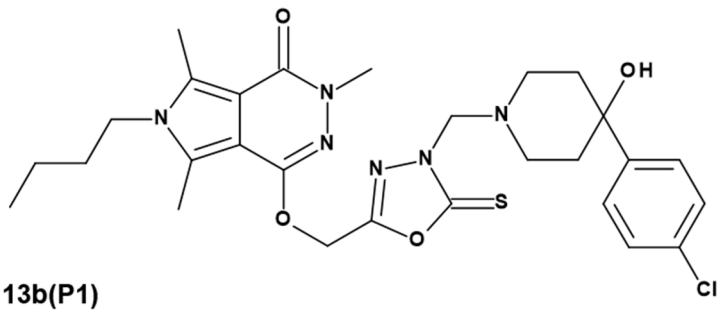

13b(P1)

Rys. 13. The structures of pyrrolo[3,4-*d*]pyridazinone derivatives which underwent the *in vivo* evaluation.

The studies in the animal model were performed in cooperation with the Department of Pharmacology of Wrocław Medical University by a team led by dr Marta Szandruk-Bender. The conducted experiments were aimed at assessing the analgesic and anti-inflammatory activity of the tested compounds, their influence on the condition of the gastric mucosa and the expression of inflammatory mediators.

The first stage of the planned research allowed us to determine the analgesic profile of **10b(P1)** and **13b(P1)** derivatives in experimental models of pain induced by noxious stimuli, i.e. the tail-flick test and the formalin test.

The tail-flick test assessed the analgesic activity associated with central mechanisms by measuring the time taken to respond to thermal stimulation induced by a heat-emitting light beam. The new derivatives, **10b(P1)** and **13b(P1)**, pyrrolo[3.4-d]pyridazinone showed statistically significant and dose-dependent analgesic activity compared to the control. At the same time, their activity was significantly lower than that of morphine. The obtained results are presented in the form of a graph in **Figure 14**.

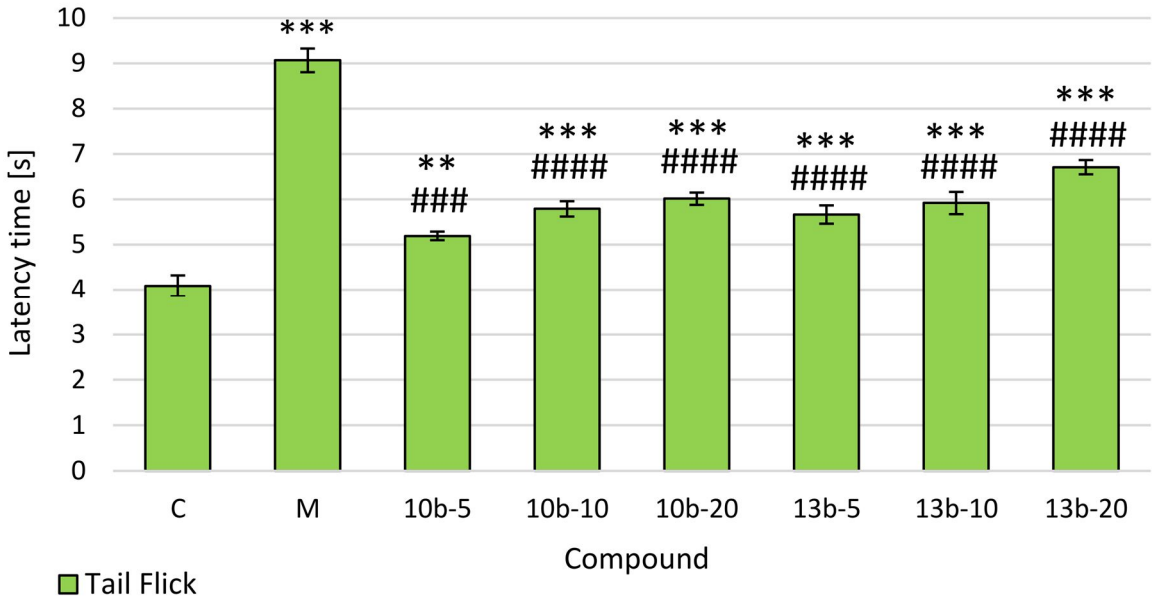

Fig. 14. The effects of compounds **10b** and **13b** on the latency time in the tail-flick test. Morphine was used as a reference drug. All compounds were administered intragastrically. Experimental groups (n=12): C – control group; M – group receiving 10 mg/kg of morphine; **10b**-5, **10b**-10, **10b**-20 – groups receiving, respectively, 5, 10, or 20 mg/kg of investigated compound **10b**; **13b**-5, **13b**-10, **13b**-20 – groups receiving, respectively, 5, 10, or 20 mg/kg of investigated compound **13b**. Data are presented as mean±SEM. Differences **p<0.01 vs. control group; ***p<0.001 vs. control group; ###p<0.001 vs.morphine group; ####p<0.0001 vs. morphine group were deemed statistically significant[53].

The obtained results indicate that both tested compounds **10b(P1)** and **13b(P1)** exert analgesic activity. Compared to the control group, they significantly extended the time after which the reaction to a harmful stimulus took place (the tail moved away by the animal). It may suggest that the **10b(P1)** and **13b(P1)** derivatives modulate central mechanisms involved in nociception.

To determine the effect of the new compounds on both central and peripheral mechanisms of pain response, the formalin test was carried out. The subcutaneous injection of formalin into the hind paw triggers a biphasic nociceptive response. The early phase, named neurogenic, is a result of direct stimulation of afferent fibres and the release of neuropeptides such as substance P. The late phase is caused by the development of inflammation. Consequently, an increase in the synthesis and release of prostaglandins occur. Therefore, the formalin test allows determining not only the influence of the tested substances on the nociception mechanisms not related to inflammation (early phase) but also on the inflammatory nociceptive reaction, as well (late phase)[3,54,55].

The examined derivatives **10b(P1)** and **13b(P1)** and the reference drugs resulted in a dose-dependent reduction in the pain reaction induced by formalin injection (paw licking time), both in the early and late phases. Compared to the control group, the most effective in the early phase turned out to be morphine and compound **13b(P1)** at the dose of 20 mg/kg, the potency of which was similar to that of the reference drug. Moreover, the antinociceptive effect of the derivative **13b(P1)** at the dose of 20 mg/kg was statistically significantly higher than that of indomethacin. The good activity of compound **13b(P1)** at the highest dose used in the early phase of the test may indicate that its mechanism of action is also due to its influence on other, non-COX-dependent pathways. This premise requires further, more in-depth research. In the late phase, the best and statistically significant effects showed morphine and both tested compounds **10b(P1)** and **13b(P1)** at the doses of 10 and 20 mg/kg. The obtained results, presented in **Figure 15**, suggest that the tested compounds probably possess central and peripheral analgesic activity.

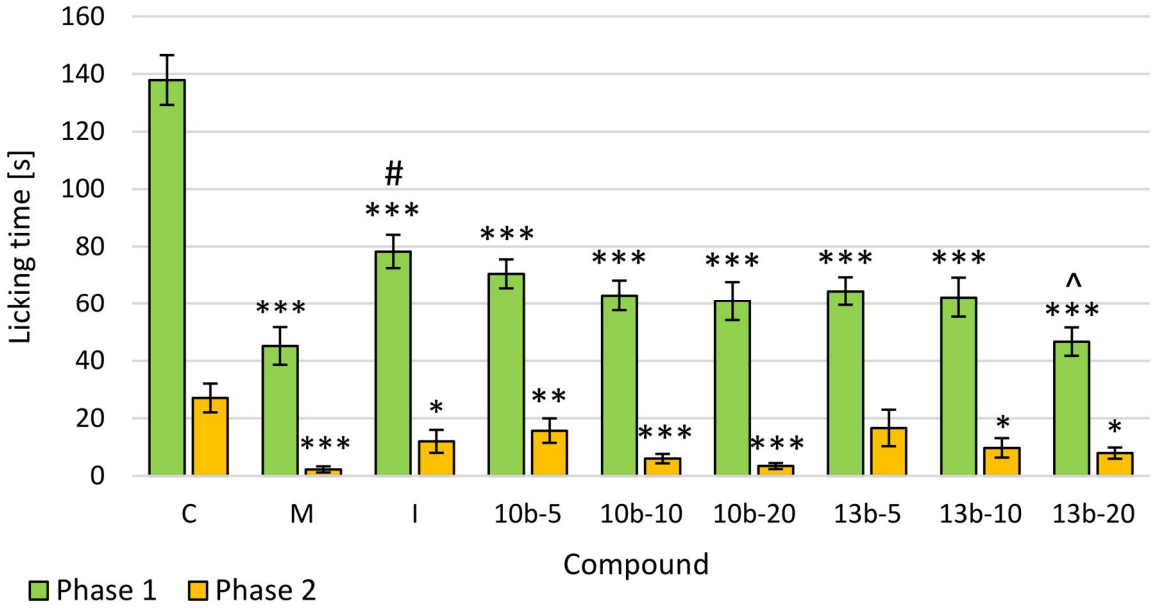

Fig. 15. The effects of compounds **10b** and **13b** on the licking time in the early (0–5 min) and late (25–30 min) phases of the formalin test. Morphine and indomethacin were used as reference drugs. All compounds were administered intragastrically. Experimental groups (n = 12): C – control group; M – group receiving 10 mg/kg of morphine; I – group receiving 10 mg/kg of indomethacin; **10b**-5, **10b**-10, **10b**-20 – groups receiving, respectively, 5, 10, or 20 mg/kg of investigated compound **10b**; **13b**-5, **13b**-10, **13b**-20 – groups receiving, respectively, 5, 10, or 20 mg/kg of investigated compound **13b**. Data are presented as mean ± SEM. Differences * $p < 0.05$ vs. control group; ** $p < 0.01$ vs. control group; *** $p < 0.001$ vs. control group; # $p < 0.05$ vs. morphine group; ^ $p < 0.05$ vs. indomethacin group were deemed statistically significant[53].

As was mentioned previously, in the late phase of the formalin test, the increased synthesis and release of prostaglandins occur. They are one of the best known and described pro-inflammatory mediators[6]. They act, especially prostaglandin E_2 (PGE_2), sensitizing, moreover they modulate the pain reaction both peripherally and centrally. PGE_2 also enhances the activity of other pro-inflammatory mediators. Therefore, the reduction of COX-dependent PGE_2 production should result in the attenuation of the nociceptive reaction[6,56,57]. Another substance that also plays an important role in mediating inflammatory nociception and influences the increased release of PGE_2 is myeloperoxidase (MPO), produced by neutrophils that infiltrate inflamed tissue. Activation of neutrophilic granulocytes in the inflamed area leads to an exaggerated MPO concentration. As a consequence, an increase in the production of reactive oxygen and nitrogen species take place[58,59]. For this reason, substances that exhibit antioxidant activity, in a somewhat indirect way, can relieve inflammation and alleviate the pain reaction at the origin of which is inflammation[48,60].

Therefore, the levels of PGE_2 and MPO in mouse plasma were determined using the enzyme-linked immunosorbent assay (ELISA). The results of the experiment are presented in the form of a graph in **Figure 16**. The lowest level of PGE2 was recorded in the groups that received compound **13b(P1)** at a dose of 20 mg/kg or indomethacin. A statistically significantly lower concentration of MPO as compared to the control was determined in the groups administered the derivative **13b(P1)** at the dose of 10 and 20 mg/kg or indomethacin. The decrease in plasma MPO concentration in animals that received compound **13b(P1)** can be explained by the fact that, unlike derivative **10b(P1)**, it showed antiradical activity in *in vitro* tests (*Section 2.4*, publication **P1**). Moreover, it is worth noting that in the case of both tested compounds **10b(P1)** and **13b(P1)**, their effect on the concentration of PGE_2 and MPO in the plasma was dose-dependent (**Fig. 16**).

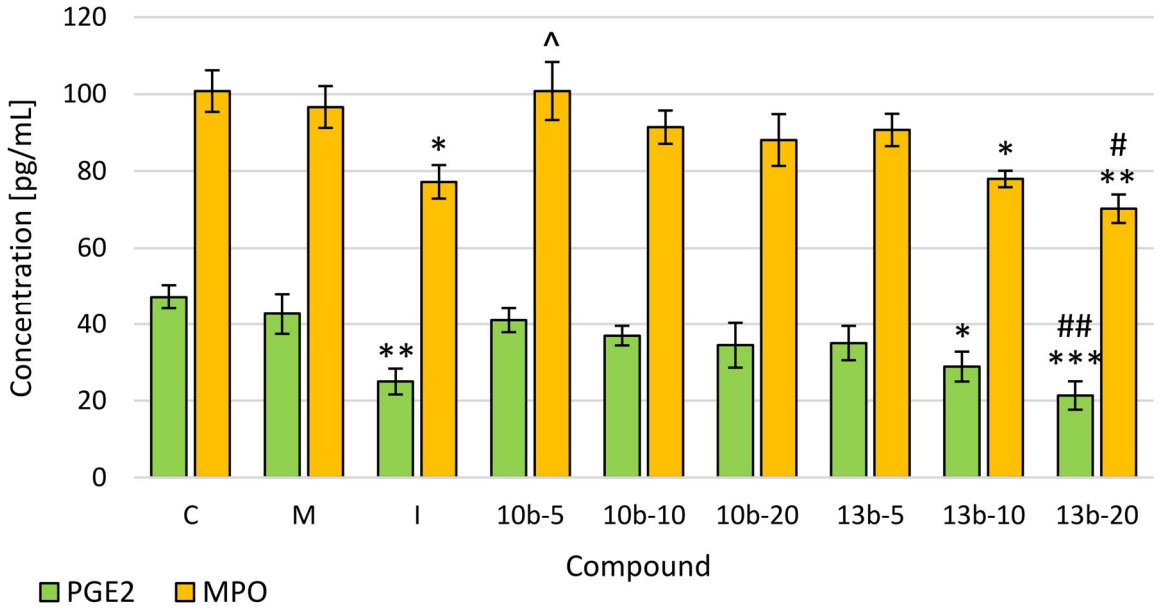

Fig. 16. The effects of compounds **10b** and **13b** on the levels of Prostaglandin E_2 (PGE_2) and Myeloperoxidase (MPO) in mice serum. Blood samples were collected before mice were sacrificed. Morphine and indomethacin were used as reference drugs. Experimental groups (n = 12): C – control group; M – group receiving 10 mg/kg of morphine; I – group receiving 10 mg/kg of indomethacin; **10b**-5, **10b**-10, **10b**-20 – groups receiving, respectively, 5, 10, or 20 mg/kg of investigated compound **10b**; **13b**-5, **13b**-10, **13b**-20 – groups receiving, respectively, 5, 10, or 20 mg/kg of investigated compound **13b**. Data are presented as mean ± SEM. Differences * $p < 0.05$ vs. control group; ** $p < 0.01$ vs. control group; *** $p < 0.001$ vs. control group; # $p < 0.05$ vs. morphine group; ## $p < 0.01$ vs. morphine group; ^ $p < 0.05$ vs. indomethacin group were deemed statistically significant[53].

This research, besides evaluating the anti-inflammatory activity, was also aimed at determining the influence of titled compounds on the condition of the gastric mucosa. The design and synthesis of molecules deprived of dangerous side effects on the gastrointestinal tract, characteristic of classic NSAIDs[15–18], was one of the main goals of this study. For this reason, a macro- and microscopic evaluation of the condition of animals' gastric mucosa was performed. The presence of macroscopically visible lesions, such as petechiae, erosions or bleeding, indicated gastrotoxic activity. The obtained results indicate, that both derivatives **10b(P1)** and **13b(P1)**, at all doses used (5, 10, 20 mg/kg), did not cause significant changes in the image of the gastric mucosa. In turn, in the indomethacin group, significant damage to the gastric mucosa was observed. The results of the macroscopic evaluation were confirmed by microscopic examinations. The photographs are provided in **Figure 17**.

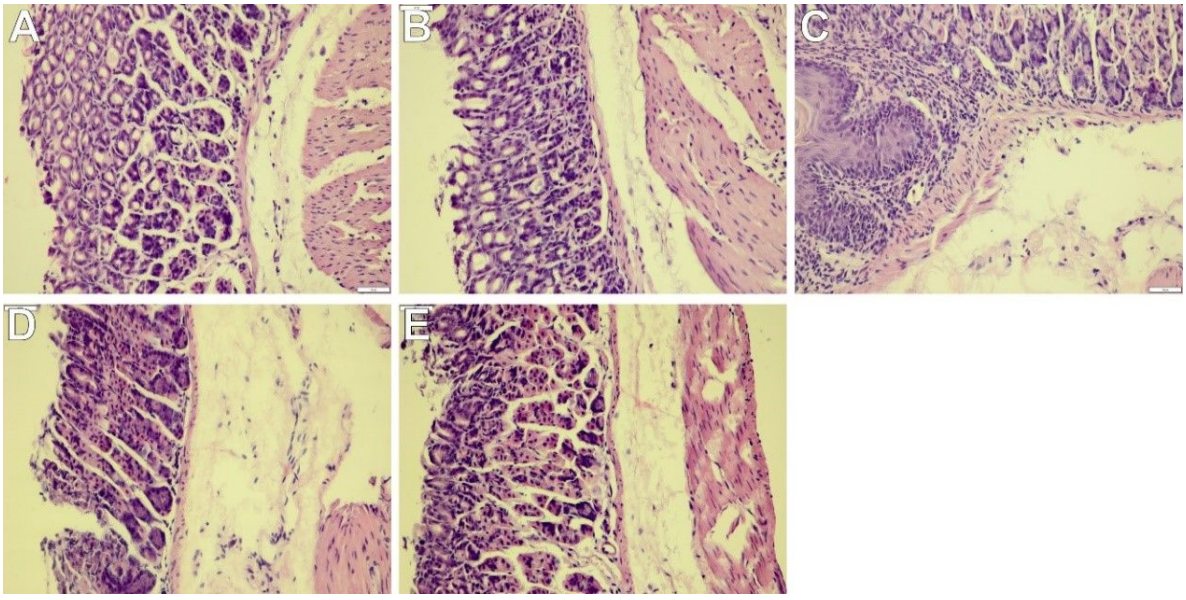

Fig. 17. Microscope appearance of stomach tissue after hematoxylin-eosin (H&E) staining demonstrated that studied compounds neither altered the normal stomach architecture nor induced ulcerations. Morphine and indomethacin were used as reference drugs. Experimental groups (n=12): Control group (**A**); group receiving 10 mg/kg morphine (**B**); group receiving 10 mg/kg indomethacin (**C**); group receiving 20 mg/kg compound 10b (**D**); group receiving 20 mg/kg compound13b (**E**); magnification 200x[53].

In the microscopic image of the gastric mucosa of animals, both in the control group and in the groups receiving test derivatives **10b(P1)** and **13b(P1)**, no pathological changes were noted (**Fig. 17A**, **D**, **E**). On the other hand, during the histopathological analysis of gastric mucosa tissue of animals given indomethacin at a dose of 10 mg/kg, numerous damage to the cells of its protective layer, necrotic foci, submucosal oedema and hyperemia of both mucosal and submucosal blood vessels were observed. (**Fig. 17C**). Morphine (10 mg/kg) did not cause

any significant changes in both the macroscopic and microscopic images of the gastric mucosa (**Fig. 17B**).

Summing up compounds **10b(P1)** and **13b(P1)** showed better antinociceptive activity *in vivo* than indomethacin, with significantly reduced gastrotoxicity, which is most likely related to the presence of 1,3,4-oxadiazole-2-thion in their structure.

Taking into account the fact that the tested derivatives of **10b(P1)** and **13b(P1)** proved to be effective in reducing inflammatory nociception in the late phase of the formalin test, it was decided to perform an experiment that would allow the assessment of their peripheral anti-inflammatory activity. Therefore, a carrageenan test was carried out, to determine the effect of compounds **10b(P1)** and **13b(P1)** on the course of acute inflammation. It was caused by an injection of a 1% carrageenan solution into the subplantar fascia area of the rat's hind paw. The absolute volume of the paw was measured using a plethysmometer and the increments in paw volume at 1, 2, 3 and 6 hours after injection of carrageenan or saline solution (control group, **C**). Additionally, the concentration of mediators such as PGE_2, MPO or tumour necrosis factor α (TNF-α) in the inflamed tissue was determined, and the effect of new pyrrolo[3,4-*d*]pyridazinone derivatives on the gastric mucosa was investigated.

In the conducted experiment, no statistically significant differences were found in the paw volume in the control group and in the groups tested before the injection of carrageenan. In contrast, the injection of 0.1mL of 1% carrageenan solution into the hind paw of animals belonging to the test groups caused a strong inflammatory reaction and a significant increase in paw volume due to oedema. Changes in the appearance and size of the animals' paws are visible in the photographs collected in **Figure 18**.

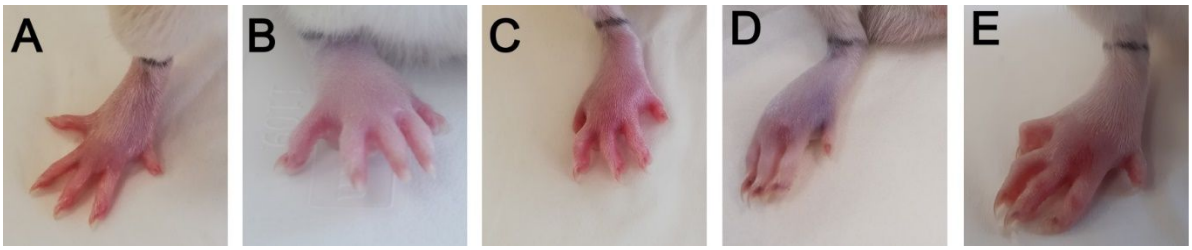

Fig. 18. The effects of compounds **10b** and **13b** on the carrageenan-induced paw oedema in rats. Indomethacin was used as a reference drug. Experimental groups: control group (**A**); carrageenan group (**B**); group receiving 10 mg/kg indomethacin (**C**); group receiving 20 mg/kg compound **10b** (**D**); group receiving 20 mg/kg compound **13b** (**E**)[61].

The greatest swelling of the paw was noted in each group 6h after the injection with carrageenan. In groups of animals that received derivatives **10b(P1)** and **13b(P1)** 2h after injection of carrageenan solution, the pace of swelling was inhibited (**Fig. 18D**, **E**). Compound **10b(P1)** at doses of 10 and 20 mg/kg was able to partially reverse the progressive increase in oedema at 2, 3 and 6h after the carrageenan injection. A similar effect, to some extent, was also noted 2, 3 and 6h after injection of carrageenan solution in all groups that received derivative **13b(P1)** (dose 5, 10 and 20 mg/kg). Moreover, in the case of compound **13b(P1)**, statistically significant differences in the volume of the paw were found at all doses used, compared to the control group at 2, 3 and 6h after induction of inflammation. Similarly, the degree of oedema growth inhibition observed in the indomethacin group (**Fig**. **18C**) was also statistically significant. The maximum effect of reducing the paw swelling compared to the carrageenan group was observed 3h after the inflammation induction in the groups that received indomethacin (oedema was inhibited in 71.2%) and compounds **10b(P1)** (oedema was inhibited in 57.5%) and **13b(P1)** (oedema was inhibited by in 62.3%) at the highest doses of 20 mg/kg. Moreover, the activity of derivatives **10b(P1)** and **13b(P1)** administered in the highest dose was comparable to that of indomethacin.

Subsequently, the concentration of mediators such as PGE_2, MPO and TNF-α, which overexpression accompany the inflammation[1–5], were determined in the supernatants obtained by homogenization of the inflamed paw tissue by ELISA assays. The obtained results present the graphs in **Figure 19**.

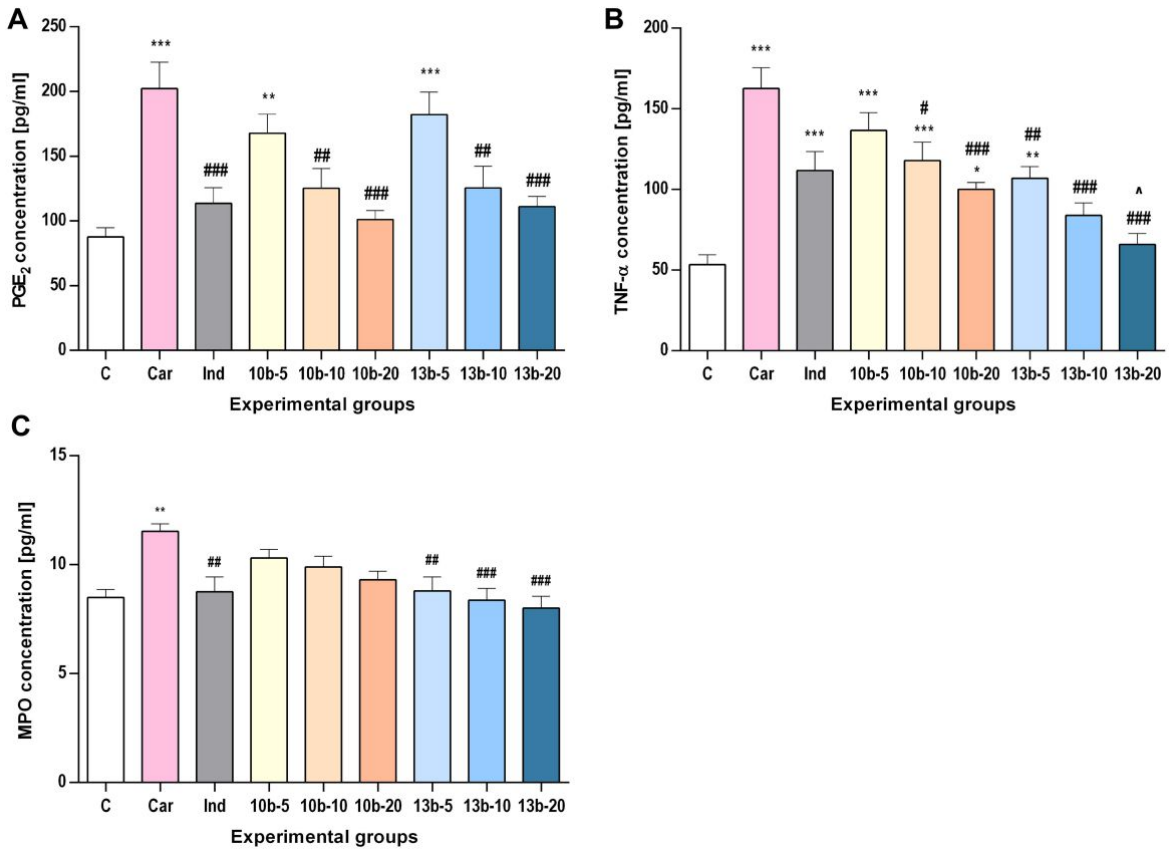

Fig. 19. 3 The impact of compounds **10b** and **13b** on PGE_2 (**A**), TNF-α (**B**), and MPO (**C**) concentrations in paw tissue. Indomethacin was used as a reference drug. Experimental groups: C – control group receiving 0.5% CMC intragastrically (i.g.) and normal saline subplantarly (s.pl.); Car – carrageenan group receiving 0.5% CMC i.g. and 1% carrageenan solution s.pl.; Ind – indomethacin group receiving 10 mg/kg of indomethacin i.g. and 1% carrageenan solution s.pl.; **10b**-5, **10b**-10, and **10b**-20 – groups receiving, respectively, 5, 10, or 20 mg/kg of investigated compound **10b** i.g. and 1% carrageenan solution s.pl.; **13b**-5, **13b**-10, and **13b**-20 – groups receiving, respectively, 5, 10, or 20 mg/kg of investigated compound **13b** i.g. and 1% carrageenan solution s.pl. Data are presented as mean values ± SEM (n=12). Differences $^{*}p<0.05$ vs control group; $^{**}p<0.01$ vs control group; $^{***}p<0.001$ vs control group; $^{\#}p<0.05$ vs carrageenan group; $^{\#\#}p<0.01$ vs carrageenan group; $^{\#\#\#}p<0.001$ vs carrageenan group; $^{\wedge}p<0.05$ vs indomethacin group were deemed statistically significant[61].

The greatest increase in the concentration of the inflammatory mediators occurred, as predicted, in the "carrageenan group". In the tissue of animals treated with compound **10b(P1)** at doses of 10 and 20 mg/kg, the level of PGE_2 was lower than in the carrageenan group and did not differ statistically significantly from the control. At the same time, in these groups (**10b**-10; **10b**-20) a partial decrease in the level of TNF-α was also noted. Derivative **10b(P1)** across the range of doses tested did not significantly affect the concentration of myeloperoxidase. The concentration of MPO in the groups receiving compound **10b(P1)** did not differ statistically significantly from those determined in the control and carrageenan groups (**Fig. 19C**). The level of PGE_2, MPO and TNF-α

in the groups administered **13b(P1)** at the doses of 10 and 20 mg/kg was statistically significantly lower compared to the "carrageenan group". It is worth noting that the amount of PGE_2 determined in the tissue of animals treated with compounds **10b(P1)** and **13b(P1)** at a dose of 10 and 20 mg/kg was comparable to the values recorded in the indomethacin group. Moreover, a similar relationship was observed in the context of MPO and TNF-α concentrations which were recorded in the groups administered the **10b(P1)** and **13b(P1)** in the entire range of the tested doses (**Fig**. **19B**, **C**). It is worth mentioning that the highest dose of compound **13b(P1)** was more effective in reducing the concentration of TNF-α in the inflamed tissue than the reference drug.

To assess the influence of the tested compounds on the condition of the gastric mucosa, macro- and microscopic analysis of organs taken from the animals participating in the study was performed. The indicator of the potential ulcerogenic effect was the presence and intensity of such changes in the image of the gastric mucosa, such as ecchymosis or erosions. **Figure 20** shows photographs of selected stomachs that were subjected to macroscopic analysis.

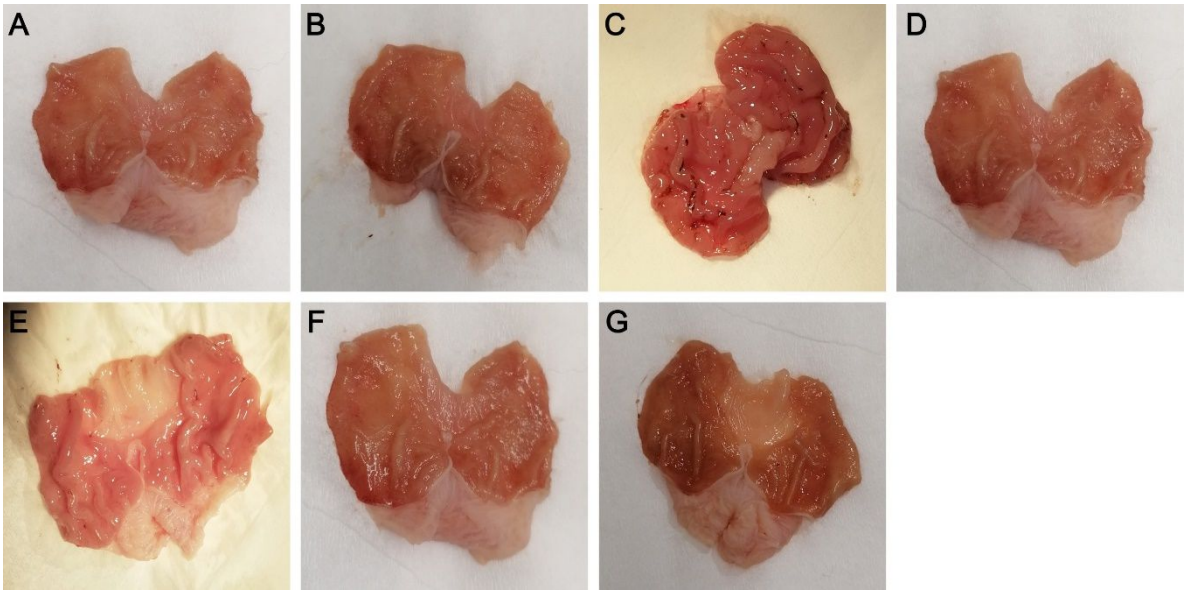

Fig. 20. The macroscopic appearance of the gastric mucosa revealed that the studied compounds caused negligible mucosal lesions. Indomethacin was used as a reference drug. Experimental groups: control group (**A**); carrageenan group (**B**); group receiving 10 mg/kg indomethacin (**C**); group receiving 10 mg/kg compound **10b** (**D**); group receiving 20 mg/kg compound **10b** (**E**); group receiving 10 mg/kg compound **13b** (**F**); group receiving 20 mg/kg compound **13b** (**G**)[61].

During the study, no damage to the gastric mucosa was observed in the control and carrageenan groups (**Fig**. **20A**, **B**). In the case of stomachs collected from animals treated with compounds **10b(P1)** and **13b(P1)**, no significant mucosal lesions were found as compared to the

control (**Fig. 20D-G**). On the other hand, in the indomethacin group, significant injuries and gastric mucosa damage were noticed. They varied in severity, from hyperemia to even hemorrhagic lesions covered with blood clots (**Fig. 20C**).

The observed macroscopic changes were confirmed by microscopic examinations. In the control and carrageenan groups as well as the groups receiving test derivatives **10b(P1)** and **13b(P1)**, no significant changes in the gastric mucosa were observed in the microscopic image. However, in the case of the carrageenan group, damage to the protective layer of the mucosa with its local thinning, crater cavities, local necrotic foci as well as submucosal oedema and hyperemia were found.

Summarizing the results obtained during the carrageenan test, we can conclude that the new pyrrolo[3,4-*d*]pyridazinone derivatives **10b(P1)** and **13b(P1)** show anti-inflammatory activity, and their mechanism of action may depend on lowering the concentration of such mediators as PGE_2, MPO or TNF-α, and reducing the infiltration of inflamed tissue. Although their activity was slightly lower than that of indomethacin, however, unlike the reference drug, they did not cause damage to the gastric mucosa, which is their undoubted advantage.

Based on the results of performed *in vivo* investigations we can conclude that 1,3,4-oxadiazole derivatives of pyrrolo[3,4-*d*]pyridazinone show a good benefit-risk ratio. Thus, this makes them attractive and promising structures for further research and development with potential application in the therapy of various inflammatory diseases.

4.2 The 1,2,4-triazole derivatives of pyrrolo[3,4-*d*]pyridazinone

4.2.1 The design and synthesis

Taking into account the promising anti-inflammatory activity of 1,3,4-oxadiazole derivatives of pyrrolo[3,4-*d*]pyridazinone and their low gastrotoxicity revealed in *in vivo* studies, it was decided to perform further optimizations and structural modifications of the compounds described in publications **P1**-**P2**.

Thoroughly analyzing the results of the experiments carried out so far, and being inspired by the reports of the scientific literature, we decided to obtain a new series of derivatives possessing an *N*-substituted 1,2,4-triazole ring in their structure. There were two important reasons for this modification.

First, the 1,2,4-triazole ring can be considered, due to its reduced acidic nature, but at the same time a similar molecular size, as a bioisostere for a free carboxyl group. Therefore, the 1,2,4-triazole moiety is an important building block of many compounds widely described in the literature. A lot of them show significant anti-inflammatory and analgesic activity with low gastrotoxicity at the same time[21,22,29,30].

Secondly, taking into account the fact that the binding pocket of the COX-2 isoenzyme is larger than that of COX-1[7–10], it was expected that the synthesis of compounds with a more complex structure, possessing an additional substituent in the 4-position of the 1,2,4-triazole ring, would significantly improve their COX-2/COX-1 selectivity ratio.

Following the results obtained so far, in particular considering the fact that in the previous series the compound **7b(P1)** turned out to be the most active, we decided to focus on the synthesis and studies of 6-*n*-butyl substituted pyrrolo[3.4-*d*]pyridazinone derivatives.

Figure 21 shows the general formulas of the two series of new *N*-substituted 1,2,4-triazole analogues of pyrrolo[3,4-*d*]pyridazinone. To the first one belong Mannich base type derivatives (**I**). In turn, the second series consists of compounds whose structure refer to the aforementioned pharmacophore theory featured by Dogruer (**II**)[46,47].

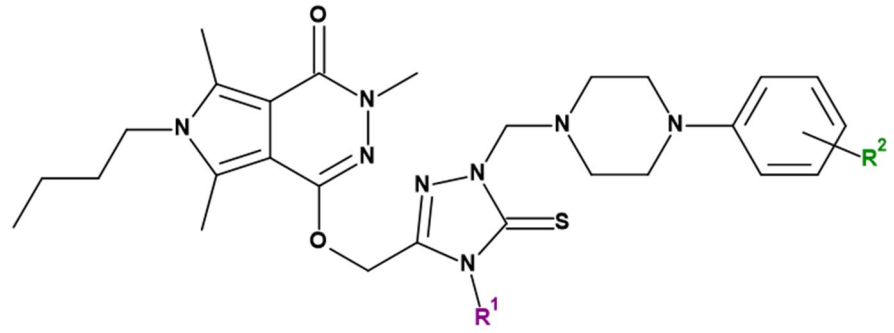

I

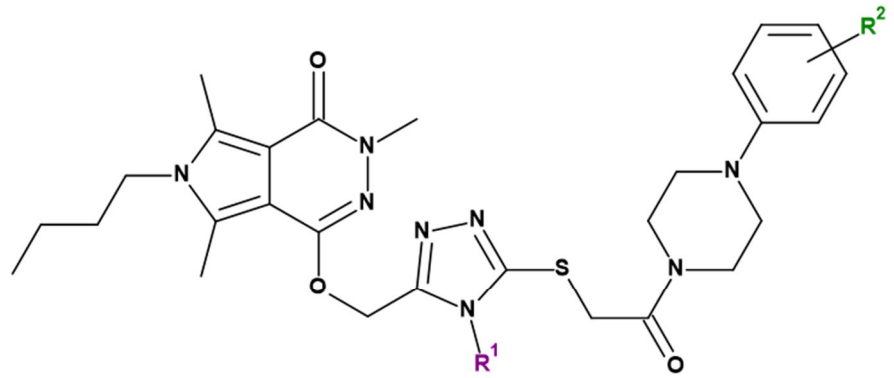

II

R^1 – CH_3, phenyl, 4-(methoxy)phenyl;

R^2 – H, CF_3, CH_3;

Fig. 21. The general structures of series **I** and **II** of 1,2,4-triazole derivatives of pyrrolo[3,4-*d*]pyridazinone.

Thus, designed molecules can be considered as structural analogues of the 1,3,4-oxadiazole derivatives described in publications **P1** and **P2**. The starting point for the synthesis of this group of compounds was the 2-(6-butyl-3,5,7-trimethyl-4-oxo-pyrrolo[3,4-d] pyridazine-1-yloxy) acetic acid hydrazide **5b(P1)** described in the publication **P1**. Condensation of this hydrazide with the appropriate *N*-substituted isothiocyanates gave thiosemicarbazide derivatives. Subsequently, they were subjected to intramolecular cyclization to form a 1,2,4-triazole ring. The last stage of the planned synthesis assumed obtaining a group of compounds with the structure shown schematically in **Figure 21**. The first series of new molecules had the structure of Mannich bases. They were obtained by the condensation of **3a-c(P3)** with appropriate arylpiperazine derivatives in the presence of formaldehyde (**Fig. 21 I**). The second series was obtained by alkylating the compounds **3a-c(P3)** with the

appropriate, previously synthesized, 1-(2-chloro-1-oxo)-ethyl derivative of arylpiperazine in ethanol in the presence of sodium ethoxide (**Fig. 21 II**).

As a result of the conducted synthesis, a total of 24 new, previously unpublished compounds were obtained, including 18 final derivatives (**Fig. 21 I**, **II**). The structure of all previously undescribed molecules has been confirmed by spectral techniques. After appropriate purification, they underwent biological evaluation.

The design, the carried-out structural modifications and the methods used for obtaining new 1,2,4-triazole derivatives of pyrrolo[3,4-*d*]pyridazinone were detailed presented and described in *Scheme 1* and *Chapters 1*, *2.1* of the publication **P3**. In the experimental part of this work and in the supplement, the analytical data, physicochemical properties and spectra (NMR, MS, IR) of all new compounds are provided.

4.2.2 *In vitro* and *in silico* investigations

The studies assessing the toxicity and biological activity of *N*-substituted 1,2,4-triazole derivatives of pyrrolo[3,4-*d*]pyridazinone were carried out in cooperation with the units of the Wrocław Medical University. At the Department of Pharmacology, enzymatic tests and all *in vitro* experiments were executed by the team led by dr Benita Wiatrak. At the Department of Inorganic Chemistry, spectral tests and molecular docking were performed by dr Edward Krzyżak, dr Aleksandra Marciniak and dr Aleksandra Kotynia.

The first stage of biological research relied on the evaluation of the cytotoxicity of new compounds. The MTT assay was performed on the NHDF cell lines. According to the standard procedure, derivatives that reduced cell viability by more than 30% are considered toxic. Compounds **4a-c(P3)**, **7a-c(P3)** as well as **5a(P3)**, **6a(P3)** and **9a(P3)** did not reveal cytotoxic effect. On the other hand, in the case of 5 compounds: **8a-c(P3)**, **9b-c(P3)**, shrunken cells, numerous granules and lysis of over 50% cells were observed. Therefore, they were excluded from further research. When observing cells that were incubated with derivatives **5b(P3)**, **5c(P3)**, **6b(P3)** and **6c(P3)**, single granules were noticed in their microscopic image, but with the retained, elongated cell shape characteristic for fibroblasts. The calculated IC_{50} values were higher than the cut ff value of 100 μM (**Table 1**, publication **P3**). For this reason, they have also been submitted for further investigations. Summing up, based on the MTT test, 5 compounds were found to be cytotoxic, the remaining 13 derivatives underwent biological evaluation. The cytotoxicity analysis of 1,2,4-triazole derivatives of pyrrolo[3,4-*d*]pyridazinone is detailed in *Section 2.2* of the publication **P3**.

The ability of the new compounds to inhibit both cyclooxygenase isoforms was determined based on the use of the commercial Cayman's COX Colorimetric Inhibitor Screening Assay (cat. No. 701050). To precisely assess the anti-cyclooxygenase activity of the new derivatives, meloxicam, diclofenac sodium and celecoxib were used as references. A detailed description of the research and the obtained results are included in *Chapter 2.3.1* of the publication **P3**.

COX inhibitory assay revealed, that 4 of the analyzed compounds preferentially block COX-2, another 4 turned out to be selective for the induced isoform COX-2. Unfortunately, 5 of them did not show the ability to inhibit cyclooxygenase. It is noteworthy that the IC_{50} values determined for new compounds were lower than those calculated for meloxicam. Moreover, the COX-2/COX-1 inhibitory ratio of the preferential COX 2 inhibitors was also better than that specified for meloxicam. However, the activity of the new structures was worse than presented by celecoxib. (**Table 2**, publication **P3**). It is also worth noting that the affinity for cyclooxygenase was shown mainly by those derivatives in which the 1,2,4-triazole ring was substituted with a small methyl substituent. On the other hand, compounds with the 4-methoxyphenyl moiety turned out to be the least effective.

The affinity of the new compounds for cyclooxygenase was also assessed using the molecular docking technique. The obtained results correlate significantly with the findings of the *in vitro* test. During attempts to dock 1,2,4-triazole derivatives to COX-1, positive values of free binding energy (ΔG°) were obtained. Among examined structures, 8 had an affinity for COX-2, and the best results were obtained for compounds with a small methyl substituent in the 1,2,4-triazole ring. A similar relationship was demonstrated in an enzymatic assay. Again, 5 compounds did not show an affinity for any of the cyclooxygenase isoenzyme. The way of interaction with COX 2 of the most effective derivatives is presented in **Figure 22**. A detailed description of molecular docking to COX is provided in *Chapter 2.3.2* of the publication **P3**.

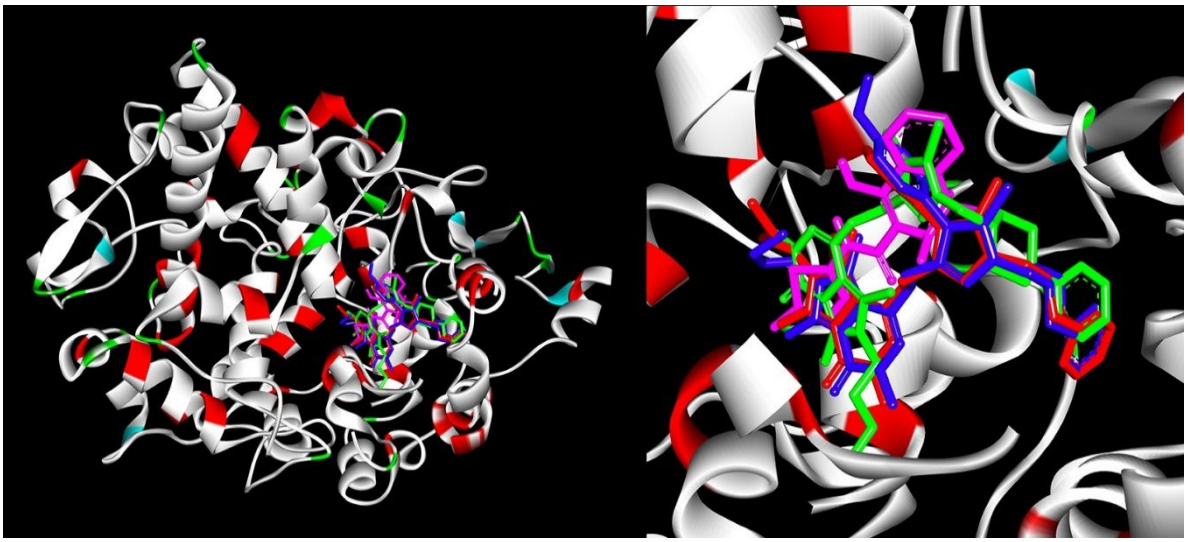

Fig. 22. The docking poses of compounds **4a(P3)** (green), **4b(P3)** (red), **4c(P3)** (blue) and meloxicam (pink) in the active site of COX-2.

The anti-inflammatory activity of the title derivatives was also assessed in a modified MTT experiment on the NHDF cell line. The model of inflammation induced by the addition of lipopolysaccharide (LPS) has been introduced. The cells were first incubated for 24h with the addition of LPS, which is a known proinflammatory factor[1,4], and then for another day with the test compounds at various concentrations. Based on the obtained results, we can conclude that all derivatives (except **5c(P3)** and **6c(P3)** in concentrations of 50 and 100 μM) increased cell survival concerning the positive control. This suggests their potentially good anti-inflammatory activity. Additionally, for compounds **6a(P3)** and **9a(P3)**, a statistically significant increase in mitochondrial activity was observed in relation to the negative control.

Subsequently, the DCF-DA and Griess assays were performed. All derivatives in the entire range of tested concentrations decreased the level of free oxygen radicals in comparison with the positive control. Moreover, in the case of compounds **6a(P3)** and **9a(P3)**, a decrease in the concentration of ROS to the level of negative control was observed. Also, in the Griess test, a statistically significant reduction in the amount of NO was noted for each compound over the entire range of tested concentrations. The derivative **9a(P3)** showed the best activity in this assay - in its case, after the incubation period, the NO concentration was close to the negative control.

A detailed description of *in vitro* experiments assessing the anti-inflammatory and antioxidant activity of new derivatives, along with the necessary tables, are included in *Chapter 2.4* of the publication **P3**.

The abovementioned enzymatic and *in vitro* experiments were supplemented with studies estimating the pharmacokinetic properties of the title compounds. Using spectroscopic methods, i.e. fluorescence quenching, CD, FTIR and molecular docking, the model of interaction of 1,2,4-triazole derivatives of pyrrolo[3,4-*d*]pyridazinone with plasma albumin was described. Based on the measurements of both CD and FTIR, it was found that in the presence of the tested compounds, changes in the secondary structure of BSA take place. It proves that the ligands interact with the protein. These findings are consistent with the results of fluorescence spectroscopy, based on which we can say that the interaction of new derivatives with BSA consists in the formation of complexes in an approximate ratio of 1: 1. According to the data obtained during molecular docking, the 1,2,4-triazole derivatives of pyrrolo[3,4-*d*]pyridazinone bind to subdomain IIIA in the hydrophobic pocket of the domain II(m) of BSA. A detailed discussion of these results with the necessary tables, formulas and spectroscopic spectra can be found in *Chapter 2.6* of the publication **P3** and in the supplementary data of this work.

Additionally, basic *in silico* investigations were performed with the use of freeware online programs. It allowed us to determine such physicochemical features, such as the topological polar surface area (TPSA), LOG P and others. These data were necessary to estimate potential pharmacokinetic parameters based on various computational models, such as Lipiński's five rule. Details can be found in *Chapter 2.7* of publication **P3**.

To summarize, the results obtained in carried out investigations were interesting and somewhat varied. Moreover, the studied group of compounds was quite numerous. Therefore, after a thorough analysis of the findings, it was possible to present some structure-activity relationships (SAR) within the 1,2,4-triazole derivatives of pyrrolo[3,4-d]pyridazinone. These dependencies were discussed in detail in *Chapter 2.5* of the publication **P3**. **Figure 23** shows schematically the most important conclusions.

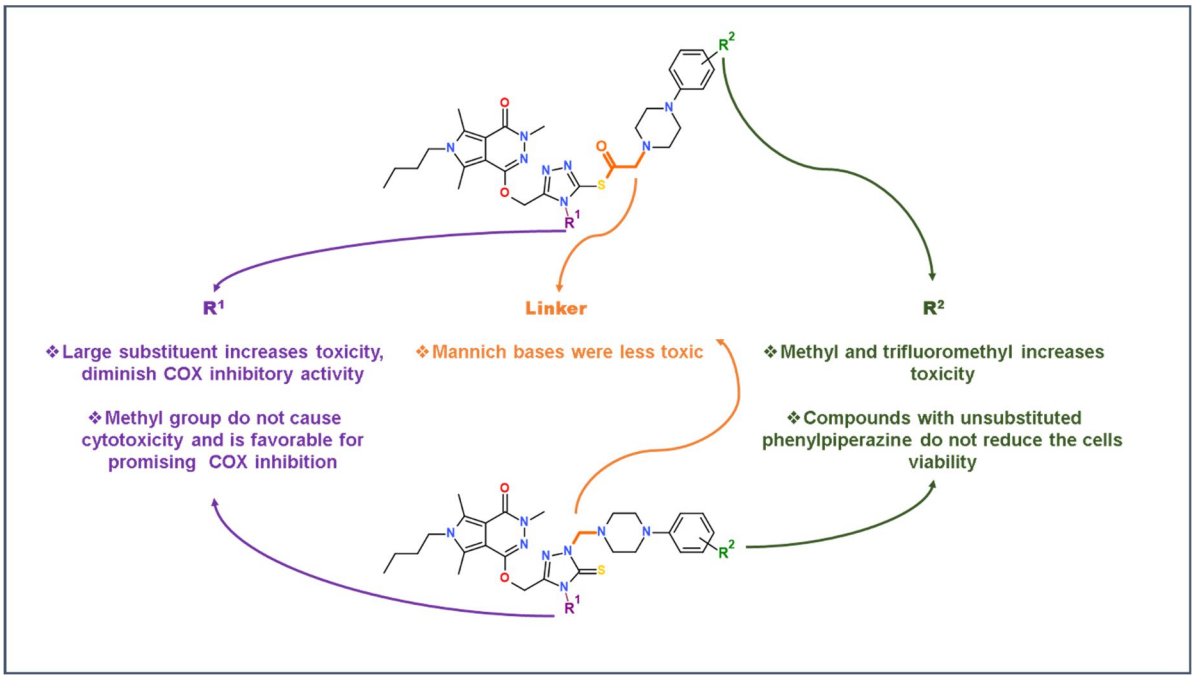

Fig. 23. The structure-activity relationships in the group of 1,2,4-triazole derivatives of pyrrolo[3,4-d]pyridazinone.

5 SUMMARY AND CONCLUSIONS

As part of the research, which is the subject of this dissertation, a total of 48 new, hitherto unknown derivatives of pyrrolo[3,4-*d*]pyridazinone were obtained. The structure of each compound was described and confirmed based on advanced spectral techniques.

The performed synthesis consisted of several stages. The first one was to obtain ester derivatives of the pyrrolo[3,4-*d*]pyridazinone core (**Fig. 5**). The proper esters gave the corresponding hydrazides by reaction with hydrazine hydrate in the next step. Subsequently, cyclic (1,3,4-oxadiazole and 1,2,4-triazole) derivatives of said hydrazides were received. As a result, we got 12 new intermediates which were necessary to obtain the title compounds with the expected analgesic and anti-inflammatory activity and low gastrotoxicity (**Fig. 4**). Consequently, three series of final derivatives were received. Series **I** and **II** compounds are the 1,3,4-oxadiazole derivatives of pyrrolo[3,4-*d*]pyridazinone, while series **III** are their 1,2,4-triazole analogues. In these compounds' structures, an arylpiperazinyl/piperidinyl moiety can be distinguished. After proper purification and confirmation of their structure, biological, spectral and molecular docking tests were carried out to assess the toxicity and biological activity of the title derivatives.

According to the assumed concept, it was possible to obtain compounds that were non-toxic and showed promising analgesic and anti-inflammatory activity. The results of the conducted research confirmed that the introduction of 1,3,4-oxadiazole or 1,2,4-triazole ring into the designed structure of title compounds allowed to obtain molecules with a good affinity for cyclooxygenase, especially for its induced COX-2 isoform. It has been proven by enzymatic experiments and molecular docking that most of the new pyrrolo[3,4-*d*]pyridazinone derivatives effectively inhibit cycloxygenase preferentially or selectively to COX-2. Moreover, some of them were more effective than meloxicam, which was used as a reference.

Moreover, it has been shown that some of the obtained derivatives act as antioxidants - they reduce the concentration of free radicals in the induced oxidative stress and exert a protective effect on chromatin. This, in turn, somewhat indirectly confirms their potentially good anti-inflammatory activity.

The promising biological activity that the new derivatives revealed in *in vitro* tests was confirmed by the results of carried out *in vivo* experiments. Two compounds were selected for such evaluation. Analyzed derivatives showed comparable, to indomethacin, analgesic and

anti-inflammatory activity in the studies performed in the animal model. Importantly, it was proved that the new pyrrolo[3,4-*d*]pyridazinone derivatives reduce the concentration of inflammatory mediators, such as MPO, TNF-α, and above all PGE_2, which may confirm that their mechanism of action is related to the inhibition of COX.

It is worth emphasizing that the tested derivatives did not cause any damage or pathological changes in the gastric mucosa, which are characteristic of classic NSAIDs. This was confirmed by macro- and microscopic analysis of the gastric mucosa of the animals participating in the study. These results proved the rightness of the modifications carried out, consisting of the introduction of 1,3,4-oxadiazole or 1,2,4-triazole ring into the structure of title molecules. It has been proven that the replacement of a free carboxyl group with bioisosteric moiety results in almost complete elimination of the side effects of the examined compounds on the gastrointestinal tract.

Taking into account the results of all the conducted research, it should be stated that the goals and assumptions adopted during the planning and implementation of this work have been fulfilled. Without any doubt, it has been proved that 1,3,4-oxadiazole and 1,2,4-triazole derivatives of pyrrolo[3,4-*d*]pyridazinone are interesting and promising compounds with a beneficial pharmacological profile. They exert good anti-inflammatory and analgesic activity and, what is very important, do not show gastrotoxicity. For this reason, these derivatives may be of significant importance in the context of the search for new compounds that could be successfully used in the effective and, above all, safe therapy of pain various inflammatory disorders.

ABSTRACT

Introduction:

Effective and safe treatment of various pain and inflammatory diseases is a significant and challenging clinical problem for modern medicine and pharmacy. The commonly used NSAIDs have limited efficiency, and their chronic use carries a considerable risk of dangerous gastrointestinal side effects, which notably limits their long-term usage. For this reason, it is necessary and justified to search for new compounds that possess potent analgesic and anti-inflammatory activity, but at the same time, are safe and free of severe side effects.

The objective of study:

The aims of the conducted research were the design and synthesis of new 1,3,4-oxadiazole and 1,2,4-triazole derivatives of pyrrolo[3,4-*d*]pyridazinone with the expected good analgesic and anti-inflammatory activity and the lack of harmful impact on the gastric mucosa. Subsequently, the evaluation of the new compounds' toxicity and the pharmacological activity profile in *in vitro* and *in vivo* experiments has been carried out.

Materials and methods:

Commercially available solvents, reagents and gcatalysts were used in the synthesis, analysis and purification of the newly received compounds. Their structure was confirmed using different spectroscopic techniques such as NMR, MS, FT-IR and elemental analysis. Toxicity and biological activity of novel derivatives were assessed using appropriate enzyme tests, cell lines and animals. Molecular docking and various types of spectral studies, such as FT-IR, CD, were also performed.

Results and conclusions:

The new 1,3,4-oxadiazole and 1,2,4-triazole derivatives of pyrrolo[3,4-*d*]pyridazinone turned out to be devoid of cytotoxic activity and most of them show good anti-inflammatory activity *in vitro*. These compounds preferentially or selectively block the induced COX-2 enzyme. Their potency is comparable to that of meloxicam. Moreover, the tested compounds show anti-radical activity and protect chromatin against damage caused by oxidative stress. Their promising biological activity was confirmed by experiments performed in an animal model. The tested compounds effectively inhibit the pain and inflammatory reaction *in vivo*, reduce the concentration of inflammatory mediators in the plasma and, what is very important, do not cause damage to the gastric mucosa. Therefore, the obtained results indicate that the pyrrolo[3,4-*d*]pyridazinone derivatives being the subject of this dissertation, are interesting and promising candidates for new, effective and safe drugs with potential application in the treatment of various types of inflammatory diseases.

PIŚMIENNICTWO

BIBLIOGRAPHY

(1) Nathan, C. Points of Control in Inflammation. *Nature* **2002**, *420* (6917), 846–852. https://doi.org/10.1038/nature01320.

(2) Serhan, C. N.; Savill, J. Resolution of Inflammation: The Beginning Programs the End. *Nat. Immunol.* **2005**, *6* (12), 1191–1197. https://doi.org/10.1038/ni1276.

(3) Negus, S. S.; Vanderah, T. W.; Brandt, M. R.; Bilsky, E. J.; Becerra, L.; Borsook, D. Preclinical Assessment of Candidate Analgesic Drugs: Recent Advances and Future Challenges. *J. Pharmacol. Exp. Ther.* **2006**, *319* (2), 507–514. https://doi.org/10.1124/JPET.106.106377.

(4) Medzhitov, R. Origin and Physiological Roles of Inflammation. *Nature* **2008**, *454* (7203), 428–435. https://doi.org/10.1038/nature07201.

(5) Medzhitov, R. Inflammation 2010: New Adventures of an Old Flame. *Cell* **2010**, *140* (6), 771–776. https://doi.org/10.1016/J.CELL.2010.03.006.

(6) Leuti, A.; Fazio, D.; Fava, M.; Piccoli, A.; Oddi, S.; Maccarrone, M. Bioactive Lipids, Inflammation and Chronic Diseases. *Adv. Drug Deliv. Rev.* **2020**, *159*, 133–169. https://doi.org/10.1016/j.addr.2020.06.028.

(7) Vane, J. R.; Botting, R. M. Mechanism of Action of Nonsteroidal Anti-Inflammatory Drugs. *Am. J. Med.* **1998**, *104* (3 A), 25–85. https://doi.org/10.1016/S0002-9343(97)00203-9.

(8) Cashman, J. N. The Mechanisms of Action of NSAIDs in Analgesia. *Drugs* **1996**, *52* (5), 13–23. https://doi.org/10.2165/00003495-199600525-00004.

(9) Blobaum, A. L.; Marnett, L. J.; Hancock, A. B. Perspective Structural and Functional Basis of Cyclooxygenase Inhibition. **2006**, *50* (7), 1425–1441. https://doi.org/10.1021/jm0613166.

(10) Marnett, L. J. Cyclooxygenase Mechanisms. *Curr. Opin. Chem. Biol.* **2000**, *4* (5), 545–552. https://doi.org/10.1016/s1367-5931(00)00130-7.

(11) Soliva, R.; Almansa, C.; G. Kalko, S.; Javier Luque, F.; Orozco, M. Theoretical Studies on the Inhibition Mechanism of Cyclooxygenase-2. Is There a Unique Recognition Site? *J. Med. Chem.* **2003**, *46* (8), 1372–1382. https://doi.org/10.1021/jm0209376.

(12) Wallace, J. L.; Devchand, P. R. Emerging Roles for Cyclooxygenase-2 in Gastrointestinal Mucosal Defense. *Br. J. Pharmacol.* **2005**, *145* (3), 275–282. https://doi.org/10.1038/sj.bjp.0706201.

(13) Cannon, C. P.; Cannon, P. J. Physiology. COX-2 Inhibitors and Cardiovascular Risk. *Science* **2012**, *336* (6087), 1386–1387. https://doi.org/10.1126/SCIENCE.1224398.

(14) Dogné, J.-M.; T. Supuran, C.; Pratico, D. Adverse Cardiovascular Effects of the Coxibs. *J. Med. Chem.* **2005**, *48* (7), 2251–2257. https://doi.org/10.1021/jm0402059.

(15) Sostres, C.; Gargallo, C. J.; Arroyo, M. T.; Lanas, A. Adverse Effects of Non-Steroidal Anti-Inflammatory Drugs (NSAIDs, Aspirin and Coxibs) on Upper Gastrointestinal Tract. *Best Pract. Res. Clin. Gastroenterol.* **2010**, *24* (2), 121–132. https://doi.org/10.1016/j.bpg.2009.11.005.

(16) Soll, A. H.; McCarthy, D. NSAID-Related Gastrointestinal Complications. *Clin. Cornerstone* **1999**, *1* (5), 42–56. https://doi.org/10.1016/s1098-3597(99)90088-1.

(17) Wallace, J. L. NSAID Gastropathy and Enteropathy: Distinct Pathogenesis Likely Necessitates Distinct Prevention Strategies. *Br. J. Pharmacol.* **2012**, *165* (1), 67–74. https://doi.org/10.1111/j.1476-5381.2011.01509.x.

(18) Laine, L. Gastrointestinal Effects of NSAIDs and Coxibs. *J. Pain Symptom Manage.* **2003**, *25* (2 SUPPL.), 32–40. https://doi.org/10.1016/s0885-3924(02)00629-2.

(19) Palkar, M. B.; Singhai, A. S.; Ronad, P. M.; Vishwanathswamy, A. H. M.; Boreddy, T. S.; Veerapur, V. P.; Shaikh, M. S.; Rane, R. A.; Karpoormath, R. Synthesis, Pharmacological Screening and in Silico Studies of New Class of Diclofenac Analogues as a Promising Anti-Inflammatory Agents. *Bioorganic Med. Chem.* **2014**, *22* (10), 2855–2866. https://doi.org/10.1016/j.bmc.2014.03.043.

(20) Manjunatha, K.; Poojary, B.; Lobo, P. L.; Fernandes, J.; Kumari, N. S. Synthesis and Biological Evaluation of Some 1,3,4-Oxadiazole Derivatives. *Eur. J. Med. Chem.* **2010**, *45* (11), 5225–5233. https://doi.org/10.1016/j.ejmech.2010.08.039.

(21) Alsayed, S. S. R.; Elshemy, H. A. H.; Abdelgawad, M. A.; Abdel-Latif, M. S.; Abdellatif, K. R. A. Design, Synthesis and Biological Screening of Some Novel Celecoxib and Etoricoxib Analogs with Promising COX-2 Selectivity, Anti-Inflammatory Activity and Gastric Safety Profile. *Bioorg. Chem.* **2017**, *70*, 173–183. https://doi.org/10.1016/j.bioorg.2016.12.008.

(22) Avci, A.; Taşci, H.; Kandemir, Ü.; Can, Ö. D.; Gökhan-Kelekçi, N.; Tozkoparan, B. Synthesis, Characterization, and in Vivo Pharmacological Evaluation of Novel Mannich Bases Derived from 1,2,4-Triazole Containing a Naproxen Moiety. *Bioorg. Chem.* **2020**, *100*, 103892. https://doi.org/10.1016/j.bioorg.2020.103892.

(23) El-Sayed, N. A.; Nour, M. S.; Salem, M. A.; Arafa, R. K. New Oxadiazoles with Selective-COX-2 and EGFR Dual Inhibitory Activity: Design, Synthesis, Cytotoxicity Evaluation and in Silico Studies. *Eur. J. Med. Chem.* **2019**, *183*, 111693. https://doi.org/10.1016/j.ejmech.2019.111693.

(24) Abdellatif, K. R. A.; Abdelall, E. K. A.; Lamie, P. F.; Labib, M. B.; El-Nahaas, E. S.; Abdelhakeem, M. M. New Pyrazole Derivatives Possessing Amino/methanesulphonyl Pharmacophore with Good Gastric Safety Profile: Design, Synthesis, Cyclooxygenase Inhibition, Anti-Inflammatory Activity and Histopathological Studies. *Bioorg. Chem.* **2020**, *95*, 103540. https://doi.org/10.1016/j.bioorg.2019.103540.

(25) Mohassab, A. M.; Hassan, H. A.; Abdelhamid, D.; Gouda, A. M.; Gomaa, H. A. M.; Youssif, B. G. M.; Radwan, M. O.; Fujita, M.; Otsuka, M.; Abdel-Aziz, M. New quinoline/1,2,4-Triazole Hybrids as Dual Inhibitors of COX-2/5-LOX and Inflammatory Cytokines: Design, Synthesis, and Docking Study. *J. Mol. Struct.* **2021**, *1244*, 130948. https://doi.org/10.1016/j.molstruc.2021.130948.

(26) Szczukowski, Ł.; Redzicka, A.; Wiatrak, B.; Krzyżak, E.; Marciniak, A.; Gębczak, K.; Gębarowski, T.; Świątek, P. Design, Synthesis, Biological Evaluation and in Silico Studies of Novel pyrrolo[3,4-D]pyridazinone Derivatives with Promising Anti-Inflammatory and Antioxidant Activity. *Bioorg. Chem.* **2020**, *102*, 104035. https://doi.org/10.1016/j.bioorg.2020.104035.

(27) Redzicka, A.; Szczukowski, Ł.; Kochel, A.; Wiatrak, B.; Gębczak, K.; Czyżnikowska, Ż. COX-1/COX-2 Inhibition Activities and Molecular Docking Study of Newly Designed and Synthesized pyrrolo[3,4-C]pyrrole Mannich Bases. *Bioorganic Med. Chem.* **2019**, *27* (17). https://doi.org/10.1016/j.bmc.2019.07.033.

(28) Szczukowski, Ł.; Krzyżak, E.; Zborowska, A.; Zając, P.; Potyrak, K.; Peregrym, K.; Wiatrak, B.; Marciniak, A.; Świątek, P. Design, Synthesis and Comprehensive Investigations of Pyrrolo[3,4-D]pyridazinone-Based 1,3,4-Oxadiazole as New Class of Selective COX-2 Inhibitors. *Int. J. Mol. Sci.* **2020**, *21* (24), 9623. https://doi.org/10.3390/IJMS21249623.

(29) Abdelazeem, A. H.; El-Din, A. G. S.; Arab, H. H.; El-Saadi, M. T.; El-Moghazy, S. M.; Amin, N. H. Design, Synthesis and Anti-Inflammatory/analgesic Evaluation of Novel Di-Substituted Urea Derivatives Bearing Diaryl-1,2,4-Triazole with Dual COX-2/sEH Inhibitory Activities. *J. Mol. Struct.* **2021**, *1240*, 130565. https://doi.org/10.1016/J.MOLSTRUC.2021.130565.

(30) Abdellatif, K. R. A.; Abdelall, E. K. A.; Elshemy, H. A. H.; Philoppes, J. N.; Hassanein, E. H. M.; Kahk, N. M. Optimization of Pyrazole-Based Compounds with 1,2,4-Triazole-3-Thiol Moiety as Selective COX-2 Inhibitors Cardioprotective Drug Candidates: Design, Synthesis, Cyclooxygenase Inhibition, Anti-Inflammatory, Ulcerogenicity, Cardiovascular Evaluation, and Molecular Modeling Studies. *Bioorg. Chem.* **2021**, *114*, 105122. https://doi.org/10.1016/J.BIOORG.2021.105122.

(31) Dal Piaz, V.; Vergelli, C.; Giovannoni, M. P.; Scheideler, M. A.; Petrone, G.; Zaratin, P. 4-Amino-3(2H)-Pyridazinones Bearing Arylpiperazinylalkyl Groups and Related Compounds: Synthesis and Antinociceptive Activity. *Farmaco* **2003**, *58* (11), 1063–1071. https://doi.org/10.1016/S0014-827X(03)00162-9.

(32) Ahmed, E. M.; Kassab, A. E.; El-Malah, A. A.; Hassan, M. S. A. Synthesis and Biological Evaluation of Pyridazinone Derivatives as Selective COX-2 Inhibitors and Potential Anti-Inflammatory Agents. *Eur. J. Med. Chem.* **2019**, 25–37. https://doi.org/10.1016/j.ejmech.2019.03.036.

(33) Li, C. S.; Brideau, C.; Chan, C. C.; Savoie, C.; Claveau, D.; Charleson, S.; Gordon, R.; Greig, G.; Gauthier, J. Y.; Lau, C. K.; Riendeau, D.; Thérien, M.; Wong, E.; Prasit, P. Pyridazinones as Selective Cyclooxygenase-2 Inhibitors. *Bioorganic Med. Chem. Lett.* **2003**, *13* (4), 597–600. https://doi.org/10.1016/S0960-894X(02)01045-4.

(34) Abouzid, K.; Bekhit, S. A. Novel Anti-Inflammatory Agents Based on Pyridazinone Scaffold; Design, Synthesis and in Vivo Activity. *Bioorganic Med. Chem.* **2008**, *16* (10), 5547–5556. https://doi.org/10.1016/j.bmc.2008.04.007.

(35) Gökçe, M.; Utku, S.; Küpeli, E. Synthesis and Analgesic and Anti-Inflammatory Activities 6-Substituted-3(2H)-Pyridazinone-2-Acetyl-2-(P-Substituted/nonsubstituted Benzal)hydrazone Derivatives. *Eur. J. Med. Chem.* **2009**, *44* (9), 3760–3764. https://doi.org/10.1016/j.ejmech.2009.04.048.

(36) Malinka, W.; Redzicka, A.; Jastrzbska Więsek, M.; Filipek, B.; Dybała, M.; Karczmarzyk, Z.; Urbańczyk-Lipkowska, Z.; Kalicki, P. Derivatives of pyrrolo[3,4-D]pyridazinone, a New Class of Analgesic Agents. *Eur. J. Med. Chem.* **2011**, *46* (10), 4992–4999. https://doi.org/10.1016/j.ejmech.2011.08.006.

(37) Mogilski, S.; Kubacka, M.; Redzicka, A.; Kazek, G.; Dudek, M.; Malinka, W.; Filipek, B. Antinociceptive, Anti-Inflammatory and Smooth Muscle Relaxant Activities of the pyrrolo[3,4-D]pyridazinone Derivatives: Possible Mechanisms of Action. *Pharmacol. Biochem. Behav.* **2015**, *133*, 99–110. https://doi.org/10.1016/j.pbb.2015.03.019.

(38) Abdel-Aziz, M.; Beshr, E. A.; Abdel-Rahman, I. M.; Ozadali, K.; Tan, O. U.; Aly, O. M. 1-(4-Methoxyphenyl)-5-(3,4,5-Trimethoxyphenyl)-1H-1,2,4-Triazole-3-Carboxamides: Synthesis, Molecular Modeling, Evaluation of Their Anti-Inflammatory Activity and Ulcerogenicity. *Eur. J. Med. Chem.* **2014**, *77*, 155–165. https://doi.org/10.1016/J.EJMECH.2014.03.001.

(39) Ünsal-Tan, O.; Özden, K.; Rauk, A.; Balkan, A. Synthesis and Cyclooxygenase Inhibitory Activities of Some N-Acylhydrazone Derivatives of isoxazolo[4,5-D]pyridazin-4(5H)-Ones. *Eur. J. Med. Chem.* **2010**, *45* (6), 2345–2352. https://doi.org/10.1016/J.EJMECH.2010.02.012.

(40) Akhtar, W.; Shaquiquzzaman, M.; Akhter, M.; Verma, G.; Khan, M. F.; Alam, M. M. The Therapeutic Journey of Pyridazinone. *European Journal of Medicinal Chemistry*. Elsevier Masson SAS 2016, pp 256–281. https://doi.org/10.1016/j.ejmech.2016.07.061.

(41) Asif, M. Annals of Medicinal Chemistry and Research Overview on Emorfazone and Other Related 3(2H) Pyridazinone Analogues Displaying Analgesic and Anti-Inflammatory Activity. **2015**.

(42) Abdellatif, K. R.; Abdelall, E. K.; Elshemy, H. A.; Lamie, P. F.; Elnahaas, E.; Amin, D. M. Design, Synthesis of New Anti-Inflammatory Agents with a Pyrazole Core: COX-1/COX-2 Inhibition Assays, Anti-Inflammatory, Ulcerogenic, Histopathological, Molecular Modeling, and ADME Studies. *J. Mol. Struct.* **2021**, *1240*, 130554. https://doi.org/10.1016/j.molstruc.2021.130554.

(43) Sağlık, B. N.; Osmaniye, D.; Levent, S.; Çevik, U. A.; Çavuşoğlu, B. K.; Özkay, Y.; Kaplancıklı, Z. A. Design, Synthesis and Biological Assessment of New Selective COX-2 Inhibitors Including Methyl Sulfonyl Moiety. *Eur. J. Med. Chem.* **2021**, *209*, 112918. https://doi.org/10.1016/J.EJMECH.2020.112918.

(44) Jacob P, J.; Manju, S. L. Identification and Development of Thiazole Leads as COX-2/5-LOX Inhibitors through in-Vitro and in-Vivo Biological Evaluation for Anti-Inflammatory Activity. *Bioorg. Chem.* **2020**, *100*, 103882. https://doi.org/10.1016/J.BIOORG.2020.103882.

(45) Abdel-Aziz, S. A.; Taher, E. S.; Lan, P.; Asaad, G. F.; Gomaa, H. A. M.; El-Koussi, N. A.; Youssif, B. G. M. Design, Synthesis, and Biological Evaluation of New Pyrimidine-5-Carbonitrile Derivatives Bearing 1,3-Thiazole Moiety as Novel Anti-Inflammatory EGFR Inhibitors with Cardiac Safety Profile. *Bioorg. Chem.* **2021**, *111*, 104890. https://doi.org/10.1016/J.BIOORG.2021.104890.

(46) Dogruer, D. S.; Sahin, M. F.; Ünlü, S.; Ito, S. Studies on Some 3(2H)-Pyridazinone Derivatives with Antinociceptive Activity. *Arch. Pharm. (Weinheim).* **2000**, *333* (4), 79–86. https://doi.org/10.1002/(SICI)1521-4184(20004)333:4<79::AID-ARDP79>3.0.CO;2-S.

(47) Dogruer, D. S.; Kupeli, E.; Yesilada, E.; Sahin, M. F. Synthesis of New 2-[1(2H)-Phthalazinon-2-Yl]acetamide and 3-[1(2H)-Phthalazinon-2-Yl]propanamide Derivatives as Antinociceptive and Anti-Inflammatory Agents. *Arch. Pharm. (Weinheim).* **2004**, *337* (6), 303–310. https://doi.org/10.1002/ardp.200200719.

(48) McGarry, T.; Biniecka, M.; Veale, D. J.; Fearon, U. Hypoxia, Oxidative Stress and Inflammation. *Free Radic. Biol. Med.* **2018**, *125*, 15–24. https://doi.org/10.1016/j.freeradbiomed.2018.03.042.

(49) Burdon, C.; Mann, C.; Cindrova-Davies, T.; Ferguson-Smith, A. C.; Burton, G. J. Oxidative Stress and the Induction of Cyclooxygenase Enzymes and Apoptosis in the Murine Placenta. *Placenta* **2007**, *28* (7), 724–733. https://doi.org/10.1016/j.placenta.2006.12.001.

(50) Gao, Z.; Zhang, H.; Liu, J.; Lau, C. W.; Liu, P.; Chen, Z. Y.; Lee, H. K.; Tipoe, G. L.; Ho, H. M.; Yao, X.; Huang, Y. Cyclooxygenase-2-Dependent Oxidative Stress Mediates Palmitate-Induced Impairment of Endothelium-Dependent Relaxations in Mouse Arteries. *Biochem. Pharmacol.* **2015**, *91* (4), 474–482. https://doi.org/10.1016/j.bcp.2014.08.009.

(51) Li, D.; Zhu, M.; Xu, C.; Ji, B. Characterization of the Baicalein-Bovine Serum Albumin Complex without or with Cu 2+or Fe 3+ by Spectroscopic Approaches. *Eur. J. Med. Chem.* **2011**, *46* (2), 588–599. https://doi.org/10.1016/j.ejmech.2010.11.038.

(52) Shi, J. hua; Pan, D. qi; Wang, X. xiou; Liu, T. T.; Jiang, M.; Wang, Q. Characterizing the Binding Interaction between Antimalarial Artemether (AMT) and Bovine Serum Albumin (BSA): Spectroscopic and Molecular Docking Methods. *J. Photochem. Photobiol. B Biol.* **2016**, *162*, 14–23. https://doi.org/10.1016/j.jphotobiol.2016.06.025.

(53) Szandruk-Bender, M.; Wiatrak, B.; Szczukowski, Ł.; Świątek, P.; Rutkowska, M.; Dzimira, S.; Merwid-Ląd, A.; Danielewski, M.; Szeląg, A. Oxadiazole Derivatives of Pyrrolo[3,4-D]pyridazinone Exert Antinociceptive Activity in the Tail-Flick and Formalin Test in Rodents and Reveal Reduced Gastrotoxicity. *Int. J. Mol. Sci.* **2020**, *21* (24), 9685. https://doi.org/10.3390/ijms21249685.

(54) Hunskaar, S.; Hole, K. The Formalin Test in Mice: Dissociation between Inflammatory and Non-Inflammatory Pain. *Pain* **1987**, *30* (1), 103–114. https://doi.org/10.1016/0304-3959(87)90088-1.

(55) Tjølsen, A.; Berge, O. G.; Hunskaar, S.; Rosland, J. H.; Hole, K. The Formalin Test: An Evaluation of the Method. *Pain* **1992**, *51* (1), 5–17. https://doi.org/10.1016/0304-3959(92)90003-T.

(56) Guerrero, A. T. G.; Verri, W. A.; Cunha, T. M.; Silva, T. A.; Schivo, I. R. S.; Dal-Secco, D.; Canetti, C.; Rocha, F. A. C.; Parada, C. A.; Cunha, F. Q.; Rgio, S.; Ferreira, H. Involvement of LTB4 in Zymosan-Induced Joint Nociception in Mice: Participation of Neutrophils and PGE2. *J. Leukoc. Biol.* **2008**, *83* (1), 122–130. https://doi.org/10.1189/JLB.0207123.

(57) Verri, W. A.; Cunha, T. M.; Magro, D. A.; Guerrero, A. T. G.; Vieira, S. M.; Carregaro, V.; Souza, G. R.; Henriques, M. D. G. M. O.; Ferreira, S. H.; Cunha, F. Q. Targeting Endothelin ETA and ETB Receptors Inhibits Antigen-Induced Neutrophil Migration and Mechanical Hypernociception in Mice. *Naunyn-Schmiedeberg's Arch. Pharmacol. 2008 3793* **2008**, *379* (3), 271–279. https://doi.org/10.1007/S00210-008-0360-1.

(58) Prokopowicz, Z.; Marcinkiewicz, J.; Katz, D. R.; Chain, B. M. Neutrophil Myeloperoxidase: Soldier and Statesman. *Arch. Immunol. Ther. Exp. 2011 601* **2011**, *60* (1), 43–54. https://doi.org/10.1007/S00005-011-0156-8.

(59) Wang, Z. Q.; Porreca, F.; Cuzzocrea, S.; Galen, K.; Lightfoot, R.; Masini, E.; Muscoli, C.; Mollace, V.; Ndengele, M.; Ischiropoulos, H.; Salvemini, D. A Newly Identified Role for Superoxide in Inflammatory Pain. *J. Pharmacol. Exp. Ther.* **2004**, *309* (3), 869–878. https://doi.org/10.1124/JPET.103.064154.

(60) Alabi, A. O.; Ajayi, A. M.; Omorogbe, O.; Umukoro, S. Anti-Nociceptive and Anti-Inflammatory Effects of an Aqueous Extract of Blended Leaves of Ocimum Gratissimum and Psidium Guajava. *Clin. Phytoscience 2019 51* **2019**, *5* (1), 1–9. https://doi.org/10.1186/S40816-019-0130-2.

(61) Szandruk-Bender, M.; Merwid-Ląd, A.; Wiatrak, B.; Danielewski, M.; Dzimira, S.; Szkudlarek, D.; Szczukowski, Ł.; Świątek, P.; Szeląg, A. Novel 1,3,4-Oxadiazole Derivatives of Pyrrolo [3,4-d]Pyridazinone Exert Anti-Inflammatory Activity without Acute Gastrotoxicity in the Carrageenan-Induced Rat Paw Edema Test. **2021**. https://doi.org/10.2147/JIR.S330614.

OŚWIADCZENIA AUTORÓW

AUTHORS' CONTRIBUTIONS

Wrocław, 30.01.2022

mgr Łukasz Szczukowski
Katedra i Zakład Chemii Leków
Uniwersytet Medyczny we Wrocławiu
50-556 Wrocław, ul. Borowska 211

OŚWIADCZENIE AUTORA

Oświadczam, że mój wkład w powstanie publikacji:

1. Ł. Szczukowski, A. Redzicka, B. Wiatrak, E. Krzyżak, A. Marciniak, K. Gębczak, T. Gębarowski, P. Świątek; *Design, synthesis, biological evaluation and in silico studies of novel pyrrolo[3,4-d]pyridazinone derivatives with promising anti-inflammatory and antioxidant activity*; **Bioorganic Chemistry**, 102 (**2020**), 104035; DOI: 10.1016/j.bioorg.2020.104035

polegał na opracowaniu koncepcji i planu wykonanych badań; zaprojektowaniu oraz zsyntetyzowaniu tytułowych związków; potwierdzeniu struktury i czystości otrzymanych pochodnych metodami spektroskopowymi; zebraniu, interpretacji oraz opisaniu wyników przeprowadzonych badań; współtworzeniu tekstu manuskryptu; korespondencji z redakcją; współtworzeniu finalnej formy publikacji;

2. Ł.Szczukowski, E. Krzyżak, A. Zborowska, P. Zając, K. Potyrak, K. Peregrym, B. Wiatrak, A. Marciniak, P. Świątek; *Design, synthesis and comprehensive investigations of pyrrolo[3,4-d]pyridazinone-based 1,3,4-oxadiazole as new class of selective COX-2 inhibitors*; **International Journal of Molecular Sciences, 2020**, 21(24), 9623; DOI: 10.3390/ijms21249623

polegał na opracowaniu koncepcji i planu wykonanych badań; zaprojektowaniu oraz zsyntetyzowaniu tytułowych związków; potwierdzeniu struktury i czystości otrzymanych pochodnych metodami spektroskopowymi; zebraniu, interpretacji oraz opisaniu wyników przeprowadzonych badań; współtworzeniu tekstu manuskryptu; korespondencji z redakcją; współtworzeniu finalnej formy publikacji;

3. Ł. Szczukowski, E. Krzyżak, B. Wiatrak, P. Jawień, A. Marciniak, A. Kotynia, P. Świątek; *New N-substituted-1,2,4-triazole derivatives of pyrrolo[3,4-d]pyridazinone with significant anti-inflammatory activity – design, synthesis and complementary in vitro, computational and spectroscopic studies*;
International Journal of Molecular Sciences, 2021, 22(20), 11235; DOI: 10.3390/ijms222011235

polegał na opracowaniu koncepcji i planu wykonanych badań; zaprojektowaniu oraz zsyntetyzowaniu tytułowych związków; potwierdzeniu struktury i czystości otrzymanych pochodnych metodami spektroskopowymi; określeniu właściwości fizykochemicznych i farmakokinetycznych metodami *in silico* nowych pochodnych, zebraniu, interpretacji oraz opisaniu wyników przeprowadzonych badań; współtworzeniu tekstu manuskryptu; korespondencji z redakcją; współtworzeniu finalnej formy publikacji;

Jednocześnie oświadczam, że wymienione powyżej publikacje, za zgodą wszystkich Współautorów, wchodzą w skład monotematycznego cyklu stanowiącego podstawę mojej rozprawy doktorskiej.

Łukasz Szczukowski

podpis autora

Uniwersytet Medyczny we Wrocławiu
KATEDRA I ZAKŁAD CHEMII LEKÓW
Kierownik
dr hab. Piotr Świątek

podpis promotora

Wrocław, 08.03.2022

dr hab. Piotr Świątek

Katedra i Zakład Chemii Leków

Uniwersytet Medyczny we Wrocławiu

50-556 Wrocław, ul. Borowska 211

OŚWIADCZENIE WSPÓŁAUTORA

Oświadczam, że mój wkład w powstanie publikacji:

1. Ł. Szczukowski, A. Redzicka, B. Wiatrak, E. Krzyżak, A. Marciniak, K. Gębczak, T. Gębarowski, P. Świątek; *Design, synthesis, biological evaluation and in silico studies of novel pyrrolo[3,4-d]pyridazinone derivatives with promising anti-inflammatory and antioxidant activity*; **Bioorganic Chemistry**, 102 (**2020**), 104035; DOI: 10.1016/j.bioorg.2020.104035

polegał na współtworzeniu koncepcji i założeń pracy, nadzorze nad przebiegiem badań, pomocy w analizie wyników, korekcie ostatecznej wersji manuskryptu.

2. Ł.Szczukowski, E. Krzyżak, A. Zborowska, P. Zając, K. Potyrak, K. Peregrym, B. Wiatrak, A. Marciniak, P. Świątek; *Design, synthesis and comprehensive investigations of pyrrolo[3,4-d]pyridazinone-based 1,3,4-oxadiazole as new class of selective COX-2 inhibitors*; **International Journal of Molecular Sciences**, **2020**, 21(24), 9623; DOI: 10.3390/ijms21249623

polegał na współtworzeniu koncepcji i założeń pracy, nadzorze nad przebiegiem badań, pomocy w analizie wyników, korekcie ostatecznej wersji manuskryptu.

3. Ł. Szczukowski, E. Krzyżak, B. Wiatrak, P. Jawień, A. Marciniak, A. Kotynia, P. Świątek; *New N-substituted-1,2,4-triazole derivatives of pyrrolo[3,4-d]pyridazinone with significant anti-inflammatory activity – design, synthesis and complementary in vitro, computational and spectroscopic studies*; **International Journal of Molecular Sciences**, **2021**, 22(20), 11235; DOI: 10.3390/ijms222011235

polegał na współtworzeniu koncepcji i założeń pracy, nadzorze nad przebiegiem badań, pomocy w analizie wyników, korekcie ostatecznej wersji manuskryptu.

Jednocześnie wyrażam zgodę, żeby wymienione powyżej publikacje mgr Łukasz Szczukowski przedstawił w formie monotematycznego cyklu stanowiącego podstawę jego rozprawy doktorskiej.

Uniwersytet Medyczny we Wrocławiu
KATEDRA I ZAKŁAD CHEMII LEKÓW
Kierownik

dr hab. Piotr Świątek
podpis współautora

Wrocław, 08.02.2022

dr inż. Benita Wiatrak

Katedra i Zakład Farmakologii

Uniwersytet Medyczny we Wrocławiu

50-345 Wrocław, ul. Mikulicza-Radeckiego 2

OŚWIADCZENIE WSPÓŁAUTORA

Oświadczam, że mój wkład w powstanie publikacji:

1. Ł. Szczukowski, A. Redzicka, B. Wiatrak, E. Krzyżak, A. Marciniak, K. Gębczak, T. Gębarowski, P. Świątek; *Design, synthesis, biological evaluation and in silico studies of novel pyrrolo[3,4d]pyridazinone derivatives with promising anti-inflammatory and antioxidant activity*; **Bioorganic Chemistry**, 102 (**2020**), 104035; DOI: 10.1016/j.bioorg.2020.104035

polegał na zaplanowaniu i przeprowadzeniu badań in vitro, opracowaniu wyników in vitro oraz na współudziale przy tworzeniu artykułu z tej części badań.

2. Ł.Szczukowski, E. Krzyżak, A. Zborowska, P. Zając, K. Potyrak, K. Peregrym, B. Wiatrak, A. Marciniak, P. Świątek; *Design, synthesis and comprehensive investigationsof pyrrolo[3,4d]pyridazinone-based 1,3,4oxadiazole as new class of selective COX-2 inhibitors*; **International Journal of Molecular Sciences**, **2020**, 21(24), 9623; DOI: 10.3390/ijms21249623

polegał na polegał na zaplanowaniu i przeprowadzeniu badań in vitro, opracowaniu wyników in vitro oraz na współudziale przy tworzeniu artykułu z tej części badań.

3. Ł. Szczukowski, E. Krzyżak, B. Wiatrak, P. Jawień, A. Marciniak, A. Kotynia, P. Świątek; *New Nsubstituted-1,2,4-triazole derivatives of pyrrolo[3,4-d]pyridazinone with significant anti-inflammatory activity – design, synthesis and complementary in vitro, computational and spectroscopic studies*; **International Journal of Molecular Sciences**, **2021**, 22(20), 11235; DOI: 10.3390/ijms222011235

polegał na polegał na zaplanowaniu i przeprowadzeniu badań in vitro, opracowaniu wyników in vitro oraz na współudziale przy tworzeniu artykułu z tej części badań.

Jednocześnie wyrażam zgodę, żeby wymienione powyżej publikacje mgr Łukasz Szczukowski przedstawił w formie monotematycznego cyklu stanowiącego podstawę jego rozprawy doktorskiej.

Beata Wiatrak

podpis współautora

Wrocław, 08.02.2022

dr Edward Krzyżak

Katedra i Zakład Chemii Nieorganicznej

Uniwersytet Medyczny we Wrocławiu

50-556 Wrocław, ul. Borowska 211a

OŚWIADCZENIE WSPÓŁAUTORA

Oświadczam, że mój wkład w powstanie publikacji:

1. Ł. Szczukowski, A. Redzicka, B. Wiatrak, E. Krzyżak, A. Marciniak, K. Gębczak, T. Gębarowski, P. Świątek; *Design, synthesis, biological evaluation and in silico studies of novel pyrrolo[3,4-d]pyridazinone derivatives with promising anti-inflammatory and antioxidant activity*; **Bioorganic Chemistry**, 102 (**2020**), 104035; DOI: 10.1016/j.bioorg.2020.104035

polegał na zbadaniu odziaływań z albuminą za pomocą spektroskopii fluorescencyjnej, dokowaniu badanych związków do Albuminy, COX-1,2, analizie otrzymanych wyników

2. Ł.Szczukowski, E. Krzyżak, A. Zborowska, P. Zając, K. Potyrak, K. Peregrym, B. Wiatrak, A. Marciniak, P. Świątek; *Design, synthesis and comprehensive investigationsof pyrrolo[3,4-d]pyridazinone-based 1,3,4-oxadiazole as new class of selective COX-2 inhibitors*; **International Journal of Molecular Sciences**, **2020**, 21(24), 9623; DOI: 10.3390/ijms21249623

polegał na zbadaniu odziaływań z albuminą za pomocą spektroskopii fluorescencyjnej, dokowaniu badanych związków do Albuminy, COX-2, analizie otrzymanych wyników

3. Ł. Szczukowski, E. Krzyżak, B. Wiatrak, P. Jawień, A. Marciniak, A. Kotynia, P. Świątek; *New N-substituted-1,2,4-triazole derivatives of pyrrolo[3,4-d]pyridazinone with significant anti-inflammatory activity – design, synthesis and complementary in vitro, computational and spectroscopic studies*; **International Journal of Molecular Sciences**, **2021**, 22(20), 11235; DOI: 10.3390/ijms222011235

polegał na zbadaniu odziaływań z albuminą za pomocą spektroskopii fluorescencyjnej, dokowaniu badanych związków do Albuminy, COX-2, analizie otrzymanych wyników

Jednocześnie wyrażam zgodę, żeby wymienione powyżej publikacje mgr Łukasz Szczukowski przedstawił w formie monotematycznego cyklu stanowiącego podstawę jego rozprawy doktorskiej.

Edward Kryzak

podpis współautora

Wrocław, 08.02.2022

dr inż. Aleksandra Marciniak

Katedra i Zakład Chemii Nieorganicznej

Uniwersytet Medyczny we Wrocławiu

50-556 Wrocław, ul. Borowska 211a

OŚWIADCZENIE WSPÓŁAUTORA

Oświadczam, że mój wkład w powstanie publikacji:

1. Ł. Szczukowski, A. Redzicka, B. Wiatrak, E. Krzyżak, A. Marciniak, K. Gębczak, T. Gębarowski, P. Świątek; *Design, synthesis, biological evaluation and in silico studies of novel pyrrolo[3,4-d]pyridazinone derivatives with promising anti-inflammatory and antioxidant activity*; **Bioorganic Chemistry**, 102 **(2020)**, 104035; DOI: 10.1016/j.bioorg.2020.104035

polegał na przeprowadzeniu pomiarów z wykorzystaniem metody spektroskopii dichroizmu kołowego oraz analizie i interpretacji otrzymanych wyników.

2. Ł.Szczukowski, E. Krzyżak, A. Zborowska, P. Zając, K. Potyrak, K. Peregrym, B. Wiatrak, A. Marciniak, P. Świątek; *Design, synthesis and comprehensive investigationsof pyrrolo[3,4-d]pyridazinone-based 1,3,4-oxadiazole as new class of selective COX-2 inhibitors*; **International Journal of Molecular Sciences, 2020**, 21(24), 9623; DOI: 10.3390/ijms21249623

polegał na przeprowadzeniu pomiarów z wykorzystaniem metody spektroskopii dichroizmu kołowego oraz analizie i interpretacji otrzymanych wyników.

3. Ł. Szczukowski, E. Krzyżak, B. Wiatrak, P. Jawień, A. Marciniak, A. Kotynia, P. Świątek; *New N-substituted-1,2,4-triazole derivatives of pyrrolo[3,4-d]pyridazinone with significant anti-inflammatory activity – design, synthesis and complementary in vitro, computational and spectroscopic studies*; **International Journal of Molecular Sciences, 2021**, 22(20), 11235; DOI: 10.3390/ijms222011235

polegał na przeprowadzeniu pomiarów z wykorzystaniem metody spektroskopii dichroizmu kołowego oraz analizie i interpretacji otrzymanych wyników.

Jednocześnie wyrażam zgodę, żeby wymienione powyżej publikacje mgr Łukasz Szczukowski przedstawił w formie monotematycznego cyklu stanowiącego podstawę jego rozprawy doktorskiej.

Aleksandra Marciniak

podpis współautora

Wrocław, 15.02.2022

dr Aleksandra Redzicka

Katedra i Zakład Chemii Leków

Uniwersytet Medyczny we Wrocławiu

50-556 Wrocław, ul. Borowska 211

OŚWIADCZENIE WSPÓŁAUTORA

Oświadczam, że mój wkład w powstanie publikacji:

Ł. Szczukowski, A. Redzicka, B. Wiatrak, E. Krzyżak, A. Marciniak, K. Gębczak, T. Gębarowski, P. Świątek; *Design, synthesis, biological evaluation and in silico studies of novel pyrrolo[3,4-d]pyridazinone derivatives with promising anti-inflammatory and antioxidant activity*; **Bioorganic Chemistry**, 102 (**2020**), 104035; DOI: 10.1016/j.bioorg.2020.104035

polegał na udziale w pracach syntetycznych oraz współtworzeniu tekstu manuskryptu

Jednocześnie wyrażam zgodę, żeby wymienione powyżej publikacje mgr Łukasz Szczukowski przedstawił w formie monotematycznego cyklu stanowiącego podstawę jego rozprawy doktorskiej.

Aleksandra Redzicka

podpis współautora

Wrocław, 17.02.2022

dr n. med. Katarzyna Gębczak

Katedra i Zakład Podstaw Nauk Medycznych

Uniwersytet Medyczny we Wrocławiu

50-556 Wrocław, ul. Borowska 211

OŚWIADCZENIE WSPÓŁAUTORA

Oświadczam, że mój wkład w powstanie publikacji:

Ł. Szczukowski, A. Redzicka, B. Wiatrak, E. Krzyżak, A. Marciniak, K. Gębczak, T. Gębarowski, P. Świątek; *Design, synthesis, biological evaluation and in silico studies of novel pyrrolo[3,4-d]pyridazinone derivatives with promising anti-inflammatory and antioxidant activity*; **Bioorganic Chemistry**, 102 (**2020**), 104035; DOI: 10.1016/j.bioorg.2020.104035

polegał na zaplanowaniu i przeprowadzeniu badań *in vitro*, interpretacji ich wyników oraz współtworzenia części manuskryptu dotyczącej badań biologicznych.

Jednocześnie wyrażam zgodę, żeby wymienione powyżej publikacje mgr Łukasz Szczukowski przedstawił w formie monotematycznego cyklu stanowiącego podstawę jego rozprawy doktorskiej.

Katarzyna Gębczak

podpis współautora

Wrocław, 14.02.2022

dr Tomasz Gębarowski

Katedra Biostruktury i Fizjologii Zwierząt

Uniwersytet Przyrodniczy we Wrocławiu

51-631 Wrocław, ul. Kożuchowska 1

OŚWIADCZENIE WSPÓŁAUTORA

Oświadczam, że mój wkład w powstanie publikacji:

Ł. Szczukowski, A. Redzicka, B. Wiatrak, E. Krzyżak, A. Marciniak, K. Gębczak, T. Gębarowski, P. Świątek; *Design, synthesis, biological evaluation and in silico studies of novel pyrrolo[3,4-d]pyridazinone derivatives with promising anti-inflammatory and antioxidant activity*; **Bioorganic Chemistry**, 102 (**2020**), 104035; DOI: 10.1016/j.bioorg.2020.104035

polegał na uczestnictwie w badaniach biologicznych

Jednocześnie wyrażam zgodę, żeby wymienione powyżej publikacje mgr Łukasz Szczukowski przedstawił w formie monotematycznego cyklu stanowiącego podstawę jego rozprawy doktorskiej.

Tomasz Gębarowski

podpis współautora

Wrocław, 15.02.2022r.

mgr Adrianna Zborowska

Studenckie Koło Naukowe przy Katedrze i Zakładzie Chemii Leków

Uniwersytet Medyczny we Wrocławiu

50-556 Wrocław, ul. Borowska 211

OŚWIADCZENIE WSPÓŁAUTORA

Oświadczam, że mój wkład w powstanie publikacji:

Ł.Szczukowski, E. Krzyżak, A. Zborowska, P. Zając, K. Potyrak, K. Peregrym, B. Wiatrak, A. Marciniak, P. Świątek; *Design, synthesis and comprehensive investigationsof pyrrolo[3,4-d]pyridazinone-based 1,3,4-oxadiazole as new class of selective COX-2 inhibitors*; **International Journal of Molecular Sciences**, **2020**, 21(24), 9623; DOI: 10.3390/ijms21249623

polegał na syntezie związków chemicznych, uczestnictwie w badaniach in vitro, oraz na udziale w przygotowaniu manuskryptu.

Jednocześnie wyrażam zgodę, żeby wymienione powyżej publikacje mgr Łukasz Szczukowski przedstawił w formie monotematycznego cyklu stanowiącego podstawę jego rozprawy doktorskiej.

Zborowska Adrianna

podpis współautora

Wrocław, 16.02.2022

mgr Katarzyna Potyrak

Studenckie Koło Naukowe przy Katedrze i Zakładzie Chemii Leków

Uniwersytet Medyczny we Wrocławiu

50-556 Wrocław, ul. Borowska 211

OŚWIADCZENIE WSPÓŁAUTORA

Oświadczam, że mój wkład w powstanie publikacji:

Ł.Szczukowski, E. Krzyżak, A. Zborowska, P. Zając, K. Potyrak, K. Peregrym, B. Wiatrak, A. Marciniak, P. Świątek; *Design, synthesis and comprehensive investigationsof pyrrolo[3,4-d]pyridazinone-based 1,3,4-oxadiazole as new class of selective COX-2 inhibitors*; **International Journal of Molecular Sciences, 2020**, 21(24), 9623; **DOI**: 10.3390/ijms21249623

polegał na współpracy przy syntezie badanych pochodnych pirolo[3,4-*d*]pirydazyny, wykonaniu doświadczeń techniką hodowli komórkowych oraz przygotowaniu tekstu manuskryptu.

Jednocześnie wyrażam zgodę, żeby wymienione powyżej publikacje mgr Łukasz Szczukowski przedstawił w formie monotematycznego cyklu stanowiącego podstawę jego rozprawy doktorskiej.

Katarzyna Potyrak

podpis współautora

Wrocław, 22.02.2022

mgr Patrycja Zając

Studenckie Koło Naukowe przy Katedrze i Zakładzie Chemii Leków

Uniwersytet Medyczny we Wrocławiu

50-556 Wrocław, ul. Borowska 211

OŚWIADCZENIE WSPÓŁAUTORA

Oświadczam, że mój wkład w powstanie publikacji:

Ł.Szczukowski, E. Krzyżak, A. Zborowska, P. Zając, K. Potyrak, K. Peregrym, B. Wiatrak, A. Marciniak, P. Świątek; *Design, synthesis and comprehensive investigationsof pyrrolo[3,4-d]pyridazinone-based 1,3,4-oxadiazole as new class of selective COX-2 inhibitors*; **International Journal of Molecular Sciences**, **2020**, 21(24), 9623; DOI: 10.3390/ijms21249623

polegał na: syntezie, ocenie biologicznej in vitro oraz pisemnym opracowaniu oryginalnego projektu.

Jednocześnie wyrażam zgodę, żeby wymienione powyżej publikacje mgr Łukasz Szczukowski przedstawił w formie monotematycznego cyklu stanowiącego podstawę jego rozprawy doktorskiej.

Zając Patrycja

podpis współautora

Wrocław, 16.02.2022

mgr Krzysztof Peregrym

Studenckie Koło Naukowe przy Katedrze i Zakładzie Chemii Leków

Uniwersytet Medyczny we Wrocławiu

50-556 Wrocław, ul. Borowska 211

OŚWIADCZENIE WSPÓŁAUTORA

Oświadczam, że mój wkład w powstanie publikacji:

Ł.Szczukowski, E. Krzyżak, A. Zborowska, P. Zając, K. Potyrak, K. Peregrym, B. Wiatrak, A. Marciniak, P. Świątek; *Design, synthesis and comprehensive investigations of pyrrolo[3,4-d]pyridazinone-based 1,3,4-oxadiazole as new class of selective COX-2 inhibitors*; **International Journal of Molecular Sciences**, **2020**, 21(24), 9623; DOI: 10.3390/ijms21249623

polegał na współpracy przy syntezie i ocenie aktywności biologicznej związków chemicznych omawianych w artykule.

Jednocześnie wyrażam zgodę, żeby wymienione powyżej publikacje mgr Łukasz Szczukowski przedstawił w formie monotematycznego cyklu stanowiącego podstawę jego rozprawy doktorskiej.

Krzysztof Peregrym

podpis współautora

Wrocław, 07.02.2022

dr Aleksandra Kotynia

Katedra i Zakład Chemii Nieorganicznej

Uniwersytet Medyczny we Wrocławiu

50-556 Wrocław, ul. Borowska 211a

OŚWIADCZENIE WSPÓŁAUTORA

Oświadczam, że mój wkład w powstanie publikacji:

Ł. Szczukowski, E. Krzyżak, B. Wiatrak, P. Jawień, A. Marciniak, A. Kotynia, P. Świątek; *New N-substituted-1,2,4-triazole derivatives of pyrrolo[3,4-d]pyridazinone with significant anti-inflammatory activity – design, synthesis and complementary in vitro, computational and spectroscopic studies*; **International Journal of Molecular Sciences, 2021**, 22(20), 11235; DOI: 10.3390/ijms222011235

polegał na przeprowadzeniu eksperymentów z wykorzystaniem metody spektroskopii FT-IR oraz analizie i interpretacji otrzymanych wyników.

Jednocześnie wyrażam zgodę, żeby wymienioną powyżej publikację mgr Łukasz Szczukowski przedstawił w formie monotematycznego cyklu stanowiącego podstawę jego rozprawy doktorskiej.

Aleksandra Kotynia

podpis współautora

Wrocław, 08.02.2022

mgr inż. Paulina Jawień

Katedra Biostruktury i Fizjologii Zwierząt

Uniwersytet Przyrodniczy we Wrocławiu

51-375 Wrocław, ul. Norwida 25/27

OŚWIADCZENIE WSPÓŁAUTORA

Oświadczam, że mój wkład w powstanie publikacji:

Ł. Szczukowski, E. Krzyżak, B. Wiatrak, P. Jawień, A. Marciniak, A. Kotynia, P. Świątek; *New N-substituted-1,2,4-triazole derivatives of pyrrolo[3,4-d]pyridazinone with significant anti-inflammatory activity – design, synthesis and complementary in vitro, computational and spectroscopic studies*; **International Journal of Molecular Sciences**, **2021**, 22(20), 11235; DOI: 10.3390/ijms222011235

polegał na zaplanowaniu i przeprowadzeniu badań in vitro.

Jednocześnie wyrażam zgodę, żeby wymienione powyżej publikacje mgr Łukasz Szczukowski przedstawił w formie monotematycznego cyklu stanowiącego podstawę jego rozprawy doktorskiej.

Paulina Jawień

podpis współautora

PUBLIKACJE WCHODZĄCE W SKŁAD ROZPRAWY

THE MANUSCRIPTS INCLUDED IN THE DISSERTATION

ISSN 0045-2068

ELSEVIER

BIO-ORGANIC CHEMISTRY

MECHANISMS FOR BIOLOGY

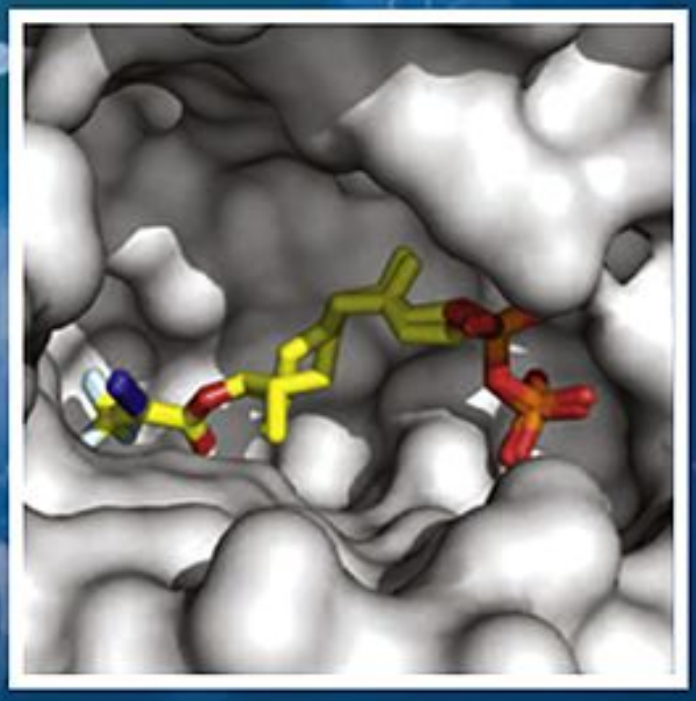

Available online at www.sciencedirect.com

ScienceDirect

Bioorganic Chemistry 102 (2020) 104035

Contents lists available at ScienceDirect

Bioorganic Chemistry

journal homepage: www.elsevier.com/locate/bioorg

Design, synthesis, biological evaluation and *in silico* studies of novel pyrrolo [3,4-*d*]pyridazinone derivatives with promising anti-inflammatory and antioxidant activity

Łukasz Szczukowski[a,*], Aleksandra Redzicka[a], Benita Wiatrak[b], Edward Krzyżak[c], Aleksandra Marciniak[c], Katarzyna Gębczak[b], Tomasz Gębarowski[b], Piotr Świątek[a]

[a] Department of Chemistry of Drugs, Wroclaw Medical University, Borowska 211, 50-556 Wroclaw, Poland
[b] Department of Basic Medical Sciences, Wroclaw Medical University, Borowska 211, 50-556 Wroclaw, Poland
[c] Department of Inorganic Chemistry, Wroclaw Medical University, Borowska 211a, 50-556, Wroclaw, Poland

ARTICLE INFO

Keywords:
Pyridazinone
Mannich bases
Molecular docking
Antioxidants
Anti-inflammatory agents
Cyclooxygenase inhibitors
1,3,4-Oxadiazole-2-thione

ABSTRACT

Novel Mannich base analogues of pyrrolo[3,4-*d*]pyridazinone **7a**,**b**-**13a**,**b** are designed and synthesized as potential anti-inflammatory agents. The title compounds are obtained *via* convenient one-pot synthesis with good yields. Their structures and properties are described by spectroscopic techniques and elemental analyses. The aim of this study is to evaluate the inhibitory activity of the new derivatives against both cyclooxygenase isoforms COX1 and COX2 as well as their cytotoxicity. The results clearly indicate that the tested compounds **7a**,**b**-**13a**,**b** are not toxic, all show better affinity towards isoform COX-2, and some of them act as selective COX-2 inhibitors. Moreover, every examined derivative of pyrrolo[3,4-*d*]pyridazinone demonstrates better inhibitory activity towards COX-2 and a superior COX-2/COX-1 selectivity ratio compared to the reference drug meloxicam. Molecular docking studies confirm that compounds **7a**,**b**-**13a**,**b** preferably bind COX-2 and all of them bind to the active site of cyclooxygenase in a way very similar to meloxicam. Subsequently, taking into account that inflammation is strongly correlated with oxidative stress and both of these processes can potentiate each other, synthesized Mannich bases are evaluated for potential antioxidant activity. Most of the investigated derivatives reduce induced oxidative and nitrosative stress. Moreover, compounds **7a**,**b**, **8a**, **10a**,**b**, **11b**, **12a**,**b**-**13a**,**b** protect chromatin from oxidative stress and decrease the number of DNA strand breaks caused by intracellular growth of free radicals. Finally, a study of the binding mechanism between compounds **7a**,**b**-**13a**,**b** and bovine serum albumin (BSA) was carried out. According to spectroscopic and molecular docking studies, all examined derivatives interact with BSA, which suggests their potential long half-life *in vivo*.

1. Introduction

The synthesis and evaluation of the biological activity of pyridazinone derivatives have been gaining more and more interest from scientists for several decades [1–3]. The core of pyridazinone is present in a number of medicaments, such as the PDE3 inhibitor zardaverine, the anti-inflammatory agent emorfazone and the antihypertensives levosimendan, indolidan and bemoradan [2,3]. Potential drug candidates whose structure is based on a pyridazinone backbone exhibit a great variety of pharmacological activities, e.g. anticancer and cytotoxic activity [4–11], antiulcer activity [12], analgesic and anti-inflammatory activity [6,13–22], vasorelaxant and platelet antiaggregatory activity [23–27]. Moreover, some derivatives of pyridazinone act as potent carbonic anhydrase [11,28] or acetylcholinesterase [29] inhibitors, histamine H_3 receptor antagonists [30,31] or anticonvulsant agents [32].

In our previous papers, we have reported the synthesis, *in vitro* and *in vivo* investigations of compounds based on a pyridazinone ring fused in a biheterocyclic scaffold of pyrrolo[3,4–*d*]pyridazinone, which were designed as potential analgesics [18,19]. In the structure of examined molecules, an arylpiperazine pharmacophore attached through 2 carbon linker to lactam nitrogen of pyrrolo[3,4-*d*]pyridazinone can be distinguished (Fig. 1). The most potent compounds, **1a** and **1b**, in the "writhing" test were much more effective than acetylsalicylic acid (ASA). On the other hand, in the "hot plate" test, both **1a** and **1b** exhibited analgesic activity at a dose only 3–5 times higher than that of

* Corresponding author.
E-mail address: lukasz.szczukowski@umed.wroc.pl (Ł. Szczukowski).

https://doi.org/10.1016/j.bioorg.2020.104035
Received 16 March 2020; Received in revised form 5 June 2020; Accepted 15 June 2020
Available online 19 June 2020

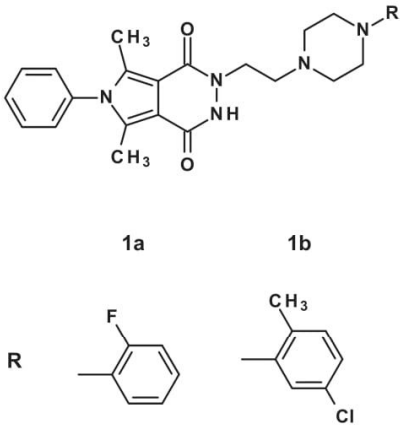

Fig. 1. Structures of previously investigated derivatives of pyrrolo[3,4-*d*]pyridazinone.

the reference drug, morphine [18]. Although **1b** showed affinity to the μ-opioid receptor in radioligand binding assay [18], our studies proved that derivatives of pyrrolo[3,4-*d*]pyridazinone exert their analgesic and anti-inflammatory effects mostly by complex, peripheral mechanisms, which is in good agreement with previous research [12,13,15,16]. The exact mechanism of action of examined compounds has not been solved yet. Nevertheless, according to many reports, a pyridazinone ring can serve as an excellent template for cyclooxygenase (COX) inhibitors, especially those with good binding affinity to the COX-2 isoform [14–16,20,22]. However, in the case of titled compounds, the key pharmacophore is not exactly pyridazinone but biheterocyclic pyrrolo [3,4–*d*]pyridazinone core. Therefore during the rational design of new derivatives, we have decided to introduce additional moiety into our structures which would enhance the potential COX-2 inhibitory activity. According to literature, a great variety of substituted five-membered heterocycles that are present in the structure of selective COX-2 inhibitors, i.e. pyrazole or isoxazole, can serve as a template for new compounds inhibiting this isoenzyme [33–40]. That is why our intention while seeking effective and safe cyclooxygenase inhibitors was to combine such five-membered nucleus with pyrrolo[3,4–*d*]pyridazinone.

Non-steroidal anti-inflammatory drugs (NSAIDs), which inhibit COX, are used worldwide for the treatment of different kinds of pain and inflammation, despite their severe side effects including gastric irritation, ulceration, nephrotoxicity, haemorrhage and cardiac toxicity [13–22]. The discovery in 1991 of the fact that cyclooxygenase exists in two isoforms –constitutive, named COX-1, and induced by different pro-inflammatory factors, named COX–2 – led to the theory that inhibition of COX-1 is responsible for adverse effects of NSAIDs, whereas desirable analgesic, antipyretic and anti-inflammatory activities of these drugs are the results of inactivation of COX-2 [16–22]. However, the introduction of a new class of selective COX-2 inhibitors (coxibs) has quickly proved this hypothesis wrong. Among these compounds, rofecoxib was withdrawn from the market in 2004 because of adverse cardiovascular effects caused by a decrease of prostacyclin (PGI_2) [16,22,37–39]. Due to these facts, therapy with NSAIDs is limited by their side effects, remains unsafe and gives unsatisfactory results. That is why there is a constant need to search for safe and effective anti-inflammatory and analgesic agents [13–22].

Therefore, in continuation of our efforts in the development of potent, safe, non-toxic antinociceptives, we report herein the design, synthesis, biological evaluation and *in silico* studies of new Mannich base derivatives of pyrrolo[3,4-*d*]pyridazinone. The main structural alteration performed on the pyrrolo[3,4-*d*]pyridazinone core consisted of the introduction of a five-membered ring of 1,3,4-oxadiazole-2-thione. Such moiety is one of the most important in medicinal chemistry and is present in plenty of compounds presenting various biological activity, including cyclooxygenase inhibiting agents as well. It can serve as bioisostere of carboxylic acids or esters [33–36]. Thereby such modification was expected to be crucial in the context of synthesis of new potential COX inhibitors based on pyrrolo[3,4-*d*]pyridazinone core. What is more, according to the literature, compounds possessing this moiety exert satisfactory antinociceptive activity and do not cause gastric irritation [41–45]. Moreover, commonly used NSAIDs, such as ibuprofen or diclofenac, were modified in the same way. Obtained derivatives of the mentioned drugs, possessing incorporated in their structure 1,3,4–oxadiazole-2-thione ring, demonstrated significant analgesic activity and were found to lack adverse gastrointestinal effects [41–43]. These new compounds had much better inhibition activity towards COX-2 isoenzyme and meaningly lower affinity to COX-1 in comparison to output structures of ibuprofen or diclofenac [41,42].

The main aim of this study was to determine whether compounds based on a pyrrolo[3,4-*d*]pyridazinone core can serve as a new class of cyclooxygenase inhibitors. Hence we performed an *in vitro* evaluation of the impact of the tested compounds on the activity of COX-1 and COX–2. Molecular docking studies illustrating the possible binding mode of the new derivatives in the active site of both cyclooxygenase isoforms were carried out as well. In inflammatory cells, an increase of reactive oxygen species (ROS) is observed. This promotes oxidative stress, which can cause oxidative damage, and in consequence, potentiate inflammation [46–48]. Taking it into consideration, we examined whether new Mannich base derivatives of pyrrolo[3,4-*d*]pyridazinone are able to affect the levels of intracellular ROS and RNS and reduce DNA damage caused by free radicals. As a supplement of the experiments determining the potential mechanism of action of investigated compounds, we carried out studies explaining the manner in which the new pyrrolo[3,4-*d*]pyridazinone analogues interact with blood proteins. The study of binding between the new drugs and proteins such as albumins is very interesting and important in pharmacy, pharmacology and biochemistry. Serum albumin is the main protein in the blood and is a significant transporter for many molecules. Therefore, serum albumin has been used to study a ligand-binding mechanism [49–54]. Spectroscopic and molecular docking studies allowed evaluation of the binding mechanism of the new derivatives to bovine serum albumin (BSA). All new structures were examined *in vitro* for cytotoxicity. The purpose of all applied biological and *in silico* investigations was to clarify, as well as possible, the pharmacological properties of new pyrrolo[3,4-*d*]pyridazinone derivatives, which may be involved in their antioxidant, analgesic and anti-inflammatory effects.

2. Results and discussion

2.1. Chemistry

The synthesis of 3,5,7-trimethyl-6-phenyl-2*H*-pyrrolo[3,4-*d*]pyridazine-1,4-dione **2a** and 6-butyl-3,5,7-trimethyl-2*H*-pyrrolo[3,4-*d*] pyridazine-1,4-dione **2b** was performed according to the protocols published previously [18,55]. Scheme 1 presents the synthesis of compounds which have not been described in the literature yet. Analytical and spectroscopic properties of all newly obtained derivatives were in good agreement with their predicted structures and are summarised in the experimental section and supplementary data.

Due to the occurrence of tautomerism in the pyridazinone ring, the alkylation of appropriate analogue of pyrrolo[3,4-*d*]pyridazine-1,4-dione **2a**-**b** with methyl chloroacetate in acetonitrile results in the formation of a mixture of isomeric ester derivatives **3a**-**b** and **4a**-**b**. After completion of the reaction, the mixture of *N*- and *O*- isomers was purified, and the isomers were separated using the column chromatography technique. Based on previous data, distinction and identification of isomeric forms were carried out by ^{1}H NMR spectra analysis

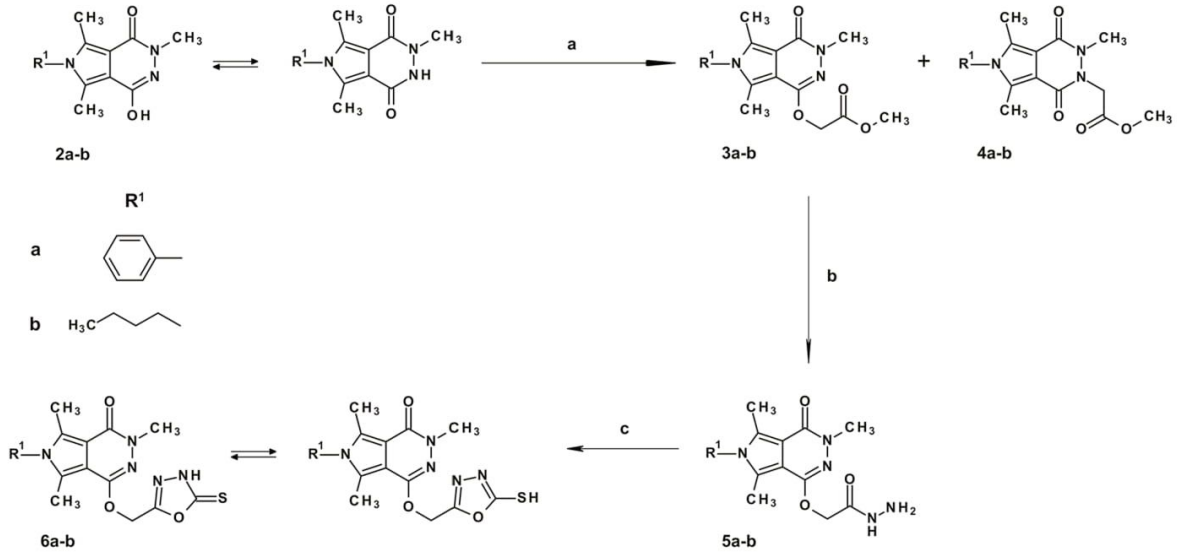

Scheme 1. Synthesis of the compounds **3a-b** – **6a-b**. Reagents and reaction conditions: (a) methyl chloroacetate, acetonitrile, K_2CO_3, reflux, 6 h; (b) hydrazine hydrate, C_2H_5OH, reflux, 5 h; (c) I. CS_2, C_2H_5OH, KOH, reflux, 6 h; II. cooling, water, stirring, acidification with 7.5% HCl.

[18]. In the case of *N*-substituted analogues **4a-b**, both methyl groups in positions 5 and 7 of the pyrrolo[3,4-*d*]pyridazinone scaffold appear as one 6-proton singlet in the ^{1}H NMR spectrum (δ ~ 2.4 ppm S, 6H, 5,7-CH_3 for **4a** and δ ~ 2.6 ppm S, 6H, 5,7-CH_3 for derivative **4b** respectively). On the other hand, when considering *O*-isomers, these methyl substituents, due to different chemical shift, occur in the spectrum as two separate 3-proton singlets (for **3a**: δ ~ 2.33 ppm S, 3H, 7–CH_3; δ ~ 2.43 ppm S, 3H, 5-CH_3, and for **3b**: δ ~ 2.56 ppm S, 3H, 7-CH_3; δ ~ 2.68 ppm S, 3H, 5-CH_3). During control experiments, it was observed that alkylation led to **3a** and **3b** with very good yield (greater than 65%), whereas compounds **4a-b** were obtained with insufficient efficiency (< 10%). This fact prevented us from further chemical modifications of *N*-isomers. The literature reports that nitrogen substitution in lactam seems to be crucial for the biological activity of pyridazinone derivatives [13,15,17,20]. Nevertheless, in the case of the biheterocyclic scaffold of pyrrolo[3,4–*d*]pyridazinone both *N*- and *O*-substituted analogues possess satisfactory antinociceptive activity, which was emphasised in our previous paper [18]. Therefore, we decided to develop the series of *O*–substituted pyrrolo[3,4-*d*]pyridazinones in this study.

In the next step, the reaction of esters **3a-b** with hydrazine hydrate (98%) in absolute ethanol allowed us to obtain the relevant hydrazides **5a-b**. The absorption bands in infrared (IR) spectra of **5a-b** ranging from 3322 to 3253 cm^{-1} for the N—H group and bands of the amidic carbonyl in the region near 1620 cm^{-1} indicate the formation of hydrazide. Then, derivatives **5a** and **5b** were transformed into key analogues **6a-b**. Initially, **5a-b** were heated at reflux in the presence of carbon disulfide in basic conditions in ethanol. Subsequently, the reaction mixture was poured onto crushed ice and acidified with hydrochloric acid. As a result, hydrazides **5a-b** were subjected to intramolecular cyclization and formation of a five-membered 1,3,4-oxadiazol-2-thione ring. Obtaining the designed compounds **6a-b** was confirmed by spectroscopic techniques: the absorption bands in IR spectra near 1590 cm^{-1} as well as the characteristic signals at around *δ* 177.9–179.2 ppm in ^{13}C NMR spectra strongly suggest the presence of a C=S bond. As was mentioned already, the introduction of this moiety is expected to be crucial in the context of low gastrotoxicity of designed structures and their good affinity towards COX-2 [41–44]. Compounds **6a-b** were the key substrates for the synthesis of new **7a,b-13a,b** derivatives of pyrrolo[3,4-*d*]pyridazinone.

Formation of final Mannich bases **7a,b-13a,b** (Scheme 2) was achieved *via* convenient and efficient one-step reaction of **6a-b** with appropriate secondary amines and formaldehyde in ethanol. The distinctive peak in the ^{1}H NMR spectrum near *δ* 4.98–5.10 ppm and the signal at around *δ* 70.01–70.42 ppm in the ^{13}C NMR spectrum clearly indicate creation of the methylene linker characteristic for Mannich bases. According to the literature, there are plenty of potent analgesics bearing an arylpiperazinyl or arylpiperidinyl group, including effective cyclooxygenase inhibitors [13,14,18–20,41,42]. Therefore, in our investigations, different amines were carefully chosen, e.g. arylpiperazines with various substituents in the phenyl ring, morpholine or substituted arylpiperidine, in order to estimate, as well as possible, the impact of this pharmacophore on the pharmacological activity of the new derivatives.

The crude products were purified by column chromatography or by crystallization from the appropriate solvent. Structures of all new compounds were established and confirmed by spectroscopic techniques: ^{1}H NMR, ^{13}C NMR, MS, FTIR, elemental analysis and on the basis of their physicochemical properties.

2.2. Cyclooxygenase (COX-1, COX-2) inhibition studies

2.2.1. In vitro cyclooxygenase inhibition assay

An evaluation of the influence of compounds **7a,b-13a,b** and meloxicam on the activity of both cyclooxygenase isoforms COX-1 and COX-2 was carried out with an incubation time of 2 min according to the procedure given by the kit manufacturer. Being aware of the severe side effects of NSAIDs such as aspirin, naproxen or ketoprofen which inhibit mostly COX-1 [16–22], we decided to compare the activity of the new Mannich bases with meloxicam, which inhibits both isoforms but has a better affinity to COX-2. We determined the concentrations of all examined compounds at which 50% inhibition of COX–1 and COX–2 occurred. Afterwards, IC_{50} values were calculated. Computing the ratio between IC_{50} values for both cyclooxygenase isoforms allowed us to determine the selectivity of the investigated structures to COX–1 and COX–2. All IC_{50} values for both enzymes and the selectivity ratio are shown in Table 1.

All investigated compounds in the *in vitro* test showed better affinity towards the COX-2 isoform than to COX-1. Moreover, all examined derivatives inhibited COX-2 more strongly than the reference drug

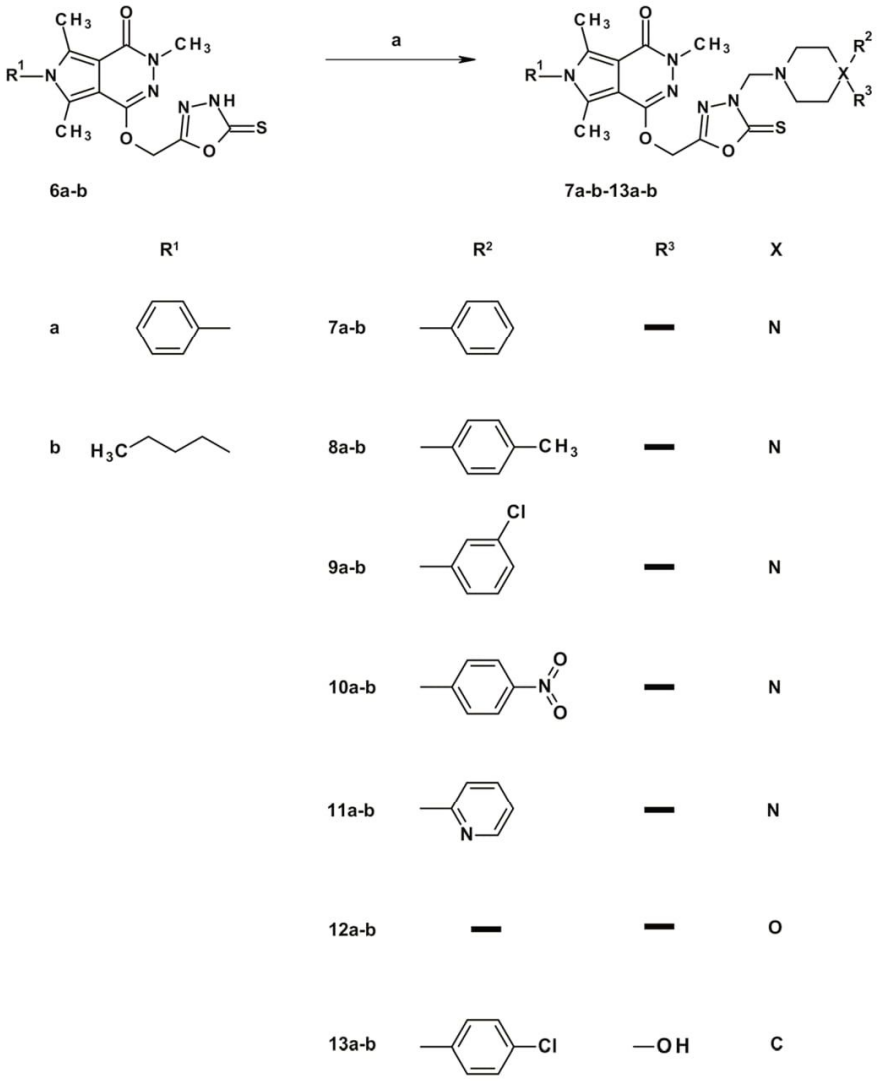

Scheme 2. Synthesis and structures of investigated Mannich base derivatives of pyrrolo[3,4–*d*]pyridazinone **7a,b-13a,b**. Reagents and reaction conditions: (a) 37% HCHO, C_2H_5OH, appropriate secondary amine, stirring 6h, RT.

meloxicam. IC_{50} values for COX-2 inhibition are similar for all 14 compounds. This could confirm that the pyrrolo[3,4-*d*]pyridazinone scaffold may serve as a good backbone for potent COX-2 inhibitors. Some of the examined compounds – **10a**-**13a** and **13b** – acted as selective COX-2 inhibitors. Derivatives with *n*-butyl substituent in position 6 – series **b** – showed better affinity towards COX-1 than those of series **a**, which have a phenyl ring substituted there. It could suggest that the aromatic substituent in that position impedes or even prevents binding of pyrrolo[3,4–*d*]pyridazinone derivatives in the active site of COX-1. This can be explained by the fact that the binding pocket in the active site of COX-2 is bigger than that of the COX-1 isoform [56]. Among compounds which inhibited COX-1 and COX-2 as well, all of them showed a better COX-2/COX-1 selectivity ratio than meloxicam. The presented results are in good agreement with previous studies, and confirm that derivatives of pyridazinone have good affinity for the COX-2 isoform [14–16,20,22].

2.2.2. Cyclooxygenase molecular docking study

The COX ligand binding site has four specific subdomains: A, B, C, D [56]. Subdomain A represents the mode of binding of flurbiprofen; subdomain B represents the mode of binding of meloxicam and piroxicam; subdomain C represents an entrance region of the enzyme binding domain, and subdomain D represents the position of the residue in position 523.

The most active COX-1 inhibiting compounds **7a**-**b**, **8a**-**b** (Table 1) bind to the enzyme by hydrogen bonds Ser530, Tyr355, Agr120(8b) and several hydrophobic (pink) or π-sigma (violet), π-cation (yellow) interactions (Table 2, Fig. 2). The main part of the compounds is in the subdomain B position, the second in the entrance region (C). The pyrrolo[3,4-*d*]pyridazinone residue takes a position very similar to meloxicam (Fig. 4). As mentioned above, the tested compounds showed better affinity towards COX-2 than to COX-1. The size of the COX-2 pocket is bigger than COX-1, which allows selective binding of larger

Table 1
IC_{50} values (mean ± SD) calculated for COX-1 and COX-2 enzymes after incubation for 2 min with the tested compounds, COX selectivity ratio, and IC_{50} values (mean ± SD) calculated for NHDF cell cultures after 48 h of incubation with the tested compounds.

Compound	Cyclooxygenase inhibition assay IC_{50} [μM]		COX selectivity ratio $IC_{50(COX-2)}/IC_{50(COX-1)}$	SRB assay IC_{50} [μM]
	COX-1	COX-2		
7a	129.2 ± 8.1	45.4 ± 2.7	0.35	414.1 ± 30.6
7b	121.8 ± 7.9	50.4 ± 9.7	0.41	191.7 ± 22.8
8a	136.5 ± 22.6	41.7 ± 3.4	0.31	654.0 ± 42.1
8b	134.5 ± 25.7	44.0 ± 2.7	0.33	166.8 ± 22.3
9a	184.3 ± 40.5	44.3 ± 2.0	0.24	124.8 ± 14.0
9b	178.2 ± 8.3	43.8 ± 4.8	0.25	96.8 ± 12.9
10a	N/C	43.9 ± 1.4	–	368.9 ± 52.1
10b	226.1 ± 25.0	44.2 ± 1.7	0.20	842.5 ± 60.6
11a	N/C	43.9 ± 2.0	–	403.5 ± 28.5
11b	286.2 ± 59.9	44.1 ± 3.5	0.15	482.5 ± 24.4
12a	N/C	43.6 ± 1.4	–	982.4 ± 72.4
12b	351.6 ± 95.5	43.4 ± 2.6	0.12	174.9 ± 14.6
13a	N/C	43.9 ± 5.1	–	169.2 ± 18.7
13b	N/C	54.4 ± 7.4	–	377.3 ± 24.6
Meloxicam	104.5 ± 5.6	57.3 ± 3.5	0.55	441.5 ± 17.1

N/C – not calculable (based on the concentrations tested)

molecules. Compounds **7a-b**, **8a-b** interact with COX-2 by hydrogen bonds with Ser530, Tyr355, Arg120 and hydrophobic interactions. Details are presented in Table 2 and Fig. 3. The orientation in the active site is very similar to the position in the COX-1 pocket. The main part of compounds is in subdomain B, and the second part is directed towards sector C or D. Additionally compounds **7a-b** are stabilised by interaction with a residue in position 523 (subdomain D). The position of the 6-substituted biheterocyclic scaffold of pyrrolo[3,4-*d*]pyridazinone is the same as meloxicam (Fig. 4). 2D interaction of derivatives **9a**,**b**-**13a**,**b** with COX-1 and COX-2 are collected in the supplementary data (**Table S1**, **Fig. S1a** and **Fig. S1b**).

2.3. Evaluation of viability

All investigated compounds **7a**,**b-13a**,**b** were evaluated for cytotoxicity in sulforhodamine B (SRB) assay. During the 48 h incubation of normal human dermal fibroblast (NHDF) cells with derivatives of pyrrolo[3,4-*d*]pyridazinone no cytotoxicity potential (viability below 70%) was observed for any of the compounds (in each concentration tested – 10, 50 and 100 μM). Regression analysis was used in order to calculate the IC_{50} values (Table 1).

2.4. Level of intracellular ROS and RNS

Reactive oxygen species (ROS) and reactive nitrogen species (RNS) are formed as a result of cellular metabolic changes. An increase of ROS and RNS, resulting in oxidative or nitrosative stress, can be caused by different factors such as hypoxia or inflammation [46]. Many studies indicate that ROS are significant pro-inflammatory mediators and oxidative stress and inflammation are strongly related to each other, coexisting processes. Cyclooxygenases 1 and 2 can affect the levels of ROS and RNS. At the same time, the rise in the level of oxygen and nitrogen free radicals may induce an increase in COX-1 and COX-2 activity [38–40]. Taking the above into consideration, we performed studies whose objective was to elucidate the potential influence of the new pyrrolo[3,4-*d*]pyridazinone derivatives on the level of ROS and RNS. In our studies, oxidative stress was induced with 100 μM H_2O_2 in the DCF-DA assay and nitrosative stress with 100 μM H_2O_2 as well in the Griess test.

The results of the DCF-DA assay are shown in Table 3, where negative values indicate a decrease in ROS level compared to the control, while positive values indicate a higher ROS level. Protective properties against oxidative stress were observed for **9a-13a** compounds – the level of oxygen free radicals was reduced compared to the control (1 h incubation of NHDF cells with 100 μM H_2O_2; without tested compounds). Derivatives **9a-13a** reduced the level of ROS in the whole range of tested concentrations with statistical significance (except **9a** in the highest concentration of 100 μM). In contrast, compound **7a** at concentrations of 10 μM and 50 μM and **8a** at 10 μM only reduced the ROS level in comparison to the control. Notably, compound **8a** at concentrations 50 μM and 100 μM caused statistically significant stronger ROS formation. Among 6-*n*-butyl substituted structures of series **b**, only **9b** and **13b** reduced the level of ROS in the lowest, 10 μM concentration, but without statistical significance. According to **7b** and **8b** at 100 μM, **9b** at 100 μM and 50 μM, **11b** at 100 μM and 50 μM, **12b** in the whole range of investigated concentrations and finally **13b** at 100 μM and 50 μM a statistically significant rise of oxygen free radical levels was observed.

The Griess assay results are shown in Table 3. Negative values

Table 2
Type of interactions and interacting residues of COX-1 and COX-2 with compounds **7a-b**, **8a-b** (rings: **1** – phenyl, **2** – pyrrole and/or pyridazinone, **3** – 1,3,4-oxadiazol-2-thione, **4** – piperazine, **5** – phenyl).

	COX-1				COX-2			
	H-bonding	π-interactions			H-bonding	π-interactions		
	Res-(distance, Å)-Atom of Ligand	Ring	Type	Residue	Res-(distance, Å)-Atom of Ligand	Ring	Type	Residue
7a	Ser530-(2.02)-O	1	π-sigma	Leu531	Ser530(3.02)-O	12,335	π-sigma	Val523,Ala527
	Tyr355-(2.58)-N	2	π-sigma	Val349,Ala527	Arg120 (2.24)-OSer119 (2.94)		π-sigma	Val349
		3	π-sigma	Val116	-S		π-sigma	Val116
		5	π-cation	Arg120			π-cation	Arg120
							π-cation	Arg120
8a	Ser530-(2.11)-OTyr355-(2.57)	2	π-sigma	Leu352,Val349	Tyr355-(2.90)-O	2	π-sigma	Leu352
	-N	3	π-sigma	Val116		4	π-sigma	Val116
		5	π-cation	Arg120				
7b	Ser530-(1.67)-OTyr355-(2.62)	2	π-sigma	Val349,Ala527	Tyr355-(2.33)-O	2	π-sigma	Val523, Ala527
	-N	3	π-sigma	Val116		5	π-sigma	Ile345
		5	π-cation	Arg120				
8b	Ser530-(2.34)-OTyr355-(2.59)	2	π-sigma	Val349	Ser530-(1.81)-O	2	π-sigma	Val349, Ala527
	-NArg120-(2.91)	3	π-sigma	Val116		5	π-sigma	Val89
	-O	5	π-sigma	Val119,Arg120,Val89		5	π-cation	Agr120

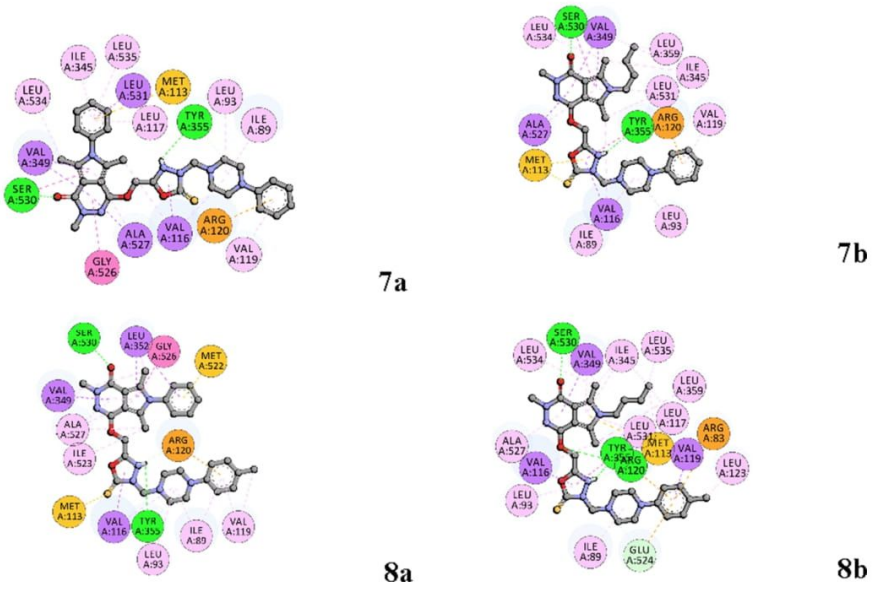

Fig. 2. 2D interaction with **COX-1** (green – hydrogen bonds, violet – π-sigma, orange – π-cation, pink – other hydrophobic). (For interpretation of the references to color in this figure legend, the reader is referred to the web version of this article.)

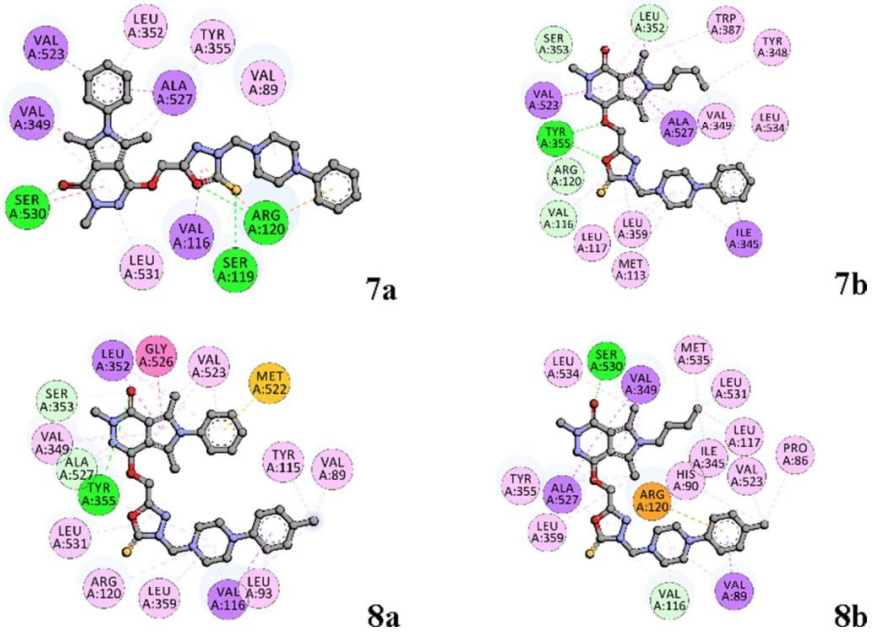

Fig. 3. 2D interaction with **COX-2** (green – hydrogen bonds, violet – π-sigma, orange – π-cation, pink – other hydrophobic). (For interpretation of the references to color in this figure legend, the reader is referred to the web version of this article.)

indicate a decrease in the nitrite ions level compared to the control, and positive values indicate that the nitrite ion level increased upon addition of the tested compounds. Most of the tested pyrrolo[3,4–*d*]pyridazinone derivatives (except for **8a**, **9a**, and **10a**) reduced RNS level after induction of nitrosative stress (with H_2O_2) for at least one of the concentrations tested. Only for compounds **7b** (50 and 100 μM), **10a** (100 μM) and **10b** (50 μM) a statistically insignificant small increase in RNS level was noted. Compounds **10a** and **10b** bear a nitric residue in the phenyl ring of the arylpiperazine pharmacophore, which may be the reason for the increase of RNS in the case of these derivatives. Derivatives **9b, 12a, 12b,** and **13b** lowered the level of RNS in the whole range of tested concentrations with statistical significance. Moreover, statistically significant reduction of nitrogen free radicals was observed in the case of **7a**, **11a** and **11b** at concentrations of 100 μM and 50 μM and **13a** at 50 μM and 10 μM, **7b** at 10 μM, **8b** at 100 μM and 10 μM, **10b** at 100 μM.

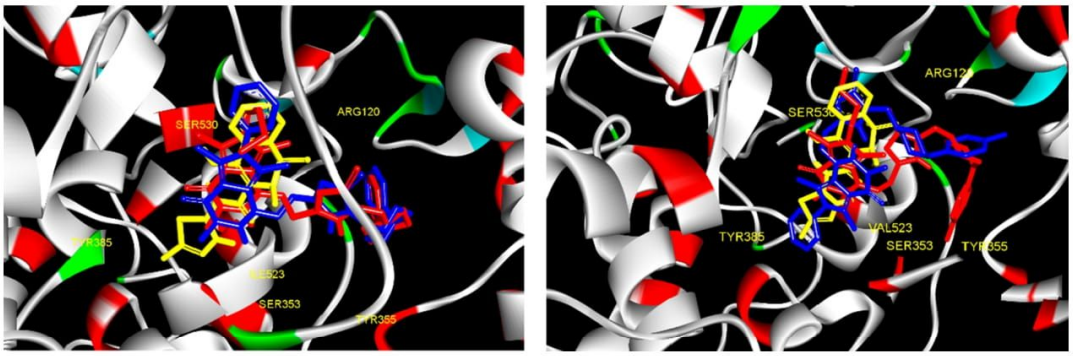

Fig. 4. Docking poses of **7a** (blue), **7b** (red) and meloxicam (yellow) under COX-1 binding domain conditions (left) and docking poses of **8a** (blue), **8b** (red) and meloxicam (yellow) under COX-2 (right). (For interpretation of the references to color in this figure legend, the reader is referred to the web version of this article.)

Table 3
ROS and RNS scavenging activity of tested compounds and an impact on the reduction of DNA damage (n = 3); the results were compared to the control and expressed as E/E_0 ratios; statistical significance calculated with post-hoc test compared to control (* $p < 0.05$; ** $p < 0.01$; *** $p < 0.001$; E_0 – cultures without tested compounds).

Compound	Conc.[μM/l]	DCF-DA assay E/E_0				GRIESS assay E/E_0				FHA assay E/E_0			
		Without H_2O_2		With H_2O_2		Without H_2O_2		With H_2O_2		Without H_2O_2		With H_2O_2	
	100	+23.0%	**	+13.4%	*								
Meloxicam	50	+15.1%	*	+11.8%									
	10	+13.7%		+4.3%									
	100	+22.6%	**	+6.6%		+12.4%		−3.5%	*	−4.3%		−14.5%	
7a	50	+21.8%	**	−9.6%		+9.7%		−5.1%	*	−5.8%		−15.9%	*
	10	+27.3%	***	−16.9%	**	+9.7%		−4.7%		−38.5%	*	−45.0%	*
	100	+16.6%	**	+17.2%	**	+11.0%		+6.1%		−28.4%	**	−35.4%	***
7b	50	+22.0%	***	+8.8%		+8.4%		+4.5%		−20.1%	*	−27.9%	*
	10	+22.0%	***	+2.6%		+9.7%		−4.7%	*	−18.1%	*	−26.0%	**
	100	+29.0%	***	+73.9%	***	+13.7%		−2.3%		−16.7%	*	−25.6%	***
8a	50	+24.6%	***	+28.7%	***	+20.4%		−2.3%		−6.7%	*	−14.9%	***
	10	+25.6%	**	−2.6%		+15.1%		−2.3%		−4.7%		−14.9%	*
	100	+22.1%	***	+20.6%	***	+4.3%		−6.0%	*	−7.0%		−16.0%	
8b	50	+22.6%	***	+9.1%		+4.3%		−5.1%		+17.8%		+6.4%	
	10	+14.1%	**	+2.2%		+5.7%		−5.5%	*	+31.6%	*	+18.9%	
	100	+18.8%	**	−3.2%		+13.7%		−2.3%		+25.3%		+11.9%	
9a	50	+19.9%	***	−12.6%	*	+20.4%		−2.3%		+18.4%		+5.8%	
	10	+22.2%	***	−15.6%	**	+15.1%		−2.3%		+6.2%		−5.2%	
	100	+18.2%	**	+30.0%	***	+9.7%		−2.3%	*	+15.7%		+4.5%	
9b	50	+18.6%	**	+14.9%	**	+5.7%		−8.8%	*	+22.2%		+10.4%	
	10	+26.2%	***	−1.6%		+3.0%		−6.8%	*	+2.0%		−7.9%	
	100	+19.8%	***	–22.7%	***	+9.7%		+4.1%		+7.7%		−3.8%	
10a	50	+29.4%	***	–22.3%	***	+12.4%		−1.1%		+3.4%		−7.7%	
	10	+30.2%	***	−19.3%	***	+12.4%		−1.9%		−16.5%		−25.4%	
	100	+20.2%	**	+5.0%		+47.2%	***	−3.5%	*	−8.8%		−17.7%	
10b	50	+19.4%	**	+4.0%		+15.1%		+5.7%		+13.5%		+2.5%	
	10	+19.8%	**	+7.2%		+7.0%		−1.1%		−20.5%	*	−28.3%	*
	100	+26.8%	***	−19.7%	***	+9.7%		−6.8%	**	−18.7%		−27.4%	
11a	50	+28.8%	***	−18.7%	***	+20.4%	*	−6.4%	*	+24.9%		+11.5%	
	10	+32.2%	***	−18.6%	***	+9.7%		−3.1%		+36.7%	**	+22.1%	*
	100	+26.1%	***	+23.8%	***	+5.7%		−8.0%	**	−8.4%		−17.3%	
11b	50	+20.2%	***	+16.7%	**	+3.0%		−9.2%	**	−2.7%		−14.8%	
	10	+17.5%	**	+8.7%		+11.0%		−3.5%		+2.8%		−7.1%	
	100	+24.2%	***	−18.4%	**	+13.7%		−7.6%	**	−18.4%	*	−27.1%	
12a	50	+18.2%	**	−19.3%	***	+13.7%		−6.8%	*	−4.9%		−15.0%	***
	10	+28.2%	***	−18.2%	***	+8.4%		−3.9%	*	+1.6%		−9.3%	
	100	+22.9%	***	+37.6%	***	+7.0%		−6.8%	*	+3.7%		−6.4%	
12b	50	+29.1%	***	+30.5%	***	+7.0%		−6.4%	*	−4.8%		−14.0%	
	10	+19.4%	*	+24.7%	***	+9.7%		−8.8%	***	−4.8%		−14.1%	
	100	+20.2%	***	−21.5%	***	+7.0%		−3.5%		−8.5%	*	−18.3%	*
13a	50	+16.9%	**	−26.5%	***	+5.7%		−6.4%	*	−13.8%		−21.3%	
	10	+25.5%	***	−20.0%	***	+5.7%		−6.4%	**	−16.2%		−25.1%	
	100	+32.6%	***	+56.4%	***	+11.0%		−2.3%	*	+5.2%		−5.0%	
13b	50	+29.0%	***	+34.8%	***	+12.4%		−6.4%	*	+0.7%		−9.0%	
	10	+29.4%	***	−3.1%		+7.0%		−8.4%	**	−37.5%		−43.5%	

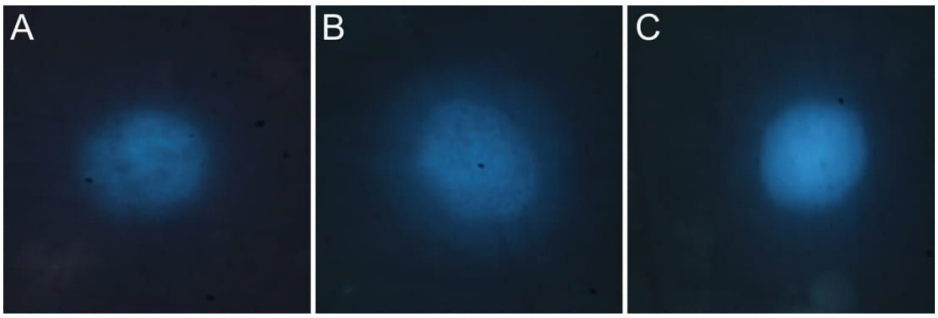

Fig. 5. Micrographs (60x) of cells showing chromatin relaxation: A) cell incubated in the complete medium; B) cell incubated with 100 μM H_2O_2 for 1 h; C) cell incubated with compound **7b** at 10 μM for 24 h and then for 1 h with 100 μM H_2O_2. Micrograph B shows a much larger nuclear halo compared to B; the larger the halo size, the greater the relaxation of chromatin, which means a higher level of DNA damage.

2.5. Fast halo assay (FHA)

Intracellular growth of oxygen and nitrogen free radicals can cause DNA strand breaks [46]. Therefore, we conducted a study to explain the potential impact of the new pyrrolo[3,4–*d*]pyridazinone derivatives on reducing the number of DNA breaks after exposure to oxidative stress. For this purpose, normal human dermal fibroblasts (NHDF) cell cultures were incubated for 24 h with the tested compounds and then for 1 h with 100 μM H_2O_2. Two controls were used in the study – cells incubated only in complete medium and a culture in which oxidative/nitrosative stress was induced exogenously (without test compounds). Examples of micrographs showing the relaxation of chromatin are shown in Fig. 5. The results were calculated as damage level ratios in the test sample compared to the control with induced stress (Table 3). Negative values in the results indicate a reduction in the level of DNA strand breaks compared to the control and positive values correspond to an increased level of damage after addition of tested compounds. Based on the results presented in Table 3, we can conclude that compounds **7b** and **8a** showed a statistically significant effect protecting DNA from oxidative/nitrosative stress (induced with H_2O_2) in the whole range of tested concentrations. A similar effect was observed for derivative **7a** at concentrations of 10 and 50 μM. DNA damage was also significantly reduced in the presence of one of the tested concentrations of compounds **10b** (10 μM), **12a** (50 μM), **13a** (100 μM), and **13b** (10 μM). Only compound **11a** at 10 μM caused a statistically significant increase in the number of DNA strand breaks. Elevated levels of damage (statistically insignificant) occurred with at least one concentration of derivatives **8b**, **9a**, **9b**, and **10b** as well.

2.6. Bovine serum albumin ligand-binding study

Bovine serum albumin (BSA) is an extensively studied model protein. Its structure is very similar to human serum albumin, but the costs of the application are much lower [49–51]. The mature BSA protein contains 583 amino acids. Among them, there are 20 Tyr and 2 Trp residues. Homologous domains I, II and III form the BSA molecule. Furthermore, each domain is composed of two sub-domains: A and B [51]. Aromatic and heterocyclic ligands can bind to hydrophobic cavities in subdomains IIA and IIIA [49]. The molecular interaction between BSA and new ligands can be monitored by optical techniques such as UV–Vis, CD or fluorescence spectroscopy. These methods are easy to use and have good sensitivity [57–60].

2.6.1. Fluorescence quenching and binding constants

Steady-state fluorescence spectroscopy was used to study fluorescence quenching of BSA by all compounds. The fluorescent behavior of BSA is due to the amino acid residues: Trp, Tyr, and Phe. However, Trp residue has the strongest fluorescence intensity. Thus, the two Trp residues of BSA are mainly responsible for its fluorescence. The fluorescence spectra were recorded for BSA in the presence of studied compounds at the excitation wavelengths λ = 280 nm (both Trp and Tyr residues are excited) and concentration range 0.0–2.0 μM. The fluorescence emission spectra for the most active COX inhibiting compounds **7a-b**, **8a-b** were shown in Fig. 6 (for all compounds in **Fig. S2a and S2b** in the supplementary data). The fluorescence intensity of BSA was decreased with increasing concentrations of compounds. This effect is especially noticeable up to the 1:1 M ratio. At higher concentrations, fluorescence quenching is smaller. A red shift was observed as **7a-8a** concentration increased. It indicates that the conformation of BSA was changed, and the amino acid residues are in a polar environment [61]. For compounds **b** series, a blue shift was observed. It means that the amino acid residues are located in a more hydrophobic environment. Fluorescence quenching and shift of λ_{max} identifies interaction with BSA and can suggest the formation of complexes (static quenching). However, it can also be the result of the collisional encounters (dynamic quenching). In order to confirm the quenching mechanism and complex formation, the fluorescence data were further analysed by the Stern-Volmer equation and dependence on temperature [53].

Fluorescence intensities were corrected for the absorption of excitation light and re-absorption of emitted light to decrease the inner filter using the following relationship:

$$F_{corr} = F_{obs} 10^{\frac{(A_{ex}+A_{em})}{2}} \quad (1)$$

where F_{corr} and F_{obs} are corrected and observed fluorescence intensities, respectively. A_{ex} and A_{em} are the absorbance values at excitation and emission wavelengths, respectively.

In most cases, the possible quenching mechanism is characterised by a linear Stern-Volmer plot and is usually analysed using the classical Stern-Volmer equation [62]:

$$\frac{F_0}{F} = 1 + k_q \tau_0 [Q] = 1 + K_{SV} [Q] \quad (2)$$

where F_0 and F are the steady-state fluorescence intensities at the maximum wavelength in the absence and presence of quencher respectively, k_q the quenching rate constant of the biomolecule, τ_0 the average lifetime of the biomolecule, [Q] is the quencher concentration, and K_{SV} is the Stern-Volmer constant.

To determine the type of quenching the linear segment was analysed. The average lifetime of the fluorophore in the excited state for a biomolecule is 10^{-8}s [63]. According to the equation, the Stern-Volmer constant and the quenching rate constant were obtained from the linear fitting of the experimental data. Obtained results are collected in Table 4 and **Table S2** (supplementary data). For dynamic quenching, the maximum scatter collision quenching constant of different quenchers with the biopolymers is reported to be 2×10^{10} $dm^3mol^{-1}s^{-1}$ [64]. The results showed that the value of k_q for all cases is much

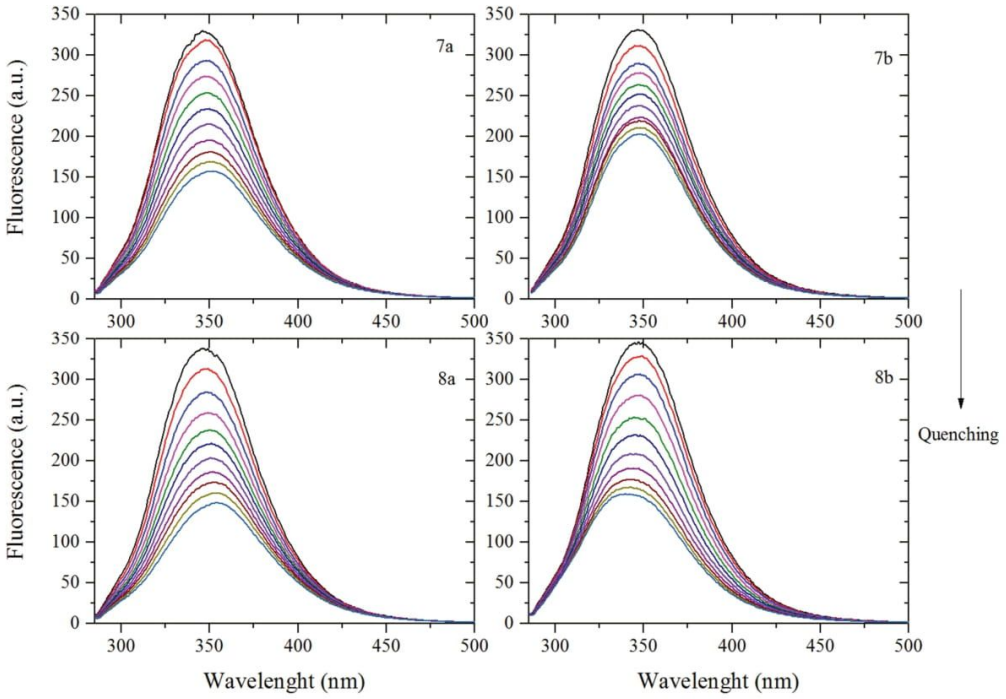

Fig. 6. Fluorescence spectra of BSA solution in presence of **7a-b**, **8a-b** (T-303 K, λ_{ex} = 280 nm). The concentration of **7a-b**, **8a-b** was: 0, 0.2, 0.4, 0.6, 0.8, 1.0, 1.2, 1.4, 1.6, 1.8, 2.0 μM.

greater, which indicated that the probable quenching mechanism of fluorescence of BSA by all compounds is not caused by a dynamic collision but by the formation of a complex.

The dynamic and static quenching can be distinguished by their dependence on temperature. The higher temperature may result in decreasing stability of the complex and thus smaller values of the static quenching constant. The fluorescence data were analysed at three different temperatures, and the fluorescence quenching constant of BSA was calculated using the Stern-Volmer equation (2). The results for the most active COX inhibiting compounds **7a-b, 8a-b** are listed in Table 4 (for all compounds in **Table S2** in the supplementary data). The Stern-Volmer quenching constant K_{SV} is inversely correlated with temperature and k_q is much greater than the value of the maximum scatter collision quenching constant. It suggests the formation of ground-state complex and involvement of static quenching between BSA and studied compounds.

For all analysed systems, the binding constants and the number of binding sites were calculated. However, in the literature, there are several models to determine the binding parameters. The values obtained from different methods of calculation could significantly differ from each other [65–67]. Therefore, two models were used to analyse the obtained data: the double logarithm regression curve, and the modified double logarithm regression curve.

Using the double logarithm regression curve, the binding constant K_b and the binding stoichiometry n were determined by the following equation [62]:

$$\log\frac{F_0 - F}{F} = \log K_b + n\log[Q] \quad (3)$$

where F_0 and F are the steady-state fluorescence intensities at the maximum wavelength in the absence and presence of quencher, respectively, and [Q] is the quencher concentration. The corresponding values were obtained from the slope and the intercept of the plot of log [(F_0-F)/F] versus log [Q]. The linear segment, corresponding to the compound/BSA molar ratio 2:1, was analysed (Table 5, Fig. 7).

The second method, the modified double logarithm regression curve, in contrast to the previous one, takes into account the total concentration of protein present in the analysed solution.

$$\log\frac{F_0 - F}{F} = n\log K_b + n\log\frac{1}{[Q] - (F_0 - F)\frac{[P]}{F_0}} \quad (4)$$

where [P] is BSA concentration. By the plot of log (F_0-F)/F vs log (1/([Q]–(F_0–F)[P]/F_0)), the binding stoichiometry n and the constant K_b were obtained (Table 5, Fig. 7).

The first method assumes a single type of quenching behaviour [54,65]. The fluorescence intensity for the fluorescent system is directly

Table 4
The Stern-Volmer constant K_{SV} and the quenching rate constant k_q for the interaction of BSA with compounds **7a-b**, **8a-b** at different temperatures.

	T[K]	$K_{SV} \times 10^5$[dm^3mol^{-1}]	$k_q \times 10^{13}$[$dm^3mol^{-1}s^{-1}$]	R^2		T[K]	$K_{SV} \times 10^5$[dm^3mol^{-1}]	$k_q \times 10^{13}$[$dm^3mol^{-1}s^{-1}$]	R^2
7a	303	8.02 ± 0.21	8.02	0.987	**7b**	303	6.22 ± 0.23	6.22	0.997
	306	7.83 ± 0.24	7.83	0.990		306	5.67 ± 0.12	5.67	0.998
	310	7.17 ± 0.20	7.17	0.992		310	5.20 ± 0.14	5.20	0.993
8a	303	8.60 ± 0.25	8.60	0.996	**8b**	303	4.84 ± 0.07	4.84	0.998
	306	8.06 ± 0.26	8.06	0.990		306	4.06 ± 0.06	4.06	0.998
	310	7.43 ± 0.22	7.43	0.992		310	3.62 ± 0.05	3.62	0.998

Table 5
Binding constants K_b and binding stoichiometry n for the interaction of BSA with studied compounds.

	Double log			Modified double log		
	K_b [dm^3mol^{-1}]	n	R^2	K_b [dm^3mol^{-1}]	n	R^2
7a	4.49×10^6	1.13	0.998	8.50×10^7	0.96	0.997
8a	1.58×10^7	1.22	0.998	8.37×10^7	1.09	0.994
9a	1.50×10^6	1.05	0.998	9.64×10^7	0.99	0.989
10a	2.55×10^6	1.10	0.996	9.20×10^7	0.93	0.987
12a	1.05×10^7	1.19	0.997	8.65×10^7	1.04	0.996
13a	3.87×10^6	1.12	0.996	8.77×10^7	0.96	0.992
7b	3.93×10^6	1.19	0.997	2.36×10^6	1.18	0.994
8b	3.87×10^5	0.99	0.996	1.58×10^6	1.07	0.992
9b	2.74×10^6	1.12	0.997	1.26×10^6	1.33	0.991
10b	2.11×10^5	0.93	0.998	1.49×10^6	0.95	0.987
12b	3.05×10^5	0.94	0.999	1.08×10^6	0.86	0.994
13b	6.63×10^5	1.02	0.995	1.49×10^6	1.32	0.993

proportional to the free concentration of protein, and the free concentration of quencher is replaced by the total concentration of a quencher. In the second method, any assumed conditions about concentration are not required [68]. As it was shown in Fig. 7, there was a good linear fit for both methods. The results show that the binding constants indicate high values, about 10^6-10^7 (Table 5). The K_b obtained from Equation (3) and (4) significantly differ from each other. It is supposed that the free concentration of the binding compound is not equal to the total concentration of the quencher. Very good interaction with BSA provides an excellent distribution of studied compounds. Structural modifications slightly change the K_b values but not spectacularly. The n value close to 1 shows one-to-one interaction.

Two models were applied in this work (double logarithm regression curve and modified double logarithm regression curve), which showed relatively high values of binding constants. It may suggest a long half-live of the drug. However, it should be noted that both models are not perfect because simplified linear equations were used. These models do not include fluorescence of free ligand, complex peptide/drug interactions or no-linear dependencies at higher concentrations of the drug.

2.6.2. Binding site identification

It is well known that in BSA molecule there are two major specific drug-binding sites, which are two hydrophobic cavities in subdomains IIA and IIIA, which are defined as site I and site II, respectively [69]. To identify the binding site of BSA that bind studied compounds, phenylbutazone and ibuprofen were used as site probes. Site I shows the binding affinity towards phenylbutazone, and site II is known to bind ibuprofen [70]. Binding constants were analysed using Equation (3). The results for the most active COX inhibiting compounds **7a-b, 8a-b** were summarized in Table 6 (for all compounds in **Table S3** in the supplementary data). It has been observed that the binding constant of all compounds with BSA in the presence of phenylbutazone and ibuprofen significantly decreases compared to the K_b value in the absence of any site markers. However, the decrease in the binding constant in the presence of ibuprofen was greater but not much more. It can be concluded that the tested compounds may be binding to both site I and site II but more preferably to site II.

2.6.3. Thermodynamic studies

The interaction forces between a small molecule and protein include hydrogen bond, van der Waals force, electrostatic and hydrophobic interactions, etc. [71]. The forces involved in the interaction are identified by the thermodynamic analysis. The signs and magnitudes of the thermodynamic parameters identify the type of interactions [72]. The enthalpy change (ΔH°), the entropic change (ΔS°) and free energy change (ΔG°) were calculated from Equation (5) and (6):

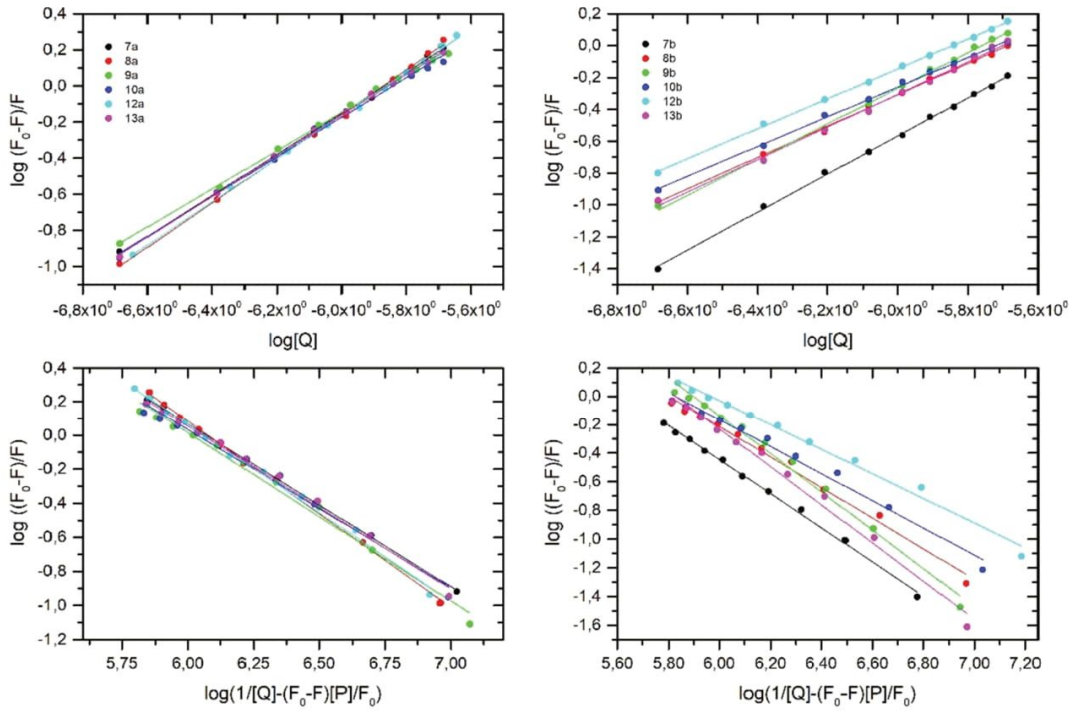

Fig. 7. Double logarithm regression curve plots (top) and the plots log $(F_0\text{-}F)/F$ vs. log $(1/([Q]–(F_0–F)[P]/F_0))$ (Modified double log) for quenching of BSA by compounds **7a-13a** (left) and **7b-13b** (right).

Table 6
Binding constant of the **7a-b, 8a-b** with BSA in the presence of site markers at 303 K.

	Site marker	logK_b	R^2		Site marker	logK_b	R^2
7a	-	6.65 ± 0.07	0.998	**7b**	-	6.59 ± 0.08	0.998
	Phenylbutazone	Ibuprofen 3.15 ± 0.04	0.999		Phenylbutazone	Ibuprofen 3.47 ± 0.22	0.969
		2.35 ± 0.03	0.998			2.77 ± 0.09	0.992
8a	-	7.20 ± 0.10	0.998	**8b**	-	5.58 ± 0.08	0.998
	Phenylbutazone	Ibuprofen 2.80 ± 0.05	0.997		Phenylbutazone	Ibuprofen 2.59 ± 0.12	0.982
		2.72 ± 0.05	0.996			2.04 ± 0.09	0.984

$$\log K_b = -\frac{\Delta H^\circ}{RT} + \frac{\Delta S^\circ}{R} \quad (5)$$

$$\Delta G^\circ = \Delta H^\circ - T\Delta S^\circ = -RT\ln K_b \quad (6)$$

where K_b is the binding constant, R is the universal gas constant.

The calculated data for the most active COX inhibiting compounds **7a-b, 8a-b** are presented in Table 7 (for all compounds in **Table S4** in the supplementary data). The results showed that the binding interaction between tested compounds and BSA were spontaneous due to the negative ΔG° values at the studied temperature range. Furthermore, both the ΔH° and ΔS° negative values indicating that the main interaction force in the binding process was van der Waals forces and/or hydrogen bonding interaction.

2.6.4. Circular dichroism spectra

Circular dichroism spectroscopy, similar to synchronous fluorescence spectroscopy, is a very powerful method to determine the changes in secondary structure in the conformation of proteins in the case of the presence of compounds that can interact with the protein molecule [73]. In this study, the changes in the structure of BSA when all fourteen analysed compounds, **7a,b-13a,b**, were absent or present in solutions were monitored. In all CD spectra, there were observed two negative bands characteristic for BSA at near 208 nm and 222 nm (supplementary data, **Fig. S3**), which is typical for the α-helical structure of the protein. Any changes in this region of the spectra suggest conformational changes in protein molecules [74].

In the presence of all analysed compounds, there was observed a reduction of values of ellipticity at 208 nm and 222 nm after adding every portion of ligands. Therefore, it can be concluded that there was a loss in the α-helix (%). No shift of the peaks was observed.

The content of α-helix can be calculated using Equation (7) and (8) [75]:

$$\alpha - \text{helix}(\%) = \frac{-\text{MRE}_{208} - 4000}{33000 - 4000} 100\% \quad (7)$$

where MRE_{208} is the MRE value observed at 208 nm, 4000 and 33,000 is the MRE value of the β-form and random coil conformation cross at 208 nm value of pure α-helix at 208 nm, respectively.

$$\text{MRE} = \frac{\text{ObservedCD(mdeg)}}{10Cnl} \quad (8)$$

where C is the molar concentration of BSA, n is the number of amino acid residues, which is 583 for BSA, l is the path length in cm.

The reduction in α-helical contents of BSA is observed in the presence of all analysed compounds (Table 8, Fig. 8). The results show that the greatest changes of α-helix (%) are observed in the case of compounds **12b** and **7a**. The α-helical content of BSA decreased here from 57.43% to 50.79% and from 55.66% to 49.46% respectively, with increasing BSA to analysed compounds molar ratio from 1:0 to 1:10. For the interaction of BSA with compound **8b**, the smallest changes were observed (Table 8 and supplementary data, **Fig. S3**). Therefore, CD studies showed that all analysed compounds bind to BSA, which is in agreement with fluorescence spectroscopy.

2.6.5. Molecular docking – Interactions with BSA

In order to determine the preferred binding sites of the compounds **7a-13a** and **7b-13b** on BSA, the binding interactions were simulated by the molecular docking method.

The simulated results for the most active COX inhibiting compounds **7a-b, 8a-b** are presented in Table 9 (for all compounds in **Table S5** in the supplementary data). As is well known, the more negative the binding free energy ΔG°, the more stable the formed complex is. The results revealed that the binding free energy for all compounds within the hydrophobic cavity in site II (m) of BSA was more negative than that within the hydrophobic cavity in the site I and site II (l). This indicates that site II (m) is favourable. However, the binding in site I is also possible. As presented in Table 9, the sum of van der Waals energy, hydrogen bonding energy, and desolvation free energy (ΔE_2) is evidently more negative than electrostatic energy (ΔE_3). Hence, it can indicate that the main interactions between studied compounds and BSA are van der Waals and hydrogen bonding interactions. Our thermodynamic studies also indicated that van der Waals and hydrogen bonding contributed to the interaction between BSA and tested compounds. In binding site II (m) studied compounds **7a** and **7b** insert into hydrophobic cavity surrounded

Table 7
Binding and thermodynamic parameters for the binding interaction between compounds **7a-b, 8a-b** and BSA.

	T [K]	logK_b	n	R^2	ΔG° [kJmol^{-1}]	ΔH° [kJmol^{-1}]	ΔS° [Jmol^{-1}K^{-1}]
7a	303,306,310	6.65 ± 0.07	1.13 ± 0.01	0.998	−38.64	−13.40	−310.80
		6.45 ± 0.14	1.10 ± 0.02	0.997			
		6.13 ± 0.18	1.05 ± 0.03	0.993			
8a	303,306,310	7.20 ± 0.10	1.22 ± 0.02	0.998	−41.94	−16.30	−400.73
		6.79 ± 0.11	1.16 ± 0.02	0.998			
		6.55 ± 0.17	1.12 ± 0.03	0.995			
7b	303,306,310	6.59 ± 0.08	1.19 ± 0.02	0.998	−37.80	−43.08	−1297.18
		5.65 ± 0.09	0.98 ± 0.02	0.998			
		4.90 ± 0.12	0.86 ± 0.03	0.996			
8b	303,306,310	5.58 ± 0.08	0.98 ± 0.08	0.998	-32.15	−19.61	−541.37
		5.13 ± 0.06	0.91 ± 0.06	0.999			
		4.91 ± 0.10	0.90 ± 0.02	0.996			

Table 8
Values of calculated α-helix (%) for BSA with the absence and presence of all analysed compounds.

	Analysed compound													
	7a	**8a**	**9a**	**10a**	**11a**	**12a**	**13a**	**7b**	**8b**	**9b**	**10b**	**11b**	**12b**	**13b**
BSA/analysed compound molar ratio	α-helix(%)													
1:0	**55.66**	**56.67**	**56.00**	**55.75**	**56.32**	**56.80**	**57.05**	**55.96**	**55.97**	**55.36**	**56.67**	**57.79**	**57.43**	**57.21**
1:0.5	53.84	55.05	54.69	54.25	54.47	55.18	55.03	54.31	54.43	54.79	55.25	55.36	55.59	55.97
1:1	52.71	54.19	53.88	53.05	53.51	54.45	54.38	53.50	53.82	53.16	54.93	54.60	54.93	55.76
1:2	51.96	53.81	53.58	52.24	52.99	54.48	53.56	52.97	53.34	52.82	53.89	54.37	53.99	54.88
1:3	51.19	53.25	53.03	51.77	52.19	53.66	53.32	52.75	53.29	52.58	52.83	54.23	53.85	54.54
1:4	51.38	53.01	52.14	51.50	52.20	53.16	52.18	52.58	52.90	52.39	52.53	53.74	53.48	54.04
1:5	50.58	52.84	51.72	51.40	52.13	52.80	51.97	52.05	52.80	52.02	52.37	53.64	52.85	53.22
1:6	50.49	52.83	51.53	51.09	51.70	52.59	51.90	51.77	52.72	51.49	51.97	53.59	52.38	53.19
1:7	49.75	52.47	51.12	51.06	51.53	52.29	51.71	51.18	52.59	51.31	51.86	53.52	52.11	53.17
1:8	49.71	52.38	50.98	51.04	51.42	52.09	51.36	51.02	52.40	51.26	51.62	53.42	51.86	53.13
1:9	49.45	52.29	50.86	50.99	51.22	51.43	51.33	50.52	52.32	51.11	51.33	53.26	50.97	53.11
1:10	**49.46**	**52.23**	**50.31**	**50.98**	**51.19**	**51.30**	**51.32**	**50.25**	**52.15**	**50.81**	**50.98**	**53.24**	**50.79**	**53.03**

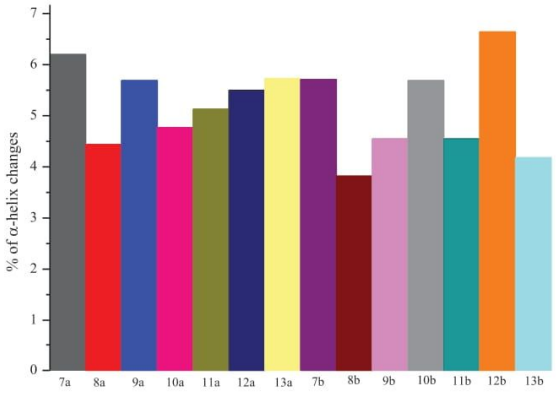

Fig. 8. Comparison of changes in α-helix (%) of BSA after adding 10 portions of each compound analysed.

Table 9
Energies of the binding complexes for **7a-b**, **8a-b** obtained from molecular docking.

	Binding site	ΔG° [kJmol^{-1}]	ΔE_1 [kJmol^{-1}]	ΔE_2 [kJmol^{-1}]	ΔE_3 [kJmol^{-1}]
7a	site I	−8.75	−10.65	−9.70	−0.96
	site II (m)	−10.73	−12.81	−11.90	−0.91
	site II (l)	−6.69	−8.77	−8.55	−0.22
8a	site I	−8.26	−10.34	−9.36	−0.99
	site II (m)	−8.90	−10.98	−10.23	−0.75
	site II (l)	−7.25	−9.34	−9.15	−0.19
7b	site I	−6.61	−9.29	−8.10	−1.19
	site II (m)	−8.11	−10.80	−10.09	−0.71
	site II (l)	−6.58	−9.26	−9.56	0.29
8b	site I	−6.79	−9.48	−8.44	−1.04
	site II (m)	−9.48	−12.17	−11.41	−0.76
	site II (l)	−7.76	−10.45	−10.37	−0.08

ΔG° – binding free energy; ΔE_1 – intermolecular interaction energy, which is the sum of van der Waals energy, hydrogen bonding energy, desolvation free energy and electrostatic energy; ΔE_2 – the sum of Van der Waals energy, hydrogen bonding energy and desolvation free energy; ΔE_3 – electrostatic energy

by various kinds of residues (Fig. 9). Hydrogen bonds with Lys211, Asp323, Arg208, Leu480, Glu353 are formed. In the site I pocket hydrogen bonds are also formed. Interactions π-sigma, π–cation, and other hydrophobic are observed. Tryptophan residue (Trp-213) is close to tested compounds. The details are presented in Fig. 9 (for all compounds in **Fig. S4 and S5** in the supplementary data).

3. Conclusions

The present study describes the synthesis of two series of Mannich base derivatives of pyrrolo[3,4–*d*]pyridazinone and their biological and *in silico* investigations. Title compounds were designed as a new class of potential cyclooxygenase inhibitors and proved such activity in *in vitro* and molecular docking studies. All analysed derivatives **7a**,**b**-**13a**,**b** showed better affinity to the COX-2 isoform and had superior COX-2/COX-1 selectivity ratio than the reference drug, meloxicam. Some of them, **10a**, **11a**, **12a,** and **13a**,**b**, appeared to be selective COX-2 inhibitors in the executed experiment. These results are in good agreement with molecular docking studies, which confirmed that tested compounds have a better affinity towards COX-2 than to COX-1 and the pyrrolo[3,4–*d*]pyridazinone scaffold takes a position very similar to that of meloxicam in the active site of the enzyme. In both experiments, the most active compounds to inhibit COX-1 were **7a**,**b,** and **8a**,**b**. Some of the newly obtained Mannich bases were able to reduce the levels of ROS and RNS in performed *in vitro* tests. What is more, derivatives **7a**,**b**, **8a**, **10a**,**b**, **11b**, **12a**,**b**-**13a**,**b** showed valuable protective properties and decreased the number of DNA strand breaks caused by intracellular growth of free radicals. Spectroscopic and molecular docking studies indicate that all analysed compounds probably form complexes with bovine serum albumin and bind favourably to site II (m) of BSA. This, in turn, could suggest a long half-life of the investigated derivatives. Finally, multiple-criteria decision analysis (MCDA) was carried out following the weighted sum model (WSM) (Fig. 10). Based on the results of MCDA, the best biological properties *in vitro* were demonstrated by compound **7b** and slightly weaker by **7a**. Derivatives **10a** and **13a**,**b** seem to be potent and promising as well.

Our research indicates that cyclooxygenase is a potential molecular target for new drug candidates based on the attractive pyrrolo[3,4-*d*]pyridazinone skeleton. As a continuation of this work, we plan further modifications of these promising structures and other pharmacological experiments, in an *in vivo* model, as well. Studies of acute and chronic gastrotoxicity of these compounds are essential to evaluate their safety. Such investigations could explain whether Mannich base derivatives of pyrrolo[3,4-*d*]pyridazinone could serve as a secure and effective analgesic and anti-inflammatory agents.

4. Experimental

4.1. Chemistry

4.1.1. Instrumentation and chemicals

All chemicals, reagents and solvents used in the current study were purchased from commercial suppliers. Dry solvents were obtained according to the standard procedures. Progress of the reaction was

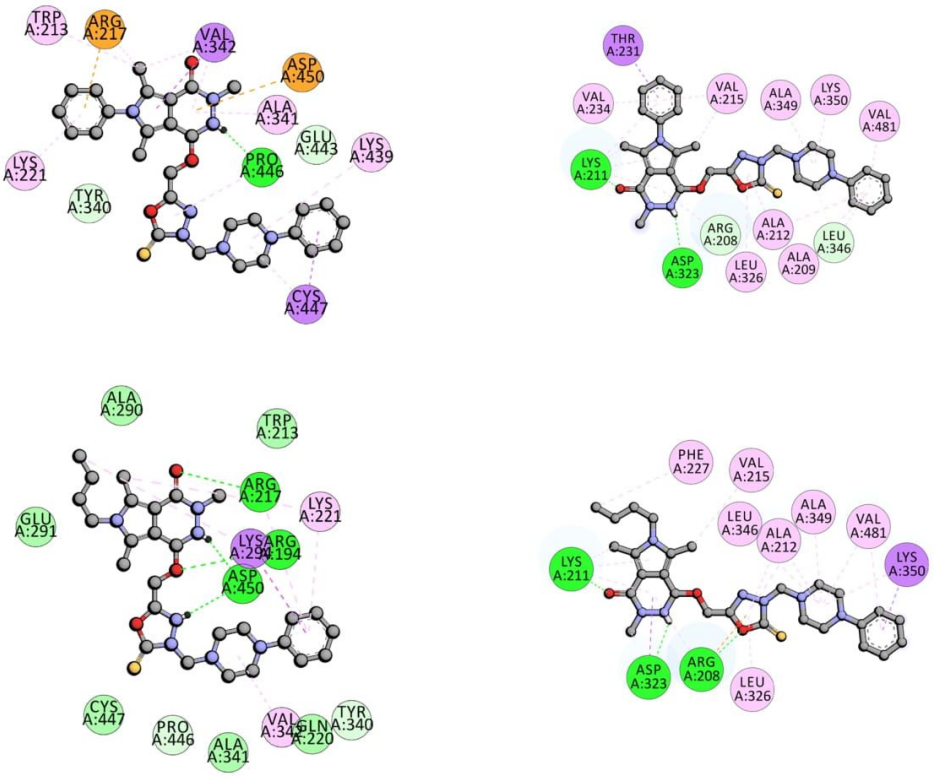

Fig. 9. 2D interaction of **7a** (top) and **7b** (bottom) with BSA in binding site I (left) and site II (right) (green – hydrogen bonds, violet – π-sigma, orange – π-cation, pink – other hydrophobic). (For interpretation of the references to color in this figure legend, the reader is referred to the web version of this article.)

monitored by thin-layer chromatography (TLC) technique on silica-gel-60-F254-coated TLC plates (Fluka Chemie GmbH) and visualised by UV light at 254 nm. Chromatographic separations were performed on a silica gel [Kieselgel 60 (70–230 mesh), Merck] column (CC). The melting points of synthesised compounds were determined by an open capillary method on Electrothermal Mel-Temp 1101D apparatus and were uncorrected. The ^{1}H NMR (300 MHz) and ^{13}C NMR (75 MHz) spectra were recorded on a Bruker 300 MHz NMR spectrometer in DMSO–d_6 or $CDCl_3$ using tetramethylsilane (TMS) as an internal reference. Chemical shifts (δ) are reported in ppm. The infrared (IR) spectra were determined on a Nicolet iS50 FT-IR Spectrometer. Samples were applied as solids and frequencies are reported in cm^{-1}. Mass spectra were recorded using a Bruker Daltonics Compact ESI-mass spectrometer. The instrument was operated in positive ion mode. Analysed compounds were dissolved in a mixture of chloroform and methanol. Elemental analyses for carbon, nitrogen and hydrogen were

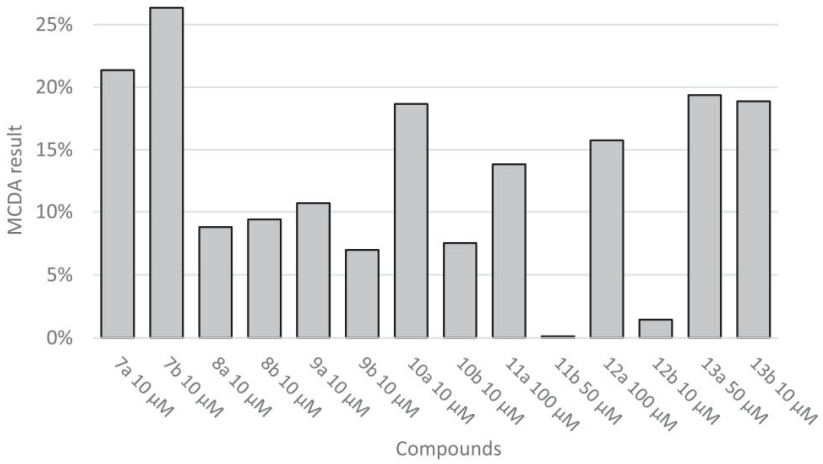

Fig. 10. Multiple-criteria decision analysis (MCDA) for results obtained in biological assays. The graph shows the results of the best-performing concentration of each compound.

run on a Carlo Erba NA–1500 analyser, and obtained results were within ± 0.4% of the theoretical values calculated for corresponding formulas.

4.1.2. Chemical synthesis

The synthesis protocols and experimental data for compounds **2a** and **2b** and all intermediates were previously reported [18,55]

4.1.2.1. General procedure for preparation of methyl ester derivatives (3a, 3b). The appropriate derivative of pyrrolo[3,4-*d*]pyridazine-1,4-dione **2a** or **2b** (0.01 mol) and K_2CO_3 (0.02 mol) were suspended in 50 mL of acetonitrile in a round bottom flask. Then, methyl chloroacetate (0.012 mol) was added and the mixture was refluxed for 6 h. After completion of the reaction (monitored by TLC) the solvent was distilled off under reduced pressure. Chloroform was added to the crude solid and filtered, collecting filtrate. The excess solvent was distilled off under reduced pressure and the residue was purified by CC using ethyl acetate as an eluent. The fractions containing product **3a** (R_f = 0.73) or **3b** (R_f = 0.69) were combined and evaporated to give white-yellowish solid methyl 2-(3,5,7-trimethyl-4-oxo-6-phenyl-pyrrolo[3,4-*d*]pyridazin-1-yl)oxyacetate **3a** or white solid methyl 2-(6-butyl-3,5,7-trimethyl-4-oxo-pyrrolo[3,4-*d*]pyridazin-1-yl)oxyacetate **3b**, which were used without further purification.

3a: Methyl 2-(3,5,7-trimethyl-4-oxo-6-phenyl-pyrrolo[3,4-*d*]pyridazin-1-yl)oxyacetate,

Yield: 68.49%; m.p.: 141–144 °C;

FT-IR (selected lines, γ_{max}, cm^{-1}): 3052, 3002 (C—H arom.), 2953, 2915, 2862 (C—H aliph.), 1749 (C═O), 1435 (C—H aliph.) 1222 (C—O), ^{1}H NMR (300 MHz, $CDCl_3$) δ: 2.32 (s, 3H, 7-CH_3), 2.43 (s, 3H, 5-CH_3), 3.55 (s, 3H, 3-CH_3), 3.79 (s, 3H, –OCH_3), 4.83 (s, 2H, O-CH_2-), 7.18–7.21 (m, 2H, ArH), 7.52–7.55 (m, 3H, ArH); ^{13}C NMR (75 MHz, $CDCl_3$) δ: 11.4, 11.8, 37.1, 51.9, 62,5, 108.7, 112.1, 124.3 127.8, 129.3, 129.7, 130.5, 136.8, 148.4, 159.4, 169.3; ESI-MS (*m/z*): calcd. for $C_{18}H_{19}N_3O_4$ [L + H]$^+$: 342.1418; found: 342.1470; Anal. calcd. (%) for $C_{18}H_{19}N_3O_4$: C:63.33, H:5.61, N:12.31, found: C:62.99, H:5.67, N:12.37,

3b: Methyl 2-(6-butyl-3,5,7-trimethyl-4-oxo-pyrrolo[3,4-*d*]pyridazin-1-yl)oxyacetate

Yield: 61.87%; m.p.: 130–133 °C;

FT-IR (selected lines, γ_{max}, cm^{-1}): 2957, 2936, 2871 (C—H aliph.), 1760 (C═O), 1228, 1182 (C—O), ^{1}H NMR (300 MHz, $CDCl_3$) δ: 0.94–0.99 (m, 3H, –CH_2-CH_2 CH_2-CH_3), 1.34–1.42 (m, 2H, –CH_2-CH_2 CH_2-CH_3), 1.59–1.66 (m, 2H, –CH_2-CH_2 CH_2-CH_3), 2.56 (s, 3H, 7-CH_3), 2.68 (s, 3H, 5-CH_3), 3.51 (s, 3H, 3-CH_3), 3.78 (s, 3H, –OCH_3), 3.87–3.93 (m, 2H, –CH_2-CH_2 CH_2-CH_3), 4.81 (s, 2H, O-CH_2–); ^{13}C NMR (75 MHz, $CDCl_3$) δ: 10.6, 11.1, 13.7, 20.0, 32.3, 37.0, 43.9, 51.9, 62.5, 108.4, 111.9, 122.6, 128.9, 148.3, 159.3, 169.3; ESI-MS (*m/z*): calcd. for $C_{16}H_{23}N_3O_4$ [L + H]$^+$: 322.1761; found: 322.1791; Anal. calcd. (%) for $C_{16}H_{23}N_3O_4$: C:59.80, H:7.21, N:13.08, found: C:59.85, H:7.17, N:13.20,

4.1.2.2. General procedure for preparation of hydrazide derivatives (5a, 5b). The mixture of adequate methyl ester (**3a** or **3b**) (0.01 mol) and hydrazine hydrate (98%) (0.1 mol) was refluxed in 50 mL of ethanol for 6 h and left overnight. The next day, the formed precipitate was filtered off, washed carefully with cold ethanol and dried. The crude product was purified by recrystallization from ethanol, resulting in a white, crystalline solid: 2-(3,5,7-trimethyl-4-oxo-6-phenyl-pyrrolo[3,4-*d*]pyridazin-1-yl)oxyacetohydrazide **5a**, or white solid: 2-(6-butyl-3,5,7-trimethyl-4-oxo-pyrrolo[3,4-*d*]pyridazin-1-yl)oxyacetohydrazide **5b**, accordingly.

5a: 2-(3,5,7-Trimethyl-4-oxo-6-phenyl-pyrrolo[3,4-*d*]pyridazin-1-yl)oxyacetohydrazide,

Yield: 86.59%; m.p.: 188–190 °C;

FT-IR (selected lines, γ_{max}, cm^{-1}): 3316 (NH, NH_2), 3253 (NH_2), 3049 (C—H arom.), 2950 (C—H aliph.), 1609 (CO-NH), ^{1}H NMR (300 MHz, $CDCl_3$) δ: 2.31 (s, 3H, 7-CH_3), 2.44 (s, 3H, 5-CH_3), 3.57 (s, 3H, 3-CH_3), 4.89 (s, 2H, O-CH_2-), 7.20–7.22 (m, 2H, ArH), 7.56–7.58 (m, 3H, ArH); ^{13}C NMR (75 MHz, $CDCl_3$) δ: 11.4, 12.1, 37.2, 64.4, 108.5, 112.1, 123.6, 127.7, 129.4, 129.8, 130.9, 136.5, 147.8, 159.2, 169.0; ESI-MS (*m/z*): calcd. for $C_{17}H_{19}N_5O_3$ [L + H]$^+$: 342.1561; found: 342.1620; Anal. calcd. (%) for $C_{17}H_{19}N_5O_3$: C:59.81, H:5.61, N:20.52, found: C:59.56, H:5.29, N:20.37,

5b: 2-(6-Butyl-3,5,7-trimethyl-4-oxo-pyrrolo[3,4-*d*]pyridazin-1-yl) oxyacetohydrazide

Yield: 82.14%; m.p.: 202–203 °C;

FT-IR (selected lines, γ_{max}, cm^{-1}): 3322 (NH, NH_2), 3268, 3208 (NH_2), 2935, 2863 (C—H aliph.), 1617 (CO-NH), ^{1}H NMR (300 MHz, $CDCl_3$) δ: 0.96–1.01 (m, 3H, –CH_2-CH_2 CH_2-CH_3), 1.42 (m, 2H, –CH_2-CH_2 CH_2-CH_3), 1.66 (m, 2H, –CH_2-CH_2 CH_2-CH_3), 2.55 (s, 3H, 7-CH_3), 2.70 (s, 3H, 5-CH_3), 3.55 (s, 3H, 3-CH_3), 3.94 (m, 2H, –CH_2-CH_2 CH_2-CH_3), 4.88 (s, 2H, O-CH_2–); ^{13}C NMR (75 MHz, $DMSOd_6$) δ: 10.1, 10.8, 13.5, 19.4, 31.6, 36.6, 63.4, 107.5, 123.1, 128.4, 147.9, 158.0, 166.6; ESI-MS (*m/z*): calcd. for $C_{15}H_{23}N_5O_4$ [L + H]$^+$: 322.1874; found: 322.1912; Anal. calcd. (%) for $C_{15}H_{23}N_5O_4$: C:56.06, H:7.21, N:21.79, found: C:56.00, H:7.24, N:21.49,

4.1.2.3. General procedure for preparation of 2-thioxo-3H-1,3,4-oxadiazol derivatives (6a, 6b). The appropriate hydrazide (**5a** or **5b**) (0.01 mol) and KOH (0.01 mol) were dissolved in ethanol (50 mL) in a round bottom flask. To this stirring mixture carbon disulphide (0.05 mol) was added and the whole was refluxed for 5–6 h till evolution of hydrogen sulfide was ceased. Then, the reaction mixture was cooled, slowly poured onto crushed ice and acidified with diluted hydrochloric acid. Formed precipitate was filtered off, washed with cold water, dried and recrystallized from ethanol giving white solid 3,5,7-trimethyl-6-phenyl-1-[(2-thioxo-3*H*-1,3,4-oxadiazol-5-yl)methoxy]pyrrolo[3,4-*d*]pyridazin-4-one **6a**, or 6-butyl-3,5,7-trimethyl-1-[(2-thioxo-3*H*-1,3,4-oxadiazol-5-yl)methoxy]pyrrolo[3,4-*d*]pyridazin-4-one **6b**, respectively.

6a: 3,5,7-Trimethyl-6-phenyl-1-[(2-thioxo-3*H*-1,3,4-oxadiazol-5-yl) methoxy]pyrrolo[3,4-*d*]pyridazin-4-one

Yield: 80.78%; m.p.: 220–222 °C;

FT-IR (selected lines, γ_{max}, cm^{-1}): 3025 (C—H arom.), 2859 (C—H aliph.), 1592 (C═S), ^{1}H NMR (300 MHz, $DMSOd_6$) δ: 2.23 (s, 3H, 7-CH_3), 2.32 (s, 3H, 5-CH_3), 3.42 (s, 3H, 3-CH_3), 5.38 (s, 2H, O-CH_2-), 7.40–7.43 (m, 2H, ArH), 7.60–7.62 (m, 3H, ArH); ^{13}C NMR (75 MHz, $DMSOd_6$) δ: 11.0, 11.6, 36.6, 57.2, 107.4, 111.0, 124.1, 127.8, 129.4, 129.8, 130.1, 135.9, 147.3, 157.9, 159.7, 177.9; ESI-MS (*m/z*): calcd. for $C_{18}H_{17}N_5O_3S$ [L + H]$^+$: 384.1125; found: 384.1171; Anal. calcd. (%) for $C_{18}H_{17}N_5O_3S$: C:56.38, H:4.47, N:18.27, found: C:56.46, H:4.38, N:17.95,

6b: 6-Butyl-3,5,7-trimethyl-1-[(2-thioxo-3*H*-1,3,4-oxadiazol-5-yl) methoxy]pyrrolo[3,4-*d*]pyridazin-4-one

Yield: 82.14%; m.p.: 215–218 °C;

FT-IR (selected lines, γ_{max}, cm^{-1}): 2930, 2860 (C—H aliph.), 1594 (C═S), ^{1}H NMR (300 MHz, $DMSOd_6$) δ: 0.88–0.93 (m, 3H, –CH_2-CH_2 CH_2-CH_3), 1.30–1.33 (m, 2H, –CH_2-CH_2 CH_2-CH_3), 1.58 (m, 2H, –CH_2-CH_2 CH_2-CH_3), 2.49 (s, 3H, 7-CH_3), 2.59 (s, 3H, 5-CH_3), 3.38 (s, 3H, 3-CH_3), 3.95–3.98 (m, 2H, –CH_2-CH_2 CH_2-CH_3), 5.33 (s, 2H, O-CH_2–); ^{13}C NMR (75 MHz, $CDCl_3$) δ: 10.1, 10.7, 13.5, 19.4, 31.5, 36.5, 43.4, 57.1, 123.9, 129.9; ESI-MS (*m/z*): calcd. for $C_{16}H_{21}N_5O_3S$ [L + H]$^+$: 364.1438; found: 364.1483; Anal. calcd. (%) for $C_{16}H_{21}N_5O_3S$: C:52.88, H:5.82, N:19.27, found: C:52.94, H:5.94, N:19.03,

4.1.2.4. General procedure for preparation of Mannich base derivatives of pyrrolo[3,4-d]pyridazine-1,4-dione (7a,b-13a,b). 37% aqueous formaldehyde (0.1 mol) was added to the solution of adequate 2-thioxo-3*H*-1,3,4-oxadiazole derivative of pyrrolo[3,4-*d*]pyridazine-1,4-dione (**6a** or **6b**) (0.01 mol) in ethanol (30 mL). The mixture was stirred at room temperature (RT) for 30 min. Next, an appropriately substituted secondary amine was added, and the stirring was continued for a further several hours at RT. The mixture was left

overnight. The formed precipitate was filtered off, thoroughly washed with cold ethanol and purified by crystallization from ethanol.

7a:3,5,7-Trimethyl-6-phenyl-1-[[4-[(4-phenylpiperazin-1-yl)methyl]-2-thioxo-1,3,4-oxadiazol −5-yl]methoxy]pyrrolo[3,4-*d*]pyridazin-4-one

Yield: 73.39%; m.p.: 189–192 °C;

FT-IR (selected lines, γ_{max}, cm^{-1}): 3055 (C—H arom.), 2924, 2833 (C—H aliph.), 1644 (C═N), ^{1}H NMR (300 MHz, $CDCl_3$) δ: 2.29 (s, 3H, 7-CH_3), 2.43 (s, 3H, 5-CH_3), 3.44 (m, 8H, CH_2 – piperazine) 3.58 (s, 3H, 3-CH_3), 5.09 (s, 2H, N-CH_2), 5.35 (s, 2H, O-CH_2), 7.18–7.21 (m, 3H, ArH), 7.43 (m, 4H, ArH) 7.53–7.55 (m, 3H, ArH); ^{13}C NMR (75 MHz, $CDCl_3$) δ: 11.4, 11.9, 37.1, 49.4, 50.2, 57.0, 70.2, 108.3, 112.0, 116.5, 120.1, 124.3, 127.7, 129.1, 129.3, 129.7, 130.8, 136.6, 147.8, 151.2, 157.6, 159.3, 178.8; ESI-MS (*m/z*): calcd. for $C_{29}H_{31}N_7O_3S$ [L + H]$^+$: 558.2282; found: 558.2350; Anal. calcd. (%) for $C_{29}H_{31}N_7O_3S$: C:62.46, H:5.60, N:17.58, found: C:62.20, H:5.50, N:17.41,

7b: 6-Butyl-3,5,7-trimethyl-1-[[4-[(4-phenylpiperazin-1-yl)methyl]-2-thioxo-1,3,4-oxadiazol-5-yl]methoxy]pyrrolo[3,4-*d*]pyridazin-4-one

Yield: 72.21%; m.p.: 196–198 °C;

FT-IR (selected lines, γ_{max}, cm^{-1}): 2943, 2880, 2830 (C—H aliph.), 1620 (C═N), 1551 (C═S), ^{1}H NMR (300 MHz, $CDCl_3$) δ: 0.95–1.00 (m, 3H, –CH_2-CH_2 CH_2-CH_3), 1.34–1.42 (m, 2H, –CH_2-CH_2 CH_2-CH_3), 1.65 (m, 2H, –CH_2-CH_2 CH_2-CH_3), 2.51 (s, 3H, 7-CH_3), 2.69 (s, 3H, 5-CH_3), 2.97–3.00 (m, 4H, CH_2 – piperazine), 3.19–3.22 (m, 4H, CH_2 – piperazine), 3.55 (s, 3H, 3-CH_3), 3.92 (m, 2H, –CH_2-CH_2 CH_2-CH_3), 5.10 (s, 2H, N-CH_2), 5.29 (s, 2H, O-CH_2), 6.90–6.96 (m, 3H, ArH), 7.24–7.28 (m, 2H, ArH); ^{13}C NMR (75 MHz, $CDCl_3$) δ: 10.6, 11.2, 13.6, 20.0, 32.3, 37.0, 43.9, 49.4, 50.2, 56.9 70.3, 108.0, 111.8, 116.4, 120.1, 122.7, 129.1, 129.3, 147.8, 151.1, 157.6, 159.2, 178.9 ESI-MS (*m/z*): calcd. for $C_{27}H_{35}N_7O_3S$ [L + H]$^+$: 538.2595; found: 538.2629; Anal. calcd. (%) for $C_{27}H_{35}N_7O_3S$: C:60.31, H:6.56, N:18.24, found: C:60.02, H:6.80, N:17.90,

8a: 3,5,7-Trimethyl-6-phenyl-1-[[4-[[4-(*p*-tolyl)piperazin-1-yl]methyl]-2-thioxo-1,3,4-oxadiazol-5-yl]methoxy]pyrrolo[3,4-*d*]pyridazin-4-one

Yield: 59.68%; m.p.: 172–174 °C;

FT-IR (selected lines, γ_{max}, cm^{-1}): 3041 (C—H arom.), 2937, 2826 (C—H aliph.), 1624 (C═N), 1556 (C═S), ^{1}H NMR (300 MHz, $CDCl_3$) δ: 2.28 (s, 3H, 7-CH_3), 2.29 (s, 3H, Ar-CH_3), 2.43 (s, 3H, 5-CH_3), 2.98–3.00 (m, 4H, CH_2 – piperazine), 3.13–3.14 (m, 4H, CH_2 – piperazine), 3.59 (s, 3H, 3-CH_3), 5.09 (s, 2H, N-CH_2), 5.33 (s, 2H, O-CH_2), 6.81–6.84 (m, 2H, ArH), 7.06–7.09 (m, 2H, ArH), 7.20–7.22 (m, 2H, ArH), 7.55–7.57 (m, 3H, ArH); ^{13}C NMR (75 MHz, $CDCl_3$) δ: 11.4, 11.9, 20.4, 37.1, 49.9, 50.2, 57.0, 70.3, 108.2, 112.0, 116.8, 127.7, 129.3, 129.6, 129.7, 130.8, 136.6, 147.9, 158.0, 179.2 ESI-MS (*m/z*): calcd. for $C_{30}H_{33}N_7O_3S$ [L + H]$^+$: 572.2438; found: 572.2513; Anal. calcd. (%) for $C_{29}H_{31}N_7O_3S$: C:63.03, H:5.82, N:17.15, found: C:62.75, H:5.52, N:16.87,

8b: 6-Butyl-3,5,7-trimethyl-1-[[4-[[4-(*p*-tolyl)piperazin-1-yl]methyl]-2-thioxo-1,3,4-oxadiazol-5-yl]methoxy]pyrrolo[3,4-*d*]pyridazin-4-one

Yield: 85.64%; m.p.: 209–211 °C;

FT-IR (selected lines, γ_{max}, cm^{-1}): 2943, 2875, 2828 (C—H aliph.), 1619 (C═N), 1551 (C═S), ^{1}H NMR (300 MHz, $CDCl_3$) δ: 0.96–1.00 (m, 3H, –CH_2-CH_2 CH_2-CH_3), 1.36–1.44 (m, 2H, –CH_2-CH_2 CH_2-CH_3), 1.63–1.68 (m, 2H, –CH_2-CH_2 CH_2-CH_3), 2.28 (s, 3H, Ar-CH_3), 2.52 (s, 3H, 7-CH_3), 2.70 (s, 3H, 5-CH_3), 2.97–3.00 (m, 4H, CH_2 – piperazine), 3.13–3.16 (m, 4H, CH_2 – piperazine), 3.55 (s, 3H, 3-CH_3), 3.89–3.95 (m, 2H, –CH_2-CH_2 CH_2-CH_3), 5.10 (s, 2H, N-CH_2), 5.29 (s, 2H, O-CH_2), 6.82–6.85 (m, 2H, ArH), 7.07–7.09 (m, 2H, ArH); ^{13}C NMR (75 MHz, $CDCl_3$) δ: 10.6, 11.3, 13.7, 20.0, 20.4, 32.3, 37.0, 43.9, 49.9, 50.2, 56.9 70.2, 108.0, 111.8, 116.8, 122.6, 129.2, 129.7, 147.8, 149.1, 157.6, 159.2, 178.9, ESI-MS (*m/z*): calcd. for $C_{28}H_{37}N_7O_3S$ [L + H]$^+$: 552.2751; found: 552.2850; Anal. calcd. (%) for $C_{28}H_{37}N_7O_3S$: C:60.96, H:6.76, N:17.77, found: C:61.21, H:6.99, N:17.40,

9a: 1-[[4-[[4-(3-Chlorophenyl)piperazin-1-yl]methyl]-2-thioxo-1,3,4-oxadiazol-5-yl]methoxy]-3,5,7-trimethyl-6-phenyl-pyrrolo[3,4-*d*]pyridazin-4-one

Yield: 57.43%; m.p.: 152–154 °C;

FT-IR (selected lines, γ_{max}, cm^{-1}): 3056 (C—H arom.), 2930, 2834 (C—H aliph.), 1645 (C═N), 1596 (C═S), ^{1}H NMR (300 MHz, $CDCl_3$) δ: 2.26 (s, 3H, 7-CH_3), 2.43 (s, 3H, 5-CH_3), 2.95–2.97 (m, 4H, CH_2 – piperazine), 3.17–3.19 (m, 4H, CH_2 – piperazine), 3.56 (s, 3H, 3-CH_3), 5.08 (s, 2H, N-CH_2), 5.31 (s, 2H, O-CH_2), 6.75–6.85 (m, 3H, ArH), 7.12–7.21 (m, 3H, ArH), 7.54–7.56 (m, 3H, ArH); ^{13}C NMR (75 MHz, $CDCl_3$) δ: 11.4, 11.9, 37.1, 48.8, 50.0, 57.0, 70.2, 108.2, 112.0, 114,2, 116.8, 119.1, 124.3, 127.7, 129.3, 129.6, 129.7, 130.1 130.8, 134.9 136.6, 147.9, 152.2, 157.7, 159.3, 178.8; ESI-MS (*m/z*): calcd. for $C_{29}H_{30}ClN_7O_3S$ [L + H]$^+$: 592.1892; found: 592.1969; Anal. calcd. (%) for $C_{29}H_{30}ClN_7O_3S$: C:58.83, H:5.11, N:16.56, found: C:58.61, H:5.30, N:16.42,

9b: 6-Butyl-1-[[4-[[4-(3-chlorophenyl)piperazin-1-yl]methyl]-2-thioxo-1,3,4-oxadiazol-5-yl]methoxy]-3,5,7-trimethyl-pyrrolo[3,4-*d*]pyridazin-4-one

Yield: 73.05%; m.p.: 173–175 °C;

FT-IR (selected lines, γ_{max}, cm^{-1}): 2954, 2838 (C—H aliph.), 1623 (C═N), 1594 (C═S), ^{1}H NMR (300 MHz, $CDCl_3$) δ: 0.95–1.00 (m, 3H, –CH_2-CH_2 CH_2-CH_3), 1.33–1.43 (m, 2H, –CH_2-CH_2 CH_2-CH_3), 1.60–1.68 (m, 2H, –CH_2-CH_2 CH_2-CH_3), 2.51 (s, 3H, 7-CH_3), 2.69 (s, 3H, 5-CH_3), 2.95–2.98 (m, 4H, CH_2 – piperazine), 3.18–3.22 (m, 4H, CH_2 – piperazine), 3.54 (s, 3H, 3-CH_3), 3.89–3.94 (m, 2H, –CH_2-CH_2 CH_2-CH_3), 5.09 (s, 2H, N-CH_2), 5.29 (s, 2H, O-CH_2), 6.76–6.86 (m, 3H, ArH), 7.14–7.19 (m, 1H, ArH); ^{13}C NMR (75 MHz, $CDCl_3$) δ: 10.6, 11.2, 13.7, 20.0, 32.3, 37.0, 43.9, 48.8, 50.0, 56.9, 70.2, 107.9, 111.8, 114.3, 116.1, 119.7, 122.6, 129.3, 130.9, 147.7, 152.2, 157.7, 159.2, 178.8; ESI-MS (*m/z*): calcd. for $C_{27}H_{34}ClN_7O_3S$ [L + H]$^+$: 572.2205; found: 572.2314; Anal. calcd. (%) for $C_{27}H_{34}ClN_7O_3S$: C:56.68, H:5.99, N:17.14, found: C:56.90, H:6.24, N:16.83,

10a: 3,5,7-Trimethyl-1-[[4-[[4-(4-nitrophenyl)piperazin-1-yl]methyl]-2-thioxo-1,3,4-oxadiazol-5-yl]methoxy]-6-phenyl-pyrrolo[3,4-*d*]pyridazin-4-one

Yield: 84.03%; m.p.: 214–217 °C;

FT-IR (selected lines, γ_{max}, cm^{-1}): 3085 (C—H arom.), 2947, 2915 (C—H aliph.), 1625 (C═N), 1593 (C═S), ^{1}H NMR (300 MHz, $CDCl_3$) δ: 2.26 (s, 3H, 7-CH_3), 2.43 (s, 3H, 5-CH_3), 2.94–2.97 (m, 4H, CH_2 – piperazine), 3.41–3.43 (m, 4H, CH_2 – piperazine), 3.55 (s, 3H, 3-CH_3), 5.09 (s, 2H, N-CH_2), 5.31 (s, 2H, O-CH_2), 6.78–6.81 (m, 2H, ArH), 7.18–7.20 (m, 2H, ArH), 7.54–7.56 (m, 3H, ArH), 8.08–8.11 (m, 2H, ArH); ^{13}C NMR (75 MHz, $CDCl_3$) δ: 11.4, 11.8, 37.1, 47.1, 49.7, 57.0, 70.0, 108.2, 111.9, 112,9, 124.2, 125.9, 127.7, 129.4, 129.8, 130.9, 136.5, 138.7, 147.8, 154.6, 157.7, 159.2, 178.8; ESI-MS (*m/z*): calcd. for $C_{29}H_{30}N_8O_5S$ [L + H]$^+$: 603.2133; found: 603.2214; Anal. calcd. (%) for $C_{29}H_{30}N_8O_5S$: C:57.80, H:5.02, N:18.59, found: C:57.57, H:5.20, N:18.30,

10b: 6-Butyl-3,5,7-trimethyl-1-[[4-[[4-(4-nitrophenyl)piperazin-1-yl]methyl]-5-thioxo-1,3,4-oxadiazol-2-yl]methoxy]pyrrolo[3,4-*d*]pyridazin-4-one

Yield: 89.74%; m.p.: 204–207 °C;

FT-IR (selected lines, γ_{max}, cm^{-1}): 2945, 2861 (C—H aliph.), 1622 (C═N), 1593 (C═S), ^{1}H NMR (300 MHz, $CDCl_3$) δ: 0.94–0.99 (m, 3H, –CH_2-CH_2 CH_2-CH_3), 1.37–1.42 (m, 2H, –CH_2-CH_2 CH_2-CH_3), 1.63 (m, 2H, –CH_2-CH_2 CH_2-CH_3), 2.48 (s, 3H, 7-CH_3), 2.68 (s, 3H, 5-CH_3), 2.97 (m, 4H, CH_2 – piperazine), 3.44 (m, 4H, CH_2 – piperazine), 3.54 (s, 3H, 3-CH_3), 3.88–3.93 (m, 2H, –CH_2-CH_2 CH_2-CH_3), 5.09 (s, 2H, N-CH_2), 5.28 (s, 2H, O-CH_2), 6.79–6.82 (m, 2H, ArH), 8.10–8.13 (m, 2H, ArH); ^{13}C NMR (75 MHz, $CDCl_3$) δ: 10.6, 11.2, 13.6, 20.0, 26.9, 32.3, 37.0, 43.9, 47.1, 49.7, 56.9, 70.0, 107.9, 111.7, 112.9, 122.6, 125.9, 129.3, 138.7, 147.7, 154.6, 157.8, 159.1, 178.8; ESI-MS (*m/z*): calcd. for $C_{27}H_{34}N_8O_5S$ [L + H]$^+$: 583.2446; found: 583.2559; Anal. calcd. (%) for $C_{27}H_{34}N_8O_5S$: C:55.66, H:5.88, N:19.23, found: C:55.90, H:6.10, N:18.99,

11a: 3,5,7-Trimethyl-6-phenyl-1-[[4-[[4-(2-pyridyl)piperazin-1-yl]methyl]-2-thioxo-1,3,4-oxadiazol-5-yl]methoxy]pyrrolo[3,4-*d*]pyridazin-4-one

Yield: 54.89%; m.p.: 183–185 °C;

FT-IR (selected lines, γ_{max}, cm^{-1}): 3054 (C—H arom.), 2922, 2838 (C—H aliph.), 1595 (C═S), ^{1}H NMR (300 MHz, $CDCl_3$) δ: 2.25 (s, 3H, 7-CH_3), 2.42 (s, 3H, 5-CH_3), 2.90–2.93 (m, 4H, CH_2 – piperazine), 3.53 (s, 3H, 3-CH_3), 3.57 (m, 4H, CH_2 – piperazine), 5.08 (s, 2H, N-CH_2), 5.29 (s, 2H, O-CH_2), 6.62–6.65 (m, 2H, ArH), 7.18–7.20 (m, 2H, ArH), 7.48–7.55 (m, 4H, ArH), 8.15–8.16 (m, 1H, ArH); ^{13}C NMR (75 MHz, $CDCl_3$) δ: 11.4, 11.8, 37.1, 45.1, 50.1, 57.0, 70.4, 107.2, 108.2, 112.0, 113,4, 124.3, 127.8, 129.4, 129.7, 130.8, 136.6, 137.5, 147.8, 147.9, 157.6, 159.2, 159.3, 178.8; ESI-MS (*m/z*): calcd. for $C_{28}H_{30}N_8O_3S$ [L + H]$^+$: 559.2234; found: 559.2310; Anal. calcd. (%) for $C_{29}H_{30}N_8O_5S$: C:60.20, H:5.41, N:20.06, found: C:59.88, H:5.50, N:19.81,

11b: 6-Butyl-3,5,7-trimethyl-1-[[4-[[4-(2-pyridyl)piperazin-1-yl]methyl]-5-thioxo-1,3,4-oxadiazol-2-yl]methoxy]pyrrolo[3,4-*d*]pyridazin-4-one:

Yield: 70.55%; m.p.: 186–188 °C;

FT-IR (selected lines, γ_{max}, cm^{-1}): 2945, 2845 (C—H aliph.), 1622 (C═N), 1592 (C═S), ^{1}H NMR (300 MHz, $CDCl_3$) δ: 0.93–0.98 (m, 3H, –CH_2-CH_2 CH_2-CH_3), 1.33–1.41 (m, 2H, –CH_2-CH_2 CH_2-CH_3), 1.60–1.65 (m, 2H, –CH_2-CH_2 CH_2-CH_3), 2.48 (s, 3H, 7-CH_3), 2.67 (s, 3H, 5-CH_3), 2.90–2.93 (m, 4H, CH_2 – piperazine), 3.50 (s, 3H, 3-CH_3), 3.57 (m, 4H, CH_2 – piperazine), 3.87–3.92 (m, 2H, –CH_2-CH_2 CH_2-CH_3), 5.08 (s, 2H, N-CH_2), 5.26 (s, 2H, O-CH_2), 6.60–6.64 (m, 2H, ArH), 7.45–7.48 (m, 1H, ArH), 8.16–8.17 (m, 1H, ArH); ^{13}C NMR (75 MHz, $CDCl_3$) δ: 10.6, 11.2, 13.7, 20.0, 32.3, 37.0, 43.9, 45.1, 50.0, 56.9, 70.4, 107.2, 107.9, 111.8, 113.5, 122.7, 129.3, 137.5, 147.7, 147.9, 157.6, 159.2, 178.8; ESI-MS (*m/z*): calcd. for $C_{26}H_{34}N_8O_3S$ [L + H]$^+$: 539.2547; found: 539.2649; Anal. calcd. (%) for $C_{26}H_{34}N_8O_3S$: C:57.97, H:6.36, N:20.80, found: C:58.30, H:6.70, N:20.49,

12a: 3,5,7-Trimethyl-1-[[4-(morpholinomethyl)-2-thioxo-1,3,4-oxadiazol-5-yl]methoxy]-6-phenyl-pyrrolo[3,4-*d*]pyridazin-4-one

Yield: 53,94%; m.p.: 189–192 °C;

FT-IR (selected lines, γ_{max}, cm^{-1}): 3040 (C—H arom.), 2927, 2855 (C—H aliph.), 1624 (C═N), ^{1}H NMR (300 MHz, $CDCl_3$) δ: 2.27 (s, 3H, 7-CH_3), 2.43 (s, 3H, 5-CH_3), 2.78–2.81 (m, 4H, CH_2 – morpholine), 3.58 (s, 3H, 3-CH_3), 3.67–3.70 (m, 4H, CH_2 – morpholine), 4.99 (s, 2H, N-CH_2), 5.31 (s, 2H, O-CH_2), 7.18–7.21 (m, 2H, ArH), 7.53–7.56 (m, 3H, ArH); ^{13}C NMR (75 MHz, $CDCl_3$) δ: 11.4, 11.9, 37.1, 50.5, 57.0, 66.7, 70.4, 108.2, 112.0, 124.3, 127.8, 129.4, 129.7, 130.9, 136.6, 147.9, 157.6, 159.3, 178.9; ESI-MS (*m/z*): calcd. for $C_{23}H_{26}N_6O_4S$ [L + H]$^+$: 483.1809; found: 483.1880; Anal. calcd. (%) for $C_{23}H_{26}N_6O_4S$: C:57.25, H:5.43, N:17.42, found: C:56.94, H:5.20, N:17.20,

12b: 6-Butyl-3,5,7-trimethyl-1-[[4-(morpholinomethyl)-2-thioxo-1,3,4-oxadiazol-5-yl]methoxy]pyrrolo[3,4-*d*]pyridazin-4-one:

Yield: 33.93%; m.p.: 157–159 °C;

FT-IR (selected lines, γ_{max}, cm^{-1}): 2960, 2935, 2875 (C—H aliph.), 1618 (C═N), 1551 (C═S), ^{1}H NMR (300 MHz, $CDCl_3$) δ: 0.94–0.99 (m, 3H, –CH_2-CH_2 CH_2-CH_3), 1.34–1.42 (m, 2H, –CH_2-CH_2 CH_2-CH_3), 1.64 (m, 2H, –CH_2-CH_2 CH_2-CH_3), 2.50 (s, 3H, 7-CH_3), 2.68 (s, 3H, 5-CH_3), 2.78–2.82 (m, 4H, CH_2 – morpholine), 3.55 (s, 3H, 3-CH_3), 3.67–3.72 (m, 4H, CH_2 – morpholine), 3.88–3.93 (m, 2H, –CH_2-CH_2 CH_2-CH_3), 5.00 (s, 2H, N-CH_2), 5.28 (s, 2H, O-CH_2); NMR (75 MHz, $CDCl_3$) δ: 10.7, 11.3, 13.7, 20.0, 32.3, 37.1, 43.9, 50.5, 56.9, 66.7, 70.4, 107.9, 111.8, 122.7, 129.3, 147.8, 157.7, 159.3, 178.9; ESI-MS (*m/z*): calcd. for $C_{21}H_{30}N_6O_4S$ [L + H]$^+$: 463.2122; found: 463.2218; Anal. calcd. (%) for $C_{21}H_{30}N_6O_4S$: C:54.53, H:6.54, N:18.17, found: C:54.90, H:6.80, N:17.85,

13a: 1-[[4-[[4-(4-Chlorophenyl)-4-hydroxy-1-piperidyl]methyl]-2-thioxo-1,3,4-oxadiazol-5-yl]methoxy]-3,5,7-trimethyl-6-phenyl-pyrrolo[3,4-*d*]pyridazin-4-one

Yield: 69.47%; m.p.: 206–208 °C;

FT-IR (selected lines, γ_{max}, cm^{-1}): 3336 (O—H), 3056 (C—H arom.), 2948, 2830, 2846 (C—H aliph.), 1554 (C═S), ^{1}H NMR (300 MHz, $CDCl_3$) δ: 1.62–166 (m, 4H, CH_2 – piperidine), 2.21 (s, 3H, 7-CH_3), 2.34 (s, 3H, 5-CH_3), 2.86–2.89 (m, 4H, CH_2 – piperidine), 3.50 (s, 3H, 3-CH_3), 4.98 (s, 2H, N-CH_2), 5.25 (s, 2H, O-CH_2), 7.11–7.14 (m, 2H, ArH), 7.19–7.20 (m, 2H, ArH), 7.31–7.34 (m, 2H, ArH), 7.47–7.49 (m, 3H, ArH); ^{13}C NMR (75 MHz, $CDCl_3$) δ: 11.4, 11.9, 37.2, 38.2, 46.6, 57.2, 70.4, 70.7, 108.3, 112.0, 124.3, 126.0, 127.8, 128.4, 129.4, 129.7, 130.8, 132.8, 136.6, 146.8, 147.9, 157.6, 159.4, 178.7; ESI-MS (*m/z*): calcd. for $C_{30}H_{31}ClN_6O_4S$ [L + H]$^+$: 607.1889 found: 607.1978; Anal. calcd. (%) for $C_{30}H_{31}ClN_6O_4S$: C:59.35, H:5.15, N:13.84, found: C:59.02H:5.40, N:13.50,

13b: 6-Butyl-1-[[4-[[4-(4-chlorophenyl)-4-hydroxy-1-piperidyl]methyl]-2-thioxo-1,3,4-oxadiazol-5-yl]methoxy]-3,5,7-trimethyl-pyrrolo[3,4-*d*]pyridazin-4-one

Yield: 83.05%; m.p.: 202–204 °C;

FT-IR (selected lines, γ_{max}, cm^{-1}): 3318 (O—H), 2961, 2933 (C—H aliph.), 1607 (C═N), 1545 (C═S), ^{1}H NMR (300 MHz, $CDCl_3$) δ: 0.94–0.99 (m, 3H, –CH_2-CH_2 CH_2-CH_3), 1.34–1.42 (m, 2H, –CH_2-CH_2 CH_2-CH_3), 1.61–1.64 (m, 2H, –CH_2-CH_2 CH_2-CH_3), 1.69–1.73 (m, 4H, CH_2 – piperidine), 2.51 (s, 3H, 7-CH_3), 2.65 (s, 3H, 5-CH_3), 2.92–2.95 (m, 4H, CH_2 – piperidine), 3.53 (s, 3H, 3-CH_3), 3.88–3.93 (m, 2H, –CH_2-CH_2 CH_2-CH_3), 5.05 (s, 2H, N-CH_2), 5.29 (s, 2H, O-CH_2), 7.27–7.30 (m, 2H, ArH), 7.38–7.41 (m, 2H, ArH); ^{13}C NMR (75 MHz, $CDCl_3$) δ: 10.6, 11.2, 13.7, 20.0, 32.3, 37.1, 38.3, 43.9, 46.7, 57.1, 70.4, 70.7, 108.0, 111.8, 122.7, 126.0, 128.4, 129.3, 132.8, 146.9, 147.8, 157.6, 159.3, 178.7; ESI-MS (*m/z*): calcd. for $C_{28}H_{35}ClN_6O_4S$ [L + H]$^+$: 587.2202; found: 587.2316; Anal. calcd. (%) for $C_{28}H_{35}ClN_6O_4S$: C:57.28, H:6.01, N:14.31, found: C:57.50, H:6.30, N:13.99,

4.2. Biological evaluation

4.2.1. Cell line

Performed *in vitro* studies were carried out on normal human dermal fibroblasts (NHDF) obtained from Sigma-Aldrich. In all studies, cells were seeded at a density of 10,000 cells/well and incubated for 24 h to regenerate in a CO_2 incubator.

4.2.2. Medium and culture conditions

The NHDF cells were cultured in a medium recommended for this cell line – DMEM with 4.5 g/mL glucose without phenol red, which was supplemented with 10% FBS and 2 mM L-glutamine and 25 μg/mL gentamicin. NHDF cells were subcultured twice a week with TrypLE. Cell culture was carried out in conditions of 5% CO_2, 37 °C, 95% humidity.

4.2.3. Tested compounds

Tested compounds **7a**,**b**-**13a**,**b** were dissolved in DMSO to reach a final concentration of 10 μM and stored at −20 °C. Before use, the solution of the compounds was heated at 37 °C, and then samples with 3 different concentrations of compounds were prepared (100 μM, 50 μM and 10 μM) for each compound. At the highest concentration of each compound, the DMSO content did not exceed 1%.

4.2.4. Cyclooxygenase inhibition assay

COX peroxidase activity was estimated by colorimetric evaluation of the occurrence of the oxidized form of N,N,N′,N′-tetramethyl-p-phenylenediamine (TMPD), which is the substrate for many enzymes with peroxidase activity. The reduction of PGG2 (prostaglandin G2) to PGH2 is caused by the oxidation of TMPD. This, in turn, results in a change in color measured at 590 nm (Victor2 microplate reader, PerkinElmer Waltham, MA, USA). The kit provided by the manufacturer includes 150 μL of assay buffer, 10 μL of heme and 10 μL of COX-1 or COX-2. All samples were made in triplicate, adding 10 μM of the analysed compounds and respectively 10 μM methanol, ethanol and DMSO. Then, 20 μL of TMPD was added to all wells. Finally, arachidonic acid was added, which activated the reaction lasting for 2 min. After this time,

TMPD oxidation was determined in a Victor2 microplate reader.

4.2.5. SRB assay

Viability evaluation was performed using the SRB dye, which binds to proteins and as a result, informs about the amount of cellular protein. After 24 h of cell regeneration, the SRB assay was carried out. One of the culture plates was fixed with a cold TCA solution with a final concentration of 10% w/v for 1 h at 4–8 °C and was a control for cultures incubated for a further 48 h with the tested compounds. The supernatant was then removed from the remaining culture plates, and the compounds were added and incubated for 48 h in 5% CO_2, 95% humidity at 37 °C. After this time, culture was also fixed with cold TCA solution. All plates were washed four times with running water and dried in air at RT. Afterwards, there was added 0.4% SRB solution in 1% v/v acetic acid for 30 min, which next was rinsed five times with 1% solution of acetic acid. Again, the plates were air-dried at RT, and then the SRB dye connected to intracellular proteins was dissolved with 10 mM Trizma base for 30 min with stirring on a shaker, and finally, the absorbance was measured at 540 nm with a Victor2 microplate reader.

4.2.6. DCF-DA assay

2′,7′-Dichlorofluorescein diacetate (DCF-DA) is a fluorescent dye allowing measurement of free radical levels. After diffusion into the cells, DCF-DA is deacetylated by esterases to a non-fluorescent compound that next, in the presence of ROS, is oxidised to 2′,7′–dichlorofluorescein (DCF). The DCF-DA solution was prepared fresh before use by dissolving 1 mg of DCF-DA in 2.05 mL of 100% ethanol and diluting in deionised water to a concentration of 10 μM. The intracellular level of free radicals was tested in two cases: after intracellular exposure to exogenous stress caused by reactive oxygen species (ROS) and without exposure to stress. The exogenous stress was induced with 100 μM H_2O_2 (hydrogen peroxide), as ROS generator. Solutions were made fresh before each use in the MEM medium without serum and phenol red. Properties of the compounds were evaluated in terms of protection against ROS formation.

After 24 h of cell regeneration, the medium was removed, and solutions of the tested compounds (each at three concentrations: 10, 50 and 100 μg/mL) were added for a further 24 h. After this time, the solutions were removed, and the cells were exposed for 1 h to oxidative stress induced by 100 μM H_2O_2 in conditions of 5% CO_2, 95% humidity, 37 °C. Finally, the DCF-DA solution was added, and cell cultures incubated for a further 1 h. The ROS level was measured after further 1 h incubation with DCF–DA solution using a Victor2 microplate reader (λ_{ex} = 485 nm, λ_{em} = 535 nm).

4.2.7. Griess assay

The Griess assay allows one to detect the presence of nitrite ions in solution and was carried out according to the supplier's protocol. Two reagents, 0.1% N-(1-naphthyl)ethylenediamine dihydrochloride and 1% sulfanilic acid, were combined in the same volume and mixed immediately before use.

This assay was carried out for two cases, as in the DCF-DA assay – protective properties against the induction of nitrite ions. The exogenous stress was induced with 100 μM H_2O_2.

After cell regeneration and 24 h of incubation with tested compounds, the supernatant solution was removed, and cells were exposed to exogenous stress (100 μM SIN-1) or incubated only in the medium for 1 h. Then, 150 μL of the solution was transferred to a new plate, and 20 μL of a mixture of Griess reagents and 130 μL of deionised water was added for 30 min at RT. Nitrite level was measured with Victor2 at a wavelength of 555 nm.

4.2.8. Fast halo assay

After treatment of the NHDF cell cultures with tested compounds, the cells were detached from the surface of the multiwell culture plates using TrypLE solution at a concentration of 0.1% in PBS for 10 min at 37 °C. The cells were transferred into tubes and trypsin was inactivated by adding medium with serum. The cells were centrifuged at 1000 × g for 5 min. The supernatant was then removed, and the cell pellets were resuspended in PBS, and the cells were again centrifuged under the same conditions. After removing the supernatant, the cells were resuspended at a density of 1000 cells/μL in PBS with Ca^{2+} and Mg^{2+}. The tubes with the cells were placed in a water bath at 37 °C. The cells were mixed with 1.25% low melting point agarose in PBS. The cells suspended in agarose solution (100 μL) were placed between slide coated with agarose (high melting point) and a coverslip. Then, the slides were put on a cooling block for 10 min to gelify. The coverslips were removed, and slides were placed in the lysis buffer overnight. The next day, slides were transferred into alkaline solution (pH = 13.0) for 30 min, and then washed twice for 5 min in neutralising buffer. Finally, slides were stained using 5 μM DAPI for 20 min and pictures were taken with a fluorescence microscope.

4.3. Molecular docking

The ground state geometric optimisations were calculated using density functional theory (DFT) with Becke's three-parameter hybrid exchange function with the Lee-Yang-Parr gradient corrected correlation (B3LYP) [76–78] functional in combination with the 6–311 + G (d,p) basis set. Harmonic vibrational wavenumbers were calculated using analytic second derivatives to confirm the convergence to minima in the potential surface. Calculations were carried out using the Gaussian 2016 A.03 software package [79].

The high-resolution crystal structure of COX-1 and COX-2 co-crystallized with meloxicam and crystal structure of BSA were selected for docking studies (Protein Data Bank, PDB ID: 4O1Z, 4 M11, 3 V03) [80]. The ligand and receptor files were prepared using AutoDock 4.2.6 software and AutoDock Tools 1.5.6. All the ligands and water molecules were removed, and then polar hydrogen atoms and Kollman charges were added to the protein structure. To prepare the ligand molecules partial charges were calculated, nonpolar hydrogens were merged, and rotatable bonds were assigned.

The interactions with COX-1, COX-2 and BSA were performed using AutoDock Script downloaded from The Scripps Research Institute (TSRI). The Lamarckian genetic algorithm was selected for the conformational search. The centres of grid boxes for COX-1 and COX-2 were set according to the meloxicam binding site in the crystal structure 4O1Z, 4 M11. The centres of grid boxes for BSA were set according to the binding site I phenylbutazone (PDB ID: 2BXC) and site II ibuprofen (PDB ID: 2BXG) on HSA [70]. The ligand-receptor complexes were further analysed using Discovery Studio 2016 software.

4.4. Spectroscopic studies

4.4.1. Fluorescence

All the fluorescence measurements were carried out on a Cary Eclipse 500 spectrophotometer. The interaction between synthesised compounds and bovine serum albumin (BSA) was studied in pH = 7.4, and the concentration of BSA was equal to 1.0×10^{-6} mol dm^{-3}. A solution of BSA was titrated by successive additions 1.0×10^{-3} mol dm^{-3} solution of studied compounds, to give a final concentration 0.2×10^{-6}–2.0×10^{-6} mol dm^{-3}. Fluorescence quenching spectra were obtained at excitation and emission wavelengths of 280 nm and 290–500 nm, respectively. In both cases, the molar ratio compound/BSA was 0.1–2.0, with 0.2 steps. All experiments were measured at three temperatures: 303, 306, and 310 K. Binding site identification studies were carried out in the presence of the two site markers, phenylbutazone (PHB) and ibuprofen (IBP) as sites I and II markers, respectively. Concentrations of BSA and site markers were set at 1.0×10^{-6} and 3.0×10^{-6} mol dm^{-3}, respectively.

4.4.2. Circular dichroism

Circular dichroism spectra were made on a Jasco J-1500 magnetic circular dichroism spectrometer. For all BSA solutions, measurements were made at RT under simulated physiological conditions at pH 7.4 in the absence and presence of analysed compounds. 10 mm path length was used. CD spectra were collected in the range of 200–250 nm at a scan rate of 50 nm min^{-1} with a response time of 1 s. All spectra were baseline corrected. The concentrations of BSA and compounds A, B were 1×10^{-6} mol dm^{-3} and 1×10^{-3} mol dm^{-3}, respectively. Experiments were performed for BSA for each analysed compound in molar ratios from 1:0 to 1:10.

4.5. Statistical analysis

Distribution normality was checked using the Shapiro-Wilk test. Because of the lack of a normal distribution, the nonparametric Kruskal-Wallis test was used (with appropriate post-hoc tests). The viability results obtained in the SRB assay allowed regression analysis to be performed for all tested compounds and IC_{50} values to be calculated. All analyses were performed using Statistica 13.1 software. The significance level of $p < 0.05$ was assumed in all tests. Based on the performed tests, it was calculated that the power of the test was greater than 80%. Multiple-criteria decision analysis (MCDA) was carried out following the weighted sum model (WSM). The weights were chosen according to the meaning of each biological test.

Declaration of Competing Interest

The authors declare that they have no known competing financial interests or personal relationships that could have appeared to influence the work reported in this paper.

Acknowledgements

This study was financially supported by a Wroclaw Medical University grant STSUB.D070.19.01. This research was financially supported by the Ministry of Health subvention according to number of STM.D070.20.021 from the IT Simple system of Wroclaw Medical University. Calculations have been carried out in Wroclaw Centre for Networking and Supercomputing (http://www.wcss.wroc.pl). The publication was prepared under a project financed from the funds granted by the Ministry of Science and Higher Education in the Regional Initiative of Excellence program for the years 2019-2022, project number 016/RID/2018/19, the amount of funding 11 998 121.30 PLN.

Appendix A. Supplementary data

Supplementary data to this article can be found online at https://doi.org/10.1016/j.bioorg.2020.104035.

References

[1] C.G. Wermuth, Are pyridazines privileged structures? Medchemcomm. 2 (2011) 935–941, https://doi.org/10.1039/c1md00074h.
[2] S. Dubey, P.A. Bhosle, Pyridazinone: An important element of pharmacophore possessing broad spectrum of activity, Med. Chem. Res. 24 (2015) 3579–3598, https://doi.org/10.1007/s00044-015-1398-5.
[3] W. Akhtar, M. Shaquiquzzaman, M. Akhter, G. Verma, M.F. Khan, M.M. Alam, The therapeutic journey of pyridazinone, Eur. J. Med. Chem. 123 (2016) 256–281, https://doi.org/10.1016/j.ejmech.2016.07.061.
[4] W. Malinka, A. Redzicka, O. Lozach, New derivatives of pyrrolo[3,4-d]pyridazinone and their anticancer effects, Farmaco. 59 (2004) 457–462, https://doi.org/10.1016/j.farmac.2004.03.002.
[5] M. Elagawany, M.A. Ibrahim, H.E. Ali Ahmed, A.S. El-Etrawy, A. Ghiaty, Z.K. Abdel-Samii, S.A. El-Feky, J. Bajorath, Design, synthesis, and molecular modelling of pyridazinone and phthalazinone derivatives as protein kinases inhibitors, Bioorganic Med. Chem. Lett. 23 (2013) 2007–2013. 10.1016/j.bmcl.2013.02.027.
[6] S. Ovais, K. Javed, S. Yaseen, R. Bashir, P. Rathore, R. Yaseen, A.D. Hameed, M. Samim, Synthesis, antiproliferative and anti-inflammatory activities of some novel 6-aryl-2-(p-(methanesulfonyl)phenyl)-4,5-dihydropyridazi-3(2H)-ones, Eur. J. Med. Chem. 67 (2013) 352–358, https://doi.org/10.1016/j.ejmech.2013.06.050.
[7] D. Dorsch, O. Schadt, F. Stieber, M. Meyring, U. Grädler, F. Bladt, M. Friese-Hamim, C. Knühl, U. Pehl, A. Blaukat, Identification and optimization of pyridazinones as potent and selective c-Met kinase inhibitors, Bioorganic Med. Chem. Lett. 25 (2015) 1597–1602, https://doi.org/10.1016/j.bmcl.2015.02.002.
[8] W. Xing, J. Ai, S. Jin, Z. Shi, X. Peng, L. Wang, Y. Ji, D. Lu, Y. Liu, M. Geng, Y. Hu, Enhancing the cellular anti-proliferation activity of pyridazinones as c-met inhibitors using docking analysis, Eur. J. Med. Chem. 95 (2015) 302–312, https://doi.org/10.1016/j.ejmech.2015.03.041.
[9] Y. Liu, S. Jin, X. Peng, D. Lu, L. Zeng, Y. Sun, J. Ai, M. Geng, Y. Hu, Pyridazinone derivatives displaying highly potent and selective inhibitory activities against c-Met tyrosine kinase, Eur. J. Med. Chem. 108 (2016) 322–333, https://doi.org/10.1016/j.ejmech.2015.11.042.
[10] L.X. Wang, X. Liu, S. Xu, Q. Tang, Y. Duan, Z. Xiao, J. Zhi, L. Jiang, P. Zheng, W. Zhu, Discovery of novel pyrrolo-pyridine/pyrimidine derivatives bearing pyridazinone moiety as c-Met kinase inhibitors, Eur. J. Med. Chem. 141 (2017) 538–551, https://doi.org/10.1016/j.ejmech.2017.10.027.
[11] M. Krasavin, A. Shetnev, S. Baykov, S. Kalinin, A. Nocentini, V. Sharoyko, G. Poli, T. Tuccinardi, M. Korsakov, T.B. Tennikova, C.T. Supuran, Pyridazinone-substituted benzenesulfonamides display potent inhibition of membrane-bound human carbonic anhydrase IX and promising antiproliferative activity against cancer cell lines, Eur. J. Med. Chem. (2019) 301–314, https://doi.org/10.1016/j.ejmech.2019.02.044.
[12] E. Barocelli, M. Chiavarini, V. Ballabeni, D. Barlocco, P. Vianello, V. Dal Piaz, M. Impicciatore, Study of the antisecretory and antiulcer mechanisms of a new indenopirydazinone derivative in rats, Pharmacol. Res. 35 (1997) 487–492, https://doi.org/10.1006/phrs.1997.0168.
[13] V. Dal Piaz, C. Vergelli, M.P. Giovannoni, M.A. Scheideler, G. Petrone, P. Zaratin, 4-Amino-3(2H)-pyridazinones bearing arylpiperazinylalkyl groups and related compounds: Synthesis and antinociceptive activity, Farmaco. 58 (2003) 1063–1071, https://doi.org/10.1016/S0014-827X(03)00162-9.
[14] E.M. Ahmed, A.E. Kassab, A.A. El-Malah, M.S.A. Hassan, Synthesis and biological evaluation of pyridazinone derivatives as selective COX-2 inhibitors and potential anti-inflammatory agents, Eur. J. Med. Chem. 171 (2019) 25–37, https://doi.org/10.1016/j.ejmech.2019.03.036.
[15] C.S. Li, C. Brideau, C.C. Chan, C. Savoie, D. Claveau, S. Charleson, R. Gordon, G. Greig, J.Y. Gauthier, C.K. Lau, D. Riendeau, M. Thérien, E. Wong, P. Prasit, Pyridazinones as selective cyclooxygenase-2 inhibitors, Bioorganic Med. Chem. Lett. 13 (2003) 597–600, https://doi.org/10.1016/S0960-894X(02)01045-4.
[16] K. Abouzid, S.A. Bekhit, Novel anti-inflammatory agents based on pyridazinone scaffold; design, synthesis and in vivo activity, Bioorganic Med. Chem. 16 (2008) 5547–5556, https://doi.org/10.1016/j.bmc.2008.04.007.
[17] M. Gökçe, S. Utku, E. Küpeli, Synthesis and analgesic and anti-inflammatory activities 6-substituted-3(2H)-pyridazinone-2-acetyl-2-(p-substituted/nonsubstituted benzal)hydrazone derivatives, Eur. J. Med. Chem. 44 (2009) 3760–3764, https://doi.org/10.1016/j.ejmech.2009.04.048.
[18] W. Malinka, A. Redzicka, M. Jastrzębska-Więsek, B. Filipek, M. Dybała, Z. Karczmarzyk, Z. Urbańczyk-Lipkowska, P. Kalicki, Derivatives of pyrrolo[3,4-d] pyridazinone, a new class of analgesic agents, Eur. J. Med. Chem. 46 (2011) 4992–4999, https://doi.org/10.1016/j.ejmech.2011.08.006.
[19] S. Mogilski, M. Kubacka, A. Redzicka, G. Kazek, M. Dudek, W. Malinka, B. Filipek, Antinociceptive, anti-inflammatory and smooth muscle relaxant activities of the pyrrolo[3,4-d]pyridazinone derivatives: Possible mechanisms of action, Pharmacol. Biochem. Behav. 133 (2015) 99–110, https://doi.org/10.1016/j.pbb.2015.03.019.
[20] J. Singh, V. Saini, A. Kumar, R. Bansal, Synthesis, molecular docking and biological evaluation of some newer 2-substituted-4-(benzo[d][1,3]dioxol-5-yl)-6-phenylpyridazin-3(2H)-ones as potential anti-inflammatory and analgesic agents, Bioorg. Chem. 71 (2017) 201–210, https://doi.org/10.1016/j.bioorg.2017.02.006.
[21] C. Barberot, A. Moniot, I. Allart-Simon, L. Malleret, T. Yegorova, M. Laronze-Cochard, A. Bentaher, M. Médebielle, J.-P. Bouillon, E. Hénon, J. Sapi, F. Velard, S. Gérard, Synthesis and biological evaluation of pyridazinone derivatives as potential anti-inflammatory agents, Eur. J. Med. Chem. 146 (2018) 139–146, https://doi.org/10.1016/j.ejmech.2018.01.035.
[22] Y. Boukharsa, W. Lakhlili, J. El harti, B. Meddah, R.Y. Tiendrebeogo, J. Taoufik, M. El Abbes Faouzi, A. Ibrahimi, M. Ansar, Synthesis, anti-inflammatory evaluation in vivo and docking studies of some new 5-(benzo[b]furan-2-ylmethyl)-6-methyl-pyridazin-3(2H)-one derivatives, J. Mol. Struct. 1153 (2018) 119–127. 10.1016/j.molstruc.2017.09.092.
[23] K. Abouzid, M. Abdel Hakeem, O. Khalil, Y. Maklad, Pyridazinone derivatives: Design, synthesis, and in vitro vasorelaxant activity, Bioorganic, Med. Chem. 16 (2008) 382–389, https://doi.org/10.1016/j.bmc.2007.09.031.
[24] R. Bansal, D. Kumar, R. Carron, C. de la Calle, Synthesis and vasodilatory activity of some amide derivatives of 6-(4-carboxymethyloxyphenyl)-4,5-dihydro-3(2H)-pyridazinone, Eur. J. Med. Chem. 44 (2009) 4441–4447, https://doi.org/10.1016/j.ejmech.2009.06.006.
[25] T. Costas, P. Besada, A. Piras, L. Acevedo, M. Yañez, F. Orallo, R. Laguna, C. Terán, New pyridazinone derivatives with vasorelaxant and platelet antiaggregatory activities, Bioorganic Med. Chem. Lett. 20 (2010) 6624–6627, https://doi.org/10.1016/j.bmcl.2010.09.031.
[26] T. Costas, M.C. Costas-Lago, N. Vila, P. Besada, E. Cano, C. Terán, New platelet aggregation inhibitors based on pyridazinone moiety, Eur. J. Med. Chem. 94 (2015) 113–122, https://doi.org/10.1016/j.ejmech.2015.02.061.
[27] Z. Hu, C. Wang, W. Han, K.A. Rossi, J.M. Bozarth, Y. Wu, S. Sheriff, J.E. Myers, J.M. Luettgen, D.A. Seiffert, R.R. Wexler, M.L. Quan, Pyridazine and pyridazinone

derivatives as potent and selective factor XIa inhibitors, Bioorganic Med. Chem. Lett. 28 (2018) 987–992, https://doi.org/10.1016/j.bmcl.2018.02.049.
[28] R. Yaseen, D. Ekinci, M. Senturk, A.D. Hameed, S. Ovais, P. Rathore, M. Samim, K. Javed, C.T. Supuran, Pyridazinone substituted benzenesulfonamides as potent carbonic anhydrase inhibitors, Bioorganic Med. Chem. Lett. 26 (2016) 1337–1341, https://doi.org/10.1016/j.bmcl.2015.12.016.
[29] W. Xing, Y. Fu, Z. Shi, D. Lu, H. Zhang, Y. Hu, Discovery of novel 2,6-disubstituted pyridazinone derivatives as acetylcholinesterase inhibitors, Eur. J. Med. Chem. 63 (2013) 95–103, https://doi.org/10.1016/j.ejmech.2013.01.056.
[30] M. Tao, R. Raddatz, L.D. Aimone, R.L. Hudkins, Synthesis and structure-activity relationships of 4,5-fused pyridazinones as histamine H 3 receptor antagonists, Bioorganic Med. Chem. Lett. 21 (2011) 6126–6130, https://doi.org/10.1016/j.bmcl.2011.08.045.
[31] R.R. Dandu, J.A. Gruner, J.R. Mathiasen, L.D. Aimone, G. Hostetler, C. Benfield, R.J. Bendesky, V.R. Marcy, R. Raddatz, R.L. Hudkins, Synthesis and evaluation of pyridazinone.phenethylamine derivatives as selective and orally bioavailable histamine H3 receptor antagonists with robust wake-promoting activity, Bioorganic Med, Chem. Lett. 21 (2011) 6362–6365, https://doi.org/10.1016/j.bmcl.2011.08.104.
[32] S. Partap, M.J. Akhtar, M.S. Yar, M.Z. Hassan, A.A. Siddiqui, Pyridazinone hybrids: Design, synthesis and evaluation as potential anticonvulsant agents, Bioorg. Chem. 77 (2018) 74–83, https://doi.org/10.1016/j.bioorg.2018.01.001.
[33] D.V. Dekhane, S.S. Pawar, S. Gupta, M.S. Shingare, C.R. Patil, S.N. Thore, Synthesis and anti-inflammatory activity of some new 4,5-dihydro-1,5- diaryl-1H-pyrazole-3-substituted-heteroazole derivatives, Bioorganic Med. Chem. Lett. 21 (2011) 6527–6532, https://doi.org/10.1016/j.bmcl.2011.08.061.
[34] A.G. Banerjee, N. Das, S.A. Shengule, P.A. Sharma, R.S. Srivastava, S.K. Shrivastava, Design, synthesis, evaluation and molecular modelling studies of some novel 5,6-diphenyl-1,2,4-triazin-3(2H)-ones bearing five-member heterocyclic moieties as potential COX-2 inhibitors: A hybrid pharmacophore approach, Bioorg. Chem. 69 (2016) 102–120, https://doi.org/10.1016/j.bioorg.2016.10.003.
[35] N.A. El-Sayed, M.S. Nour, M.A. Salem, R.K. Arafa, New oxadiazoles with selective-COX-2 and EGFR dual inhibitory activity: Design, synthesis, cytotoxicity evaluation and in silico studies, Eur. J. Med. Chem. 183 (2019) 111693, , https://doi.org/10.1016/j.ejmech.2019.111693.
[36] S. Bansal, M. Bala, S.K. Suthar, S. Choudhary, S. Bhattacharya, V. Bhardwaj, S. Singla, A. Joseph, Design and synthesis of novel 2-phenyl-5-(1,3-diphenyl-1H-pyrazol-4-yl)-1, 3,4-oxadiazoles as selective COX-2 inhibitors with potent anti-inflammatory activity, Eur. J. Med. Chem. 80 (2014) 167–174, https://doi.org/10.1016/j.ejmech.2014.04.045.
[37] K.R.A. Abdellatif, W.A.A. Fadaly, Design, synthesis, cyclooxygenase inhibition and biological evaluation of new 1,3,5-triaryl-4,5-dihydro-1H-pyrazole derivatives possessing amino/methanesulfonyl pharmacophore, Bioorg. Chem. 70 (2017) 57–66, https://doi.org/10.1016/j.bioorg.2016.11.008.
[38] K.R.A. Abdellatif, E.K.A. Abdelall, P.F. Lamie, M.B. Labib, E.S. El-Nahaas, M.M. Abdelhakeem, New pyrazole derivatives possessing amino/methanesulphonyl pharmacophore with good gastric safety profile: Design, synthesis, cyclooxygenase inhibition, anti-inflammatory activity and histopathological studies, Bioorg. Chem. 95 (2020) 103540, , https://doi.org/10.1016/j.bioorg.2019.103540.
[39] S.S.R. Alsayed, H.A.H. Elshemy, M.A. Abdelgawad, M.S. Abdel-Latif, K.R.A. Abdellatif, Design, synthesis and biological screening of some novel celecoxib and etoricoxib analogs with promising COX-2 selectivity, anti-inflammatory activity and gastric safety profile, Bioorg. Chem. 70 (2017) 173–183, https://doi.org/10.1016/j.bioorg.2016.12.008.
[40] M.A.M.S. El-Sharief, S.Y. Abbas, A.M.S. El-Sharief, N.M. Sabry, Z. Moussa, S.M. El-Messery, A.R. Elsheakh, G.S. Hassan, M.T. El Sayed, 5-Thioxoimidazolidine-2-one derivatives: Synthesis, anti-inflammatory activity, analgesic activity, COX inhibition assay and molecular modelling study, Bioorg. Chem. 87 (2019) 679–687, https://doi.org/10.1016/j.bioorg.2019.03.075.
[41] K. Manjunatha, B. Poojary, P.L. Lobo, J. Fernandes, N.S. Kumari, Synthesis and biological evaluation of some 1,3,4-oxadiazole derivatives, Eur. J. Med. Chem. 45 (2010) 5225–5233, https://doi.org/10.1016/j.ejmech.2010.08.039.
[42] M.B. Palkar, A.S. Singhai, P.M. Ronad, A.H.M. Vishwanathswamy, T.S. Boreddy, V.P. Veerapur, M.S. Shaikh, R.A. Rane, R. Karpoormath, Synthesis, pharmacological screening and in silico studies of new class of Diclofenac analogues as a promising anti-inflammatory agents, Bioorganic Med. Chem. 22 (2014) 2855–2866, https://doi.org/10.1016/j.bmc.2014.03.043.
[43] S.V. Bhandari, K.G. Bothara, M.K. Raut, A.A. Patil, A.P. Sarkate, V.J. Mokale, Design, Synthesis and Evaluation of Antiinflammatory, Analgesic and Ulcerogenicity studies of Novel S-Substituted phenacyl-1,3,4-oxadiazole-2-thiol and Schiff bases of Diclofenac acid as Nonulcerogenic Derivatives, Bioorganic Med. Chem. 16 (2008) 1822–1831, https://doi.org/10.1016/j.bmc.2007.11.014.
[44] M. Koksal, I. Ozkan-Dagliyan, T. Ozyazici, B. Kadioglu, H. Sipahi, A. Bozkurt, S.S. Bilge, Some Novel Mannich Bases of 5-(3,4-Dichlorophenyl)-1,3,4-oxadiazole-2(3H)-one and Their Anti-Inflammatory Activity, Arch. Pharm. (Weinheim). 350 (2017), https://doi.org/10.1002/ardp.201700153.
[45] A.G. Banerjee, N. Das, S.A. Shengule, R.S. Srivastava, S.K. Shrivastava, Synthesis, characterization, evaluation and molecular dynamics studies of 5, 6-diphenyl-1,2,4-triazin-3(2 H)-one derivatives bearing 5-substituted 1,3,4-oxadiazole as potential anti-inflammatory and analgesic agents, Eur. J. Med. Chem. 101 (2015) 81–95, https://doi.org/10.1016/j.ejmech.2015.06.020.
[46] T. McGarry, M. Biniecka, D.J. Veale, U. Fearon, Hypoxia, oxidative stress and inflammation, Free Radic. Biol. Med. 125 (2018) 15–24, https://doi.org/10.1016/j.freeradbiomed.2018.03.042.
[47] Z. Gao, H. Zhang, J. Liu, C.W. Lau, P. Liu, Z.Y. Chen, H.K. Lee, G.L. Tipoe, H.M. Ho, X. Yao, Y. Huang, Cyclooxygenase-2-dependent oxidative stress mediates palmitate-induced impairment of endothelium-dependent relaxations in mouse arteries, Biochem. Pharmacol. 91 (2015) 474–482, https://doi.org/10.1016/j.bcp.2014.08.009.
[48] C. Burdon, C. Mann, T. Cindrova-Davies, A.C. Ferguson-Smith, G.J. Burton, Oxidative Stress and the Induction of Cyclooxygenase Enzymes and Apoptosis in the Murine Placenta, Placenta. 28 (2007) 724–733, https://doi.org/10.1016/j.placenta.2006.12.001.
[49] D. Li, M. Zhu, C. Xu, B. Ji, Characterization of the baicalein-bovine serum albumin complex without or with Cu 2+ or Fe 3+ by spectroscopic approaches, Eur. J. Med. Chem. 46 (2011) 588–599, https://doi.org/10.1016/j.ejmech.2010.11.038.
[50] Y.Q. Wang, H.M. Zhang, G.C. Zhang, W.H. Tao, Z.H. Fei, Z.T. Liu, Spectroscopic studies on the interaction between silicotungstic acid and bovine serum albumin, J. Pharm. Biomed. Anal. 43 (2007) 1869–1875, https://doi.org/10.1016/j.jpba.2007.01.001.
[51] J. hua Shi, D. qi Pan, X. xiou Wang, T.T. Liu, M. Jiang, Q. Wang, Characterizing the binding interaction between antimalarial artemether (AMT) and bovine serum albumin (BSA): Spectroscopic and molecular docking methods, J. Photochem. Photobiol. B Biol. 162 (2016) 14–23. 10.1016/j.jphotobiol.2016.06.025.
[52] A.A. Al-Mehizia, A.H. Bakheit, S. Zargar, M.A. Bhat, M.M. Asmari, T.A. Wani, Evaluation of Biophysical Interaction between Newly Synthesized Pyrazoline Pyridazine Derivative and Bovine Serum Albumin by Spectroscopic and Molecular Docking Studies, J. Spectrosc. 2019 (2019) 3848670, https://doi.org/10.1155/2019/3848670.
[53] T.A. Wani, A.H. Bakheit, S. Zargar, M.A. Bhat, A.A. Al-Majed, Molecular docking and experimental investigation of new indole derivative cyclooxygenase inhibitor to probe its binding mechanism with bovine serum albumin, Bioorg. Chem. 89 (2019) 103010, , https://doi.org/10.1016/j.bioorg.2019.103010.
[54] S. Zargar, S. Alamery, A.H. Bakheit, T.A. Wani, Poziotinib and bovine serum albumin binding characterization and influence of quercetin, rutin, naringenin and sinapic acid on their binding interaction, Spectrochim. Acta - Part A Mol. Biomol. Spectrosc. 235 (2020) 118335, , https://doi.org/10.1016/j.saa.2020.118335.
[55] W. Malinka, Synthesis of some pyrrolo[3,4-d]pyridazinones and their preliminary anticancer, antimycobacterial and CNS screening, Pharmazie. 56 (2001) 384–389.
[56] P. Świątek, M. Strzelecka, R. Urniaz, K. Gębczak, T. Gębarowski, K. Gąsiorowski, W. Malinka, Synthesis, COX-1/2 inhibition activities and molecular docking study of isothiazolopyridine derivatives, Bioorg. Med. Chem. 25 (2017) 316–326, https://doi.org/10.1016/j.bmc.2016.10.036.
[57] Y. Li, W. He, J. Liu, F. Sheng, Z. Hu, X. Chen, Binding of the bioactive component Jatrorrhizine to human serum albumin, Biochim. Biophys. Acta - Gen. Subj. 1722 (2005) 15–21, https://doi.org/10.1016/j.bbagen.2004.11.006.
[58] M.M. Alanazi, A.A. Almehizia, A.H. Bakheit, N.A. Alsaif, H.M. Alkahtani, T.A. Wani, Mechanistic interaction study of 5,6-Dichloro-2-[2-(pyridin-2-yl)ethyl]isoindoline-1,3-dione with bovine serum albumin by spectroscopic and molecular docking approaches, Saudi Pharm. J. 27 (2019) 341–347, https://doi.org/10.1016/j.jsps.2018.12.001.
[59] T.A. Wani, A.H. Bakheit, S. Zargar, H. Rizwana, A.A. Al-Majed, Evaluation of competitive binding interaction of neratinib and tamoxifen to serum albumin in multidrug therapy, Spectrochim. Acta - Part A Mol. Biomol. Spectrosc. 227 (2020) 117691, , https://doi.org/10.1016/j.saa.2019.117691.
[60] T.A. Wani, A.H. Bakheit, S. Zargar, M.A. Hamidaddin, I.A. Darwish, Spectrophotometric and molecular modelling studies on in vitro interaction of tyrosine kinase inhibitor Linifanib with bovine serum albumin, PLoS One. 12 (2017) e0176015, , https://doi.org/10.1371/journal.pone.0176015.
[61] G.Z. Chen, X.Z. Huang, J.G. Xu, Z.Z. Zheng, Z.B. Wang, The Methods of Fluorescence Analysis, 2nd ed., Science Press, Beijing, 1990.
[62] J.R. Lakowicz, ed., Principles of Fluorescence Spectroscopy, 3rd ed, Springer US, Boston, MA, 2006. 10.1007/978-0-387-46312-4.
[63] J.R. Lakowicz, G. Weber, Quenching of fluorescence by oxygen, Probe for structural fluctuations in macromolecules, Biochemistry. 12 (1973) 4161–4170, https://doi.org/10.1021/bi00745a020.
[64] W.R. Ware, Oxygen quenching of fluorescence in solution: an experimental study of the diffusion process, J. Phys. Chem. 66 (1962) 455–458, https://doi.org/10.1021/j100809a020.
[65] X.L. Wei, J.B. Xiao, Y. Wang, Y. Bai, Which model based on fluorescence quenching is suitable to study the interaction between trans-resveratrol and BSA?, Spectrochim, Acta - Part A Mol. Biomol. Spectrosc. 75 (2010) 299–304, https://doi.org/10.1016/j.saa.2009.10.027.
[66] M. Van De Weert, L. Stella, Fluorescence quenching and ligand binding: A critical discussion of a popular methodology, J. Mol. Struct. 998 (2011) 145–150, https://doi.org/10.1016/j.molstruc.2011.05.023.
[67] S. Bi, D. Song, Y. Tian, X. Zhou, Z. Liu, H. Zhang, Molecular spectroscopic study on the interaction of tetracyclines with serum albumins, Spectrochim. Acta - Part A Mol. Biomol, Spectrosc. 61 (2005) 629–636, https://doi.org/10.1016/j.saa.2004.05.028.
[68] S. Bi, L. Ding, Y. Tian, D. Song, X. Zhou, X. Liu, H. Zhang, Investigation of the interaction between flavonoids and human serum albumin, J. Mol. Struct. 703 (2004) 37–45, https://doi.org/10.1016/j.molstruc.2004.05.026.
[69] G. Sudlow, D.J. Birkett, D.N. Wade, The Characterization of Two Specific Drug Binding Sites on Human Serum Albumin, Mol. Pharmacol. 11 (1975) 824–832.
[70] J. Ghuman, P.A. Zunszain, I. Petitpas, A.A. Bhattacharya, M. Otagiri, S. Curry, Structural basis of the drug-binding specificity of human serum albumin, J. Mol. Biol. 353 (2005) 38–52, https://doi.org/10.1016/j.jmb.2005.07.075.
[71] I.M. Klotz, J.M. Urquhart, The Binding of Organic Ions by Proteins. Effect of Temperature, J. Am. Chem. Soc. 71 (1949) 847–851, https://doi.org/10.1021/ja01171a024.
[72] P.D. Ross, S. Subramanian, Thermodynamics of Protein Association Reactions:

Forces Contributing to Stability, Biochemistry. 20 (1981) 3096–3102, https://doi.org/10.1021/bi00514a017.
[73] S.M. Kelly, T.J. Jess, N.C. Price, How to study proteins by circular dichroism, Biochim. Biophys. Acta - Proteins, Proteomics. 1751 (2005) 119–139, https://doi.org/10.1016/j.bbapap.2005.06.005.
[74] S. Kelly, N. Price, The Use of Circular Dichroism in the Investigation of Protein Structure and Function, Curr. Protein Pept. Sci. 1 (2005) 349–384, https://doi.org/10.2174/1389203003381315.
[75] Q.L. Lu, Z.X., Cui, T., Shi, Applications of Circular Dichroism (CD) and Optical Rotatory Dispersion (ORD) in Molecular Biology, 1st ed, Science Press: Beijing, 1987.
[76] A.D. Becke, Density-functional thermochemistry. III. The role of exact exchange, J. Chem. Phys. 98 5648 (1993), https://doi.org/10.1063/1.464913.
[77] C. Lee, W. Yang, R.G. Parr, Development of the Colle-Salvetti correlation-energy formula into a functional of the electron density, Phys. Rev. B. 37 (1988) 785–789, https://doi.org/10.1103/PhysRevB.37.785.
[78] J.P. Perdew, Y. Wang, Accurate and simple analytic representation of the electron-gas correlation energy, Phys. Rev. B. 45 (1992) 13244–13249, https://doi.org/10.1103/PhysRevB.45.13244.
[79] M.J. Frisch, G.W. Trucks, H.B. Schlegel, G.E. Scuseria, M.A. Robb, J.R. Cheeseman, G. Scalmani, V. Barone, G.A. Petersson, H. Nakatsuji, X. Li, M. Caricato, A. V Marenich, J. Bloino, B.G. Janesko, R. Gomperts, B. Mennucci, H.P. Hratchian, J. V Ortiz, A.F. Izmaylov, J.L. Sonnenberg, D. Williams-Young, F. Ding, F. Lipparini, F. Egidi, J. Goings, B. Peng, A. Petrone, T. Henderson, D. Ranasinghe, V.G. Zakrzewski, J. Gao, N. Rega, G. Zheng, W. Liang, M. Hada, M. Ehara, K. Toyota, R. Fukuda, J. Hasegawa, M. Ishida, T. Nakajima, Y. Honda, O. Kitao, H. Nakai, T. Vreven, K. Throssell, J.A. Montgomery Jr., J.E. Peralta, F. Ogliaro, M.J. Bearpark, J. J. Heyd, E.N. Brothers, K.N. Kudin, V.N. Staroverov, T.A. Keith, R. Kobayashi, J. Normand, K. Raghavachari, A.P. Rendell, J.C. Burant, S.S. Iyengar, J. Tomasi, M. Cossi, J.M. Millam, M. Klene, C. Adamo, R. Cammi, J.W. Ochterski, R.L. Martin, K. Morokuma, O. Farkas, J.B. Foresman, D.J. Fox, Gaussian 16, Revision A.03, (2016).
[80] S. Xu, D.J. Hermanson, S. Banerjee, K. Ghebreselasie, G.M. Clayton, R.M. Garavito, L.J. Marnett, Oxicams bind in a novel mode to the cyclooxygenase active site via a two-water-mediated h-bonding network, J. Biol. Chem. 289 (2014) 6799–6808, https://doi.org/10.1074/jbc.M113.517987.

International Journal of
Molecular Sciences

IMPACT FACTOR 4.556

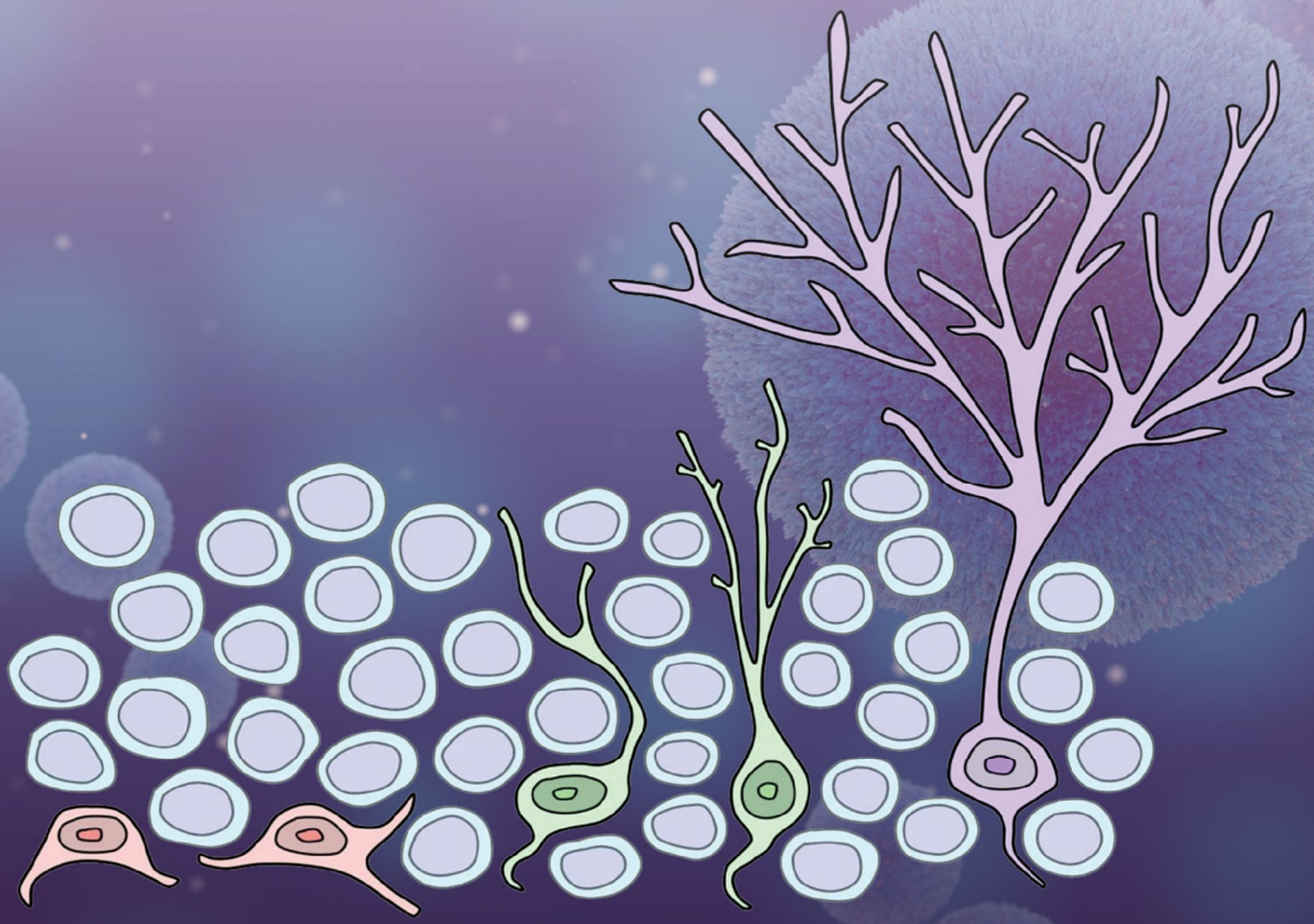

Epigenetic Regulation of the Hippocampus, with Special Reference to Radiation Exposure

Volume 21 · Issue 24 | December (II) 2020

MDPI

mdpi.com/journal/ijms
ISSN 1422-0067

International Journal of
Molecular Sciences

MDPI

Article

Design, Synthesis and Comprehensive Investigations of Pyrrolo[3,4-*d*]pyridazinone-Based 1,3,4-Oxadiazole as New Class of Selective COX-2 Inhibitors

Łukasz Szczukowski [1,*], Edward Krzyżak [2], Adrianna Zborowska [3], Patrycja Zając [3], Katarzyna Potyrak [3], Krzysztof Peregrym [3], Benita Wiatrak [4,5], Aleksandra Marciniak [2] and Piotr Świątek [1]

1 Department of Medicinal Chemistry, Wroclaw Medical University, Borowska 211, 50-556 Wroclaw, Poland; piotr.swiatek@umed.wroc.pl
2 Department of Inorganic Chemistry, Wroclaw Medical University, Borowska 211a, 50-556 Wroclaw, Poland; edward.krzyzak@umed.wroc.pl (E.K.); aleksandra.marciniak@umed.wroc.pl (A.M.)
3 Student Scientific Club of Medicinal Chemistry, Wroclaw Medical University, Borowska 211, 50-556 Wroclaw, Poland; adrianna.zborowska@student.umed.wroc.pl (A.Z.); patrycja.zajac@student.umed.wroc.pl (P.Z.); katarzyna.potyrak@student.umed.wroc.pl (K.P.); krzysztof.peregrym@student.umed.wroc.pl (K.P.)
4 Department of Basic Medical Sciences, Wroclaw Medical University, Borowska 211, 50-556 Wroclaw, Poland; benita.wiatrak@umed.wroc.pl
5 Department of Pharmacology, Wroclaw Medical University, Mikulicza-Radeckiego 2, 50-345 Wroclaw, Poland
* Correspondence: lukasz.szczukowski@umed.wroc.pl; Tel.: +48-71-784-03-90

Received: 23 November 2020; Accepted: 11 December 2020; Published: 17 December 2020

Abstract: The long-term use of Non-Steroidal Anti-Inflammatory Drugs (NSAIDs) in treatment of different chronic inflammatory disorders is strongly restricted by their serious gastrointestinal adverse effects. Therefore, there is still an urgent need to search for new, safe, and efficient anti-inflammatory agents. Previously, we have reported the Mannich base-type derivatives of pyrrolo[3,4-*d*]pyridazinone which strongly inhibit cyclooxygenase, have better affinity to COX-2 isoenzyme and exert promising anti-oxidant activity. These findings encouraged us to perform further optimization of that structure. Herein, we present the design, synthesis, molecular docking, spectroscopic, and biological studies of novel pyrrolo[3,4-*d*]pyridazinone derivatives bearing 4-aryl-1-(1-oxoethyl)piperazine pharmacophore **5a,b**–**6a,b**. The new compounds were obtained via convenient, efficient, one-pot synthesis. According to in vitro evaluations, novel molecules exert no cytotoxicity and act as selective COX-2 inhibitors. These findings stay in good correlation with molecular modeling results, which additionally showed that investigated compounds take a position in the active site of COX-2 very similar to Meloxicam. Moreover, all derivatives reduce the increased level of reactive oxygen and nitrogen species and prevent DNA strand breaks caused by oxidative stress. Finally, performed spectroscopic and molecular docking studies demonstrated that new compound interactions with bovine serum albumin (BSA) are moderate, formation of complexes is in one-to-one ratio, and binding site II (subdomain IIIA) is favorable.

Keywords: selective COX-2 inhibitors; double pharmacophore approach; anti-inflammatory activity; anti-oxidant agents; molecular docking; 1,3,4-oxadiazole; DNA protection

1. Introduction

The prostaglandin-endoperoxide synthase (PGH synthase), more widely known as cyclooxygenase (COX), is a membrane-bound enzyme that catalyzes the conversion of arachidonic acid into bioactive

lipids such as prostaglandins (PGs) and thromboxane (TX) [1–6]. These mediators are essential to maintain homeostasis and play a crucial role in various pathological conditions such as induction of pain and control of inflammation. Cyclooxygenase exists in three isoforms that differ from each other in terms of structure and function [1–4]. A constitutive form of the enzyme, named COX-1, is expressed in normal cells. It synthesizes PGs involved in the physiological processes related mainly to the gastrointestinal and cardiovascular systems. For instance, activation of COX-1 in gastric mucosa leads to prostaglandin I_2 (PGI_2) formation, commonly called prostacyclin, which exerts cytoprotective effects by increasing secretion of mucus and bicarbonate and improving local blood flow. Prostacyclin produced in endothelial cells reduces platelet aggregation and causes vasodilation [1–8]. COX-2, on the contrary, is mostly an inducible form of cyclooxygenase, which level under normal, physiological conditions, is very low. Its expression immediately increases due to various pro-inflammatory and pathogenic stimuli. Induction of isoform COX-2 occurs in areas affected by inflammation, infection, neurodegeneration or cell mutation [1–3,9,10]. Finally, the third isoform named COX-3, a variant of COX-1, is expressed mainly in the brain and spinal cord [1,2,11].

Both cyclooxygenase isoforms, COX-1 and COX-2, are molecular targets for salicylates and aspirin-like drugs, more often called presently Non-steroidal and Anti-Inflammatory Drugs (NSAIDs). It was discovered in 1971 by Vane that popular antipyretic and anti-inflammatory drug—aspirin diminish prostanoid biosynthesis. Inhibition of COX expressed in malfunctioning tissue affected by injury or infection results in pain relief and reduction of inflammation. Unfortunately, at the same time, the decreased level of prostaglandins in normal cells causes dangerous side effects characteristic for NSAIDs [1–10,12–14].

Non-steroidal and Anti-Inflammatory Drugs, which act as non-selective cyclooxygenase inhibitors (e.g., Ibuprofen, Diclofenac), are reported to cause different upper and lower gastrointestinal (GI) adverse effects including dyspepsia, heartburn, ulceration, or bleeding, which are the consequence of weakened mucosal protection. Moreover, the free carboxylic group, which is characteristic for most of NSAIDs, is irritating in direct contact with mucosa cells. Those drugs are not ionized in acidic stomach environment, but get dissociated when got into epithelial cells. The effect of ionic trap is responsible for topical mucosal damage. Selective COX-2 inhibitors (COXIBs) exert similar analgesic and anti-inflammatory properties to traditional NSAIDs and, at the same time, show very low gastrotoxicity. Nevertheless, some gastric complications could occur anyway during therapy with COXIBs because COX-2 is also, to some extent, engaged in gastroduodenal mucosa defense. Additionally, chronic use of COXIBs can elevate the risk of serious cardiovascular complications [7–10,12–16].

Severe adverse effects of both non-selective and selective NSAIDs significantly restrict the usage of these drugs, especially in long-term therapy. Therefore, there is still an urgent prompt for search and develop new, potent, selective, and primarily safe cyclooxygenase inhibitors, which could be deprived of side effects distinctive for known NSAIDs [7,8,14,17–19].

Our previous study reported the synthesis and biological evaluatio of several pyrrolo[3,4-*d*] pyridazinone derivatives with promising anti-inflammatory and anti-oxidant activity. All designed compounds efficiently inhibit cyclooxygenase, have a better affinity to isoenzyme COX-2 and show a superior COX-2/COX-1 selectivity ratio compared to Meloxicam, which was used as the reference drug. According to a molecular docking study, novel Mannich base-type derivatives of pyrrolo[3,4-*d*]pyridazinone take a position in COX's active site very similar to Meloxicam [20,21]. In relation to performed multiple-criteria decision analysis (MCDA), the most potent compound in formerly carried out study was 6-butyl-3,5,7-trimethyl-1-[[3-[(4-phenylpiperazin-1-yl)methyl]-2-thioxo-1,3,4-oxadiazol-5-yl]methoxy] pyrrolo[3,4-*d*]pyridazin-4-one **1** (Figure 1) [20].

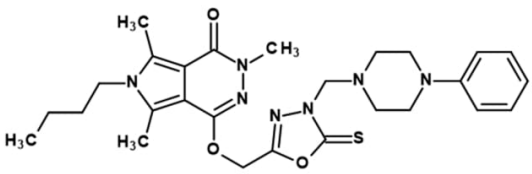

Figure 1. The structure of the most potent new Mannich base-type derivative of pyrrolo[3,4-*d*]pyridazinone.

These findings encouraged us to perform further modifications on the investigated scaffold of pyrrolo[3,4-*d*]pyridazin-4-one, based on the structural optimalization of derivative **1** to obtain more effective molecules.

As was mentioned already, derivatives of pyrrolo[3,4-*d*]pyridazinone are proved to have promising analgesic and anti-inflammatory activity (Figure 2, I) [22,23]. We have previously introduced to the biheterocyclic scaffold of pyrrolo[3,4-*d*]pyridazinone, the five-membered moiety of 1,3,4-oxiadiazole-2-thione [20]. This modification was inspired by the fact that in the structure of selective COX-2 inhibitors—COXIBS, characteristic five-membered heterocyclic rings such as isoxazole (Valdecoxib) or pyrrazole (Celecoxib) can be distinguished (Figure 2, II) [18]. Moreover, 1,3,4-oxiadiazole-2-thione can serve as a bioisostere of the carboxylic group [17,24–26]. There are plenty of compounds containing the mentioned ring that lack gastrointestinal toxicity while presenting promising anti-inflammatory and analgesic activity. Replacement of irritating free carboxylic group by 1,3,4-oxiadiazole-2-thione moiety in popular NSAIDs, such as Diclofenac or Ibuprofen, allowed to obtain structures with significantly reduced gastrotoxicity and improved COX-2 affinity (Figure 2, III) [27,28]. Finally, the current study's key modification was the introduction to the new derivatives, the arylpiperazine pharmacophore, through a flexible 2-oxoethyl linker. This structural alteration closely refers to the theory featured by Dogruer (Figure 2, IV) [29,30]. According to this hypothesis, the presence of carbonyl moiety in the alkyl chain could enhance the analgesic and anti-inflammatory activity of new structures.

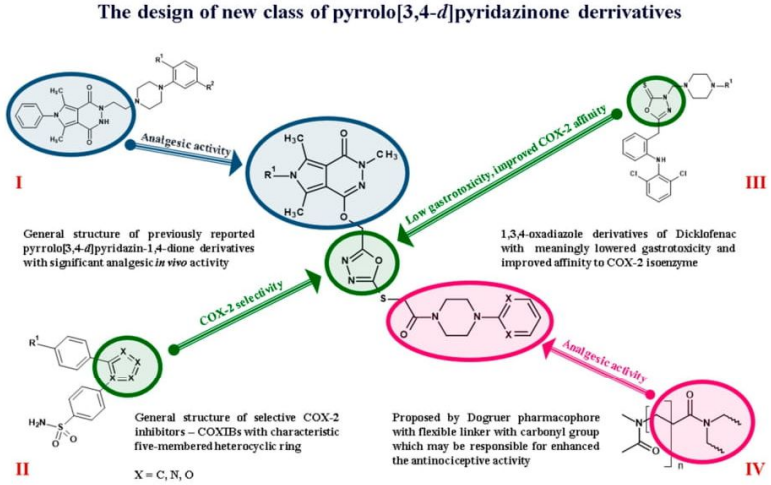

Figure 2. The outline of the concept of the uprising of novel pyrrolo[3,4-*d*]pyridazinone derivatives.

Taking the above into consideration, we can conclude that new pyrrolo[3,4-*d*]pyridazinone derivatives were designed and synthesized on the base of the idea of the double pharmacophore approach. The 1,3,4-oxadiazole-2-thione moiety is one of the most valid in contemporary medicinal chemistry. It is present in a great variety of compounds that exert diverse biological activities, including cyclooxygenase inhibitors, as well [18,19,31,32]. On the other hand, arylpiperazine pharmacophore

occurs in many potent antinociceptive and anti-inflammatory agents [20,22,23,27–30]. Herein, in the structure of title compounds, both 1,3,4-oxadiazole, arylpiperazine pharmacophore and flexible 2-oxoethyl linker, proposed by Dogruer [29,30], could be recognized (Figure 2). Hopefully, such a synthetic approach will result in the obtainment of potent bioactive molecules.

Currently, we present the synthesis, comprehensive in vitro and in silico evaluation of pyrrolo[3,4-*d*]pyridazinone derivatives designed as a potential novel class of analgesic anti-inflammatory agents inhibiting cyclooxygenase. This study's aim is to determine the impact of the mentioned elongated 2-oxyethyl linker on the anti-inflammatory and anti-oxidant activity of new pyrrolo[3,4-*d*]pyridazinone derived compounds. All performed complex investigations focus on possibly the most precise explanation of the probable mechanism of action of new molecules. Moreover, we determine their cytotoxicity and model of interaction with blood proteins.

2. Results and Discussion

2.1. Chemistry

The objective of this study was the design and synthesis of novel pyrrolo[3,4-*d*]pyridazinone derivatives. The structures of final compounds **5a,b**–**6a**,**b** (Scheme 1) were based on already published in the literature the structure–activity relationships of different analgesic and anti-inflammatory agents (Figure 2).

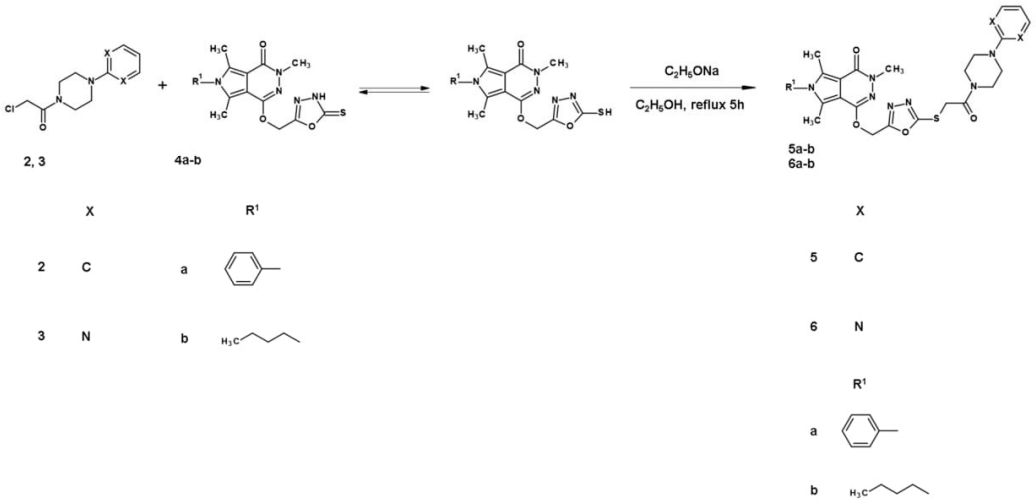

Scheme 1. The synthesis and structures of final pyrrolo[3,4-*d*]pyridazinone derivatives **5a,b**–**6a,b**.

The first step of the planned synthesis assumed the obtainment of appropriate arylpiperazine pharmacophores. The alkylation of 1-phenylpiperazine or 1-(2-pyrimidyl)-piperazine with chloroacetyl chloride led to the formation of 1-(2-chloro-1-oxoethyl)-4-phenylpiperazine **2** and 1-(2-chloro-1-oxoethyl)-4-(2-pyrimidyl)-piperazine **3**, respectively. This stage was performed according to previously reported protocols [33]. The synthesis of 3,5,7-trimethyl-6-phenyl-1-[(2-thioxo-3*H*-1,3,4-oxadiazol-5-yl)methoxy]pyrrolo[3,4-*d*]pyridazin-4-one **4a** and 6-butyl-3,5,7-trimethyl-1-[(2-thioxo-3*H*-1,3,4-oxadiazol-5-yl)methoxy]pyrrolo[3,4-*d*] pyridazin-4-one **4b** was carried out also in accordance to our procedure which has been published already [20]. Scheme 1 presents the synthesis of compounds which have not been described in the literature yet. All spectroscopic and analytical properties of all afresh received derivatives were in good agreement with their predicted structures and are summarized in the experimental section and in Supplementary Data.

The title compounds **5a**,**b**–**6a**,**b** were synthesized with satisfactory yield in a convenient way through the alkylation of key pyrrolo[3,4-*d*]pyridazinone analogues **4a** and **4b** with arylpiperazine

derivatives **2** or **3**, respectively. The final reactions were carried out in ethanol in the presence of sodium ethoxide, which played the role of hydrogen chloride binding factor (Scheme 1). The thin-layer chromatography technique was used to monitor the progress of the reaction. The precipitated crude products were filtered off, washed with ethanol, and purified by crystallization from proper solvent.

Due to the occurrence of tautomerism in the 1,3,4-oxadiazole-2-thione ring, the alkylation of appropriate analogue of pyrrolo[3,4-*d*]pyridazinone **4a**,**b** with Suitable 2-chloro-1-oxoethylarylpiperazine derivative **2**, **3** may result in obtainment of a mixture of isomeric *N*- and *S*–forms. In the current study, the applied reagents and reaction conditions allowed the formation of, exclusively, *S*-isomers **5a**,**b**–**6a**,**b** (Scheme 1). Such a conclusion was drawn based on the analysis of the NMR spectra.

When considering the ^{13}C NMR spectra of compounds **4a**,**b**, the significant peak near 177.89–178.90 ppm, which is typical for carbon atom which forms C=S bond, can be distinguished. The lack of this characteristic signal in the ^{13}C NMR spectra of the final structures **5a**,**b**–**6a**,**b** (experimental section and Supplementary Data) indicates that the title compounds were formed via *S*-alkylation of 1,3,4-oxadiazole-2-thiole derivatives of pyrrolo[3,4-*d*]pyridazinone **4a**,**b** (Scheme 1). This is also confirmed by the presence of characteristic peak near 165.36-165.42 ppm in ^{13}C NMR spectra of **5a**,**b**–**6a**,**b** which can be assigned to carbon C2 in 1,3,4-oxadiazole, which binds sulfur via single bond.

Continuing the analysis of the ^{13}C NMR spectra of final molecules **5a**,**b**–**6a**,**b** we can observe peaks which are the signals of carbon atoms present in 2-oxoethyl linker. A peak near 164.59–164.81 ppm is typical for carbonyl (C=O), whereas a signal in the area of 32.32 ppm is assigned to carbon atom 1C (-CH_2-). Furthermore, the presence of an additional two-proton singlet, which appears, depending on the considering derivative, in the range of 4.33-4.42 ppm in ^{1}H NMR spectra of **5a**,**b**–**6a**,**b** could be equated with methylene group present in 2-oxoethyl linker.

In our former study, the compounds bearing phenylpiperazine moiety (Figure 1) appeared to be the most potent in performed experiments [20]. That is why we have decided to introduce the same pharmacophore to one series of novel derivatives. In the second series, a pyrimidine ring is present to evaluate the impact of this terminal aromatic six-membered ring on new compound activity. Moreover, the structure of new agents will allow us to estimate the influence of elongated 2-oxoethyl linker and the substitution of the sulfur atom in 1,3,4-oxadiazole-2-thiol ring on the pharmacological activity of new pyrrolo[3,4-*d*]pyridazinone derivatives

The crude intermediate and final products were purified by crystallization from the suitable solvent. Structures of all newly synthesized derivatives were established and confirmed by spectroscopic techniques including ^{1}H NMR, ^{13}C NMR, MS, FT-IR, elemental analysis and based on their physicochemical properties.

2.2. Cyclooxygenase (COX-1, COX-2) Inhibition Studies

2.2.1. In Vitro Cyclooxygenase Inhibition Assay

The tested compounds' ability to inhibit the activity of COX-1 and COX-2 was assessed by Cayman's COX Colorimetric Inhibitor Screening Assay (cat. no. 701050). Each sample was prepared in triplicate at a concentration of 100 μM. The study started with 2 min incubation at RT, and then peroxidase activity was measured with Varioskan LUX microplate reader (Thermo Scientific) at a wavelength of 590 nm. The outcome is shown as the IC_{50} values, i.e., the concentrations at which a 50% inhibition of enzyme activity appeared for both COX-1 and COX-2. Meloxicam, which shows better affinity to COX-2 than to COX-1, therefore is used by patients with GI complications, was used as a reference compound. The results for both enzymes are presented in the table below. The study showed that the tested structures inhibit the activity of COX-2 enzymes and have no impact on the COX-1 isoform (Table 1). The most active compound appeared to be **6a**, in which 50% inhibition of COX-2 enzyme activity occurred at the lowest concentration. Taking these results into account, it is worth emphasizing that both isoforms of cyclooxygenase have slight but important structural

differences in their active sites. The isoleucine (Ile) residue in position 523 in COX-1 isoform is replaced by valine (Val) when considering isoform COX-2. Furthermore, in the case of COX-1, in position 434 occurs isoleucine (Ile) and in position 513 histidine (His), while in COX-2 valine (Val) and arginine (Arg), respectively. Due to these differences, the size of the COX-2 pocket is bigger than that of COX-1, which allows selective binding of larger molecules [1–5]. In the case of the COX-2 enzyme, investigated compounds displayed lower activity than the reference.

Table 1. IC_{50} values determined for COX-1 and COX-2 enzymes; data are presented as mean and SD (standard deviation).

Compound	Cyclooxygenase Inhibition Assay IC50 [μM]	
	COX-1	COX-2
5a	ND [1]	658.7 (15.0)
5b	ND [1]	257.4 (11.3)
6a	ND [1]	160.2 (6.8)
6b	ND [1]	371.0 (10.1)
Meloxicam	83.7 (1.8)	59.2 (2.4)

[1] ND—not detectable at tested concentrations.

When comparing the COX inhibitory activity of new compounds **5a,b–6a,b** with previously reported Mannich base-type derivatives of pyrrolo[3,4-*d*]pyridazinone [20] we can point out some important differences between these two series. Most of formerly studied compounds had the affinity towards both isoenzymes of cyclooxygenase, with superior activity on COX-2, while molecules described in this manuscript act as selective COX-2 inhibitors. Basing on these findings, and with reference to investigations performed earlier by Malinka et al. [22,23] we can try to speculate about some structure–activity relationships in the group of analgesic and anti-inflammatory agents based on pyrrolo[3,4-*d*]pyridazinone core.

Malinka et al. reported the synthesis and extensive biological evaluation of new derivatives of pyrrolo[3,4-*d*]pyridazinone with promising antinociceptive activity. In the structure of described compounds, the characteristic arylpiperazine/piperidine pharmacophore can be recognized. It was attached directly to the pyridazinone core via different flexible linkers such as ethyl, propyl or 2-hydroxypropyl. Despite good pharmacological activity, the exact mechanism of action of these compounds has not been solved yet [22,23].

Inspired by those results we decided to continue this work and modify the pyrrolo[3,4-*d*]pyridazinone scaffold by incorporation of the five-membered 1,3,4-oxadiazole-2-thione moiety with the hope of receiving potent cyclooxygenase inhibitors with good affinity towards COX-2. As was mentioned before, we have achieved the intended goal. The 1,3,4-oxadiazole ring is supposed to enhance COX inhibitory activity of our compounds [20]. When considering derivatives **5a,b–6a,b** we can infer that introduction of arylpiperazine pharmacophore via flexible 2-oxoethyl linker to the pyrrolo[3,4-*d*]pyridazinone-based 1,3,4-oxadiazole molecules resulted in their COX-2 selectivity. The fact that in the current study we report molecules received by *S*, not *N* alkylation of 1,3,4-oxadiazole-2-thiol, could also be significant. Nevertheless, certainly further extensive studies and subsequent structural modifications of future derivatives are needed, because the increase of selectivity led to a decrease of activity.

2.2.2. Cyclooxygenase Molecular Docking Study

To estimate the possible binding interactions of synthesized compounds inside the active site of cyclooxygenase, a molecular docking study was performed. AutoDock software was used. The scoring function binding free energy (ΔG°) for interaction with COX-1 for all tested compounds showed a positive value. This result is in very good correlation with a biological evaluation, which indicated no activity towards the COX-1. The docking results for interactions with COX-2 are assumed in Table 2. The ΔG° is negative for all compounds. The lowest value was found for **6b**. For all compounds,

the sum of van der Waals energy, hydrogen bonding energy, and desolvation free energy (ΔE_2) is more negative than electrostatic energy (ΔE_3). It indicates that the main interactions are van der Waals and hydrogen bonding interactions. For **6a** and **5b**, inhibit constants obtained from molecular docking showed lower values than for **6b** and **5a**.

Table 2. Energies of the binding complexes **5a, 6a, 5b, and 6b** with COX-2 obtained from molecular docking.

	$\Delta G°$ [kJmol^{-1}]	$\Delta E1$ [kJmol^{-1}]	$\Delta E2$ [kJmol^{-1}]	$\Delta E3$ [kJmol^{-1}]	K_i [μM]
5a	−20.44	−30.18	−30.43	0.25	285.75
5b	−26.75	−39.20	−38.87	−0.33	20.39
6a	−30.54	−40.52	−40.88	−0.37	4.44
6b	−21.06	−33.52	−35.69	2.13	202.61
Meloxicam	−34.02	−37.74	−37.32	−0.42	1.09

$\Delta G°$—binding free energy; ΔE_1—intermolecular interaction energy, which is the sum of van der Waals energy, hydrogen bonding energy, desolvation free energy and electrostatic energy; ΔE_2—the sum of van der Waals energy, hydrogen bonding energy and desolvation free energy; ΔE_3—electrostatic energy, K_i—inhibit constans.

Inside the COX-2 active site, no conventional hydrogen bond interaction was found. Hydrophobic interactions play an important role. The details are presented in Figure 3. The COX ligand binding site has four specific subdomains: A, B, C, and D. Subdomain A represents the mode of binding of flurbiprofen; subdomain B represents the mode of binding of Meloxicam and Piroxicam; subdomain C represents an entrance region of the enzyme binding domain, and subdomain D represents the position of the residue in position 523 [34]. The size of the COX-2 pocket is bigger than that of COX-1., It allows the selective binding of larger molecules. The position of studied compounds was found very similar to Meloxicam (Figure 4).

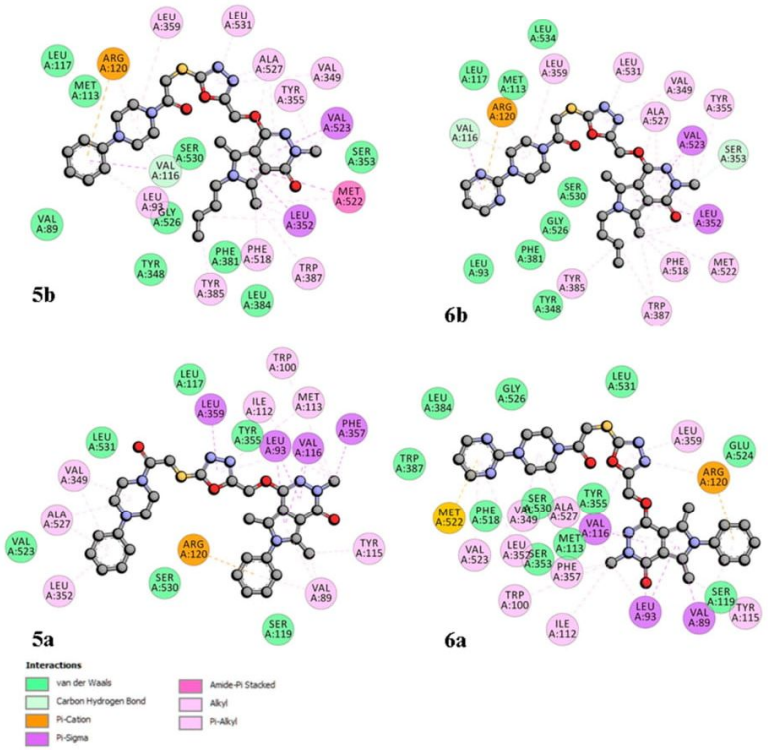

Figure 3. 2D interaction plot of **5a**, **5b**, **6a**, **6b** with COX-2.

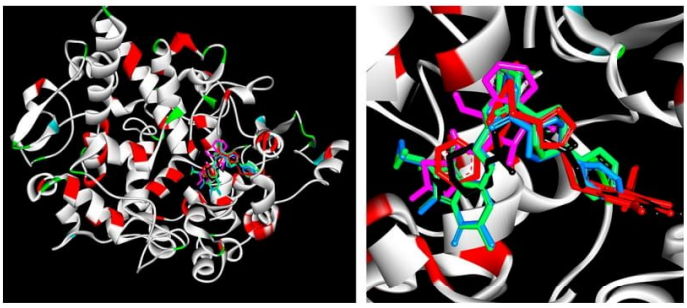

Figure 4. Docking poses of studied compounds **5a**,**b**–**6a**,**b** and Meloxicam (pink) inside COX-2.

2.3. Evaluation of Viability

Dependence between viability and concentration was observed for all investigated compounds (Figure 5). The study showed that the metabolic activity of **5b** and **5a** decreases as the concentration increases, whereas **6a** toxicity at 50 μM concentration is higher than at 100 μM, but it is within experimental error. None of the cases showed a decrease of viability under 30%, indicating a lack of tested compound cytotoxic potential. Furthermore, **5a** and **5b** at 10 μM concentration presumably improve the proliferation of Normal Human Dermal Fibroblasts (NHDF) cells. Merely **6a** at 50-100 μM concentration range revealed mild cytotoxicity of a dozen or so percent.

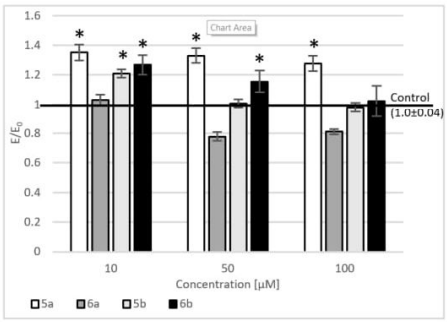

Figure 5. Effect of tested compounds on Normal Human Dermal Fibroblasts (NHDF) cells; metabolic activity measured in MTT assay; Control—cell culture incubated without tested substances; * $p < 0.05$—significant difference compared to control.

2.4. Level of Intracellular Reactive Oxygen Species, Nitric Oxide, and DNA Damage

For all tested compounds, a relationship between the level of free oxygen radicals, nitric oxide or the number of DNA strand breaks and concentration was observed (Table 3). The results showed that the level of free oxygen radicals after using all tested compounds is the lowest at a concentration of 10 μM. After using compounds **5a**, **5b**, **6b**, a decrease in the level of free oxygen radicals below the positive control was noticed (cell culture treated with only 100 μM H_2O_2) in the entire range of tested concentrations. Compound **6a** at concentrations of 50 and 100 μM did not reduce the level of free oxygen radicals. Regarding the nitric oxide (NO) level, a reduction in NO levels was observed after incubating the culture with the tested compounds compared to the positive control after incubation at a concentration of 10 and 50 μM for **6b** and **5a**, 10 μM for **5b** and in the entire concentration range for **6a**. At the same time, a reduction in the amount of DNA strand damage after incubation with the investigated compounds was demonstrated for all tested concentrations for **6b** and **5a**, at 10 and 50 μM for compound **5b** and the lowest tested concentration for compound **6a** (Scheme 2).

Table 3. Reactive oxygen species (ROS) and reactive nitrogen species (RNS) scavenging activity of tested compounds and an impact on the DNA damage ($n = 3$); the results were compared to the positive control and expressed as E/E_0 ratios; statistical significance calculated with post-hoc test compared to control (* $p < 0.05$; E0—culture incubated with 100 μM H_2O_2 but without test compounds); data are presented as mean and SEM.

Compound	Concentration [μM]	ROS	RNS	DNA Damage
5a	10	−33.1 (0.04) *	−3.7 (0.03)	−68 (0.1) *
	50	−34.2 (0.06) *	−5.9 (0.02)	−47 (0.08) *
	100	−28.7 (0.03) *	12.1 (0.02) *	−38 (0.1) *
5b	10	−29.0 (0.02) *	−6.7 (0.03) *	−59 (0.08) *
	50	−9.7 (0.02) *	3.4 (0.04)	−12 (0.07) *
	100	−0.5 (0.04)	9.8 (0.04)	5.7 (0.2)
6a	10	−7.4 (0.03)	−11.0 (0.07) *	−2.4 (0.1)
	50	12.3 (0.05)	−6.9 (0.05)	26 (0.06) *
	100	18.9 (0.06) *	−4.1 (0.04)	24 (0.08) *
6b	10	−24.1 (0.05) *	−7.9 (0.05) *	−70 (0.06) *
	50	−12.6 (0.04) *	−1.4 (0.04)	−22 (0.09) *
	100	−1.8 (0.02)	4.6 (0.02)	−9.7 (0.1) *

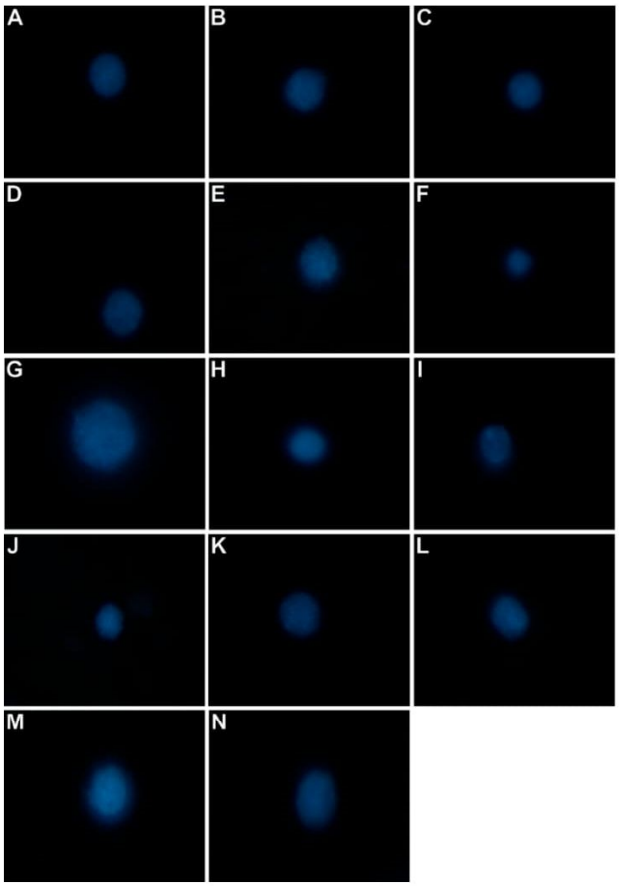

Scheme 2. Micrographs (60×) of cells showing chromatin relaxation: (**A**) compound **5a** at 10 μM; (**B**) compound **5a** at 50 μM; (**C**) compound **5a** at 100 μM; (**D**) compound **5b** at 10 μM; (**E**) compound **5b** at 50 μM; (**F**) compound **5b** at 100 μM; (**G**) compound **6a** at 10 μM; (**H**) compound **6a** at 50 μM; (**I**) compound **6a** at 100 μM; (**J**) compound **6b** at 10 μM; (**K**) compound **6b** at 50 μM; (**L**) compound **6b** at 100 μM; (**N**) cell incubated in the complete medium; (**M**) cell incubated with 100 μM H_2O_2 for 1 h.

Correlation coefficients between the DNA damage assay results and the level of free oxygen radicals or nitric oxide were calculated (Table 4). In all cases, strong positive correlations were observed between the levels of reactive oxygen species (ROS) and NO as well as DNA strand breakage. These results may suggest a strong reparative effect (scavenging of free radicals and repair of DNA strand breaks) of the tested compounds in a state of increased exogenous stress (incubation of cell cultures with H_2O_2), possibly by inhibiting COX-2.

Table 4. Pearson correlation coefficients between DNA damage and ROS or NO levels.

Compound	ROS Level vs. DNA Damage	NO Level vs. DNA Damage
5a	0.589	0.650
5b	0.998	0.991
6a	0.953	0.888
6b	0.951	0.950

2.5. Fluorescence Quenching and Binding Constants

To investigate the binding properties of **5a**, **6a**, **5b**, and **6b** to Bovine Serum Albumin, the fluorescence spectra were recorded in the range of 300–500 nm upon excitation at 280 nm (both Trp and Tyr residues are excited) and concentration range 0.0–2.0 μM (Figure 6). When different amounts of tested compounds were titrated, BSA's fluorescence intensity decreased, suggesting that all compounds could interact with BSA and quench its intrinsic fluorescence. The presence of **5a**, **6a**, **5b**, and **6b** also caused a blue shift in the maximum emission wavelength of protein. It indicates that BSA's conformation and the amino acid residues are located in a more hydrophobic environment and are less exposed to the solvent [35]. Fluorescence quenching and shift of λ_{max} identify interaction with BSA and suggest the formation of complexes (static quenching). However, it can also be the result of the collisional encounters (dynamic quenching). To confirm the quenching mechanism and complex formation, the fluorescence data were further analyzed by the Stern–Volmer equation and dependence on temperature [36].

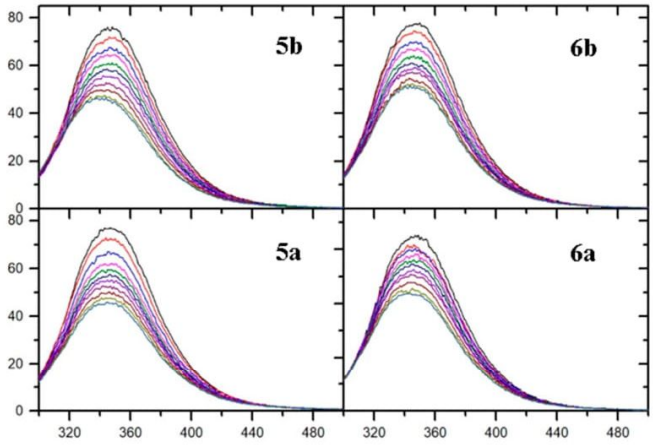

Figure 6. Fluorescence spectra of Bovine Serum Albumin solution in the presence of **5a**, **5b** and **6a**, **6b** (T-294 K, λex = 280 nm). The concentration of **5a**, **5b** and **6a**, **6b** was: 0, 0.2, 0.4, 0.6, 0.8, 1.0, 1.2, 1.4, 1.6, 1.8, 2.0 μM.

The fluorescence data were analyzed at three different temperatures, 294, 301, 308 K, using Stern–Volmer Equation [37] (Equation (S1) in the Supplementary Data) after correction due to the infer filter effect (Equation (S2) in the Supplementary Data). The Stern–Volmer (K_{SV}) constant was determined by the linear fitting. The calculated results are collected in Table 5. The K_{SV} values decreasing with

increasing temperature, and the quenching rate constant (k_q) values are much greater than the value of the maximum scatter collision quenching constant (2×10^{10} $dm^3 \cdot mol^{-1} \cdot s^{-1}$ [38]). It indicated that the probable quenching mechanism is static rather than dynamic, and it suggested the formation of a ground-state complex.

Table 5. The Stern–Volmer constant K_{SV} and the quenching rate constant k_q, binding constants K_b and number of binding sites n, thermodynamic parameters for the interaction of BSA with studied compounds at different temperatures.

	Quenching			Binding			Thermodynamic		
	T [K]	$K_{sv} \times 10^5$ [$dm^3 \cdot mol^{-1}$]	$k_q \times 10^{13}$ [$dm^3 \cdot mol^{-1} \cdot s^{-1}$]	$\log K_b$	$K_b \times 10^4$ [$dm^3 \cdot mol^{-1}$]	n	ΔG° [$kJmol^{-1}$]	ΔH° [$kJmol^{-1}$]	ΔS° [$Jmol^{-1}K^{-1}$]
	294	4.44	4.44	5.09 ± 0.14	12.30	0.91 ± 0.02	−29.31	−133.03	−352.78
5a	301	2.45	4.45	4.90 ± 0.30	7.94	0.92 ± 0.05			
	308	2.09	2.09	4.01 ± 0.13	1.02	0.77 ± 0.03			
	294	4.44	4.44	5.09 ± 0.14	12.30	0.91 ± 0.02	−29.31	−133.03	−352.78
5b	301	2.45	4.45	4.90 ± 0.30	7.94	0.92 ± 0.05			
	308	2.09	2.09	4.01 ± 0.13	1.02	0.77 ± 0.03			
	294	2.12	2.12	4.86 ± 0.05	7.24	0.92 ± 0.01	−27.51	−108.79	−276.43
6a	301	1.27	1.17	4.50 ± 0.13	3.16	0.89 ± 0.02			
	308	1.13	2.74	3.98 ± 0.27	0.96	0.81 ± 0.04			
	294	2.90	2.90	4.93 ± 0.07	8.51	0.91 ± 0.01	−27.37	−77.15	−169.33
6b	301	1.80	1.80	4.41 ± 0.29	2.57	0.85 ± 0.05			
	308	1.74	4.43	4.31 ± 0.26	2.04	0.84 ± 0.04			

The binding constants and the number of binding sites were calculated using a double logarithm regression curve (Equation (S3) in the Supplementary Data). As is shown in Figure 7 there is a good linear fit for all studied compounds. The calculated results are listed in Table 5. The results showed that the binding constants indicate values about 10^5 $dm^3 \cdot mol^{-1}$ at 294 K and decreasing with increasing temperature. The differences between **5a**, **6a**, **5b**, and **6b** compounds are not great. The number of the binding site is close to 1, shows one-to-one interaction. The interaction of 14 anti-inflammatory drugs with human serum albumin was investigated by F. Mohammadnia [39]. The binding constants were found with the range 10^2 $dm^3 \cdot mol^{-1}$ (acetaminophen) to 1.88×10^7 $dm^3 \cdot mol^{-1}$ for Meloxicam. Therefore, K_b values of studied compounds show that the interactions with BSA are moderate. Similar values were obtained for many compounds with biological activity [20,36,40–44].

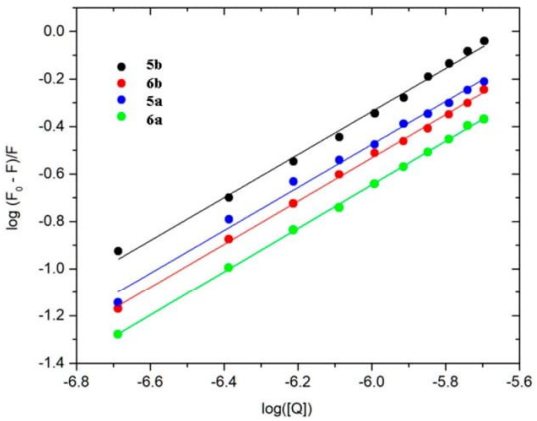

Figure 7. Double logarithm regression plots for quenching of BSA by **5a**, **5b**, **6a**, and **6b.**

2.6. Site Markers Studies and Molecular Docking

BSA, as well as human serum albumin (HSA), is known to possess two binding sites, which are situated in subdomains IIA and IIIA [45]. To confirm the binding sites on BSA involved in **5a**, **6a**, **5b**, and **6b** binding, phenylbutazone (PHB) and ibuprofen (IBP) were used as site probes [46]. Binding

constants were analyzed using Equation (S3) (in the Supplementary Data). Calculated values were found as 5.50×10^3 (**5b**), 4.79×10^3 (**6b**), 4.17×10^3 (**5a**), 3.24×10^3 (**6a**). The results show that binding constant Kb of all tested compounds with BSA in the presence of IBP considerably decline compared to compound BSA only (Table 5.). In the presence of PHB, Kb value showed smaller difference compared to no marker: 4.27×10^4 (**5b**), 3.31×10^4 (**6b**), 4.07×10^4 (**5a**), 2.51×10^4 (**6a**). It can be suggested that **5a**, **5b**, **6a**, **6b** mainly bind to the subdomain IIIA of BSA.

The binding interactions between studied compounds and BSA were simulated by the molecular docking method. The results were presented in Table 6. The results demonstrated that the binding free energy within the hydrophobic cavity in site II (subdomain IIIA) of BSA was more negative than that within the hydrophobic cavity in site I (subdomain IIA). It indicates that site II is favorable. Such outcome is consistent with the results observed in the site marker fluorescence studies. The sum of van der Waals energy, hydrogen bonding energy, and desolvation free energy (ΔE_2) is more negative than electrostatic energy (ΔE_3). Hence, it can indicate that the main interactions are van der Waals and hydrogen bonding interactions. In binding site IIIA studied compounds are surrounded by various kinds of residues (Figure 8). Hydrogen bonds with Arg208 (**5a**, **5b**, **6a**, **6b**) and Lys211 (**6b**) are formed. The π-sigma and other hydrophobic interactions are observed. The details are presented in Figure 8.

Table 6. Energies of the binding complexes BSA with **5a, 5b, 6a, and 6b** obtained from molecular docking.

	Binding Site	ΔG° [kJmol^{-1}]	ΔE_1 [kJmol^{-1}]	ΔE_2 [kJmol^{-1}]	ΔE_3 [kJmol^{-1}]
5a	site I	−31.43	−41.42	−40.88	−0.54
	site II	−38.96	−48.94	−48.44	−0.46
5b	site I	−27.38	−39.83	−38.70	−1.13
	site II	−38.87	−51.37	−51.03	−0.33
6a	site I	−34.73	−44.72	−40.34	−4.39
	site II	−36.94	−47.10	−44.51	−2.59
6b	site I	−30.55	−43.01	−38.70	−4.31
	site II	−39.12	−51.62	−49.49	−0.46

ΔG°—binding free energy; ΔE_1—intermolecular interaction energy, which is the sum of van der Waals energy, hydrogen bonding energy, desolvation free energy and electrostatic energy; ΔE_2—the sum of van der Waals energy, hydrogen bonding energy and desolvation free energy; ΔE_3—electrostatic energy.

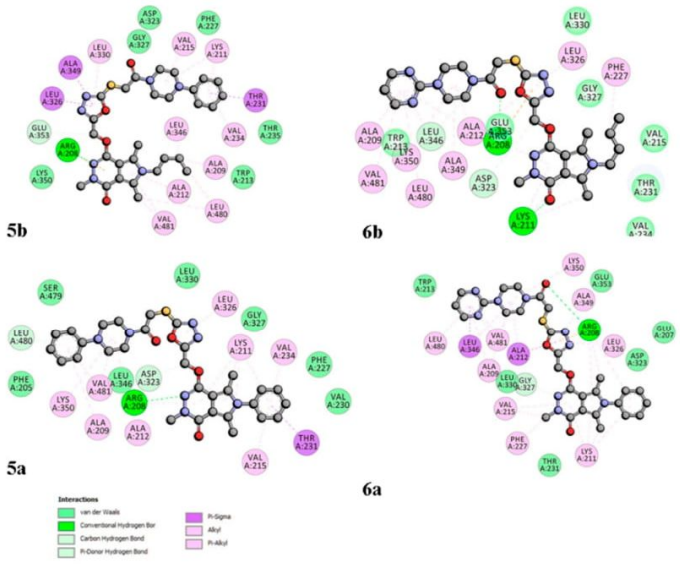

Figure 8. 2D interaction plot of **5a**, **5b**, **6a**, **6b** with BSA in the binding site II (subdomain IIIA).

The interaction forces between a small molecule and protein include hydrogen bond, van der Waals force, electrostatic and hydrophobic interactions, etc. [47]. The thermodynamic parameters enthalpy change (ΔH°), the entropic change (ΔS°) and free energy change (ΔG°) were calculated from Equations (S4) and (S5) in the Supplementary Data. The results are listed in Table 5. We can conclude that the binding interaction between tested compounds and BSA were spontaneous due to the negative ΔG°. Both the ΔH° and ΔS° negative values indicate that the main interaction force in the binding process was van der Waals forces and/or hydrogen bonding interaction.

2.7. Circular Dichroism Spectra

Circular dichroism (CD) spectroscopy is a useful method to determine the secondary structure changes in the conformation of proteins. It can check the interaction between the protein molecule and new pharmaceutical compounds [48]. In this study, we had monitored the changes in BSA structure when four analyzed compounds: **5a**, **5b**, **6a**, and 6b were absent or present in solutions. In all CD spectra, we observed two negative bands at near 208 nm and 222 nm, typical for the α-helical structure of the protein (Figure 9). Any changes in this region suggest conformational changes in protein molecules [49].

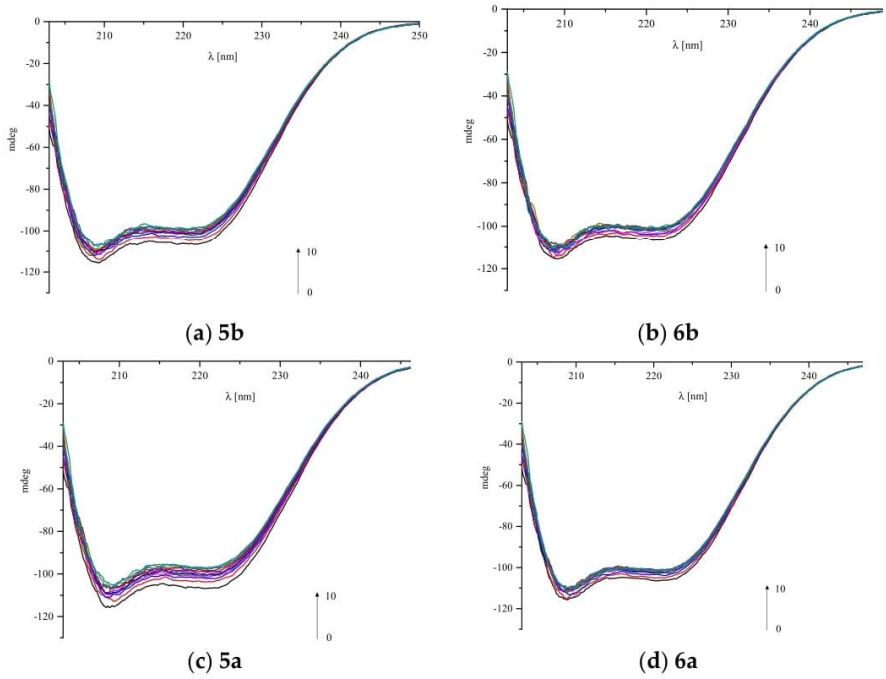

Figure 9. CD spectra of BSA in the absence and presence of all analyzed compounds. BSA to analyzed compounds molar ratios was changing from 1:0 to 1:10.

Figure 9 shows that we observed the reduction of ellipticity values at 208 nm and 222 nm in the presence of all analyzed compounds. Any shift of the peaks was not observed. To measure the observed change size, we calculated the α-helix(%) values after adding every portion of each analyzed compound (Table 7).

Table 7. The values of calculated α-helix(%) for BSA with the absence and presence of all analyzed compounds.

BSA/Analyzed Compound Molar Ratio	α-helix(%)			
	5a	**5b**	**6a**	**6b**
1:0	**54.05**	**53.55**	**53.78**	**53.46**
1:0.5	51.08	52.15	52.77	52.45
1:1	50.51	51.11	51.72	51.83
1:2	49.94	50.50	51.70	51.26
1:3	49.70	50.47	51.45	50.91
1:4	49.62	49.81	51.49	50.47
1:5	49.48	49.78	51.40	50.23
1:6	48.85	49.51	50.28	50.15
1:7	48.57	49.21	50.29	50.10
1:8	48.23	48.85	50.31	49.97
1:9	48.11	48.06	50.24	49.82
1:10	**47.59**	**47.76**	**50.11**	**49.76**

Numbers in bold represent the initial and final values of α-helical content of BSA in carried out experiment.

The content of α-helix can be calculated using Equations (1) and (2) [50]:

$$\alpha - helix(\%) = \frac{-MRE_{208} - 4000}{33,000 - 4000} 100\% \quad (1)$$

where MRE_{208} is the MRE value observed at 208 nm, 4000 and 33,000 is the MRE value of the β-form and random coil conformation cross at 208 nm value of pure α-helix at 208 nm, respectively.

$$MRE = \frac{ObservedCD[mdeg]}{10Cnl} \quad (2)$$

C is the molar concentration of BSA, n is the number of amino acid residues 583 for BSA, and l is the path length in cm.

The results collected in Figures 9 and 10 and Table 7 show that greater changes of α-helix(%) are observed in the case of **5b** and **5a**. The α-helical content of BSA decreased from 53.55% to 47.76% and from 54.05% to 47.59%, respectively, when BSA to analyzed compounds molar ratio was increasing from 1:0 to 1:10. The smallest changes were observed after adding **6a** to BSA (from 53.78% to 50.11%, Table 7, Figure 9). Above 1:6 BSA to **6a** molar ratio, there was no longer any changes. The greatest changes in the CD spectra are observed in case of 1:0.5 and 1:1 molar ratios. This result is consistent with the fluorescence measurements and molecular docking studies, where it was proved that analyzed compounds can form complexes with BSA in 1:1 ratios. Further changes observed after adding next portions of analyzed ligands may be caused by the interaction of hydrophobic sites of the protein with hydrophobic groups in compounds. Changes in the α-helical content of BSA for all four compounds are compared in Figure 10.

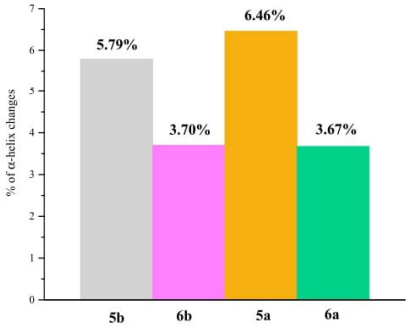

Figure 10. Changes in α-helix(%) of BSA after adding 10 portions of the compound—the comparison for **5a**, **5b**, **6a**, and **6b**.

3. Materials and Methods

3.1. Chemistry

3.1.1. Instrumentation and Chemicals

All chemicals, reagents, and solvents used in the current study were purchased from commercial suppliers (Chemat, Gdańsk, Poland; Archem, Łany, Poland; Alchem, Wrocław, Poland) and used without further purification. Dry solvents were obtained according to the standard procedures. Progress of the reaction was monitored by thin-layer chromatography (TLC) technique on silica-gel-60-F254-coated TLC plates (Fluka Chemie GmbH) and visualized by UV light at 254 or 366 nm. Chromatographic separations and purifications were performed on a silica-gel [Kieselgel 60 (70–230 mesh), Merck] column (CC). The melting points of received products were determined by an open capillary method on Electrothermal Mel-Temp 1101D apparatus (Cole-Parmer, Vernon Hills, IL, USA) and were uncorrected. The ^{1}H NMR (300 MHz) and ^{13}C NMR (75 MHz) spectra were recorded on a Bruker 300 MHz NMR spectrometer (Bruker Analytische Messtechnik GmbH, Rheinstetten, Germany) in $CDCl_3$ or DMSO-d_6 using tetramethylsilane (TMS) as an internal reference. Chemical shifts (δ) are reported in ppm. Spectra were recorded and read using TopSpin 3.6.2. Bruker Daltonik, GmbH, Bremen, Germany) The infrared (IR) spectra were determined on a Nicolet iS50 FT-IR Spectrometer (Thermo Fisher Scientific, Waltham, MA, USA). Samples were applied as solids, and frequencies are reported in cm^{-1}. Spectra were read using OMNIC Spectra 2.0 Thermo Fisher Scientific, Waltham, MA, USA) Mass spectra were recorded using a Bruker Daltonics Compact ESI-mass spectrometer (Bruker Daltonik, GmbH, Bremen, Germany). The instrument was operated in positive ion mode. Analyzed compounds were dissolved in a mixture of chloroform and methanol. Elemental analyses for carbon, nitrogen and hydrogen were run on a Carlo Erba NA-1500 analyzer (Thermo Fisher Scientific, Waltham, MA, USA), and obtained results were within ± 0.4% of the theoretical values calculated for corresponding formulas.

3.1.2. Chemical Synthesis

The synthesis protocols and experimental data for derivatives **4a**,**b** and all intermediates were previously reported[20,33].

General procedure for preparation of title derivatives of pyrrolo[3,4-d]pyridazinone 5a,b–6a,b.

The appropriate derivative of pyrrolo[3,4-*d*]pyridazinone 4a or 4b (0.001 mol) was suspended in 30mL of anhydrous ethanol in a round bottom flask. Then, the 1mL of 1M sodium exthoxide (0.001 mol) and appropriate arylpiperazine derivative 2 or 3 was added, and the mixture was refluxed for 6h. The reaction progress was monitored by TLC. The mixture was left overnight. After cooling, the precipitate was formed. The solid was filtered off, washed thoroughly with ethanol, and afterwards purified by crystallization from ethanol.

5a: 3,5,7-trimethyl-1-[[2-[2-oxo-2-(4-phenylpiperazin-1-yl)ethyl]sulfanyl-1,3,4-oxadiazol-5-yl] methoxy]-6-phenyl-pyrrolo[3,4-*d*]pyridazin-4-one
White solid, Yield: 76,91%; m.p.: 186–188 °C
FT-IR (selected lines, γ_{max}, cm^{-1}): 3067 (C-H arom.), 2916 (C-H aliph.), 1646 (C=N)
^{1}H NMR (300 MHz, $CDCl_3$): δ= 2.27 (s, 3H, 7-CH_3), 2.45 (s, 3H, 5-CH_3), 3.19–3.21 (m, 2H, CH_2-piperazine), 3.22–3.26 (m, 2H, CH_2-piperazine), 3.59 (s, 3H, 3-CH_3), 3.76 (m, 2H, CH_2-piperazine), 3.84 (m, 2H, CH_2-piperazine), 4.41(s, 2H, S-CH_2), 5.49 (s, 2H, O-CH_2), 6.95-6.98 (m, 3H, ArH), 7.19–7.22 (m, 2H, ArH), 7.31–7.33 (m, 2H, ArH), 7.54–7.57 (m, 3H, ArH)
^{13}C NMR (75 MHz, $CDCl_3$): δ= 11.41, 11.84, 36.96, 37.10, 42.25, 46.04, 49.45, 49.82, 57.01, 108.42, 112.07, 116.94, 124.24, 127.79, 129.34, 129.73, 130.74, 136.68, 148.06, 159.32, 163.88, 164.60, 165.43
HR-MS (*m*/*z*): calcd. for $C_{30}H_{31}N_7O_4S$ $[L+H]^+$: 586.2243; found: 586.2231; Anal. calcd. (%) for $C_{30}H_{31}N_7O_4S$: C:61.52, H:5.34, N:16.74, found: C:61.81, H:5.19, N:16.50,

5b: 6-butyl-3,5,7-trimethyl-1-[[2-[2-oxo-2-(4-phenylpiperazin-1-yl)ethyl]sulfanyl-1,3,4-oxadiazol-5-yl]methoxy]pyrrolo[3,4-*d*]pyridazin-4-one
Whitish solid, Yield: 69,44%; m.p.: 141–143 °C
FT-IR (selected lines, γ_{max}, cm^{-1}): 2964, 2925, 2871 (C-H aliph.), 1645 (C=N)
^{1}H NMR (300 MHz, $CDCl_3$): δ= 0.87-0.92 (m,3H, -CH_2-CH_2 CH_2-CH_3), 1.27–1.39 (m, 2H, -CH_2-CH_2 CH_2-CH_3), 1.57 (m, 2H, -CH_2-CH_2-CH_2-CH_3), 2.40–2.42 (s, 3H, 7-CH_3), 2.60–2.61 (s, 3H, 5-CH_3), 3.13 (m, 2H, CH_2-piperazine), 3.19 (m, 2H, CH_2-piperazine), 3.46–3.47 (s, 3H, 3-CH_3), 3.70 (m, 2H,-CH_2-CH_2-CH_2-CH_3), 3.77–3.83 (m, 4H, CH_2-piperazine), 4.33 (s, 2H, S-CH_2), 5.36–5.37 (s, 2H, O-CH_2), 6.88-6.90 (m, 3H, ArH), 7.19-7.23 (m, 2H, ArH)
^{13}C NMR (75 MHz, $CDCl_3$): δ= 10.65, 11.19, 13.69, 20.04, 32.32, 36.90, 37.02, 42.21, 43.94, 46.02, 49.53, 49.88, 56.93, 108.15, 111.85, 122.59, 129.15, 129.36, 147.95, 159.24, 163.95, 164.61, 165.38
HR-MS (*m*/*z*): calcd. for $C_{28}H_{35}N_7O_4S$ $[L+H]^+$: 566.2549; found: 566.2544; Anal. calcd. (%) for $C_{28}H_{35}N_7O_4S$: C:59.45, H:6.24, N:17.33, found: C:59.67, H:6.28, N:17.04,

6a: 3,5,7-trimethyl-1-[[2-[2-oxo-2-(4-pyrimidin-2-ylpiperazin-1-yl)ethyl]sulfanyl-1,3,4-oxadiazol-5-yl]methoxy]-6-phenyl-pyrrolo[3,4-*d*]pyridazin-4-one
White solid, Yield: 85,27 %; m.p.: 237–239 °C
FT-IR (selected lines, γ_{max}, cm^{-1}): 3079 (C-H arom.) 2916 (C-H aliph.), 1645 (C=N)
^{1}H NMR (300 MHz, $CDCl_3$): δ= 2.25 (s, 3H, 7-CH_3), 2.43 (s, 3H, 5-CH_3), 3.58 (s, 3H, 3-CH_3), 3.64–3.66 (m,2H, CH_2-piperazine), 3.73–3.75 (m, 2H, CH_2-piperazine), 3.84–3.86 (m, 2H, CH_2-piperazine), 3.91–3.92 (m, 2H, CH_2-piperazine), 4.41 (s, 2H, S-CH_2), 5.47 (s, 2H, O-CH_2), 6.54-6.58 (m, 1H, ArH), 7.18–7.20 (m, 2H, ArH), 7.53–7.55 (m, 3H, ArH), 8.32–8.34 (m, 2H, ArH)
^{13}C NMR (75 MHz, $CDCl_3$): δ= 11.40, 11.84, 37.09, 37.13, 42.20, 43.33, 43.59, 45.94, 57.01, 108.42, 110.73, 112.07, 124.24, 127.79, 129.34, 129.73, 130.72, 136.68, 148.05, 157.82, 159.31, 161.40, 163.86, 164.78, 165.42
HR-MS (*m*/*z*): calcd. for $C_{28}H_{29}N_9O_4S$ $[L+H]^+$: 588.2132; found: 588.2136; Anal. calcd. (%) for $C_{28}H_{29}N_9O_4S$: C:57.23, H:4.97, N:21.45, found: C:56.99, H:4.82, N:21.25,

6b: 6-butyl-3,5,7-trimethyl-1-[[2-[2-oxo-2-(4-pyrimidin-2-ylpiperazin-1-yl)ethyl]sulfanyl-1,3,4-oxadiazol-5-yl]methoxy]pyrrolo[3,4-*d*]pyridazin-4-one
Whitish solid, Yield: 72,47%; m.p.: 198–200 °C
FT-IR (selected lines, γ_{max}, cm^{-1}): 2954, 2931, 2918 (C-H aliph.), 1640 (C=N)
^{1}H NMR (300 MHz, $CDCl_3$): δ= 0.95–1.00 (m, 3H, -CH_2-CH_2 CH_2-CH_3), 1.35-1.43 (m, 2H, -CH_2-CH_2-CH_2-CH_3), 1.62–1.67 (m, 2H, -CH_2-CH_2 CH_2-CH_3), 2.50 (s, 3H, 7-CH_3), 2.69 (s, 3H, 5-CH_3), 3.55 (s,3H, 3-CH_3), 3.65-3.69 (m, 2H, CH_2-piperazine), 3.74–3.77 (m, 2H, CH_2-piperazine), 3.87–3.89 (m, 2H,-CH_2-CH_2-CH_2-CH_3), 3,91–3,98 (m, 2H, CH_2-piperazine), 4.42 (s, 2H, S-CH_2-), 5.45 (s, 2H, O-CH_2), 6.57-6.60(t, 1H, ArH), 8.35–8.37 (m, 2H, ArH)
^{13}C NMR (75 MHz, $CDCl_3$): δ= 10.64, 11.19, 13.69, 20.04, 32.32, 37.02, 37.07, 42.18, 43.42, 43.68, 43.94, 45.92, 56.94, 108.15, 110.69, 111.85, 122.60, 129.13, 147.95, 157.77, 159.24, 161.07, 163.92, 164.81, 165.36
HR-MS (*m*/*z*): calcd. for $C_{26}H_{33}N_9O_4S$ $[L+H]^+$: 568.2460; found: 568.2449; Anal. calcd. (%) for $C_{26}H_{33}N_9O_4S$: C:55.01, H:5.86, N:22.21, found: C:55.27, H:5.91, N:22.15,

3.2. Cell Line

The study was conducted on a NHDF purchased from Lonza (Basel, Switzerland). These cells were a regular line of skin fibroblasts obtained from 54-years-old women.

Cells were grown at 37 °C in a humidified 5% CO_2/95% air atmosphere incubator and passaged twice a week.

3.3. Cell Culture Media

The cells were cultured in a Dulbecco Modified Eagle Medium (DMEM) without phenol red, which was supplemented with 10% fetal bovine serum (FBS), 2 mM L-glutamine, 1.25 μg/mL amphotericin B, and 100 μg/mL gentamicin. Prepared culture medium was stored at 4–8 °C until full exploit, but not longer than a month.

3.4. Tested Compounds

Investigated derivatives of pyrrolo[3,4-*d*]pyridazinone were received from the Department of Chemistry of Drugs at Wroclaw Medical University. The compounds were dissolved with DMSO to a final concentration of 1mM. All prepared stock solutions were left at –20 °C for up to 6 months. Stock solutions were dissolved in the culture medium to accomplish the final concentrations of 100 μM, 50 μM and 10 μM for each compound.

3.5. Experimental Design

Cells were seeded into 96-well culture plates at a density of 10,000 cells/well, except fast halo assay (FHA) assay, in which cells were seeded into 24-well culture plates at the density of 25,000 cells/well. The cells were then allowed to adhere overnight. After this time, the medium was removed, and tested compounds were added for a further 24 h of incubation in 5% CO_2, 95% humidity, 37 °C in MTT assay. Subsequently, the supernatant was removed, then the cells were washed with PBS, and the MTT assay was performed. For other assays, in the first step, the cells were incubated with the 100 μM H_2O_2 for 1h, then the supernatant was removed, and the cells were washed, and the cells were treated with tested compounds for the next 1 h.

The study included 2 control samples. A negative control, used as a reference, was a cell culture incubated in medium but without tested compounds. The positive control was used in the FHA and the level of oxygen free radicals and nitric oxide, which was a 1-h incubation of NHDF cells with 100 μM H_2O_2 without tested compounds.

Cell viability was assessed by metabolic activity in MTT assay, oxygen free radicals in DCF-DA assay and nitric oxide levels in Griess assay. FHA assay, which was used as well, allowed to estimate the number of DNA double-strand breaks (DSBs). The Cayman COX Inhibitor Screening Assay measured COX inhibition activity.

3.6. MTT Assay

The MTT assay was used to estimate the effects of investigated compounds on the metabolic activity of NHDF cells. The study started with the incubation of a proper cell line with tested compounds for 24 h at 37 °C. After that, the supernatant was replaced with 1 mg/mL MTT solution dissolved in MEM and plates were left for 2 h at 37 °C. Subsequently, the medium was removed, and for the next 30 min, the formazan crystals were dissolving in 100 μl of isopropanol. Absorbance was measured with Varioskan LUX microplate reader (Thermo Scientific, Waltham, MA, USA) at a wavelength of 570 nm.

3.7. Level of Reactive Oxygen Species

The DCF-DA assay was used to evaluate the level of ROS. The NHDF cells were cultured with 100 μM H_2O_2 to induce exogenous stress. Then, the solution was removed, cells were washed, and compounds were added for 1 h, and afterward, the medium was removed. The cells were washed with PBS, and 25 μM of DCF-DA solution dissolved in MEM without serum and phenol red was added. At this point, cultures were incubated for 1 h at 37 °C. The level of ROS was determined by fluorescence excitation at 485 nm and emission at 535 nm using a Varioskan LUX microplate reader (Thermo Scientific, Waltham, MA, USA).

3.8. Griess Assay

The Griess assay allows the establishment of nitric oxide production in the NHDF cell line. The Greiss reagent is a 1:1 mixture of 1% sulfanilamide in 5% phosphoric acid and 0.1% N-(1-Naphthyl)ethylenediamine dihydrochloride had to be prepared promptly before use.

After treatment with 100 μM H_2O_2, cell cultures were incubated with tested compounds for 1 h, and after that, 50 μl of the supernatant solution was moved into a new plate, while 50 μl of a Griess

reagent was added and then left for the next 20 min at RT, in the darkness. Absorbance was measured at 548 nm with a Varioskan LUX microplate reader (Thermo Scientific, Waltham, MA, USA).

3.9. Fast Halo Assay

DSBs (DBSBs) in DNA were evaluated via the FHA. After incubating for 24 h with tested compounds (due to procedures previously described), cells were separated from the plate surface using TrypLE solution for 3 min. In the next step, cells were moved into the tube to inactivate the TrypLE solution, an equivalent quantity of medium was added. After cell centrifugation at 1000× *g* for 5 min and removing the supernatant, the cell pellet was washed using PBS and again centrifuged as previously. Afterward, the supernatant was removed, and the cells were suspended in PBS within a density of 1000 cells per 1 µl. In the next step, the tubes filled with cell suspension was placed in a water bath, and 120 ul of 1.25% low melting agarose in PBS was added. The obtained mixture was promptly compressed between a coverslip and an agarose-coated slide (high melting point) for 10 min. After that time, when gel formation on the cooling block was observed, coverslips were removed, while slides were put in the lysis buffer and left for 24h. The slides were moved afterward into an alkaline solution (pH = 13) for 30 min and, after that time, put twice in neutralizing buffer to wash. The slides were colored by 5 µM DAPI within 20 min and promptly evaluated using a fluorescence microscope. Having taken the photos, the cell nucleus diameter to halo diameter ratio was studied as a degree of DNA damage.

3.10. Fluorescence Spectroscopic Studies

Spectroscopic fluorescence studies were performed using a Cary Eclipse 500 spectrophotometer (Agilent, Santa Clara, CA, USA). A concentration of BSA was 5.0×10^{-6} mol·dm^{-3}. A solution of BSA was titrated by successive additions 1.0×10^{-3} mol·dm^{-3} solution of studied compounds to give a final concentration 0.2×10^{-6}–2.0×10^{-6} mol·dm^{-3}. Experiments were carried out at three temperatures: 294, 301, and 308 K in pH = 7.4. Quenching spectra were recorded at excitation and an emission wavelength of 280 nm and 300–500 nm. The molar ratio compound/BSA was 0.1–2.0 with 0.2 steps. Binding site identification studies were indicated in the presence of the two site markers, phenylbutazone (PHB) and ibuprofen (IBP), as sites I and II markers, respectively. Concentrations of BSA and site markers were set at 1.0×10^{-6} and 3.0×10^{-6} mol dm^{-3}, respectively.

3.11. Molecular Docking

The ground-state structures were calculated using density functional theory (DFT) with Becke's three-parameter hybrid exchange function with the Lee-Yang–Parr gradient corrected correlation (B3LYP) [51–53] functional in combination with 6–311+G (d,p) basis set. Calculations were carried out using the Gaussian 2016 A.03 software package [54]. From the Protein Data Bank (http://www.rcsb.org), the following crystal structure was selected for docking studies: 4O1Z, 4M11, 3V03. The ligand and receptor files were prepared using AutoDock 4.2.6 software and AutoDock Tools 1.5.6. All the ligands and water molecules were removed, and then polar hydrogen atoms and Kollman charges were added to the protein structure. To prepare the ligand molecules, partial charges were calculated, nonpolar hydrogens were merged, and rotatable bonds were assigned. The interactions with COX-1, COX-2 and BSA were performed using AutoDock Script downloaded from The Scripps Research Institute (TSRI). The centers of grid boxes for COX-1 and COX-2 were set according to the Meloxicam binding site in the crystal structure 4O1Z, 4M11. The centers of grid boxes for BSA were set according to the binding site I phenylbutazone (PDB ID: 2BXC) and site II ibuprofen (PDB ID: 2BXG) on HSA [46]. The Lamarckian genetic algorithm was selected for the conformational search. The running times of the genetic algorithm and the evaluation times were set to 250 and 2.5million, respectively. After the molecular docking, the ligand-receptor complexes were further analyzed using Discovery Studio software (http://accelrys.com/).

3.12. Circular Dichroism

CD spectra were measured on Jasco J-1500 magnetic circular dichroism spectrometer. Spectra were collected in the range of 205–250 nm at a scan rate speed of 50 nm/min with 1 s response time and 10 mm path length. All spectra were measured once, each measurement with triple accumulation, and they were baseline corrected. All measurements for BSA solutions were made at RT under simulated physiological conditions in pH 7.4 in the absence and presence of analyzed compounds. Phosphate buffer was the solvent. Concentrations of BSA and analyzed compounds were: 1×10^{-6} mol/dm^3 for BSA and 1×10^{-3} mol/dm^3 for 5b, 6b, 5a, and 6a. Experiments were performed for BSA to each analyzed compound in molar ratios from 1:0 to 1:10.

3.13. Statistical Analysis

All results are presented as mean ± SEM (standard error of the mean) relative to the control (E/E_0), where E is the culture with the tested substance, and E_0 is the negative control (without H_2O_2 and tested compounds) or positive control (with H_2O_2 but without tested compounds). Statistical significance was calculated compared to the positive control for DCF-DA, Griess, and FHA assays or negative control for MTT assay.

The data have a normal distribution, so the ANOVA was used (with Tukey post-hoc tests). The significance level was set at $p < 0.05$. The relationship between DNA DSBs and free radical levels was shown by calculating Pearson correlation coefficients.

4. Conclusions

According to performed experiments, new derivatives of pyrrolo[3,4-*d*]pyridazinone exert promising anti-inflammatory and anti-oxidant activity. On the basis of our previous work [20] and inspired by Dogruer's theory [29,30], we have decided to introduce the elongated, flexible 2-oxoethyl linker between 1,3,4-oxadiazole-2-thione ring and arylpiperazine moiety. The design of new compounds is therefore based on the double pharmacophore approach. We have combined in the structure of final derivatives the 1,3,4-oxadiazole moiety, which is one of the most important in medicinal chemistry and arylpiperazine pharmacophore, which can be distinguished in many potent anti-inflammatory agents [17,18,20,22,27,28,34,55]. Biological evaluation and molecular docking study clearly indicate that performed structural modification resulted in the good affinity of some of the new compounds to COX-2 isoenzyme and lack of activity towards COX-1. However, the inhibition activity is lower than that of Meloxicam, investigated structures take a position in the active site of COX-2 very similar to that reference drug. Probably, further structural optimization and changes in the type of arylpiperazine pharmacophore may result in enhanced COX-2 inhibitory activity. Nevertheless, what is worth to emphasize, the results of the COX Colorimetric Inhibitor Screening Assay stay in very good correlation with molecular docking. Furthermore, the compound which showed the best activity towards COX-2 in biological evaluation—**6a** is characterized by the lowest values of K_i when considering molecular docking study. As was mentioned before, there are slight structural differences between both cyclooxygenase isoforms, and the binding pocket of COX-2 is bigger than that of COX-1. It could explain the fact that the introduction of elongated 2-oxoethyl linker results in COX-2 selectivity of new derivatives. The fact that arylpiperazine pharmacophore is connected with 1,3,4-oxadiazole ring via sulfur, not nitrogen atom as formerly [20], could also impact the activity and cyclooxygenase selectivity of new compounds.

Promising anti-oxidant activity of new derivatives may suggest an additional mechanism of action involved in their anti-inflammatory activity. Needless to say, inflammation is firmly correlated with oxidative stress, and both processes can potentiate one another. In inflammatory cells, an excessive amount of ROS can be stated. This, in turn, promotes oxidative stress, which can cause oxidative damage, and in consequence, potentiate inflammation [56–58]. Therefore, the ability of scavenging

free radicals and DNA protection properties can be very useful in the context of therapy of different inflammatory disorders.

Finally, both molecular docking study and spectroscopic investigations indicate that title compounds bind to BSA in a moderate manner and form complexes in a one-to-one ratio. According to performed experiments, investigated derivatives interact with BSA by means of complex formation. The favorable binding site of BSA is the hydrophobic cavity in site II (subdomain IIIA). According to CD results, the compounds **5a**,**b** caused greater changes of α-helix(%), which may suggest stronger binding of derivatives bearing phenylpiperazine pharmacophore. Such a result may indicate the potential long half-life on title compounds in vivo.

Summarizing, novel derivatives of pyrrolo[3,4-*d*]pyridazinone exert satisfactory anti-inflammatory and anti-oxidant activity. All compounds present selective inhibition activity towards COX-2 isoenzyme in both biological and molecular docking studies. Moreover, investigated structures possess the ability to scavenge reactive oxygen and nitrogen species. Such properties make the novel pyrrolo[3,4-*d*]pyridazinone derivatives the promising agents in the context of the development of new potent and safe analgesic and anti-inflammatory drug-candidates.

Supplementary Materials: The following are available online at http://www.mdpi.com/1422-0067/21/24/9623/s1.

Author Contributions: Ł.S.: concept of the study, chemistry: design and synthesis, formal analysis, writing—original draft preparation; writing—review and editing.; visualization; supervision; E.K.: spectroscopic and molecular docking study, formal analysis, writing—original draft preparation; writing—review and editing; A.Z.: synthesis, biological in vitro evaluation, writing—original draft preparation; P.Z.: synthesis, biological in vitro evaluation, writing—original draft preparation; K.P. (Katarzyna Potyrak) synthesis, in vitro biological evaluation, writing—original draft preparation; K.P. (Krzysztof Peregrym) synthesis, biological in vitro evaluation, writing—original draft preparation; B.W.: biological in vitro investigations, formal analysis, writing—original draft preparation; writing—review and editing; visualization A.M.: spectroscopic investigations, formal analysis, writing—original draft preparation; writing—review and editing; P.Ś. concept of the study, writing—original draft preparation; writing—review and editing; supervision. All authors have read and agreed to the published version of the manuscript.

Funding: This research was financially supported by the Ministry of Health subvention according to the number of STM.D070.20.021 from the IT Simple system of Wroclaw Medical University. This study was financially supported by a Wroclaw Medical University grant STSUB.D070.19.011

Acknowledgments: Calculations have been carried out in Wroclaw Center for Networking and Supercomputing (http://www.wcss.wroc.pl).

Conflicts of Interest: The authors declare no conflict of interest.

References

1. Marnett, L.J. Cyclooxygenase mechanisms. *Curr. Opin. Chem. Biol.* **2000**, *4*, 545–552. [CrossRef]
2. Blobaum, A.L.; Marnett, L.J.; Hancock, A.B. PerspectiVe Structural and Functional Basis of Cyclooxygenase Inhibition. *J. Med. Chem.* **2007**, *50*, 1425–1441. [CrossRef] [PubMed]
3. Vane, J.R.; Botting, R.M. Mechanism of action of nonsteroidal anti-inflammatory drugs. *Am. J. Med.* **1998**, *104*, 2S–8S.
4. Smith, W.L.; Urade, Y.; Jakobsson, J. Enzymes of the Cyclooxygenase Pathways of Prostanoid Biosynthesis. *Chem. Rev* **2011**, *111*, 5821–5865. [CrossRef]
5. Cashman, J.N. The Mechanisms of Action of NSAIDs in Analgesia. *Drugs* **1996**, *52*, 13–23. [CrossRef]
6. Leuti, A.; Fazio, D.; Fava, M.; Piccoli, A.; Oddi, S.; Maccarrone, M. Bioactive lipids, inflammation and chronic diseases. *Adv. Drug Deliv. Rev.* **2020**, *159*, 133–169. [CrossRef]
7. Sostres, C.; Gargallo, C.J.; Arroyo, M.T.; Lanas, A. Adverse effects of non-steroidal anti-inflammatory drugs (NSAIDs, aspirin and coxibs) on upper gastrointestinal tract. *Best Pract. Res. Clin. Gastroenterol.* **2010**, *24*, 121–132. [CrossRef]
8. Bidaut-Russell, M.; Gabriel, S.E. Adverse gastrointestinal effects of NSAIDs: Consequences and costs. *Best Pract. Res. Clin. Gastroenterol.* **2001**, *15*, 739–753. [CrossRef]
9. Laine, L. Gastrointestinal effects of NSAIDs and coxibs. *J. Pain Symptom Manag.* **2003**, *25*, 32–40. [CrossRef]

10. Wallace, J.L.; Devchand, P.R. Emerging roles for cyclooxygenase-2 in gastrointestinal mucosal defense. *Br. J. Pharmacol.* **2005**, *145*, 275–282. [CrossRef]
11. Chandrasekharan, N.V.; Dai, H.; Lamar, K.; Roos, T.; Evanson, N.K.; Tomsik, J.; Elton, T.S.; Simmons, D.L. COX-3, a cyclooxygenase-1 variant inhibited by acetaminophen and other analgesic/antipyretic drugs: Cloning, structure, and expression PCOX-1 proteins). COX-3 and one of the PCOX-1 proteins (PCOX-1a) are made from the COX-1 gene but retain intron 1 in their mRNAs. PCOX-1 proteins additionally contain an in-frame deletion of exons 5-8 of the COX-1 mRNA. COX-3 and PCOX mRNAs. *Proc. Natl. Acad. Sci. USA* **2002**, *99*, 13926–13931.
12. Soll, A.H.; McCarthy, D. NSAID-related gastrointestinal complications. *Clin. Cornerstone* **1999**, *1*, 42–56. [CrossRef]
13. Wallace, J.L. NSAID gastropathy and enteropathy: Distinct pathogenesis likely necessitates distinct prevention strategies. *Br. J. Pharmacol.* **2012**, *165*, 67–74. [CrossRef] [PubMed]
14. García Rodríguez, L.A.; Barreales Tolosa, L. Risk of Upper Gastrointestinal Complications Among Users of Traditional NSAIDs and COXIBs in the General Population. *Gastroenterology* **2007**, *132*, 498–506. [CrossRef] [PubMed]
15. Takeuchi, K. Pathogenesis of NSAID-induced gastric damage: Importance of cyclooxygenase inhibition and gastric hypermotility. *World J. Gastroenterol.* **2012**, *18*, 2147–2160. [CrossRef]
16. Esposito, G.; Pagano, E.; Ii, F.; Kaji, I.I.; Scarpignato, C.; Colucci, R.; Pellegrini, C.; Fornai, M.; Tirotta, E.; Antonioli, L.; et al. Pathophysiology of NSAID-Associated Intestinal Lesions in the Rat: Luminal Bacteria and Mucosal Inflammation as Targets for Prevention. *Front. Pharmacol.* **2018**, *9*, 1340.
17. Koksal, M.; Ozkan-Dagliyan, I.; Ozyazici, T.; Kadioglu, B.; Sipahi, H.; Bozkurt, A.; Bilge, S.S. Some Novel Mannich Bases of 5-(3,4-Dichlorophenyl)-1,3,4-oxadiazole-2(3H)-one and Their Anti-Inflammatory Activity. *Arch. Pharm.* **2017**, *350*. [CrossRef]
18. El-Sayed, N.A.; Nour, M.S.; Salem, M.A.; Arafa, R.K. New oxadiazoles with selective-COX-2 and EGFR dual inhibitory activity: Design, synthesis, cytotoxicity evaluation and in silico studies. *Eur. J. Med. Chem.* **2019**, *183*, 111693. [CrossRef]
19. Banerjee, A.G.; Das, N.; Shengule, S.A.; Sharma, P.A.; Srivastava, R.S.; Shrivastava, S.K. Design, synthesis, evaluation and molecular modelling studies of some novel 5,6-diphenyl-1,2,4-triazin-3(2H)-ones bearing five-member heterocyclic moieties as potential COX-2 inhibitors: A hybrid pharmacophore approach. *Bioorg. Chem.* **2016**, *69*, 102–120. [CrossRef]
20. Szczukowski, Ł.; Redzicka, A.; Wiatrak, B.; Krzyżak, E.; Marciniak, A.; Gębczak, K.; Gębarowski, T.; Świątek, P. Design, synthesis, biological evaluation and in silico studies of novel pyrrolo[3,4-d]pyridazinone derivatives with promising anti-inflammatory and antioxidant activity. *Bioorg. Chem.* **2020**, *102*, 104035. [CrossRef]
21. Wakulik, K.; Wiatrak, B.; Szczukowski, Ł.; Bodetko, D.; Szandruk-Bender, M.; Dobosz, A.; Piotr', P.; Atek, P.; Asiorowski, K.G. Effect of Novel Pyrrolo[3,4-d]pyridazinone Derivatives on Lipopolysaccharide-Induced Neuroinflammation. *Int. J. Mol. Sci. Artic.* **2020**, *21*, 2575. [CrossRef]
22. Malinka, W.; Redzicka, A.; Jastrzbska Więsek, M.; Filipek, B.; Dybała, M.; Karczmarzyk, Z.; Urbańczyk-Lipkowska, Z.; Kalicki, P. Derivatives of pyrrolo[3,4-d]pyridazinone, a new class of analgesic agents. *Eur. J. Med. Chem.* **2011**, *46*, 4992–4999. [CrossRef]
23. Mogilski, S.; Kubacka, M.; Redzicka, A.; Kazek, G.; Dudek, M.; Malinka, W.; Filipek, B. Antinociceptive, anti-inflammatory and smooth muscle relaxant activities of the pyrrolo[3,4-d]pyridazinone derivatives: Possible mechanisms of action. *Pharmacol. Biochem. Behav.* **2015**, *133*, 99–110. [CrossRef]
24. Kohara, Y.; Imamiya, E.; Kubo, K.; Wada, T.; Inada, Y.; Naka, T. A new class of angiotensin II receptor antagonists with a novel acidic bioisostere. *Bioorganic Med. Chem. Lett.* **1995**, *5*, 1903–1908. [CrossRef]
25. Kohara, Y.; Kubo, K.; Imamiya, E.; Wada, T.; Inada, Y.; Naka, T. Synthesis and Angiotensin II Receptor Antagonistic Activities of Benzimidazole Derivatives Bearing Acidic Heterocycles as Novel Tetrazole Bioisosteres 1. *J. Med. Chem.* **1996**, *39*, 5228–5235. [CrossRef]
26. Tagad, H.D.; Hamada, Y.; Nguyen, J.T.; Hamada, T.; Abdel-Rahman, H.; Yamani, A.; Nagamine, A.; Ikari, H.; Igawa, N.; Hidaka, K.; et al. Design of pentapeptidic BACE1 inhibitors with carboxylic acid bioisosteres at P1′ and P4 positions. *Bioorganic Med. Chem.* **2010**, *18*, 3175–3186. [CrossRef]

27. Palkar, M.B.; Singhai, A.S.; Ronad, P.M.; Vishwanathswamy, A.H.M.; Boreddy, T.S.; Veerapur, V.P.; Shaikh, M.S.; Rane, R.A.; Karpoormath, R. Synthesis, pharmacological screening and in silico studies of new class of Diclofenac analogues as a promising anti-inflammatory agents. *Bioorganic Med. Chem.* **2014**, *22*, 2855–2866. [CrossRef]
28. Manjunatha, K.; Poojary, B.; Lobo, P.L.; Fernandes, J.; Kumari, N.S. Synthesis and biological evaluation of some 1,3,4-oxadiazole derivatives. *Eur. J. Med. Chem.* **2010**, *45*, 5225–5233. [CrossRef] [PubMed]
29. Dogruer, D.S.; Sahin, M.F.; Ünlü, S.; Ito, S. Studies on some 3(2H)-pyridazinone derivatives with antinociceptive activity. *Arch. Pharm.* **2000**, *333*, 79–86. [CrossRef]
30. Dogruer, D.S.; Kupeli, E.; Yesilada, E.; Sahin, M.F. Synthesis of New 2-[1(2H)-Phthalazinon-2-yl]acetamide and 3-[1(2H)-Phthalazinon-2-yl]propanamide Derivatives as Antinociceptive and Anti-inflammatory Agents. *Arch. Pharm.* **2004**, *337*, 303–310. [CrossRef] [PubMed]
31. Dekhane, D.V.; Pawar, S.S.; Gupta, S.; Shingare, M.S.; Patil, C.R.; Thore, S.N. Synthesis and anti-inflammatory activity of some new 4,5-dihydro-1,5- diaryl-1H-pyrazole-3-substituted-heteroazole derivatives. *Bioorg. Med. Chem. Lett.* **2011**, *21*, 6527–6532. [CrossRef]
32. Bansal, S.; Bala, M.; Suthar, S.K.; Choudhary, S.; Bhattacharya, S.; Bhardwaj, V.; Singla, S.; Joseph, A. Design and synthesis of novel 2-phenyl-5-(1,3-diphenyl-1H-pyrazol-4-yl)-1, 3,4-oxadiazoles as selective COX-2 inhibitors with potent anti-inflammatory activity. *Eur. J. Med. Chem.* **2014**, *80*, 167–174. [CrossRef] [PubMed]
33. Gupta, S.; Pandey, D.; Mandalapu, D.; Bala, V.; Sharma, V.; Shukla, M.; Yadav, S.K.; Singh, N.; Jaiswal, S.; Maikhuri, J.P.; et al. Design, synthesis and biological profiling of aryl piperazine based scaffolds for the management of androgen sensitive prostatic disorders. *Medchemcomm* **2016**, *7*, 2111–2121. [CrossRef]
34. Świątek, P.; Strzelecka, M.; Urniaz, R.; Gębczak, K.; Gębarowski, T.; Gąsiorowski, K.; Malinka, W. Synthesis, COX-1/2 inhibition activities and molecular docking study of isothiazolopyridine derivatives. *Bioorg. Med. Chem.* **2017**, *25*, 316–326. [CrossRef] [PubMed]
35. Chen, G.Z.; Huang, X.Z.; Xu, J.H.; Zneng, Z.Z.; Wang, Z.B. *The Methods of Fluorescence Analysis, 2ed ed.*; Science Press: Beijing, China, 1990.
36. Wani, T.A.; Bakheit, A.H.; Zargar, S.; Bhat, M.A.; Al-Majed, A.A. Molecular docking and experimental investigation of new indole derivative cyclooxygenase inhibitor to probe its binding mechanism with bovine serum albumin. *Bioorg. Chem.* **2019**, *89*, 103010. [CrossRef] [PubMed]
37. Lakowicz, J.R. (Ed.) *Principles of Fluorescence Spectroscopy*, 3rd ed.; Springer US: Boston, MA, USA, 2006; ISBN 978-0-387-31278-1.
38. Ware, W.R. Oxygen quenching of fluorescence in solution: An experimental study of the diffusion process. *J. Phys. Chem.* **1962**, *66*, 455–458. [CrossRef]
39. Mohammadnia, F.; Fatemi, M.H.; Taghizadeh, S.M. Study on the interaction of anti-inflammatory drugs with human serum albumin using molecular docking, quantitative structure–activity relationship, and fluorescence spectroscopy. *Luminescence* **2020**, *35*, 266–273. [CrossRef]
40. Dufour, C.; Dangles, O. Flavonoid-serum albumin complexation: Determination of binding constants and binding sites by fluorescence spectroscopy. *Biochim. Biophys. Acta Gen. Subj.* **2005**, *1721*, 164–173. [CrossRef]
41. Abdelhameed, A.S.; Bakheit, A.H.; Mohamed, M.S.; Eldehna, W.M.; Abdel-Aziz, H.A.; Attia, M.I. Synthesis and biophysical insights into the binding of a potent anti-proliferative non-symmetric bis-isatin derivative with bovine serum albumin: Spectroscopic and molecular docking approaches. *Appl. Sci.* **2017**, *7*, 617. [CrossRef]
42. Suryawanshi, V.D.; Walekar, L.S.; Gore, A.H.; Anbhule, P.V.; Kolekar, G.B. Spectroscopic analysis on the binding interaction of biologically active pyrimidine derivative with bovine serum albumin. *J. Pharm. Anal.* **2016**, *6*, 56–63. [CrossRef]
43. Wani, T.A.; Bakheit, A.H.; Al-Majed, A.R.A.; Bhat, M.A.; Zargar, S. Study of the interactions of bovine serum albumin with the new anti-inflammatory agent 4-(1,3-dsioxo-1,3-dihydro-2H-isoindol-2-yl)-N-[(4-ethoxy-phenyl) methylidene]benzohydrazide using a multi-spectroscopic approach and molecular docking. *Molecules* **2017**, *22*, 1258. [CrossRef]
44. Krzyżak, E.; Szkatuła, D.; Wiatrak, B.; Gębarowski, T.; Marciniak, A. Synthesis, Cyclooxygenases Inhibition Activities and Interactions with BSA of N-substituted 1H-pyrrolo[3,4-c]pyridine-1,3(2H)-diones Derivatives. *Molecules* **2020**, *25*, 2934. [CrossRef]
45. Sudlow, G.; Birkett, D.J.; Wade, D.N. The Characterization of Two Specific Drug Binding Sites on Human Serum Albumin. *Mol. Pharmacol.* **1975**, *11*, 824–832. [PubMed]

46. Ghuman, J.; Zunszain, P.A.; Petitpas, I.; Bhattacharya, A.A.; Otagiri, M.; Curry, S. Structural basis of the drug-binding specificity of human serum albumin. *J. Mol. Biol.* **2005**, *353*, 38–52. [CrossRef] [PubMed]
47. Klotz, I.M.; Urquhart, J.M. The Binding of Organic Ions by Proteins. Effect of Temperature. *J. Am. Chem. Soc.* **1949**, *71*, 847–851. [CrossRef]
48. Kelly, S.; Price, N. The Use of Circular Dichroism in the Investigation of Protein Structure and Function. *Curr. Protein Pept. Sci.* **2005**, *1*, 349–384. [CrossRef] [PubMed]
49. Kelly, S.M.; Jess, T.J.; Price, N.C. How to study proteins by circular dichroism. *Biochim. Biophys. Acta Proteins Proteom.* **2005**, *1751*, 119–139. [CrossRef]
50. Lu, Z.X.; Cui, T.; Shi, Q.L. *Applications of Circular Dichroism (CD) and Optical Rotatory Dispersion (ORD) in Molecular Biology*, 1st ed.; Science Press: Beijing, China, 1987.
51. Becke, A.D. Density-functional thermochemistry. III. The role of exact exchange. *J. Chem. Phys.* **1993**, *98*, 5648. [CrossRef]
52. Lee, C.; Yang, W.; Parr, R.G. Development of the Colle-Salvetti correlation-energy formula into a functional of the electron density. *Phys. Rev. B* **1988**, *37*, 785–789. [CrossRef]
53. Perdew, J.P.; Wang, Y. Accurate and simple analytic representation of the electron-gas correlation energy. *Phys. Rev. B* **1992**, *45*, 13244–13249. [CrossRef]
54. Frisch, M.J.; Trucks, G.W.; Schlegel, H.B.; Scuseria, G.E.; Robb, M.A.; Cheeseman, J.R.; Scalmani, G.; Barone, V.; Petersson, G.A.; Nakatsuji, H.; et al. *Gaussian~16 {R}evision {A}.03 2016*; Gaussian Inc.: Wallingford, CT, USA, 2016.
55. Redzicka, A.; Szczukowski, Ł.; Kochel, A.; Wiatrak, B.; Gębczak, K.; Czyżnikowska, Ż. COX-1/COX-2 inhibition activities and molecular docking study of newly designed and synthesized pyrrolo[3,4-c]pyrrole Mannich bases. *Bioorg. Med. Chem.* **2019**, *27*, 3918–3928. [CrossRef]
56. McGarry, T.; Biniecka, M.; Veale, D.J.; Fearon, U. Hypoxia, oxidative stress and inflammation. *Free Radic. Biol. Med.* **2018**, *125*, 15–24. [CrossRef] [PubMed]
57. Gao, Z.; Zhang, H.; Liu, J.; Lau, C.W.; Liu, P.; Chen, Z.Y.; Lee, H.K.; Tipoe, G.L.; Ho, H.M.; Yao, X.; et al. Cyclooxygenase-2-dependent oxidative stress mediates palmitate-induced impairment of endothelium-dependent relaxations in mouse arteries. *Biochem. Pharmacol.* **2015**, *91*, 474–482. [CrossRef] [PubMed]
58. Burdon, C.; Mann, C.; Cindrova-Davies, T.; Ferguson-Smith, A.C.; Burton, G.J. Oxidative Stress and the Induction of Cyclooxygenase Enzymes and Apoptosis in the Murine Placenta. *Placenta* **2007**, *28*, 724–733. [CrossRef] [PubMed]

International Journal of
Molecular Sciences

IMPACT FACTOR 5.923

Indexed in: PubMed

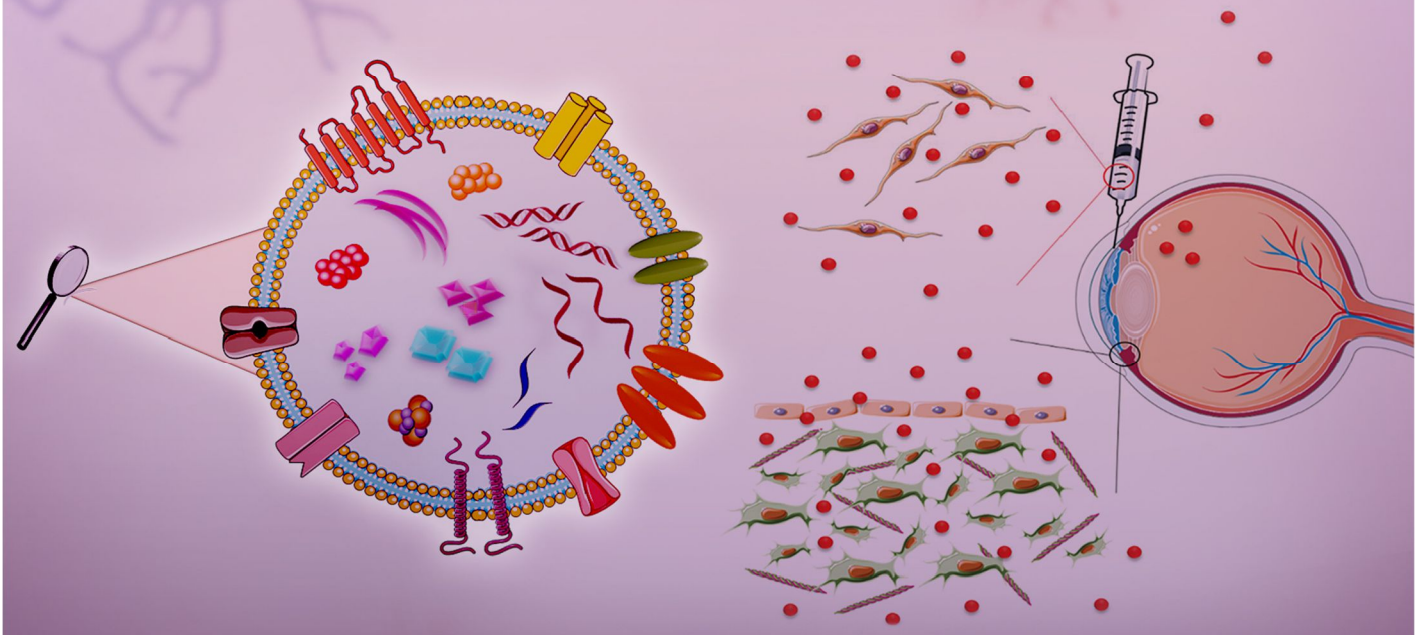

Stem Cells and Their Derivates in the Treatment of Glaucoma

Volume 22 · Issue 20 | October (II) 2021

MDPI

mdpi.com/journal/ijms
ISSN 1422-0067

International Journal of
Molecular Sciences

MDPI

Article

New *N*-Substituted-1,2,4-triazole Derivatives of Pyrrolo[3,4-*d*]pyridazinone with Significant Anti-Inflammatory Activity—Design, Synthesis and Complementary In Vitro, Computational and Spectroscopic Studies

Łukasz Szczukowski [1,*], Edward Krzyżak [2], Benita Wiatrak [3], Paulina Jawień [3], Aleksandra Marciniak [2], Aleksandra Kotynia [2] and Piotr Świątek [1,*]

[1] Department of Medicinal Chemistry, Wroclaw Medical University, Borowska 211, 50-556 Wroclaw, Poland
[2] Department of Inorganic Chemistry, Wroclaw Medical University, Borowska 211a, 50-556 Wroclaw, Poland; edward.krzyzak@umed.wroc.pl (E.K.); aleksandra.marciniak@umed.wroc.pl (A.M.); aleksandra.kotynia@umed.wroc.pl (A.K.)
[3] Department of Pharmacology, Wroclaw Medical University, Mikulicza-Radeckiego 2, 50-345 Wroclaw, Poland; benita.wiatrak@umed.wroc.pl (B.W.); paulina.jawien@umed.wroc.pl (P.J.)
* Correspondence: lukasz.szczukowski@umed.wroc.pl (Ł.S.); piotr.swiatek@umed.wroc.pl (P.Ś.); Tel.: +48-71-784-0391 (P.Ś.)

Citation: Szczukowski, Ł.; Krzyżak, E.; Wiatrak, B.; Jawień, P.; Marciniak, A.; Kotynia, A.; Świątek, P. New *N*-Substituted-1,2,4-Triazole Derivatives of Pyrrolo[3,4-*d*] pyridazinone with Significant Anti-Inflammatory Activity—Design, Synthesis and Complementary In Vitro, Computational and Spectroscopic Studies. *Int. J. Mol. Sci.* **2021**, *22*, 11235. https://doi.org/10.3390/ijms222011235

Academic Editors: Andrzej Kutner, Geoffrey Brown and Enikö Kallay

Received: 23 September 2021
Accepted: 14 October 2021
Published: 18 October 2021

Abstract: Regarding that the chronic use of commonly available non-steroidal and anti-inflammatory drugs (NSAIDs) is often restricted by their adverse effects, there is still a current need to search for and develop new, safe and effective anti-inflammatory agents. As a continuation of our previous work, we designed and synthesized a series of 18 novel *N*-substituted-1,2,4-triazole-based derivatives of pyrrolo[3,4-*d*]pyridazinone **4a-c-9a-c**. The target compounds were afforded via a convenient way of synthesis, with good yields. The executed cell viability assay revealed that molecules **4a-7a**, **9a**, **4b-7b**, **4c-7c** do not exert a cytotoxic effect and were qualified for further investigations. According to the performed in vitro test, compounds **4a-7a**, **9a**, **4b**, **7b**, **4c** show significant cyclooxygenase-2 (COX-2) inhibitory activity and a promising COX-2/COX-1 selectivity ratio. These findings are supported by a molecular docking study which demonstrates that new derivatives take position in the active site of COX-2 very similar to *Meloxicam*. Moreover, in the carried out in vitro evaluation within cells, the title molecules increase the viability of cells pre-incubated with the pro-inflammatory lipopolysaccharide and reduce the level of reactive oxygen and nitrogen species (RONS) in induced oxidative stress. The spectroscopic and molecular modeling study discloses that new compounds bind favorably to site II(m) of bovine serum albumin. Finally, we have also performed some in silico pharmacokinetic and drug-likeness predictions. Taking all of the results into consideration, the molecules belonging to series **a** (**4a-7a**, **9a**) show the most promising biological profile.

Keywords: cyclooxygenase; 1,2,4-triazole; pyridazinone; SAR; molecular docking; anti-inflammatory activity; antioxidant activity; ADME

1. Introduction

The inflammatory response that leads to homeostasis restoration is provoked by various exogenous and endogenous harmful stimuli and inducers, such as injury, tissue malfunctioning or infection. Its course, purpose and aftermath depend on the trigger. Characteristic symptoms that occur in inflamed areas are edema, reddening, hypersensitivity and often pain, which plays an important warning and protective role and promotes the organism's reflex and behavioral response to minimize the effects of tissue damage. The inflammation is a complicated process coordinated by a great variety of mediators whose expression and complex network of relationships are still not satisfactorily understood. Numerous proinflammatory mediators of different origins could be divided into the following

groups: vasoactive amines, vasoactive peptides, fragments of complement components and lipid mediators, such as eicosanoids, cytokines, chemokines and proteolytic enzymes. A lot of those aforementioned agents, besides affecting the target cells and tissues, could also induce the production of other elements. The best possible understanding and explanation of the mechanisms responsible for inflammatory mediators' expression, action and mutual dependence is essential in the effective management of different inflammatory diseases. Suitable pharmacological treatment and natural tissue healing processes cause acute pain and inflammation to disappear after some days. Nevertheless, the lack of or ineffective pharmacotherapy may trigger dangerous pathophysiological changes, which lead to the evolution of chronic inflammation and pain syndrome [1–5].

Most drugs commonly used in the treatment of pain and inflammatory disorders act as, mainly non-selective, inhibitors of both isoforms of cyclooxygenase (COX) and belong to a varied and spacious group of medicines named as non-steroidal and anti-inflammatory drugs (NSAIDs) [6–10]. The analgesic, antipyretic and anti-inflammatory effects associated with the administration of these medicaments are related to the reduction of COX-dependent prostaglandins (PGs) production, which belong, alongside with leukotrienes and lipoxins, to the above-mentioned group of eicosanoids [4–10]. Because PGs, except for the mediation of inflammation, play a crucial role in homeostasis maintenance and exert a protective effect, e.g., in the gastrointestinal and cardiovascular system, such decreased COX activity may also lead to dangerous side effects [6,7,11–15]. Usually, in patients receiving NSAIDs, adverse effects related to the gastroduodenal tract, such as heartburn, dyspepsia, stomach ache or even ulceration, may occur [11–14]. Initially, it was believed that a constitutive isoform named COX-1 is engaged in various physiological processes, while the development of pain and inflammation is under control of the mediators produced by the inducible form—COX-2 [6–10,13,15]. However, the introduction of selective COX-2 inhibitors—COXIBs, which were supposed to spare gastric mucosa, have quickly disproved this theory. Although any significant harmful impact of COXIBs on the gastrointestinal tract has not been noticed, the therapy with those drugs has been shown to carry a serious risk of hazardous cardiovascular incidents, which can even lead to patient death. Consequently, some COXIBs have been withdrawn from the market, and among them, the case of *Rofecoxib* became the most shameful [11–17].

Therefore, there is still a current need to search for and develop new, safe and efficient analgesic and anti-inflammatory compounds, since severe adverse effects often restrict the long-term usage of already known and available NSAIDs [11–14]. New drug candidates with potential application in the treatment of various inflammatory disorders can be received either through the structural alteration of already known NSAIDs, such as *Diclofenac* [18], *Naproxen* [19], *Celecoxib* [20], *Ibuprofen* [21], or by developing fully novel classes of cyclooxygenase inhibitors. When considering the design of new anti-inflammatory agents, one of the most popular and effective synthetic approaches in contemporary medicinal chemistry relies on replacing the free carboxylic group with different bioisosteric five-membered heterocyclic rings, such as 1,3,4-oxadiazole [18–22], 1,3-thiazole [23–25], pyrazole [26,27] or 1,2,4-triazole [28–33]. According to the leading investigations, such a strategy can be successfully applied to modify widespread used NSAIDs and other promising compounds not introduced in the market yet. As a result, potent cyclooxygenase inhibitors with an improved affinity towards COX-2 isoform and reduced gastrotoxicity can be received [18,19,22,23,30,31].

In our former studies, we have reported the synthesis and comprehensive biological evaluation of new 1,3,4-oxadiazole-based derivatives of pyrrolo [3,4-*d*]pyridazinone designed as a new class of COX inhibitor. The investigated compounds exerted promising in vitro cyclooxygenase inhibitory activity and acted as specific or selective COX-2 inhibitors. It is worth emphasizing that each examined molecule showed a superior COX-2/COX-1 selectivity ratio than *Meloxicam*, which was used as a reference drug. These findings were supported by the results of molecular docking studies, which revealed that tested 1,3,4-oxadiazole derivatives of pyrrolo[3,4-*d*]pyridazinone take place in the

active site of cyclooxygenase very similar to that of *Meloxicam* [34,35]. Subsequently, the most potent molecules have been investigated in vivo. It has been demonstrated by the enzyme-linked immunosorbent assay (ELISA) tests that the measured concentrations of inflammatory mediators—prostaglandin E_2 (PGE_2) and myeloperoxidase (MPO) in mice serum—were decreased after the application of our derivatives. Moreover, the macro- and microscopic histopathological assessment of gastric mucosa proved that novel compounds caused negligible stomach lesions andno histopathological changes were observed. These results confirmed the safe gastric profile of investigated molecules [36].

Encouraged by those promising results, we have decided to modify the structure of the above-mentioned derivatives by replacing the 1,3,4-oxadiazole with 4-substituted-1,2,4-triazole pharmacophore to obtain even more effective compounds. The introduction of this five-membered ring was inspired by the leading research described in the most recent literature [28–33]. The 1,2,4-triazole is an important moiety present in numerous potent bioactive molecules with a wide range of therapeutic applications [28–32]. It also acts as a valuable building block used in the design and synthesis of promising analgesic and anti-inflammatory agents, especially those with a good affinity towards an inducible COX-2 isoform [28,30–32]. Needless to say, different five-membered heterocycles serve as the structural core of the previously mentioned selective COX-2 inhibitors—COXIBs [17,20,25]. Considering that the binding pocket of COX-2 isoenzyme is bigger than that of COX-1 [6–10], we expect that the presence of expanded 4-substituted-1,2,4-triazole residues will enhance the COX-2 selectivity of titled compounds.

In summing up, here we report herein the design, synthesis and complex in vitro and in silico investigations of a new series of 4-substituted-1,2,4-triazole-based derivatives of pyrrolo[3,4-*d*]pyridazinone. First of all, we have determined the cytotoxic effect of the new compounds. After excluding toxic derivatives from further studies, we have defined the potential affinity and binding mode of the novel structures to both isoforms of cyclooxygenase. The investigations were carried out using in vitro enzymatic assay and computational studies, as well. Afterwards, have we estimated the antioxidant activity of the title compounds. Finally, the interaction binding manner of novel 1,2,4-triazole-based derivatives of pyrrolo[3,4-*d*]pyridazinone with bovine serum albumin (BSA) has been established. All of the performed experiments focused on the most precise determination of the possible mechanism of action and pharmacokinetic properties of new molecules and their potential application in the treatment of inflammatory disorders.

2. Results

2.1. Chemistry

The aim of the present study was the design and synthesize a new series of *N*-substituted-1,2,4-triazole derivatives of pyrrolo[3,4-*d*]pyridazinone. Scheme 1 presents all of the performed chemical modifications and structures of novel molecules (each new compounds' structural formula is also presented in Table S1 in Supplementary Data). The thin layer chromatography (TLC) technique was used to monitor the progress of the reaction. The structure and purity of all of the new derivatives were established and confirmed based on the spectra analysis: ^{1}H and ^{13}C nuclear magnetic resonance (NMR), Fourier transform infrared (FT-IR), electrospray ionization mass spectrometry (ESI-MS). All of the analytical and spectroscopic properties of every newly obtained compound were in good agreement with their predicted structures. The Experimental Section and Supplementary Data provide detailed information concerning the analytical and spectroscopic data, reactants, solvents and reactions environment. The synthetic pathway and structure of the starting molecule 2-(6-butyl-3,5,7-trimethyl-4-oxo-pyrrolo[3,4-*d*]pyridazin-1-yl)oxyacetohydrazide 1 has already been published in our previous paper [34].

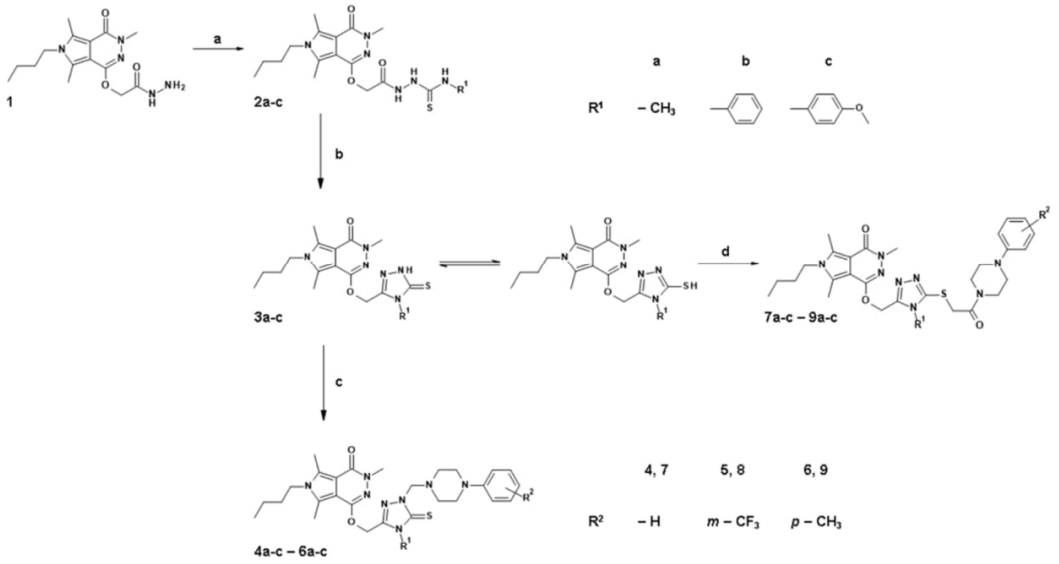

Scheme 1. Synthesis of the intermediates **2a-c-3a-c** and the title compounds **4a-c-9a-c**. Reagents and reaction conditions: (**a**) N substituted isothiocyanate, ethanol, reflux, 0.5–2 h; (**b**) I. 5% NaOH (aq), reflux, 2 h; II. Cooling, crushed ice, stirring, acidification with 7.5% HCl; (**c**) 37% HCHO, 4 aryl piperazine derivative, methanol, RT 5 h; (**d**) C_2H_5ONa, 1 (2-chloro-1-oxoethyl)-4-aryl piperazine derivative, ethanol, reflux, 5 h.

The first step of the current synthesis relied on forming adequate *N*-substituted-(aminothioxomethyl)hydrazides **2a-c**. The aforementioned hydrazide **1** was refluxed in ethanol in the presence of the appropriate *N*-substituted isothiocyanate for 30 to 120 min. The mixture was then cooled down, and the formed precipitate was filtered off, washed thoroughly with ethanol and purified by crystallization from this solvent. Compounds **2a-c** were obtained with a good to excellent yield (up to 94%). Their formation was confirmed by spectral analysis. When considering the ^{1}H NMR spectra of molecules **2a-c**, a characteristic peak of protons linked to *N*1, *N*2 and *N*3 nitrogens of thiosemicarbazide moiety were recorded as three singlets in the range of δ 7.89–10.18 ppm. The methylene group connecting the pyrrolo[3,4-*d*]pyridazinone core and hydrazine residue appears as two proton singlets within δ 4.70-4.76 ppm in the ^{1}H NMR and as a signal about δ 63.74–63.84 ppm in the ^{13}C NMR spectra, respectively. Moreover, in the ^{13}C NMR spectra of compounds **2a-c**, a signal near δ 182 ppm is assigned to the carbon atom forming the C=S bond. Finally, in both the ^{1}H and ^{13}C NMR spectra of structures **2a-c**, new peaks characteristic for the methyl group in series **a** and phenyl or 4-methoxyphenyl substituent in series **b** and **c** can be distinguished.

Subsequently, the synthesis of key 1,2,4-triazole derivatives of pyrrolo[3,4-*d*]pyridazinone **3a-c** was carried out. First, compounds **2a-c** underwent alkaline cyclization by refluxing in a 5% aqueous sodium hydroxide solution for about 2 h. Then, the reaction mixture was poured onto crushed ice and acidified with 7.5% hydrochloric acid solution, affording the corresponding *N*-substituted-1,2,4-triazoles **3a-c**. Finally, the formed white or yellowish precipitate of compounds **3a-c** was filtered off, washed with cold water and recrystallized from a proper solvent. In reference to the NMR spectra of structures **3a-c**, the change in the chemical shift of the signal of methylene linker can be easily observed. The signal of the protons of this group is shown at δ 5.12–5.30 ppm in the ^{1}H NMR, while the signal of a carbon atom is recorded about δ 57.85–58.09 ppm in the ^{13}C NMR spectra, accordingly. Moreover, the presence of the distinctive peak near δ 168.04–169.12 ppm in the ^{13}C NMR spectra, which is identified with the triazole carbon forming C=S bond, alongside with the signal characteristic for a *N*H proton observed in the range of δ 13.82–14.04-ppm in the ^{1}H NMR spectra may suggest that derivatives **3a-c** occur in the thione form.

The final stage of the planned synthesis relied on the formation of titled *N*-substituted-1,2,4-triazole derivatives of pyrrolo[3,4-*d*]pyridazinone **4a-c-9a-c**. As it has already been mentioned, the concept of their structure was inspired by the leading literature data and our own previous investigations. As it was depicted on Scheme 1, the final molecules **4a-c-9a-c** could be divided into two series.

Compounds **4a-c-6a-c** are the new Mannich base-type derivatives of pyrrolo[3,4-*d*]pyridazinone based 1,2,4-triazoles. These molecules were obtained via an effective and convenient one-step reaction, carried out at room temperature. The corresponding derivative **3a-c** was stirred with the appropriate 4-aryl piperazine derivative and formaldehyde in methanol for several hours and left overnight. The distinctive two-proton singlet in the ^{1}H NMR spectrum observed about δ 5.15–5.29 ppm. The signal at around δ 69.39–69.66 ppm in the ^{13}C NMR spectrum clearly indicates the creation of the methylene linker, characteristic for Mannich bases. What is obvious, in both the ^{1}H and ^{13}C NMR spectra of compounds **4a-c-6a-c**, are the signals assigned to aryl piperazine pharmacophore have been recorded.

On the other hand, the structure of the final compounds **7a-c-9a-c** was inspired by the pharmacophore theory featured by Dogruer [37]. Therefore, in the case of these derivatives, the 4-aryl piperazine moiety is connected with a five-membered 1,2,4-triazole ring via a flexible 2-oxoethylene linker. First of all, suitable 2-chloro-1-oxoethylaryl piperazine derivatives were afforded according to the synthetic protocols which have already been reported [38]. Due to the occurrence of possible tautomerism in the mentioned five-membered ring, the alkylation of 1,2,4-triazole analogue of pyrrolo[3,4-*d*]pyridazinone **3a-c** with 2-chloro-1-oxoethylaryl piperazine derivative may result in the formation of a mixture of *N*- and *S*-isoforms. Based on our former study, we have engaged the same synthetic conditions [35]. Therefore, the title compounds **7a-c-9a-c** were obtained by refluxing the 4-substituted-1,2,4-triazole derivatives of pyrrolo[3,4-*d*]pyridazinone **3a-c** with the appropriate 2-chloro-1-oxoethylaryl piperazine for several hours in ethanol in the presence of sodium ethoxide (Scheme 1). The crude products were filtered off, washed thoroughly with ethanol and purified by crystallization from this solvent. The lack of characteristic peak in the ^{13}C NMR spectra observed about δ 169.72–170.78 ppm, which was assigned to a carbon atom, forming a C=S bond (Experimental Section, Supplementary Data), strongly suggests that the final compounds **7a-c-9a-c** were formed via *S*-alkylation of 1,2,4-triazole derivatives of pyrrolo[3,4-*d*]pyridazinone **3a-b** (Scheme 1). This claim is supported by the presence of a distinctive signal shown near δ 152.25–152.62 ppm in the ^{13}C NMR spectra of **7a-c-9a-c**, which can be identified with carbon atom C3 in 1,2,4-triazole ring binding sulphur atom via a single bond (Ar-<u>C</u>-*S*-CH_2). Furthermore, a peak recorded about δ 165.49–165.72 ppm is typical for carbon atoms in carbonyl moiety (<u>C</u>=O). On the other hand, the signal which occurs near δ 41.98–42.23 ppm is assigned to carbon atom C1 (-<u>C</u>H_2-) of the 2-oxoethylene linker. Moreover, the two-proton singlet in the range of δ 4.37–4.42 ppm in the ^{1}H NMR spectra of **7a-c-9a-c** is assigned with the protons of carbon atom C1 in the mentioned linker. More detailed information is provided in the Experimental Section and Supplementary Data.

2.2. Evaluation of Viability

To estimate the effect of the new compounds on normal cells, a 3-(4, 5-Dimethylthiazol-2-yl)-2, 5-diphenyltetrazolium bromide (MTT) test was performed according to ISO 10993 part 5 Appendix C. The percentage of survival and the assessment of changes in the morphology of normal human dermal fibroblasts (NHDF) after contact with the tested compounds are presented in Table 1. The derivatives with 4-phenylpiperazine moiety, **4a-c** and **7a-c** and compounds **5a**, **6a**, **9a**, did not reduce the viability of NHDF cells below 70% in the tested concentration ranges. In the case of these molecules, no significant differences in cell survival were observed at a concentration of 100 μM. However, NHDF cell survival after 24-hour incubation was less than 50% for compounds **8a**, **8b**, **8c**, **9b** and **9c**, and the concentration at which 50% cell survival was observed has been calculated for these molecules. Therefore, these derivatives were excluded from further experiments.

Furthermore, due to the low level of cytotoxicity (less than 30% of dead cells compared to the control—culture without test compounds in a complete medium only), the theoretical IC_{50} values for compounds **5b**, **6b**, **5c** and **6c** were calculated. In all of the cases, it was noted that an increase in cell viability was observed at the reduced concentration (10 and 50 μM).

Table 1. The cell viability [IC_{50} (SEM) n = 3] and the evaluation of the morphology of cells treated with the tested compounds.

	IC_{50} [μM]	Cell Morphology in Culture
4a	Non-toxic	normal morphology for fibroblasts—elongated cells, single granular cells in 1 of 10 assessed fields of view
5a	Non-toxic	normal morphology for fibroblasts—elongated cells, single granular cells in 1 of 10 assessed fields of view
6a	Non-toxic	normal morphology for fibroblasts—elongated cells, single granular cells in 1 of 10 assessed fields of view
7a	Non-toxic	normal morphology for fibroblasts—elongated cells, single granular cells in 1 of 10 assessed fields of view
8a	35.60 (4.46)	many granules, cells shrunken, cell lysis was observed
9a	Non-toxic	normal morphology for fibroblasts—elongated cells, single granular cells in 1 of 10 assessed fields of view
4b	Non-toxic	normal morphology for fibroblasts—elongated cells, single granular cells in 1 of 10 assessed fields of view
5b	200.00 (7.05)	granularities were observed in 3–5 fields of view from 10 analyzed fields, cells with an elongated shape characteristic of fibroblasts
6b	156.25 (6.70)	granularities were observed in 3–5 fields of view from 10 analyzed fields, cells with an elongated shape characteristic of fibroblasts
7b	Non-toxic	normal morphology for fibroblasts—elongated cells, single granular cells in 1 of 10 assessed fields of view
8b	22.72 (2.25)	many granules, cells shrunken, cell lysis was observed
9b	30.80 (3.04)	many granules, cells shrunken, cell lysis was observed
4c	Non-toxic	normal morphology for fibroblasts—elongated cells, single granular cells in 1 of 10 assessed fields of view
5c	166.67 (3.35)	granularities were observed in 3–5 fields of view from 10 analyzed fields, cells with an elongated shape characteristic of fibroblasts
6c	103.89 (2.75)	granularities were observed in 3–5 fields of view from 10 analyzed fields, cells with an elongated shape characteristic of fibroblasts
7c	Non-toxic	normal morphology for fibroblasts—elongated cells, single granular cells in 1 of 10 assessed fields of view
8c	18.97 (1.84)	many granules, cells shrunken, cell lysis was observed
9c	28.56 (4.59)	many granules, cells shrunken, cell lysis was observed

Note: Cytotoxic compounds which were excluded from further investigations are marked in red.

On the microscopic image, few granules were observed in the NHDF cells in the tested concentration range for the compounds **4a-7a**, **9a**, **4b**, **7b**, **4c** and **7c**. Cell shrinkage and separation from the surface of the culture wells were not observed. These changes were classified according to the criterion of grade 1—low toxicity. Similar changes in the cell morphology were observed in the systems containing 100 μM for **5b**, **6b** and **5c**. In this case, a slightly greater number of endoplasmic granules were observed without any effect on the cell contraction. In this case, low toxicity was considered as well.

With reference to derivative **6c** at a concentration of 100 μM, the cells in the range of 10–15% contracted and detached from the medium. The appearance of fine granules inside the cytoplasmic cells was observed. However, at the reduced concentration of the tested compounds from individual endoplasmic pellets, a culture density comparable to that of the control culture was observed. Cell lysis was not observed. Regardless of the tested derivatives, there was no significant change in the NHDF cells compared to the control.

2.3. Cyclooxygenase (COX-1, COX-2) Inhibition Studies

2.3.1. In Vitro COX Inhibition Assay

Inhibition of COX-1 and COX-2 activity of the tested compounds was assessed after 2 min incubation at 100 μM concentration using the Cayman's COX Colorimetric Inhibitor Screening Assay Kit (Cat # 701050). The IC_{50} values and the COX-2/COX-1 selectivity ratios were calculated for each investigated and reference compound (*Meloxicam*, *Celecoxib* and *Diclofenac*). The results are shown in Table 2. The derivatives **4a-7a**, **9a**, **4b**, **7b** and **4c** revealed COX-2 inhibitory activity comparable to *Meloxicam*. Four of the studied molecules: **5a**, **7a**, **4b** and **7b**, also inhibited the constitutive isoform COX-1, but this activity was significantly lower. Compounds **5b**, **6b**, **5c-7c** did not exert any cyclooxygenase inhibition

profile in the performed in vitro investigations. The analysis of these data allows us to conclude that the derivatives of series **a**, with methyl substituent in the 1,2,4-triazole ring, demonstrate possibly the best COX inhibitory activity. Better affinity towards COX-2 can be explained by the bigger binding pocket of that isoenzyme. Large and expanded molecules, like those from series **b** and **c**, with aryl substituent in the 1,2,4-triazole moiety, revealed poor or no inhibitory activity towards COX.

2.3.2. Molecular Docking Study

The molecular docking analysis was carried out to explore the binding interactions of the tested compounds inside the active site of cyclooxygenase. The binding free energy (ΔG°) for the interaction with COX-1 for all of the studied compounds showed positive value. The energies obtained for the interactions with COX-2 are presented in Table 3. The ΔG° is negative for all of the compounds from series **a**, and for **4b**, **7b** and **4c**. The lowest value was found for compounds number **4** in each series (**4a-c**). The energies ΔE_2, ΔE_3 indicate that the main interactions are van der Waals and hydrogen bonding. The size of the COX-2 pocket is bigger than COX-1, which allows for the selective binding of larger molecules. However, the analyzed compounds are relatively large, especially the compounds from the **b** and **c** series, with phenyl and 4-methoxyphenyl rings. It can make some difficulties in the efficient docking to even COX-2.

Table 2. The IC_{50} [μM] values determined for COX-1 and COX-2.

Compound	IC_{50} [μM] (SD)		COX-2/COX-1 Selectivity Ratio
	COX-1	COX-2	
4a	NA	45.24 (0.018)	-
5a	95.75 (0.1)	48.24 (0.04)	0.50
6a	NA	43.85 (0.035)	-
7a	70.96 (0.2)	48.48 (0.037)	0.68
9a	NA	42.64 (0.015)	-
4b	79.47 (0.06)	47.83 (0.039)	0.60
5b	NA	NA	-
6b	NA	NA	-
7b	86.30 (0.005)	49.79 (0.001)	0.58
4c	NA	48.50 (0.027)	-
5c	NA	NA	-
6c	NA	NA	-
7c	NA	NA	-
Meloxicam	83.7 (0.03)	59.2 (0.06)	0.71
Celecoxib	56 (0.1)	0.30 (0.08)	0.005
Diclofenac	3.5 (0.04)	16.6 (0.03)	4.74

Note: Data are shown as standard deviation (SD), NA stands for "not applicable".

Inside the COX-2 active site, some hydrogen bonds interactions were found, especially for the compounds belonging to series **a**: SER530, TYR355, ARG120, SER120. Moreover, various kinds of π interactions are observed. The details are presented in Figures 1–3. In addition, the position of the studied compounds was found very similar to *Meloxicam* (Figure 4).

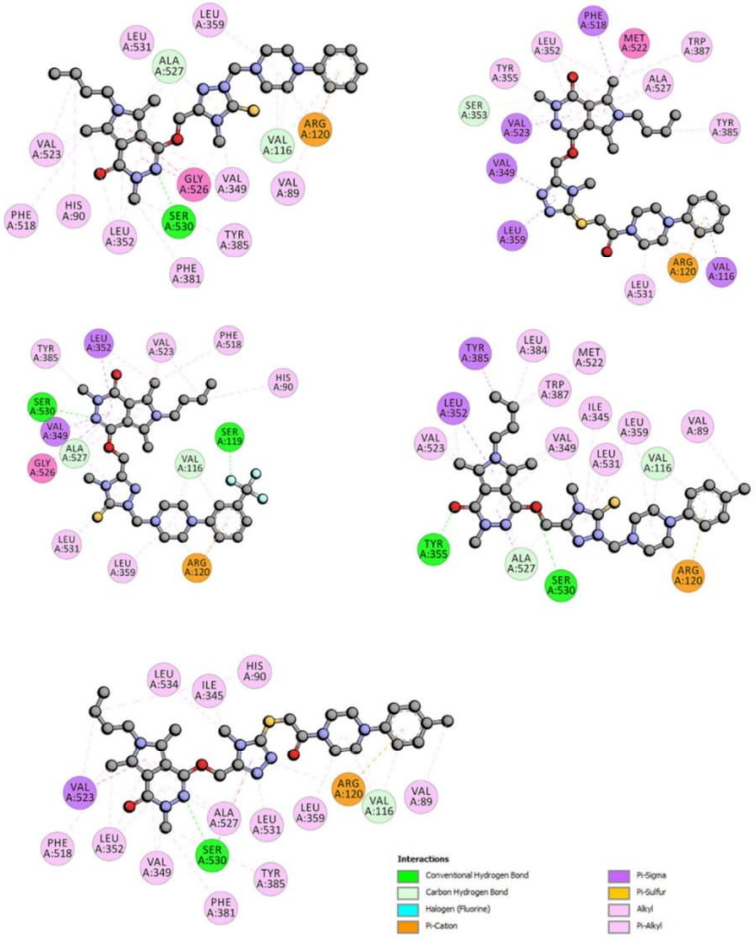

Figure 1. Two-dimensional interaction plot of **4a-7a**, **9a** with COX-2.

2.4. Anti-Inflammatory and Antioxidant Activity within Cells

The titled *N*-substituted-1,2,4-triazole derivatives of pyrrolo[3,4-*d*]pyridazinone were further evaluated for their anti-inflammatory potential in NHDF cells pre-incubated with the proinflammatory agent lipopolysaccharide (LPS) at a concentration of 50 μg/mL.

The NHDF cell line was firstly treated with LPS for 24 h to induce inflammation. Then, the culture was washed and incubated with the test compounds for 24 h at a concentration range of 10–100 μM. All of the tested molecules increased the cell viability compared to the positive control (except **5c** and **6c** in the concentration range of 50–100 μM). This fact can suggest that the investigated derivatives could probably exert a good ability to reduce cell inflammation (Figure 5). For the remaining tested compounds, the increase in the activity of mitochondria was statistically significantly higher than in the positive control. At the same time, compounds **6a** and **9a** showed a greater increase in mitochondrial activity than the negative control in the entire range of the tested concentrations.

Table 3. Energies of the interactions of the tested compounds with COX-2 were obtained from the molecular study.

	ΔG° [kJmol^{-1}]	ΔE_1 [kJmol^{-1}]	ΔE_2 [kJmol^{-1}]	ΔE_3 [kJmol^{-1}]	K_i [μM]
4a	−22.57	−33.81	−34.52	0.75	109
5a	−15.38	−27.84	−28.67	0.84	2010
6a	−23.28	−34.48	−35.44	0.96	83
7a	−11.32	−23.83	−23.83	0.00	10,250
9a	−21.02	−33.48	−33.41	−0.16	206
4b	−20.40	−32.85	−34.36	1.50	226
5b	11.60	−2.17	−3.89	1.76	-
6b	13.29	−0.83	−0.25	1.08	-
7b	−5.93	−19.64	−19.10	−0.84	90,800
4c	−8.07	−21.82	−23.24	1.42	38,200
5c	29.63	14.67	11.87	2.71	-
6c	52.36	36.65	35.44	1.21	-
7c	6.18	−8.78	−8.66	−0.12	-
Meloxicam	−34.02	−37.74	−37.32	−0.42	1.09
Celecoxib	−30.17	−36.40	−36.11	−0.08	5.13
Diclofenac	−29.59	−35.82	−30.18	−5.63	6.50

Notes: ΔG°—binding free energy; ΔE_1—intermolecular interaction energy, which is the sum of van der Waals energy, hydrogen bonding energy, desolvation free energy and electrostatic energy; ΔE_2—the sum of van der Waals energy, hydrogen bonding energy and desolvation free energy; ΔE_3—electrostatic energy, K_i—inhibit constants.

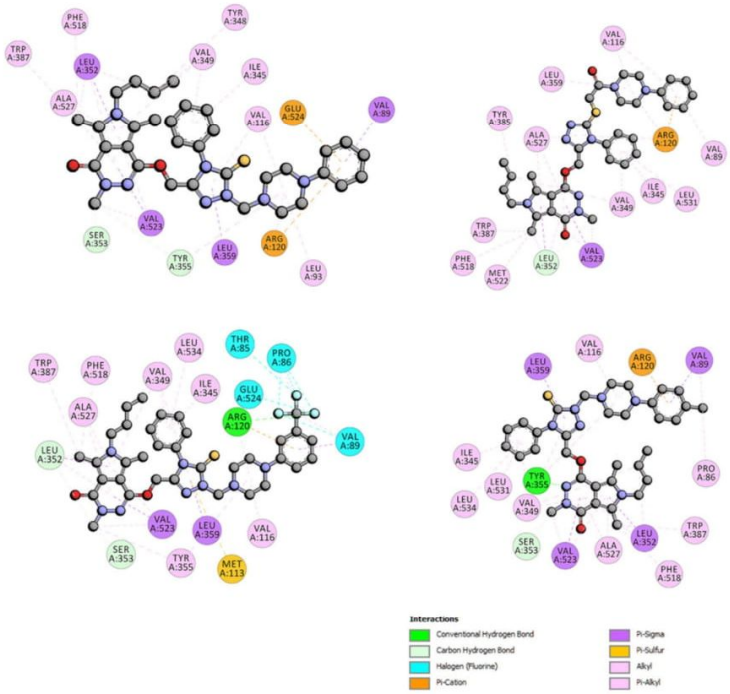

Figure 2. Two-dimensional interaction plot of **4b-7b** with COX-2.

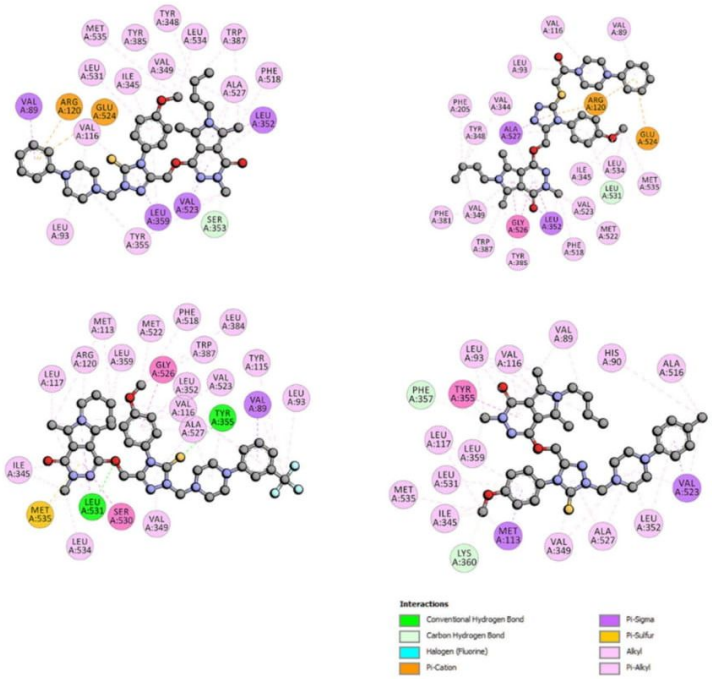

Figure 3. Two-dimensional interaction plot of **4c-7c** with COX-2.

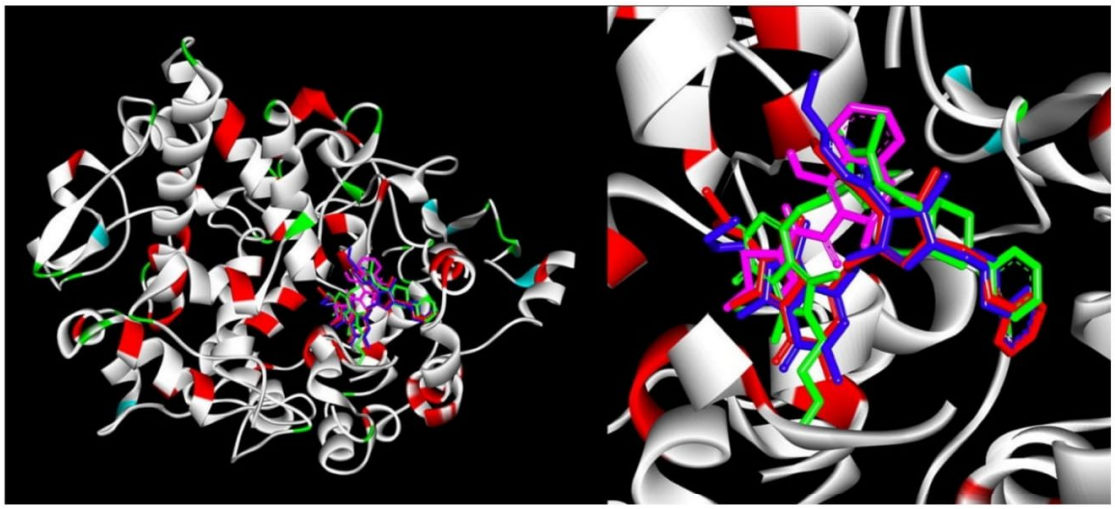

Figure 4. Docking poses of **4a** (green), **4b** (red), **4c** (blue) and *Meloxicam* (pink) inside COX-2.

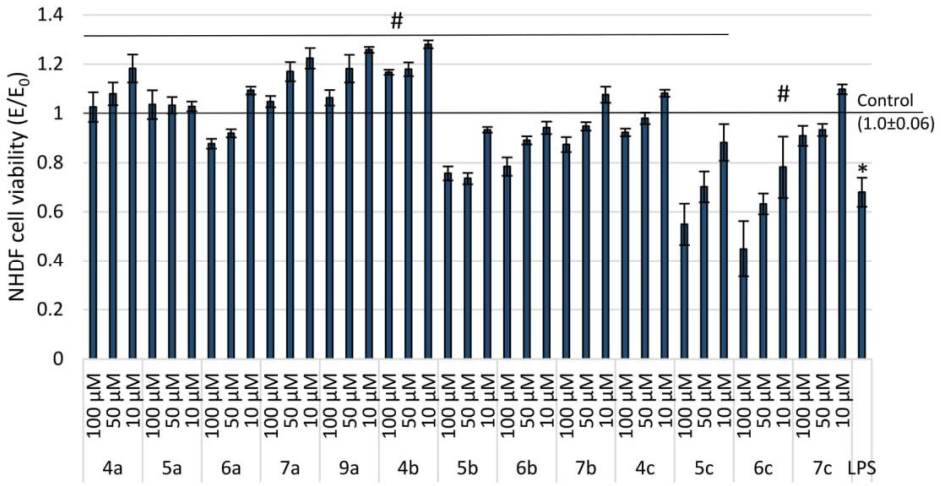

Figure 5. Impact of investigated compounds on NHDF cells after incubation with 50 µg/mL LPS measured through MTT assay; # $p < 0.05$—significant difference compared to the control with 50 µg/mL LPS and without compounds; * $p < 0.05$—significant difference compared to a negative control without 50 µg/mL LPS and compounds.

Needless to say, such factors like hypoxia or inflammation can increase the intracellular level of reactive oxygen and nitrogen species (RONS). As a consequence, oxidative and/or nitrosative stress can develop in inflamed tissue [39]. According to many studies, the aforementioned processes often co-exist and potentiate one another [39,40]. Being aware that there is an increased level of free oxygen radicals and nitric oxide (NO) in inflammation, we evaluated whether the tested compounds exhibit antiradical activity in the dichlorofluorescin diacetate (DCF-DA) and Griess assays and assessed the levels of reactive oxygen species (ROS) and NO, respectively (Figure 6A,B).

The dependence on the concentration of the new derivatives of pyrrolo[3,4-*d*]pyridazinone and their antioxidant activity has been demonstrated in the executed experiments (Figure 6). The higher the concentration of the tested compound, the stronger the scavenging of oxygen free radicals has been noticed. All of the tested compounds statistically significantly decreased the level of ROS as compared to the positive control. Moreover, the derivatives **6a** and **9a** scavenged oxygen free radicals to the level of the negative control in the whole range of the tested concentrations. At the same time, all of the examined molecules showed a statistically significant reduction in the NO level, as compared to the positive control. Compound **9a** was the only one that lowered NO levels to negative control levels over the whole range of the investigated concentrations.

2.5. Structure-Activity Relationship Study

When considering the composition of 18 title compounds reported in this paper, we can point out three characteristic and variable structural elements which could have the impact on the toxicity and the biological activity of the investigated derivatives (Figure 7). The first one is the substituent in position 4 in the 1,2,4-triazole ring. We have introduced there residues of a different size and character. Based on this structural element, we have divided title compounds into three main series: (**a**) with methyl group, (**b**) with phenyl ring and (**c**) with 4-methoxyphenyl moiety. The second one is the aryl piperazine pharmacophore—being more precise, the substituent or its lack in its phenyl ring. In this case, we can also demonstrate three groups of compounds. The first one is those with unsubstituted phenylpiperazine moiety (**4a-c**, **7a-c**). In the second class (**5a-c**, **8a-c**) we can distinguish the derivatives with the trifluoromethyl group in position 3. On the other hand, compounds **6a-c**, **9a-c** possess a substituent completely different in the size and electronic character—a methyl residue in position 4 of phenyl ring. Finally, when taking

into consideration the way in which the aryl piperazine pharmacophore is linked with 1,2,4-triazole moiety, we can divide the target compounds into two groups. Mannich base-type derivatives are the first one (**4a-c-6a-c**), while the second one consists of structures with flexible oxoethylene linker (**7a-c-9a-c**) received via *S*-alkylation of 1,2,4-triazole.

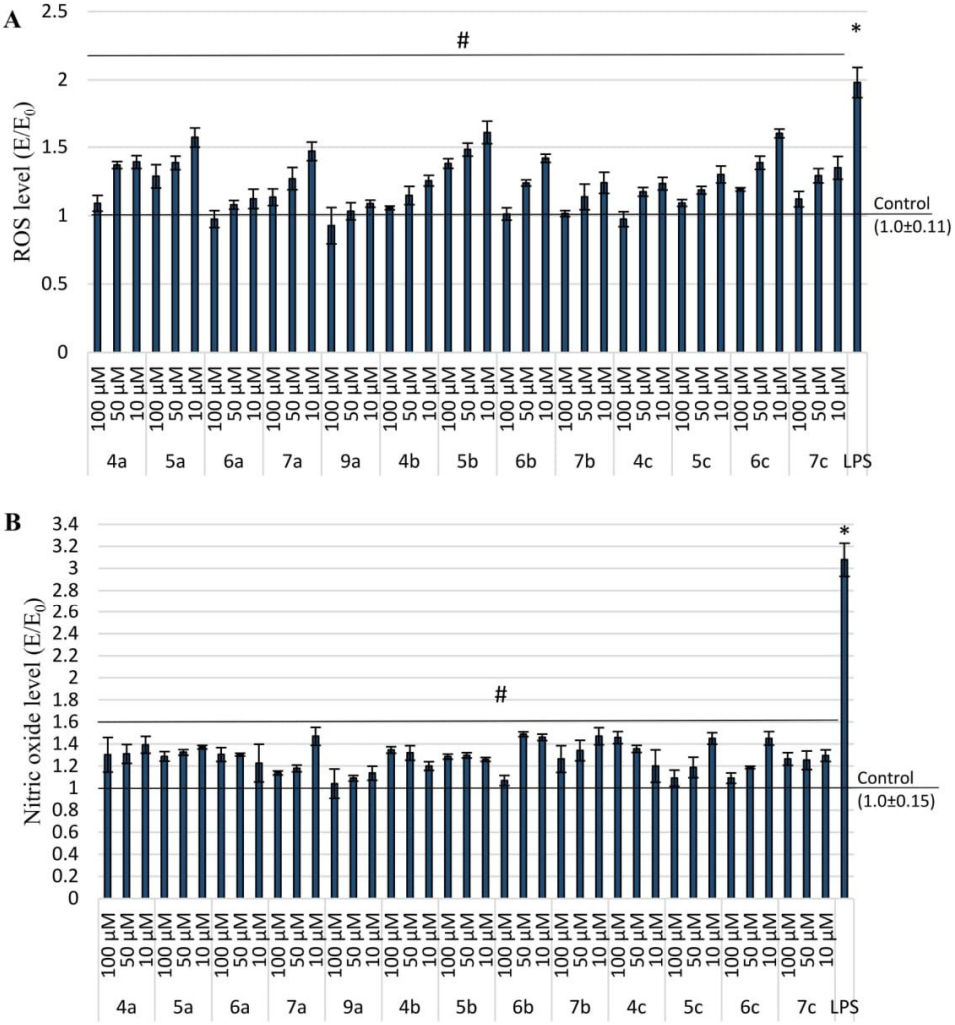

Figure 6. Impact of investigated compounds on NHDF cells after incubation with 50 µg/mL LPS; (**A**) DCF-DA assay and (**B**) Griess assay; # $p < 0.05$—significant difference compared to the control with 50 µg/mL LPS and without compounds; * $p < 0.05$—significant difference compared to a negative control without 50 µg/mL LPS and compounds.

When analyzing the results of the cell viability evaluation, we can see that there is a significant relationship between the structure and cytotoxicity of the titled compounds. First of all, in every series, **a**, **b** and **c** molecules with unsubstituted phenylpiperazine, that is **4** and **7**, appeared to be non-toxic. On the contrary, all of the derivatives with both the trifluoromethyl group and oxoethylene linker (**8a-c**) caused cell lysis. Such an effect was also observed in the case of compounds possessing 4-methylphenylpiperazine pharmacophore connected via the oxoethylene group with 1,2,4-triazole, which are **9b** and **9c**. Continuing our considerations, it is worth noticing that the data shown in the Table 1 clearly indicate that out of six compounds from series **a** (methyl residue in 1,2,4-triazole), as many as five derivatives (**4a-7a**, **9a**) did not reveal a cytotoxic effect at all. Therefore, the

presence of a small substituent in that place appear to be the most favorable. Moreover, Mannich base derivatives (**4a-c-6a-c**) were found to be less toxic than compounds with oxoethylene linker (**7a-c-9a-c**).

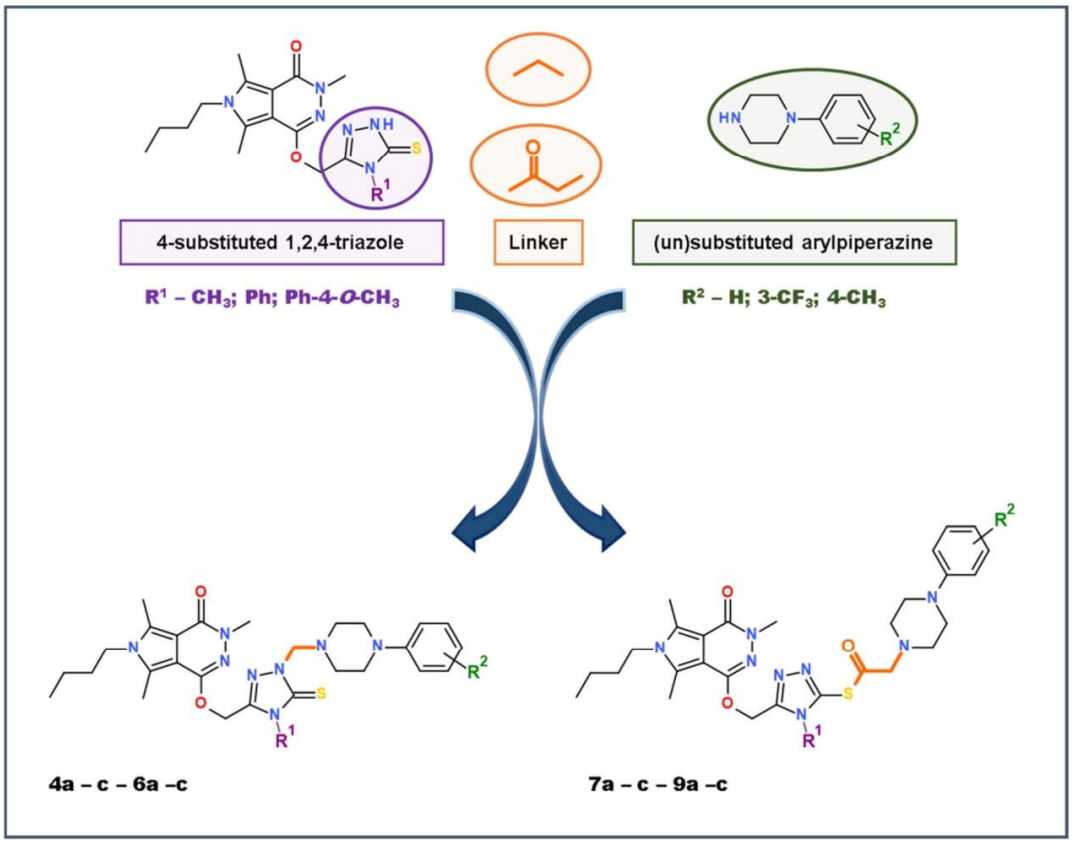

Figure 7. The concept of design and synthesis of target *N*-substituted-1,2,4-triazole-based derivatives of pyrrolo[3,4-*d*]pyridazinone.

We can assume that the introduction of a large substituent into position 4 of 1,2,4-triazole ring, with the simultaneous presence of substituted aryl piperazine pharmacophore, leads to an increase of cytotoxicity, which may be caused by large molecular weight. In this case, the nature and size of the residue in the triazole ring seems to be substantial. The compounds with a small methyl group in the position 4 of 1,2,4-triazole ring and/or unsubstituted phenylpiperazine pharmacophore did not affect the cell viability at all (except **8a**). Summing up, the cytotoxic effect grew up alongside with increased molecular weight and the size of molecule. Derivatives **8a-c**, **9b-c** were excluded from further investigations.

Considering COX inhibition studies, derivatives **5b**, **6b**, **5c-7c**, did not show any activity in in vitro assay and their binding free energy (ΔG°) for interaction with both of the isoenzymes presented positive values. Thus, a large substituent in 1,2,4-triazole ring led to a decrease in the biological activity. From series **b** and **c** only **4b**, **7b** and **4c** revealed potential COX inhibition. Compounds **4a-7a**, **9a** demonstrated good cyclooxygenase inhibitory activity, especially towards COX-2 isoform (Table 2). It is worth to mention, that **5a**, **7a**, **4b** and **7b** inhibited also COX-1 isoform in vitro, but it was not confirmed by the results of the molecular docking studies. Moreover, the IC_{50} values of active compounds determined for both COX-1 and COX-2 were very similar to that defined for *Meloxicam*. Taking into

consideration the results obtained in in vitro COX inhibition assay and in the molecular docking studies, the most promising appeared to be derivatives from series **a**.

Analyzing the result of performed in vitro anti-inflammatory and antioxidant activity evaluation within cells, we did not notice such meaningful differences between the investigated compounds. All of the derivatives exerted a good ability to reduce induced inflammation, except **5c** and **6c**. Once more, structures which belong to series **a** turned out to be the most potent.

Taking all of the above into account, we can suppose that the nature of aryl piperazine pharmacophore and the linker had the main impact on the compounds' toxicity. On the other hand, the substituent in the position 4 of 1,2,4-triazole had the influence on both the cytotoxicity and the COX inhibitory activity.

Our consideration concerning the structure-activity relationships in the group of the investigated target molecules are summarized in Figure 8.

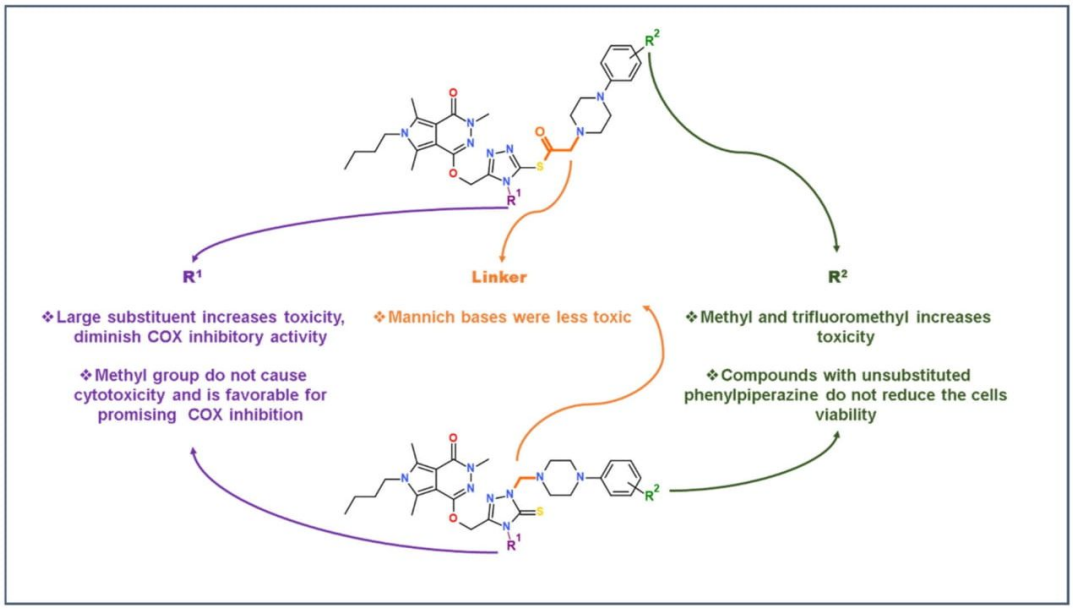

Figure 8. The structure-activity relationships in the group of investigated molecules.

2.6. Bovine Serum Albumin (BSA) Ligand-Binding Assay

The interaction of new compounds with blood proteins affects their pharmacokinetics in vivo. Therefore, we have performed experiments which were aimed at the estimation of the binding mode of the target compounds with the bovine serum albumin (BSA). Its structure is very similar to human serum albumin (HSA), and therefore can be used instead of human protein, especially since the costs of the application of bovine protein are significantly lower [41,42]. The mature BSA protein consists of 583 amino acids and is formed by 3 homologous domains, I, II and III, which in turn are composed of 2 subdomains: A and B [42]. Aromatic and heterocyclic ligands can bind to hydrophobic cavities in the subdomains IIA and IIIA [41]. The molecular interaction between new ligands and bovine serum albumin can be monitored by optical techniques such as circular dichroism (CD), FT-IR, ultraviolet–visible (UV-vis) or fluorescence spectroscopy [43].

2.6.1. Fluorescence Quenching of BSA, Binding Constants, Thermodynamic Studies

In this study, we checked the binding properties of the analyzed compounds to bovine serum albumin (BSA). Due to this, the fluorescence spectra were recorded in the range of 300–500 nm upon excitation at 280 nm, where both Trp and Tyr residues are excited,

and concentration range 0.0–2.0 μM (Figure 9). After the addition of each portion of the analyzed compound, the fluorescence intensity of BSA decreased. It suggests that all compounds could interact with BSA. The analyzed compounds can interact with BSA in two ways: forming a complex (what means static quenching) or due to collisions between molecules (dynamic quenching). The analysis by the Stern–Volmer equation, in dependence on temperature, can explain which way of interaction is observed in the case of our compounds [44].

The Stern–Volmer Equation (1) [45] at three different temperatures 297, 303, 308 K, was used for all of the fluorescence data after correction due to the infer filter effect (2):

$$F_{corr} = F_{obs} 10^{\frac{(A_{ex}+A_{em})}{2}} \quad (1)$$

where, F_{corr} and F_{obs} are the corrected and observed fluorescence intensities, respectively. A_{ex} and A_{em} are the absorbance values at excitation and emission wavelengths, respectively.

$$\frac{F_O}{F} = 1 + k_q \tau [Q] = 1 + K_{SV} \quad (2)$$

where F_0 and F are the steady-state fluorescence intensities at the maximum wavelength in the absence and presence of quencher, respectively, k_q the quenching rate constant of the biomolecule, τ_0 the average lifetime of the biomolecule, [Q] is the quencher concentration and K_{sv} is the Stern–Volmer constant.

The Stern–Volmer (K_{SV}) constant was determined by linear fitting. The calculated results are collected in Table 4. When the temperature increases, the K_{SV} values also decrease. Furthermore, the quenching rate constant (k_q) values are much greater than the value of the maximum scatter collision quenching constant equal to 2×10^{10} $dm^3 \cdot mol^{-1} \cdot s^{-1}$ [46]. Thus, all of the above indicate that the static quenching mechanism is more probable than dynamic and suggests forming the ground–state complex.

A double logarithm regression curve (3) was used to calculate the binding constants and the number of binding sites:

$$\log \frac{F_0 - F}{F} = \log K_b + n \log [Q] \quad (3)$$

where F_0 and F are the steady-state fluorescence intensities at the maximum wavelength in the absence and presence of quencher, respectively, [Q] is the quencher concentration.

Figure 10 shows a good linear fit for all of the studied compounds. The results listed in Table 4 made visible that the binding constants indicate values of about 10^5 $dm^3 \cdot mol^{-1}$ at 297 K and decrease in higher temperatures. Similar values were obtained for many biologically active compounds [44,47–51]. Thus, the number of binding sites is close to 1 for all of the studied compounds, which means a one-to-one interaction.

Small molecules can interact with proteins in various ways, such as a hydrogen bond, van der Waals force, electrostatic and hydrophobic interactions, etc. [52]. The values of the thermodynamic parameters, enthalpy change (ΔH°), the entropic change (ΔS°) and free energy change (ΔG°), indicate the manners of these interactions.

The thermodynamic parameters were calculated from Equations (4) and (5):

$$\log K_b = -\frac{\Delta H^\circ}{RT} + \frac{\Delta S^\circ}{R} \quad (4)$$

$$\Delta G^\circ = \Delta H^\circ - T\Delta S^\circ = -RT \ln K_b \quad (5)$$

where K_b is the binding constant, R is the universal gas constant.

The results are listed in Table 4. The negative ΔG° values indicate that the interaction between BSA and the analyzed compounds was spontaneous. Simultaneously, the ΔH° and ΔS° also had negative values. Due to this, it can be concluded that van der Waals forces and/or hydrogen bonds were the main interaction types in the binding process.

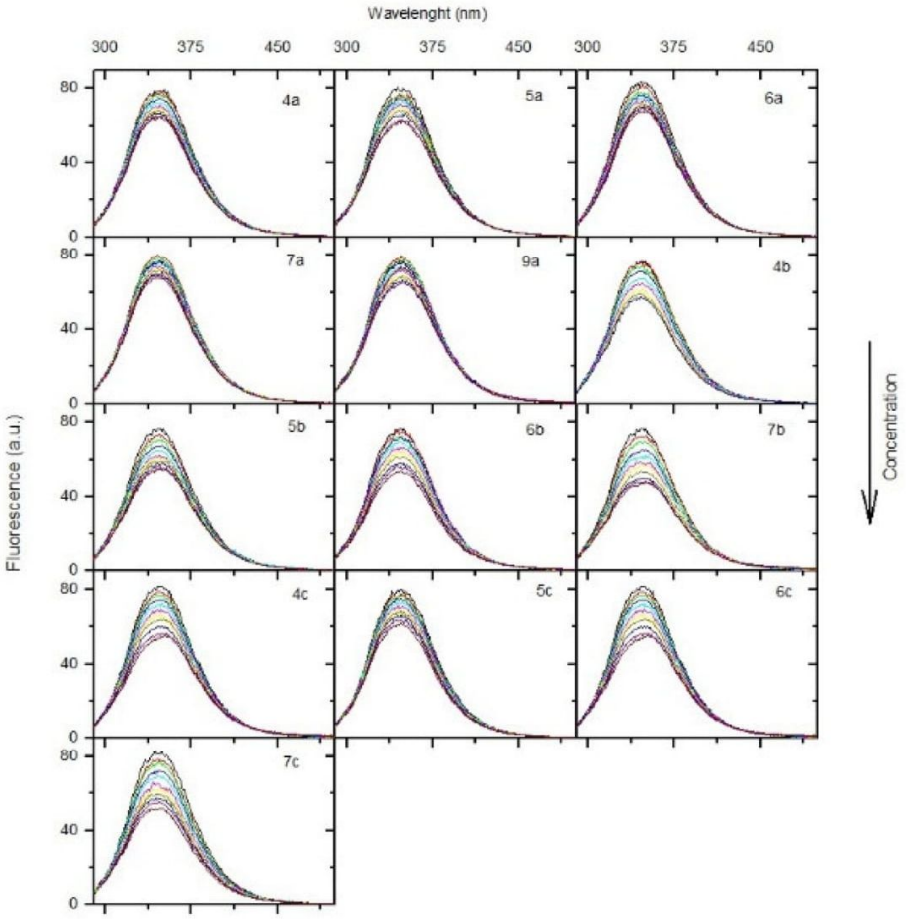

Figure 9. Fluorescence spectra of BSA solution in the presence of studied compounds (T-297 K, λex = 280 nm). The concentration of derivatives from series a, b and c increased gradually as follows: 0, 0.2, 0.4, 0.6, 0.8, 1.0, 1.2, 1.4, 1.6, 1.8, 2.0 μM.

2.6.2. Circular Dichroism Spectra

Circular dichroism spectroscopy is a good method to determine the changes in the secondary structure in the conformation of proteins and to check if the analyzed compounds can interact with protein molecules [53]. In this study, we investigated the changes in the structure of BSA when all of the analyzed compounds were absent or present in solutions. Two negative bands characteristic for BSA, at near 208 nm and 222 nm, were observed in all of the CD spectra (Table S6 in Supplementary Data), which is typical for the α-helical structure of the protein. Any changes in this region mean conformational changes in protein molecules [54]. On the CD spectra shown in Table S6, a reduction of ellipticity values at 208 nm and 222 nm after adding every portion of the analyzed compounds can be seen. The loss in the α-helix(%) was observed. The content of the α-helix was calculated using Equations (6) and (7):

$$\alpha - \text{helix}(\%) = \frac{-\text{MRE}_{208} - 4000}{33000 - 4000} 100\% \quad (6)$$

where MRE_{208} is the MRE value observed at 208 nm, 4000 and 33,000 is the MRE value of the β-form and random coil conformation cross at 208 nm value of pure α-helix at 208 nm, respectively.

$$MRE = \frac{ObservedCD[mdeg]}{10Cnl} \quad (7)$$

where C is the molar concentration of BSA, n is the number of amino acid residues, which is 583 for BSA, l is the path length in cm [55].

Table 4. The Stern–Volmer constant K_{sv} and the quenching rate constant k_q, the binding constants K_b and number of binding sites n and the thermodynamic parameters for the interaction of BSA with studied compounds at different temperatures.

		Quenching			Binding		Thermodynamic		
	T [K]	**$K_{sv} \times 10^5$ [dm^3mol^{-1}]**	**$k_q \times 10^{13}$ [$dm^3mol^{-1}\cdot s^{-1}$]**	**$logK_b$**	**$K_b \times 10^4$ [dm^3mol^{-1}]**	**n**	**ΔG° [$kJmol^{-1}$]**	**ΔH° [$kJmol^{-1}$]**	**ΔS° [$Jmol^{-1}K^{-1}$]**
	297	0.82	0.82	4.95 ± 0.09	8.91	1.00 ± 0.02			
4a	303	0.56	0.56	4.65 ± 0.09	4.47	0.98 ± 0.02	−28.20	−95.14	−225.40
	308	0.24	0.24	4.35 ± 0.27	2.24	0.99 ± 0.05			
	297	0.89	0.89	4.91 ± 0.14	8.13	0.99 ± 0.02			
5a	303	0.97	0.97	4.74 ± 0.04	5.50	0.96 ± 0.01	−28.20	−95.17	−225.50
	308	0.80	0.80	4.30 ± 0.07	2.00	0.89 ± 0.01			
	297	0.51	0.51	4.69 ± 0.13	4.90	0.99 ± 0.02			
6a	303	0.40	0.40	4.27 ± 0.14	1.86	0.94 ± 0.02	−27.07	−186.69	−537.43
	308	0.14	0.14	3.51 ± 0.22	0.33	0.89 ± 0.04			
	297	0.66	0.66	4.67 ± 0.07	4.68	0.97 ± 0.01			
7a	303	0.27	0.27	4.09 ± 0.20	1.23	0.94 ± 0.03	−26.89	−222.14	−657.43
	308	0.10	0.10	3.26 ± 0.21	0.99	0.87 ± 0.04			
	297	1.71	1.71	4.91 ± 0.05	4.90	0.94 ± 0.01			
9a	303	0.48	0.48	4.52 ± 0.09	1.86	0.97 ± 0.02	−27.89	−108.40	−271.08
	308	0.20	0.20	4.23 ± 0.18	0.33	0.98 ± 0.03			
	297	1.76	1.76	4.82 ± 0.20	6.61	0.92 ± 0.03			
4b	303	0.97	0.97	4.47 ± 0.22	2.95	0.91 ± 0.03	−27.75	−156.84	−434.67
	308	0.42	0.42	3.82 ± 0.20	0.61	0.86 ± 0.02			
	297	1.72	1.72	4.76 ± 0.12	5.75	0.92 ± 0.02			
5b	303	0.97	0.97	4.22 ± 0.13	1.66	0.93 ± 0.02	−26.92	−131.53	−352.20
	308	0.25	0.25	3.94 ± 0.17	0.87	0.92 ± 0.03			
	297	1.78	1.78	4.91 ± 0.15	8.13	0.95 ± 0.02			
6b	303	0.52	0.52	4.32 ± 0.12	2.09	0.93 ± 0.02	−27.90	−167.25	−469.18
	308	0.48	0.48	3.86 ± 0.06	0.72	0.90 ± 0.01			
	297	3.07	3.07	4.97 ± 0.17	9.33	0.91 ± 0.03			
7b	303	1.95	1.95	4.53 ± 0.16	3.39	0.87 ± 0.02	−28.36	−142.60	−384.65
	308	0.78	0.78	4.07 ± 0.10	1.17	0.86 ± 0.02			
	297	0.59	0.59	4.82 ± 0.19	5.61	1.01 ± 0.03			
4c	303	0.24	0.24	4.37 ± 0.40	2.34	0.99 ± 0.08	−27.44	−135.07	−362.40
	308	0.37	0.37	3.97 ± 0.12	0.93	0.90 ± 0.02			
	297	0.81	0.81	4.97 ± 0.18	9.33	1.01 ± 0.03			
5c	303	0.60	0.60	4.51 ± 0.10	3.24	0.95 ± 0.02	−28.29	−136.72	−365.09
	308	0.36	0.36	4.11 ± 0.13	1.29	0.92 ± 0.02			
	297	2.68	2.68	4.98 ± 0.12	9.55	0.92 ± 0.02			
6c	303	0.76	0.76	4.61 ± 0.03	4.07	0.95 ± 0.01	−28.34	−111.23	−279.08
	308	0.31	0.31	4.28 ± 0.12	1.91	0.96 ± 0.02			
	297	2.37	2.37	4.97 ± 0.20	9.33	0.93 ± 0.03			
7c	303	1.03	1.03	4.53 ± 0.10	3.39	0.92 ± 0.02	−28.48	−162.47	−451.14
	308	0.41	0.41	3.94 ± 0.18	0.87	0.88 ± 0.03			

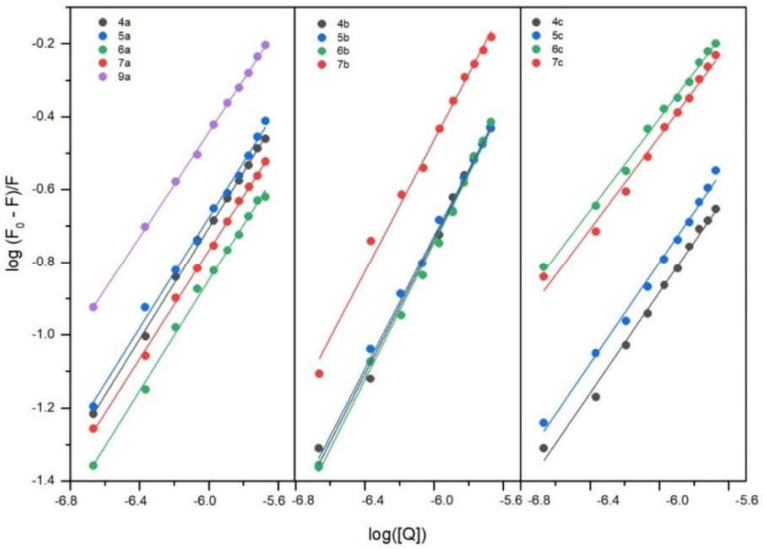

Figure 10. Fluorescence spectra of BSA solution in presence of studied compounds (T-297 K, λex = 280 nm). The concentration of a, b and c was as follows: 0, 0.2, 0.4, 0.6, 0.8, 1.0, 1.2, 1.4, 1.6, 1.8, 2.0 μM.

The reduction in the α-helical contents of BSA is observed in the presence of all of the analyzed compounds. The changes after adding every portion of analyzed ligands are presented in Table 5. The observed changes ranged from 2.72% for **7a** to 5.88% for **7b** (Figure 11). Thus, CD studies showed that all of the analyzed compounds could interact with BSA, which agrees with the fluorescence spectroscopy.

Table 5. The values of the calculated α-helix(%) for BSA with the absence and presence of all analyzed compounds.

BSA/Analyzed Compound Molar Ratio	α-Helix [%]												
	4a	**5a**	**6a**	**7a**	**9a**	**4b**	**5b**	**6b**	**7b**	**4c**	**5c**	**6c**	**7c**
1:0	51.83	52.15	51.93	51.59	51.90	51.08	52.80	52.44	52.87	52.70	53.10	53.49	52.77
1:0.5	51.35	51.52	51.28	50.49	50.79	51.40	51.05	51.89	51.78	52.64	52.24	52.41	52.07
1:1	51.16	50.62	50.74	49.99	50.74	50.48	50.86	49.81	51.75	51.66	52.49	51.81	51.22
1:5	49.80	50.26	49.59	48.79	49.76	49.74	51.21	49.15	49.92	51.10	50.36	50.74	50.31
1:10	48.09	47.56	47.45	48.87	46.94	47.00	48.53	47.66	46.99	47.45	50.12	48.01	48.19

2.6.3. Fourier Transform Infrared Spectroscopic Measurements

The interaction of BSA with a series of investigated compounds was evaluated by analyzing changes in the protein secondary structure. The backbone conformation of BSA is related to the shape and intensity variation of the Amide I bond (C=O—stretching) and Amide II bond (C–N—stretching coupled with N–H bending) detected in the range 1700–1600 cm^{-1} [56]. Shi et al. mention that the Amide I bond is more sensitive than the Amide II bond for changes in the secondary structure [42]. The major signals found for free BSA: 1658 cm^{-1} and 1550 cm^{-1} are related to the α-helix structure and contribution of 53.8% (Table 6). It corresponds well with the CD measurements. The second large share has the β-sheet structure, which accounts for 29.2% and manifests as 1638 cm^{-1}, 1630 cm^{-1} and 1618 cm^{-1} peaks (Table 6, Table S7a). For all of the measurement BSA-compound complexes, it was observed that there was a tendency to decrease the intensity of the 1650 cm^{-1} and 1545 cm^{-1} signals with an increase of the compound concentration

(Table S8 in Supplementary Data). This clearly proves that all of the presented compounds interact with BSA, and binding to a protein is demonstrated by changing its secondary structure. A reduction in the α-helix structures in BSA was observed for all of the studied compounds after binding them to the protein. These results are in good agreement with fluorescence and CD spectroscopy. The majority of the changes were exhibited in It is with good correspondence the **5b, 5c, 6b, 6c** and **7c** compounds. Moreover, the certain losing β-sheet structure occurred, especially for the **5c, 6c** and **7c**. These findings correspond to a rise in the percentage of β-turn and β-antiparallel in the secondary structure of BSA. Moreover, the higher contribution of disordered random coil stood out in the samples containing **5c, 6c** and **7c**.

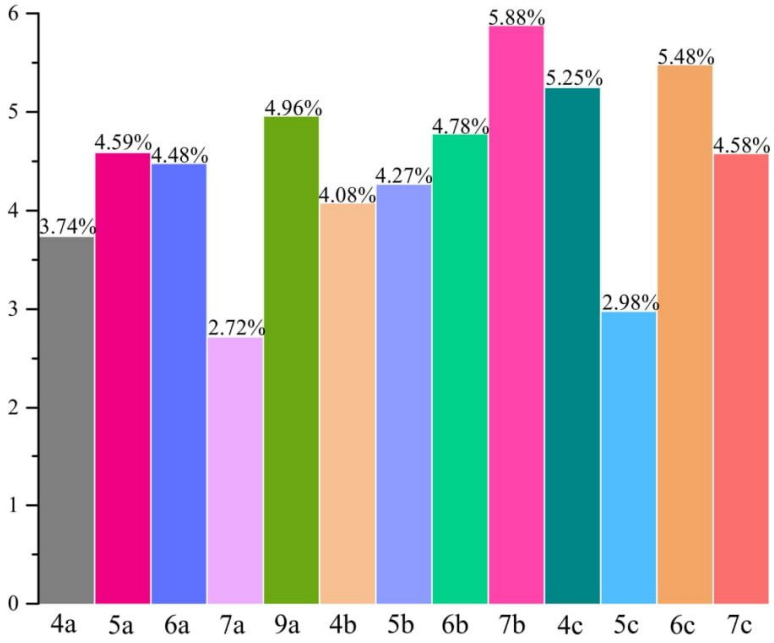

Figure 11. The comparison of changes in the α-helix(%) of BSA after adding 10 portions of each analyzed compound.

2.6.4. Site Markers Studies and Molecular Docking

In the BSA molecule, there are two binding sites situated in subdomains IIA and IIIA [57]. To confirm the binding sites where the analyzed compounds can be bound, *Phenylbutazone* (PHB) and *Ibuprofen* (IBP) were used as site probes [58]. Equation (3) was used to analyze the results here. The obtained results are collected in Table 7. The values of K_b of all of the tested compounds with BSA in the presence of IBP and PHB decline compared to compounds without BSA (Table 7). However, in the case of the values with PHB, the differences are smaller than in the case of IBP. Therefore, the results suggest that all of the studied compounds mainly bind to subdomain IIIA of BSA.

Table 6. Secondary structure of free BSA and BSA-drug complexes at pH = 7.5 calculated from Amide I bond obtained by FT-IR.

Compound	α-Helix [%]	β-Sheet [%]	β-Turn [%]	β-Anti [%]	Random-Coil [%]
Free—BSA	53.8	29.2	6.6	1.6	8.8
4a—BSA	50.2	16.5	11.8	11.8	9.7
5a—BSA	50.4	16.5	8.9	15.4	8.8
6a—BSA	50.3	17.8	4.9	19.5	7.5
7a—BSA	51.7	17.1	8.5	15.6	7.1
9a—BSA	51.8	16.2	5.8	18.4	7.8
4b—BSA	50.2	14.3	11.7	16.4	7.4
5b—BSA	49.7	13.8	13.7	12.5	10.3
6b—BSA	49.8	12.4	12.3	13.4	12.1
7b—BSA	51.5	14.2	15.6	9.9	8.8
4c—BSA	50.1	17.3	13.2	8.3	11.1
5c—BSA	49.1	6.1	16.4	3.6	24.8
6c—BSA	49.9	5.6	18.8	4.1	21.6
7c—BSA	48.3	6.6	18.6	4.2	22.3

Table 7. The binding constant of the studied compounds with BSA in the presence of site markers *Phenylbutazone* (PHB) and *Ibuprofen* (IBP) at 297 K.

	Site Marker	$logK_b$		Site Marker	$logK_b$		Site Marker	$logK_b$
	-	4.95 ± 0.09		-	4.82 ± 0.20		-	4.82 ± 0.19
4a	BSA + IBP	3.50 ± 0.07	**4b**	BSA + IBP	3.55 ± 0.19	**4c**	BSA + IBP	3.30 ± 0.08
	BSA + PHP	4.54 ± 0.05		BSA + PHP	4.55 ± 0.07		BSA + PHP	4.57 ± 0.12
	-	4.91 ± 0.14		-	4.76 ± 0.12		-	4.97 ± 0.18
5a	BSA + IBP	3.60 ± 0.09	**5b**	BSA + IBP	3.45 ± 0.05	**5c**	BSA + IBP	3.27 ± 0.09
	BSA + PHP	4.36 ± 0.07		BSA + PHP	4.25 ± 0.13		BSA + PHP	4.58 ± 0.05
	-	4.69 ± 0.13		-	4.91 ± 0.15		-	4.98 ± 0.12
6a	BSA + IBP	3.40 ± 0.11	**6b**	BSA + IBP	3.60 ± 0.12	**6c**	BSA + IBP	3.68 ± 0.06
	BSA + PHP	4.10 ± 0.09		BSA + PHP	4.46 ± 0.15		BSA + PHP	4.63 ± 0.05
	-	4.67 ± 0.07		-	4.97 ± 0.17		-	4.97 ± 0.20
7a	BSA + IBP	3.37 ± 0.09	**7b**	BSA + IBP	3.20 ± 0.08	**7c**	BSA + IBP	3.50 ± 0.14
	BSA + PHP	4.20 ± 0.11		BSA + PHP	4.39 ± 0.07		BSA + PHP	4.58 ± 0.09
	-	4.91 ± 0.05						
9a	BSA + IBP	3.50 ± 0.09						
	BSA + PHP	4.55 ± 0.10						

The binding interactions between the tested compounds and BSA were studied by the molecular docking method. The simulated results were listed in Table 8. The results revealed that the binding free energy for all of the compounds within the hydrophobic cavity in site II (m) of BSA was more negative than that within the hydrophobic cavity in site I and site II(l). This indicates that site II (m) is favorable. The value of electrostatic energy (ΔE_3) is much less than ΔE_2. It can indicate that the main interactions are van der Waals and hydrogen bonding interactions. The position of the compounds with the lowest binding free energy from all of the studied series in site II (m) compared to *Ibuprofen* is shown in Figure 12. The compounds are surrounded by various kinds of residues (Figure 13). Hydrogen bonds with Arg208, Leu326, Leu346 are formed. The π-sigma and other hydrophobic interactions are observed.

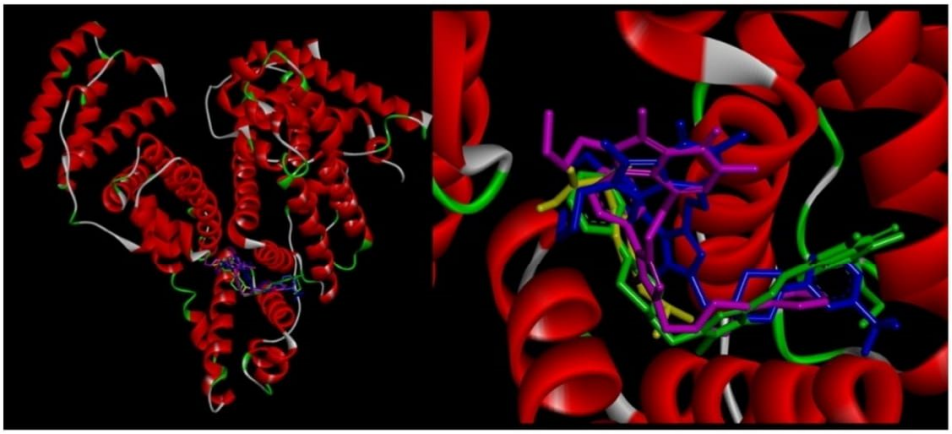

Figure 12. Docking poses of **4a** (pink), **4b** (green), **5c** (blue) and *Ibuprofen* (yellow) inside BSA site II (m).

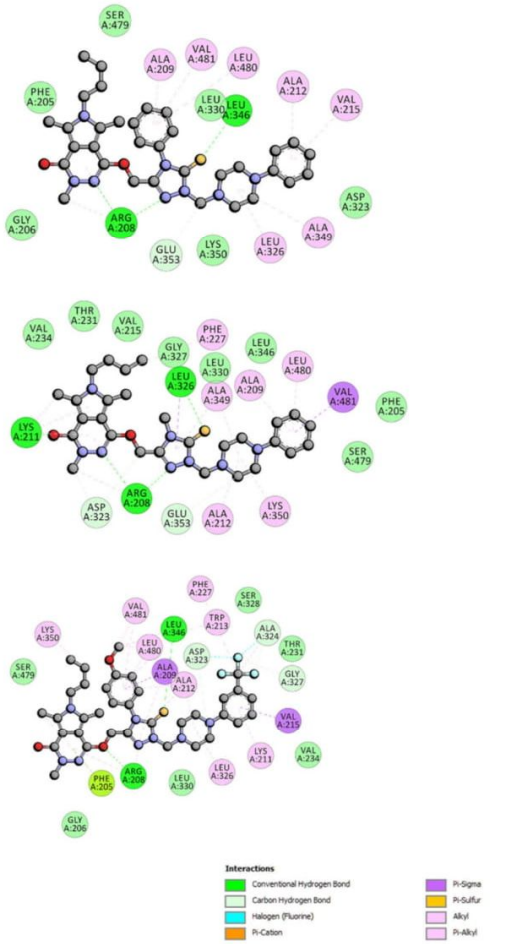

Figure 13. Two-dimensional interaction plot of **4b**, **4a**, and **5c** with BSA in site 2 (m).

Table 8. Energies of the binding complexes BSA with studied compounds obtained from molecular docking.

	Binding Site	ΔG° [kJmol^{-1}]	ΔE_1 [kJmol^{-1}]	ΔE_2 [kJmol^{-1}]	ΔE_3 [kJmol^{-1}]
	site I	−31.02	−42.22	−37.66	−4.56
4a	site II(m)	−40.08	−51.33	−46.73	−4.60
	site II(l)	−27.42	−38.66	−39.88	1.21
	site I	−29.93	−42.38	−39.00	−3.38
5a	site II(m)	−38.22	−50.74	−46.89	−3.85
	site II(l)	−28.88	−41.38	−42.38	1.00
	site I	−30.18	−42.79	−38.67	−4.10
6a	site II(m)	−38.03	−49.28	−46.48	−2.80
	site II(l)	−31.30	−42.55	−43.72	1.17
	site I	−30.51	−43.01	−42.93	−0.04
7a	site II(m)	−35.69	−48.20	−47.36	−0.84
	site II(l)	−28.55	−41.04	−40.38	−0.67
	site I	−31.06	−43.55	−43.35	−0.21
9a	site II(m)	−35.44	−47.95	−47.19	−0.76
	site II(l)	−25.16	−37.62	−37.12	−0.50
	site I	−35.53	−47.98	−44.02	−4.01
4b	site II(m)	−41.17	−53.62	−50.20	−3.43
	site II(l)	−25.37	−37.87	−38.03	0.20
	site I	−32.02	−45.73	−41.05	−4.68
5b	site II(m)	−39.54	−53.30	−50.95	−2.30
	site II(l)	−30.47	−44.18	−45.06	0.84
	site I	−33.56	−46.02	−41.08	−4.22
6b	site II(m)	−41.17	−53.63	−51.00	−2.63
	site II(l)	−28.30	−40.76	−39.67	−1.08
	site I	−29.30	−43.01	−42.64	−0.37
7b	site II(m)	−39.67	−53.38	−52.83	−0.55
	site II(l)	−23.57	−37.28	−37.57	0.29
	site I	−34.48	−48.19	−43.76	−4.43
4c	site II(m)	−38.79	−52.50	−49.87	−2.63
	site II(l)	−28.34	−45.01	−43.09	1.08
	site I	−31.51	−46.48	−42.18	−4.26
5c	site II(m)	−42.48	−57.81	−54.88	−2.93
	site II(l)	−22.40	−37.37	−39.17	1.80
	site I	−31.77	−45.48	−42.39	−3.09
6c	site II(m)	−37.20	−50.91	−47.82	−3.09
	site II(l)	−24.03	−37.75	−36.12	−1.63
	site I	−27.21	−42.17	−41.08	−1.09
7c	site II(m)	−38.12	−53.08	−52.37	−0.71
	site II(l)	−33.89	−48.86	−48.91	0.05

ΔG°—binding free energy; ΔE_1—intermolecular interaction energy, which is the sum of van der Waals energy, hydrogen bonding energy, desolvation free energy and electrostatic energy; ΔE_2—the sum of van der Waals energy, hydrogen bonding energy and desolvation free energy; ΔE_3—electrostatic energy.

2.7. In Silico Pharmacokinetic and Druglikeness Prediction

The derivatives **4a-7a**, **9a**, **4b-7b**, **4c-7c** were predicted for their possible pharmacokinetic (absorption distribution metabolism excretion; ADME) and drug-likeness properties using the SWISSADME server (http://www.swissadme.ch/index.php, accessed on 9 September 2021). The simulated results concerning the physicochemical features in the context of the Lipinski's rule of five (Ro5) [59] are presented in the Table 9. The compounds **4a-6a**, **4b** and **6b** meet the conditions of the Ro5, and therefore are supposed to show good oral bioavailability and membrane permeability. These findings are supported by the

results collected in Table 10. Most of the investigated molecules are predicted to be highly absorbed through the gastrointestinal (GI) tract. On the other hand, none of them are expected to cross blood–brain barrier (BBB). The water solubility was found to be rather poor (Table 10).

Table 9. Predicted physicochemical properties of studied compounds using SWISSADME server.

Compound	Physicochemical Properties—Lipinski's Rule of Five (Ro5)				
	#H-Bond Acceptors	#H-Bond Donors	Log $P_{o/w}$ (MLOGP)	MW [g/mol]	#Violations
4a	5	0	2.88	550.72	1
5a	8	0	3.36	618.72	1
6a	5	0	3.07	564.75	1
7a	6	0	2.99	578.73	2
9a	6	0	3.18	592.76	2
4b	5	0	3.89	612.79	1
5b	8	0	4.35	680.79	2
6b	5	0	4.08	626.81	1
7b	5	0	3.99	640.80	2
4c	6	0	3.58	642.81	2
5c	9	0	4.03	710.81	2
6c	6	0	3.76	656.84	2
7c	7	0	3.68	670.82	2

Table 10. Predicted ADME parameters of studied compounds using SWISSADME server.

Compound	Pharmacokinetics			
	GI Absorption	BBB Permeant	P-gp Substrate	Water Solubility
4a	High	No	Yes	Moderately soluble
5a	High	No	Yes	Poorly soluble
6a	High	No	Yes	Moderately soluble
7a	High	No	Yes	Poorly soluble
9a	High	No	Yes	Poorly soluble
4b	High	No	Yes	Poorly soluble
5b	Low	No	Yes	Poorly soluble
6b	High	No	Yes	Poorly soluble
7b	Low	No	Yes	Poorly soluble
4c	High	No	Yes	Poorly soluble
5c	Low	No	Yes	Poorly soluble
6c	High	No	Yes	Poorly soluble
7c	Low	No	Yes	Poorly soluble

According to the results presented in Table 11, the derivatives **4a-6a**, **4b**, **6b** not only do not violate the Lipinski's rule of five, but also fulfill the descriptors of Veber's rule [59,60]. This factors, alongside with the promising bioavailability score and calculated values of topological polar surface area (TPSA) (<140 $Å^2$) [61], can suggest that our compounds could be easily transported through biological membranes.

Table 11. Predicted drug-likeness properties of studied compounds using SWISSADME server.

Compound	Drug-Likeness			
	Lipinski	Veber	Bioavailability Score	TPSA [Å^2]
4a	Yes, 1 violation	Yes	0.55	110.37
5a	Yes, 1 violation	Yes	0.55	110.37
6a	Yes, 1 violation	Yes	0.55	110.37
7a	No, 2 violations	No, 1 violation	0.17	128.61
9a	No, 2 violations	No, 1 violation	0.17	128.61
4b	Yes, 1 violation	Yes	0.55	110.37
5b	No, 2 violations	No, 1 violation	0.17	110.37
6b	Yes, 1 violation	Yes	0.55	110.37
7b	No, 2 violations	No, 1 violation	0.17	128.61
4c	No, 2 violations	No, 1 violation	0.17	119.60
5c	No, 2 violations	No, 1 violation	0.17	119.60
6c	No, 2 violations	No, 1 violation	0.17	119.60
7c	No, 2 violations	No, 1 violation	0.17	137.84

3. Materials and Methods

3.1. Chemistry

3.1.1. Instrumentation and Chemicals

All of the chemicals, solvents and reagents used during chemical synthesis, purification and other experiments were delivered by commercially available suppliers (Alchem, Wrocław, Poland; Chemat, Gdańsk, Poland; Archem, Łany, Poland) and were used without further purification. Dry solvents were received according to the standard procedures. The reaction progress was monitored using the thin-layer chromatography (TLC) technique on silica-gel-60-F254-coated TLC plates, which were observed in UV light at 254 or 366 nm. The melting points of all of the new compounds were determined on the Electrothermal Mel-Temp 1101D apparatus (Cole-Parmer, Vernon Hills, IL, USA) using the open capillary method and were uncorrected. The ^{1}H NMR (300 MHz) and ^{13}C NMR (75 MHz) spectra were recorder on the Bruker 300 MHz NMR spectrometer (Bruker Analytische Messtechnik GmbH, Rheinstetten, Germany). The samples were dissolved in $CDCL_3$ or DMSO-d_6, and tetramethylsilane (TMS) was used as an internal reference. Chemical shifts (δ) were reported in ppm. The infrared (IR) spectra were determined on the Nicolet iS50 FT-IR Spectrometer (Thermo Fisher Scientific, Waltham, MA, USA). The samples were applied as solids, and the frequencies were reported in cm^{-1}. Mass spectra (MS) were recorded using the Bruker Daltonics Compact ESI-Mass Spectrometer (Bruker Daltonik, GmbH, Bremen, Germany), operating in the positive ion mode. The analyzed compounds were dissolved in a methanol–chloroform mixture. All of the new reported derivatives were determined to have purities of >95% by the above-mentioned methods, unless stated otherwise.

3.1.2. Chemical Synthesis

The synthesis protocols and experimental data for compound **1** and all of the intermediates have already been reported [34].

General Procedure for Preparation of *N*-Substituted(aminothioxomethyl)hydrazide Derivatives of Pyrrolo[3,4-*d*]pyridazinone (**2a-c**)

The 2-(6-butyl-3,5,7-trimethyl-4-oxo-pyrrolo[3,4-*d*]pyridazin-1-yl)oxyacetohydrazide **1** (0.001 mol) was suspended in anhydrous ethanol (25 mL), and the mixture was heated under reflux until the hydrazide dissolved completely. Then, the appropriate *N*-substituted isothiocyanate (0.0011 mol) was added, and the reflux was continued for a further 0.5–2 h till the product precipitated. Finally, the mixture was cooled down, and the solid was filtered off, thoroughly washed with ethanol and purified by crystallization from this solvent.

2a:1-[[2-(6-butyl-3,5,7-trimethyl-4-oxo-pyrrolo[3,4-*d*]pyridazin-1-yl)oxyacetyl]amino]-3-methyl-thiourea

Yield: 87.56%; m.p.: 207–209 °C;

FT-IR (selected lines, γ_{max}, cm^{-1}): 3263 (N-H), 2960, 2937, 2875 (C-H aliph.), 1698 (C=O), 1372 (C=S), 1231 (C-O), ^{1}H NMR (300 MHz, DMSO-d_6) δ: 0.88–0.93 (m, 3H, -CH_2-CH_2 CH_2-CH_3), 1.27–1.35 (m, 2H, -CH_2-CH_2 CH_2-CH_3), 1.57 (m, 2H, -CH_2-CH_2 CH_2-CH_3), 2.51 (s, 3H, 7-CH_3), 2.58 (s, 3H, 5-CH_3), 2.85 (s, 3H, *N*-CH_3), 3.38 (s, 3H, 3-CH_3), 3.94–3.99 (m, 2H, -CH_2-CH_2 CH_2-CH_3), 4.70 (s, 2H, *O*-CH_2-); 7.88 (s, 1H, *N*H), 9.31 (s, 1H, *N*H), 9.96 (s, 1H, *N*H); ^{13}C NMR (75 MHz, DMSO-d_6) δ: 10.65, 11.33, 13.99, 19.91, 31.27, 32.06, 37.04, 63.74, 108.00, 111.23, 123.58, 129.07, 148.57, 158.46, 167.62, 182.59; MS (ESI-MS) (*m*/*z*): calcd. for $C_{17}H_{26}N_6O_3S$ $[L+H]^+$: 395.1860; found: 395.1839.

2b:1-[[2-(6-butyl-3,5,7-trimethyl-4-oxo-pyrrolo[3,4-*d*]pyridazin-1-yl)oxyacetyl]amino]-3-phenyl-thiourea

Yield: 89.88%; m.p.: 214–216 °C;

FT-IR (selected lines, γ_{max}, cm^{-1}): 3323, 3237 (N-H), 3049 (C-H arom.), 2961, 2938, 2876 (C-H aliph.), 1689 (C=O), 1360 (C=S); ^{1}H NMR (300 MHz, DMSO-d_6) δ: 0.88–0.93 (m, 3H, -CH_2-CH_2 CH_2-CH_3), 1.28–1.35 (m, 2H, -CH_2-CH_2 CH_2-CH_3), 1.58 (m, 2H, -CH_2-CH_2 CH_2-CH_3), 2.53 (s, 3H, 7-CH_3), 2.58 (s, 3H, 5-CH_3), 3.36 (s, 3H, 3-CH_3), 3.94–3.99 (m, 2H, -CH_2-CH_2 CH_2-CH_3), 4.77 (s, 2H, *O*-CH_2-); 7.16–7.18 (m, 1H, Ar-H), 7.30–7.42 (m, 4H, Ar-H), 9.56 (s, 1H, *N*H), 9.71 (s, 1H, *N*H), 10.18 (s, 1H, *N*H); ^{13}C NMR (75 MHz, DMSO-d_6) δ: 10.65, 11.36, 13.99, 19.91, 32.06, 37.03, 63.84, 108.01, 111.25, 123.57, 125.64, 128.56, 129.09, 139.50, 148.57, 158.46; MS (ESI-MS) (*m*/*z*): calcd. for $C_{22}H_{28}N_6O_3S$ $[L+H]^+$: 457.2016; found: 457.1985.

2c:1-[[2-(6-butyl-3,5,7-trimethyl-4-oxo-pyrrolo[3,4-*d*]pyridazin-1-yl)oxyacetyl]amino]-3-[(4-methoxy)phenyl]-thiourea

Yield: 94.12%; m.p.: 217–219 °C;

FT-IR (selected lines, γ_{max}, cm^{-1}): 3321, 3219 (N-H), 3051 (C-H arom.), 2957, 2872, 2836 (C-H aliph.), 1678 (C=O), 1348 (C=S); ^{1}H NMR (300 MHz, DMSO-d_6) δ: 0.88–0.93 (m, 3H, -CH_2-CH_2 CH_2-CH_3), 1.28–1.35 (m, 2H, -CH_2-CH_2 CH_2-CH_3), 1.58 (m, 2H, -CH_2-CH_2 CH_2-CH_3), 2.53 (s, 3H, 7-CH_3), 2.58 (s, 3H, 5-CH_3), 3.36 (s, 3H, 3-CH_3), 3.73 (s, 3H, *O*-CH_3), 3.94–3.97 (m, 2H, -CH_2-CH_2 CH_2-CH_3), 4.76 (s, 2H, *O*-CH_2-); 6.87–6.90 (m, 2H, Ar-H), 7.22–7.25 (m, 2H, Ar-H), 9.44 (s, 1H, *N*H), 9.61 (s, 1H, *N*H), 10.14 (s, 1H, *N*H); ^{13}C NMR (75 MHz, DMSO-d_6) δ: 10.65, 11.35, 13.99, 19.91, 32.06, 37.03, 55.67, 63.84, 108.02, 111.25, 113.78 123.57, 127.77, 129.08, 132.31, 148.59, 157.32, 158.46, 167.69; MS (ESI-MS) (*m*/*z*): calcd. for $C_{23}H_{30}N_6O_4S$ $[L+H]^+$: 487.2122; found: 487.2087.

General Procedure for Preparation of 4-Substituted-2*H*-1,2,4-triazole Derivatives of Pyrrolo[3,4-*d*]pyridazinone (**3a-c**)

The appropriate *N*-substituted-(aminothioxomethyl)hydrazide derivative of pyrrolo [3,4-*d*]pyridazinone (**2a-c**) (0.0001 mol) was dissolved in a 5% aqueous solution of sodium hydroxide (25 mL), and the mixture was stirred and refluxed for about 2–3 h. Afterward, it was poured onto crushed ice and carefully acidified to pH 2–3 with 7.5% hydrochloric acid (aq), resulting in the formation of a white or yellowish solid of adequate 4-substituted-1,2,4-triazole derivative (**3a-c**). Finally, the afforded precipitate was filtered off, washed with ice-cold water and recrystallized from ethanol.

3a:6-butyl-3,5,7-trimethyl-1-[(4-methyl-3-thioxo-2*H*-1,2,4-triazol-5-yl)methoxy]pyrrolo [3,4-*d*]pyridazin-4-one

Yield: 83.12%; m.p.: 117–120 °C;

FT-IR (selected lines, γ_{max}, cm^{-1}): 3425 (N-H), 3120, 3050 (C-H arom.), 2935, 2871(C-H aliph.), 1544 (C=N), 1340 (C=S); ^{1}H NMR (300 MHz, DMSO-d_6) δ: 0.86–0.91 (m, 3H, -CH_2-CH_2 CH_2-CH_3), 1.26–1.33 (m, 2H, -CH_2-CH_2 CH_2-CH_3), 1.56 (m, 2H, -CH_2-CH_2 CH_2-CH_3), 2.42 (s, 3H, 7-CH_3), 2.57 (s, 3H, 5-CH_3), 3.40 (s, 3H, 3-CH_3), 3.50 (s, 3H, triazole-*N*-CH_3),

3.92–3.97 (m, 2H, -$\underline{CH_2}$-CH_2 CH_2-CH_3), 5.30 (s, 2H, *O*-CH_2-), 13.82 (s, 1H, *N*H); ^{13}C NMR (75 MHz, DMSO-d_6) δ: 10.64, 11.18, 13.97, 19.89, 30.65, 32.01, 37.03, 43.83, 58.09, 107.62, 111.18, 123.42, 129.38, 148.07, 148.89, 158.40, 168.05; HR-MS (ESI-MS) (*m*/*z*): calcd. for $C_{17}H_{24}N_6O_2S$ [L+H]$^+$: 377.1754; found: 377.1736.

3b:6-butyl-3,5,7-trimethyl-1-[(4-phenyl-3-thioxo-2*H*-1,2,4-triazol-5-yl)methoxy]pyrrolo [3,4-*d*]pyridazin-4-one

Yield: 81.69%; m.p.: 123–125 °C;

FT-IR (selected lines, γ_{max}, cm^{-1}): 3414 (N-H), 3037 (C-H arom.), 2957, 2928, 2871 (C-H aliph.), 1543 (C=N); ^{1}H NMR (300 MHz, DMSO-d_6) δ: 0.86–0.91 (m, 3H, -CH_2-CH_2 CH_2-$\underline{CH_3}$), 1.24–1.31 (m, 2H, -CH_2-CH_2 $\underline{CH_2}$-CH_3), 1.53 (m, 2H, -CH_2-$\underline{CH_2}$ CH_2-CH_3), 2.25 (s, 3H, 7-CH_3), 2.53 (s, 3H, 5-CH_3), 3.32 (s, 3H, 3-CH_3), 3.88–3.93 (m, 2H, -$\underline{CH_2}$-CH_2 CH_2-CH_3), 5.12 (s, 2H, *O*-CH_2-); 7.45 (m, 5H, Ar-H), 14.04 (s, 1H, *N*H); ^{13}C NMR (75 MHz, DMSO-d_6) δ:10.59, 11.20, 13.97, 19.86, 31.97, 36.95, 43.76, 57.85, 107.38, 111.05, 123.31, 128.28, 129.19, 129.69, 129.91, 133.86, 147.76, 148.60, 158.28, 168.90; MS (ESI-MS) (*m*/*z*): calcd. for $C_{22}H_{26}N_6O_2S$ [L+H]$^+$: 439.1911; found: 439.1874.

3c:6-butyl-3,5,7-trimethyl-1-[[4-(4-methoxy)phenyl-3-thioxo-2*H*-1,2,4-triazol-5-yl] methoxy]pyrrolo[3,4-*d*]pyridazin-4-one

Yield: 84.49%; m.p.: 129–131 °C;

FT-IR (selected lines, γ_{max}, cm^{-1}): 3414 (N-H), 3041 (C-H arom.), 2956, 2931, 2872 (C-H aliph.), 1543 (C=N);^{1}H NMR (300 MHz, DMSO-d_6) δ: 0.87–0.92 (m, 3H, -CH_2-CH_2 CH_2-$\underline{CH_3}$), 1.31 (m, 2H, -CH_2-CH_2 $\underline{CH_2}$-CH_3), 1.54 (m, 2H, -CH_2-$\underline{CH_2}$ CH_2-CH_3), 2.29 (s, 3H, 7-CH_3), 2.54 (s, 3H, 5-CH_3), 3.31 (s, 3H, 3-CH_3), 3.74 (s, 3H, Ar-*O*-CH_3) 3.92 (m, 2H, -$\underline{CH_2}$-CH_2 CH_2-CH_3), 5.12 (s, 2H, *O*-CH_2-); 6.96–6.99 (m, 2H, Ar-H), 7.31–7.34 (m, 2H, Ar-H), 13.99 (s, 1H, *N*H); ^{13}C NMR (75 MHz, DMSO-d_6) δ:10.59, 11.20, 13.98, 19.88, 31.99, 36.95, 43.78, 55.84, 57.85, 107.46, 111.06, 114.79, 115.18, 123.34, 126.32, 129.19, 129.54, 129.97, 147.83, 148.88, 158.29, 160.13, 169.12; MS (ESI-MS) (*m*/*z*): calcd. for $C_{13}H_{28}N_6O_3S$ [L+H]$^+$: 469.2016; found: 469.1976.

General Procedure for Preparation of Mannich Base-Type Derivatives of Pyrrolo[3,4-*d*]pyridazinone (**4a-c-6a-c**)

Aqueous formaldehyde of 37% (0.01 mol, ~1mL) was added to the solution of adequate 4-substituted-1,2,4-triazole derivative of pyrrolo[3,4-*d*]pyridazinone (**3a**, **3b** or **3c**) (0.001 mol) in methanol (30 mL). The mixture was stirred at room temperature (RT) for 30 min. Subsequently, a corresponding aryl piperazine derivative (0.0015 mol) was added, and the stirring was continued for a further several hours at RT. The mixture was left overnight. The formed precipitate was filtered off, thoroughly washed with cold methanol and purified by crystallization from methanol.

4a:6-butyl-3,5,7-trimethyl-1-[[4-methyl-2-[(4-phenylpiperazin-1-yl)methyl]-3-thioxo-2*H*-1,2,4-triazol-5-yl]methoxy]pyrrolo[3,4-*d*]pyridazin-4-one

Yield: 72.35%; m.p.: 186–188 °C;

FT-IR (selected lines, γ_{max}, cm^{-1}): 3019 (C-H arom.), 2962, 2937, 2874 (C-H aliph.), 1549 (C=N) 1272 (C=S); ^{1}H NMR (300 MHz, $CDCl_3$) δ: 0.94–0.99 (m, 3H, -CH_2-CH_2 CH_2-$\underline{CH_3}$), 1.34–1.41 (m, 2H, -CH_2-CH_2 $\underline{CH_2}$-CH_3), 1.60–1.66 (m, 2H, -CH_2-$\underline{CH_2}$ CH_2-CH_3), 2.43 (s, 3H, 7-CH_3), 2.68 (s, 3H, 5-CH_3), 2.98–2.99 (m, 4H, CH_2—piperazine), 3.18–3.19 (m, 4H, CH_2—piperazine), 3.57 (s, 3H, 3-CH_3), 3.67 (s, 3H, triazole-*N*-CH_3), 3.94–3.97 (m, 2H, -$\underline{CH_2}$-CH_2 CH_2-CH_3), 5.21 (s, 2H, *N*-CH_2-*N*) 5.31 (s, 2H, *O*-CH_2-); 6.82–6.91 (m, 3H, Ar-H), 7.22–7.27 (m, 2H, Ar-H); ^{13}C NMR (75 MHz, $CDCl_3$) δ: 10.65, 11.30, 13.69, 20.04, 31.69, 32.32, 37.05, 43.99, 49.29, 50.42, 57.54, 69.49, 108.05, 111.84, 116.32, 119.89, 122.24, 129.10, 129.43, 146.76, 147.95, 151.28, 159.17, 169.74; HRMS (ESI-MS) (*m*/*z*): calcd. for $C_{28}H_{38}N_8O_2S$ [L+H]$^+$: 551.2911; found: 551.2894.

5a:6-butyl-3,5,7-trimethyl-1-[[4-methyl-2-[[4-[3-(trifluoromethyl)phenyl]piperazin-1-yl]methyl]-3-thioxo-2*H*-1,2,4-triazol-5-yl]methoxy]pyrrolo[3,4-*d*]pyridazin-4-one

Yield: 64.84%; m.p.: 198–200 °C;

FT-IR (selected lines, γ_{max}, cm^{-1}): 2963, 2935, 2876, 3843 (C-H aliph.), 1650 (C=N), 1242 (C=S); ^{1}H NMR (300 MHz, $CDCl_3$) δ: 0.94–0.98 (m, 3H, -CH_2-CH_2 CH_2-CH_3), 1.34–1.41 (m, 2H, -CH_2-CH_2 CH_2-CH_3), 1.60–1.63 (m, 2H, -CH_2-CH_2 CH_2-CH_3), 2.42 (s, 3H, 7-CH_3), 2.68 (s, 3H, 5-CH_3), 2.96–2.99 (m, 4H, CH_2—piperazine), 3.22–3.25 (m, 4H, CH_2—piperazine), 3.57 (s, 3H, 3-CH_3), 3.67 (s, 3H, triazole-*N*-CH_3), 3.87–3.92 (m, 2H, -CH_2-CH_2 CH_2-CH_3), 5.21 (s, 2H, *N*-CH_2-*N*) 5.31 (s, 2H, *O*-CH_2-); 7.01–7.07 (m, 3H, Ar-H), 7.30–7.35 (m, 1H, Ar-H); ^{13}C NMR (75 MHz, $CDCl_3$) δ: 10.65, 11.27, 13.67, 20.04, 31.71, 32.32, 37.04, 43.99, 48.77, 50.23, 57.51, 69.39, 108.05, 111.83, 112.39, 115.99, 118.93, 122.21, 129.45, 129.56, 131.22, 131.64, 146.84, 147.91, 151.32, 159.16, 169.78; MS (ESI-MS) (*m*/*z*): calcd. for $C_{29}H_{37}F_3N_8O_2S$ $[L+H]^+$: 619.2785; found: 619.2748.

6a:6-butyl-3,5,7-trimethyl-1-[[4-methyl-2-[[4-[(4-methyl)phenyl]piperazin-1-yl]methyl]-3-thioxo-2*H*-1,2,4-triazol-5-yl]methoxy]pyrrolo[3,4-*d*]pyridazin-4-one

Yield: 68.98%; m.p.: 181–183 °C;

FT-IR (selected lines, γ_{max}, cm^{-1}): 2962, 2933, 2878, 2855, 2826 (C-H aliph.), 1633 (C=N), 1248 (C=S); ^{1}H NMR (300 MHz, $CDCl_3$) δ: 0.94–0.98 (m, 3H, -CH_2-CH_2 CH_2-CH_3), 1.34–1.42 (m, 2H, -CH_2-CH_2 CH_2-CH_3), 1.63 (m, 2H, -CH_2-CH_2 CH_2-CH_3), 2.26 (s, 3H, Ar-CH_3), 2.43 (s, 3H, 7-CH_3), 2.67 (s, 3H, 5-CH_3), 2.99 (m, 4H, CH_2—piperazine), 3.15 (m, 4H, CH_2—piperazine), 3.57 (s, 3H, 3-CH_3), 3.67 (s, 3H, triazole-*N*-CH_3), 3.87–3.92 (m, 2H, -CH_2-CH_2 CH_2-CH_3), 5.21 (s, 2H, *N*-CH_2-*N*) 5.31 (s, 2H, *O*-CH_2-); 6.85 (m, 2H, Ar-H), 7.05–7.08 (m, 2H, Ar-H); ^{13}C NMR (75 MHz, $CDCl_3$) δ: 10.66, 11.33, 13.70, 20.05, 20.44 31.70, 32.33, 37.06, 43.99, 50.34, 57.54, 69.43, 108.04, 111.82, 112.26, 116.81, 122.26, 129.41, 129.67, 146.77, 147.95, 159.18, 169.72; MS (ESI-MS) (*m*/*z*): calcd. for $C_{29}H_{40}N_8O_2S$ $[L+H]^+$: 565.3068; found: 565.3019.

4b:6-butyl-3,5,7-trimethyl-1-[[4-phenyl-2-[(4-phenylpiperazin-1-yl)methyl]-3-thioxo-2*H*-1,2,4-triazol-5-yl]methoxy]pyrrolo[3,4-*d*]pyridazin-4-one

Yield: 69.02%; m.p.: 129–131 °C;

FT-IR (selected lines, γ_{max}, cm^{-1}): 2932, 2828 (C-H aliph.), 1543 (C=N), 1269 (C=S); ^{1}H NMR (300 MHz, $CDCl_3$) δ: 0.94–0.99 (m, 3H, -CH_2-CH_2 CH_2-CH_3), 1.36–1.38 (m, 2H, -CH_2-CH_2 CH_2-CH_3), 1.61 (m, 2H, -CH_2-CH_2 CH_2-CH_3), 2.34 (s, 3H, 7-CH_3), 2.65 (s, 3H, 5-CH_3), 3.06 (m, 4H, CH_2—piperazine), 3.22 (m, 4H, CH_2—piperazine), 3.46 (s, 3H, 3-CH_3), 3.84–3.89 (m, 2H, -CH_2-CH_2 CH_2-CH_3), 5.16 (s, 2H, *N*-CH_2-*N*) 5.30 (s, 2H, *O*-CH_2-); 6.87–6.94 (m, 3H, Ar-H), 7.24–7.29 (m, 2H, Ar-H) 7.39 (m, 2H, Ar-H); 7.45–7.46 (m, 3H, Ar-H); ^{13}C NMR (75 MHz, $CDCl_3$) δ: 10.62, 11.23, 13.71, 20.03, 32.31, 36.97, 43.92, 49.36, 50.52, 57.09, 69.64, 108.05, 111.74, 116.39, 119.98, 122.18, 127.67 129.13, 129.63, 130.03, 133.80 146.79, 147.81, 151.31, 159.11, 170.52; MS (ESI-MS) (*m*/*z*): calcd. for $C_{33}H_{40}N_8O_2S$ $[L+H]^+$: 613.3068; found: 613.2995.

5b:6-butyl-3,5,7-trimethyl-1-[[4-phenyl-2-[[4-[3-(trifluoromethyl)phenyl]piperazin-1-yl]methyl]-3-thioxo-2*H*-1,2,4-triazol-5-yl]methoxy]pyrrolo[3,4-*d*]pyridazin-4-one

Yield: 65.29%; m.p.: 118–120 °C;

FT-IR (selected lines, γ_{max}, cm^{-1}): 2935, 2872, 2850 (C-H aliph.), 1268 (C=S); ^{1}H NMR (300 MHz, $CDCl_3$) δ: 0.94–0.99 (m, 3H, -CH_2-CH_2 CH_2-CH_3), 1.33–1.40 (m, 2H, -CH_2-CH_2 CH_2-CH_3), 1.59–1.61 (m, 2H, -CH_2-CH_2 CH_2-CH_3), 2.33 (s, 3H, 7-CH_3), 2.65 (s, 3H, 5-CH_3), 3.05–3.07 (m, 4H, CH_2—piperazine), 3.24–3.26 (m, 4H, CH_2—piperazine), 3.46 (s, 3H, 3-CH_3), 3.84–3.89 (m, 2H, -CH_2-CH_2 CH_2-CH_3), 5.16 (s, 2H, *N*-CH_2-*N*) 5.30 (s, 2H, *O*-CH_2-); 7.04–7.09 (m, 3H, Ar-H), 7.32–7.39 (m, 3H, Ar-H); 7.46–7.48 (m, 3H, Ar-H); ^{13}C NMR (75 MHz, $CDCl_3$) δ: 10.62, 11.20, 13.69, 20.02, 32.31, 36.96, 43.92, 48.84, 50.34, 57.08, 69.54, 108.01, 111.72, 112.44, 116.01, 119.00, 122.15, 126.08, 127.65, 129.15, 129.60, 129.66, 130.07, 131.23, 131.65, 133.75, 146.87, 147.78, 151,37, 159.09, 170.52; MS (ESI-MS) (*m*/*z*): calcd. for $C_{34}H_{39}F_3N_8O_2S$ $[L+H]^+$: 681.2942; found: 681.2864.

6b:6-butyl-3,5,7-trimethyl-1-[[4-phenyl-2-[[4-[(4-methyl)phenyl]piperazin-1-yl] methyl]-3-thioxo-2*H*-1,2,4-triazol-5-yl]methoxy]pyrrolo[3,4-*d*]pyridazin-4-one

Yield: 61.74%; m.p.: 108–111 °C;

FT-IR (selected lines, γ_{max}, cm^{-1}): 2959, 2935, 2860, 2832 (C-H aliph.), 1618 (C=N), 1234 (C=S); ^{1}H NMR (300 MHz, $CDCl_3$) δ: 0.94–0.99 (m, 3H, -CH_2-CH_2 CH_2-CH_3), 1.36–1.38 (m, 2H, -CH_2-CH_2 CH_2-CH_3), 1.61 (m, 2H, -CH_2-CH_2 CH_2-CH_3), 2.27 (s, 3H, Ar-CH_3), 2.34 (s, 3H, 7-CH_3), 2.66 (s, 3H, 5-CH_3), 3.07 (m, 4H, CH_2—piperazine), 3.18 (m, 4H, CH_2—piperazine), 3.46 (s, 3H, 3-CH_3), 3.84–3.90 (m, 2H, -CH_2-CH_2 CH_2-CH_3), 5.16 (s, 2H, *N*-CH_2-*N*) 5.30 (s, 2H, *O*-CH_2-); 6.86 (m, 2H, Ar-H), 7.06–7.09 (m, 2H, Ar-H); 7.39 (m, 2H, Ar-H), 7.45–7.46 (m, 3H, Ar-H); ^{13}C NMR (75 MHz, $CDCl_3$) δ: 10.63, 11.26, 13.71, 20.04, 32.32, 36.97, 43.92, 50.47, 57.09, 69.60, 108.02, 111.74, 116.84, 122.20, 127.68 129.11, 129.64, 129.69, 130.02, 133.80, 146.80, 147.81, 159.11, 170.52; MS (ESI-MS) (*m*/*z*): calcd. for $C_{34}H_{42}N_8O_2S$ $[L+H]^+$: 627.3224; found: 627.3176.

4c:6-butyl-1-[[4-(4-methoxyphenyl)-2-[(4-phenylpiperazin-1-yl)methyl]-3-thioxo-2*H*-1, 2,4-triazol-5-yl]methoxy]-3,5,7-trimethyl-pyrrolo[3,4-*d*]pyridazin-4-one

Yield: 71.07%; m.p.: 169–170 °C;

FT-IR (selected lines, γ_{max}, cm^{-1}): 2961, 2933, 2860, 2838 (C-H aliph.), 1651 (C=N); ^{1}H NMR (300 MHz, $CDCl_3$) δ: 0.94–0.99 (m, 3H, -CH_2-CH_2 CH_2-CH_3), 1.34–1.41 (m, 2H, -CH_2-CH_2 CH_2-CH_3), 1.62 (m, 2H, -CH_2-CH_2 CH_2-CH_3), 2.36 (s, 3H, 7-CH_3), 2.66 (s, 3H, 5-CH_3), 3.05–3.07 (m, 4H, CH_2—piperazine), 3.20–3.22 (m, 4H, CH_2—piperazine), 3.47 (s, 3H, 3-CH_3), 3.81 (s, 3H, *O*-CH_3) 3.85–3.90 (m, 2H, -CH_2-CH_2 CH_2-CH_3), 5.15 (s, 2H, *N*-CH_2-*N*) 5.29 (s, 2H, *O*-CH_2-); 6.84–6.95 (m, 5H, Ar-H), 7.24–7.28 (m, 4H, Ar-H); ^{13}C NMR (75 MHz, $CDCl_3$) δ: 10.62, 11.26, 13.72, 20.05, 32.33, 36.97, 43.94, 49.36, 50.52, 55.51, 57.11, 69.66, 108.08, 111.74, 114.83, 116.39, 119.97, 122.19, 126.21 129.13, 147.11, 147.88, 151.31, 159.11, 160.48, 170.75; HRMS (ESI-MS) (*m*/*z*): calcd. for $C_{34}H_{42}N_8O_3S$ $[L+H]^+$: 643.3173; found: 643.3194.

5c:6-butyl-1-[[4-(4-methoxyphenyl)-2-[[4-[3-(trifluoromethyl)phenyl]piperazin-1-yl] methyl]-3-thioxo-2*H*-1,2,4-triazol-5-yl]methoxy]-3,5,7-trimethyl-pyrrolo[3,4-*d*] pyridazin-4-one

Yield: 59.73%; m.p.: 163–165 °C;

FT-IR (selected lines, γ_{max}, cm^{-1}): 2964, 2935, 2870, 2840 (C-H aliph.), 1650 (C=N), 1248 (C=S); ^{1}H NMR (300 MHz, $CDCl_3$) δ: 0.94–0.99 (m, 3H, -CH_2-CH_2 CH_2-CH_3), 1.34–1.41 (m, 2H, -CH_2-CH_2 CH_2-CH_3), 1.62 (m, 2H, -CH_2-CH_2 CH_2-CH_3), 2.36 (s, 3H, 7-CH_3), 2.66 (s, 3H, 5-CH_3), 3.04 (m, 4H, CH_2—piperazine), 3.24–3.26 (m, 4H, CH_2—piperazine), 3.47 (s, 3H, 3-CH_3), 3.81 (s, 3H, *O*-CH_3), 3.85–3.90 (m, 2H, -CH_2-CH_2 CH_2-CH_3), 5.15 (s, 2H, *N*-CH_2-*N*) 5.29 (s, 2H, *O*-CH_2-); 6.92–6.95 (m, 2H, Ar-H), 7.04–7.09 (m, 3H, Ar-H), 7.29–7.37 (m, 3H, Ar-H); ^{13}C NMR (75 MHz, $CDCl_3$) δ: 10.61, 11.20, 13.68, 20.03, 32.32, 36.95, 43.93, 48.83, 50.34, 55.51, 57.10, 69.57, 108.09, 111.75, 112.42, 114.84, 116.04, 118.98, 122.15, 126.18, 128.83, 129.14, 129.59, 131.24, 147.18, 147.85, 151.37, 159.09, 160.51, 170.78; HRMS (ESI-MS) (*m*/*z*): calcd. for $C_{35}H_{41}F_3N_8O_3S$ $[L+H]^+$: 711.3047; found: 711.3031.

6c:6-butyl-1-[[4-(4-methoxyphenyl)-2-[[4-[(4-methyl)phenyl]piperazin-1-yl]methyl]-3-thioxo-2*H*-1,2,4-triazol-5-yl]methoxy]-3,5,7-trimethyl-pyrrolo[3,4-*d*]pyridazin-4-one

Yield: 74.21%; m.p.: 151–153 °C;

FT-IR (selected lines, γ_{max}, cm^{-1}): 2958, 2934, 2860, 2837 (C-H aliph.), 1651 (C=N), 1247 (C=S); ^{1}H NMR (300 MHz, $CDCl_3$) δ: 0.94–0.99 (m, 3H, -CH_2-CH_2 CH_2-CH_3), 1.36–1.41 (m, 2H, -CH_2-CH_2 CH_2-CH_3), 1.62 (m, 2H, -CH_2-CH_2 CH_2-CH_3), 2.27 (s, 3H, Ar-CH_3), 2.37 (s, 3H, 7-CH_3), 2.66 (s, 3H, 5-CH_3), 3.07 (m, 4H, CH_2—piperazine), 3.17 (m, 4H, CH_2—piperazine), 3.47 (s, 3H, 3-CH_3), 3.81 (s, 3H, *O*-CH_3) 3.85–3.90 (m, 2H, -CH_2-CH_2 CH_2-CH_3), 5.15 (s, 2H, *N*-CH_2-*N*) 5.29 (s, 2H, *O*-CH_2-); 6.85 (m, 2H, Ar-H), 6.92–6.95 (m, 2H, Ar-H), 7.07–7.09 (m, 2H, Ar-H), 7.25–7.29 (m, 2H, Ar-H); ^{13}C NMR (75 MHz, $CDCl_3$) δ: 10.63, 11.28, 13.72, 20.05, 20.46, 32.33, 36.97, 43.94, 50.43, 55.51, 57.11, 69.61, 108.08, 111.74, 114.82, 116.86,

117.24, 122.21, 126.22, 128.85, 129.10, 129.71, 147.12, 147.88, 159.11, 160.48, 170.75; HRMS (ESI-MS) (*m*/*z*): calcd. for $C_{35}H_{44}N_8O_3S$ [L+H]$^+$: 657.3330; found: 657.3316.

General Procedure for Preparation of S-Substituted Derivatives of Pyrrolo[3,4-*d*]pyridazinone (**7a-c-9a-c**)

The appropriate 4-substituted-1,2,4-triazole derivative of pyrrolo[3,4-*d*]pyridazinone (**3a**, **3b** or **3c**) (0.001 mol) was suspended in 30 mL of anhydrous ethanol in a round bottom flask. Next, the 1 mL of 1M sodium ethoxide (0.001 mol) and the appropriate 2-chloro-1-oxoethyl aryl piperazine derivative was added, and the mixture was refluxed for 4–6 h. TLC monitored the reaction progress. After the completion of synthesis, the mixture was cooled, and the precipitate was formed. Finally, the solid was filtered off, washed thoroughly with ethanol and, afterward, purified by crystallization from this solvent.

7a:6-butyl-3,5,7-trimethyl-1-[[4-methyl-3-[2-oxo-2-(4-phenylpiperazin-1-yl)ethyl] sulfanyl-2*H*-1,2,4-triazol-5-yl]methoxy]pyrrolo[3,4-*d*]pyridazin-4-one

Yield: 62.52%; m.p.: 183–184 °C;

FT-IR (selected lines, γ_{max}, cm^{-1}): 3054 (C-H arom.), 2961, 2922, 2873 (C-H aliph.), 1639 (C=O), 1268 (C=S); ^{1}H NMR (300 MHz, $CDCl_3$) δ: 0.93–0.98 (m, 3H, -CH_2-CH_2 CH_2-CH_3), 1.33–1.41 (m, 2H, -CH_2-CH_2 CH_2-CH_3), 1.59–1.62 (m, 2H, -CH_2-CH_2 CH_2-CH_3), 2.41 (s, 3H, 7-CH_3), 2.68 (s, 3H, 5-CH_3), 3.17–3.19 (m, 2H, CH_2—piperazine), 3.23 (m, 2H, CH_2—piperazine), 3.57 (s, 3H, 3-CH_3), 3.66 (s, 3H, triazole-*N*-CH_3), 3.78 (m, 4H, CH_2—piperazine), 3.86–3.91 (m, 2H, -CH_2-CH_2 CH_2-CH_3), 4.38 (s, 2H, *S*-CH_2) 5.44 (s, 2H, *O*-CH_2-); 6.92–6.94 (m, 3H, Ar-H), 7.28–7.31 (m, 2H, Ar-H); ^{13}C NMR (75 MHz, $CDCl_3$) δ: 10.64, 11.21, 13.68, 20.04, 30.54, 32.32, 36.57, 37.02, 42.21, 43.93, 46.11, 49.33, 49.74, 57.45, 108.27, 111.86, 116.80, 120.80, 122.29, 129.19, 129.29, 148.33, 151.80, 152.30, 159,19, 165.55; HRMS (ESI-MS) (*m*/*z*): calcd. for $C_{29}H_{38}N_8O_3S$ [L+H]$^+$: 579.2860; found: 579.2843.

8a:6-butyl-3,5,7-trimethyl-1-[[4-methyl-3-[2-oxo-2-[4-[3-(triflouromethyl)phenyl] piperazin-1-yl]ethyl]sulfanyl-2*H*-1,2,4-triazol-5-yl]methoxy]pyrrolo[3,4-*d*] pyridazin-4-one

Yield: 56.41%; m.p.: 201–202 °C;

FT-IR (selected lines, γ_{max}, cm^{-1}): 2964, 2934, 2919 (C-H aliph.) 1226 (C=S); ^{1}H NMR (300 MHz, $CDCl_3$) δ: 0.93–0.98 (m, 3H, -CH_2-CH_2 CH_2-CH_3), 1.33–1.41 (m, 2H, -CH_2-CH_2 CH_2-CH_3), 1.59–1.62 (m, 2H, -CH_2-CH_2 CH_2-CH_3), 2.42 (s, 3H, 7-CH_3), 2.68 (s, 3H, 5-CH_3), 3.23 (m, 2H, CH_2—piperazine), 3.31 (m, 2H, CH_2—piperazine), 3.57 (s, 3H, 3-CH_3), 3.68 (s, 3H, triazole-*N*-CH_3), 3.80–3.84 (m, 4H, CH_2—piperazine), 3.86–3.91 (m, 2H, -CH_2-CH_2 CH_2-CH_3), 4.41 (s, 2H, *S*-CH_2) 5.44 (s, 2H, *O*-CH_2-); 7.08–7.16 (m, 3H, Ar-H), 7.35–7.41 (m, 1H, Ar-H); ^{13}C NMR (75 MHz, $CDCl_3$) δ: 10.64, 11.22, 13.68, 20.04, 30.68, 32.32, 36.56, 37.02, 42.01, 43.94, 45.90, 48.85, 49.21, 57.33, 108.21, 111.83, 112.97, 117.10, 119.54, 122.29, 129.25, 129.79, 131.43, 131.85, 148.26, 150.69, 151.83, 152.31, 159,17, 165.51; MS (ESI-MS) (*m*/*z*): calcd. for $C_{30}H_{37}F_3N_8O_3S$ [L+H]$^+$: 647.2734; found: 647.2680.

9a:6-butyl-3,5,7-trimethyl-1-[[4-methyl-3-[2-oxo-2-[4-[4-(methyl)phenyl]piperazin-1-yl] ethyl]sulfanyl-2*H*-1,2,4-triazol-5-yl]methoxy]pyrrolo[3,4-*d*]pyridazin-4-one

Yield: 59.49%; m.p.: 190–191 °C;

FT-IR (selected lines, γ_{max}, cm^{-1}): 2960, 2919, 2851 (C-H aliph.), 1643 (C=O) 1227 (C=S); ^{1}H NMR (300 MHz, $CDCl_3$) δ: 0.93–0.98 (m, 3H, -CH_2-CH_2 CH_2-CH_3), 1.34–1.41 (m, 2H, -CH_2-CH_2 CH_2-CH_3), 1.62 (m, 2H, -CH_2-CH_2 CH_2-CH_3), 2.27 (s, 3H, Ar-CH_3), 2.41 (s, 3H, 7-CH_3), 2.68 (s, 3H, 5-CH_3), 3.11 (m, 4H, CH_2—piperazine), 3.57 (s, 3H, 3-CH_3), 3.66 (s, 3H, triazole-*N*-CH_3), 3.78 (m, 4H, CH_2—piperazine), 3.86–3.91 (m, 2H, -CH_2-CH_2 CH_2-CH_3), 4.38 (s, 2H, *S*-CH_2) 5.44 (s, 2H, *O*-CH_2-); 6.86 (m, 2H, Ar-H), 7.08–7.11 (m, 2H, Ar-H); ^{13}C NMR (75 MHz, $CDCl_3$) δ: 10.64, 11.22, 13.68, 20.04, 20.45 30.54, 32.32, 36.67, 37.03, 42.26, 43.93, 46.16, 49.88, 50.27, 57.46, 108.28, 111.87, 117.14, 122.29, 129.19, 129.81, 148.33, 151.84, 152.29, 159,19, 165.50; MS (ESI-MS) (*m*/*z*): calcd. for $C_{30}H_{40}N_8O_3S$ [L+H]$^+$: 593.3017; found: 593.3092.

7b:6-butyl-3,5,7-trimethyl-1-[[4-phenyl-3-[2-oxo-2-(4-phenylpiperazin-1-yl)ethyl] sulfanyl-2*H*-1,2,4-triazol-5-yl]methoxy]pyrrolo[3,4-*d*]pyridazin-4-one

Yield: 53.83%; m.p.: 126–128 °C;

FT-IR (selected lines, γ_{max}, cm^{-1}): 3053 (C-H arom.), 2929, 2871 (C-H aliph.), 1636 (C=O); ^{1}H NMR (300 MHz, $CDCl_3$) δ: 0.94–0.99 (m, 3H, -CH_2-CH_2 CH_2-CH_3), 1.33–1.41 (m, 2H, -CH_2-CH_2 CH_2-CH_3), 1.59–1.61 (m, 2H, -CH_2-CH_2 CH_2-CH_3), 2.33 (s, 3H, 7-CH_3), 2.66 (s, 3H, 5-CH_3), 3.17 (m, 2H, CH_2—piperazine), 3.23 (m, 2H, CH_2—piperazine), 3.46 (s, 3H, 3-CH_3), 3.78 (m, 4H, CH_2—piperazine), 3.84–3.89 (m, 2H, -CH_2-CH_2 CH_2-CH_3), 4.42 (s, 2H, *S*-CH_2) 5.31 (s, 2H, *O*-CH_2-); 6.89–6.94 (m, 3H, Ar-H), 7.29–7.34 (m, 4H, Ar-H), 7.44–7.46 (m, 3H, Ar-H); ^{13}C NMR (75 MHz, $CDCl_3$) δ: 10.61, 11.19, 13.70, 20.04, 32.32, 36.32, 42.18, 43.87, 46.13, 49.26, 49.72, 56.94, 108.24, 111.78, 116.76, 120.72, 122.21, 126.65, 129.27, 129.91, 130.21, 132.60, 148.15, 150.76, 152.28, 159,13, 165.54; MS (ESI-MS) (*m*/*z*): calcd. for $C_{34}H_{40}N_8O_3S$ $[L+H]^+$: 641.3017; found: 641.2935.

8b:6-butyl-3,5,7-trimethyl-1-[[4-phenyl-3-[2-oxo-2-[4-[3-(triflouromethyl)phenyl] piperazin-1-yl]ethyl]sulfanyl-2*H*-1,2,4-triazol-5-yl]methoxy]pyrrolo[3,4-*d*] pyridazin-4-one

Yield: 60.84%; m.p.: 141–143 °C;

FT-IR (selected lines, γ_{max}, cm^{-1}): 3053 (C-H arom.), 2959, 2930, 2872 (C-H aliph.), 1635 (C=O); ^{1}H NMR (300 MHz, $CDCl_3$) δ: 0.94–0.99 (m, 3H, -CH_2-CH_2 CH_2-CH_3), 1.33–1.40 (m, 2H, -CH_2-CH_2 CH_2-CH_3), 1.59–1.61 (m, 2H, -CH_2-CH_2 CH_2-CH_3), 2.33 (s, 3H, 7-CH_3), 2.65 (s, 3H, 5-CH_3), 3.22 (m, 2H, CH_2—piperazine), 3.30 (m, 2H, CH_2—piperazine), 3.45 (s, 3H, 3-CH_3), 3.81–3.84 (m, 4H, CH_2—piperazine), 3.86–3.89 (m, 2H, -CH_2-CH_2 CH_2-CH_3), 4.39 (s, 2H, *S*-CH_2) 5.31 (s, 2H, *O*-CH_2-); 7.06–7.15 (m, 3H, Ar-H), 7.31–7.35 (m, 2H, Ar-H), 7.37–7.40 (m, 1H, Ar-H), 7.44–7.46 (m, 3H, Ar-H); ^{13}C NMR (75 MHz, $CDCl_3$) δ: 10.61, 11.18, 13.69, 20.03, 32.31, 36.02, 36.94, 41.98, 43.87, 45.92, 48.76, 49.17, 56.92, 108.21, 108.23, 111.78, 112.93, 116.94, 119.44, 122.20, 125.95, 126.64, 128.92, 129.76, 129.92, 130.25, 131.43, 131.86, 132.57, 148.13. 150.85, 152.34, 152.34, 159.13, 165.65; MS (ESI-MS) (*m*/*z*): calcd. for $C_{35}H_{39}F_3N_8O_3S$ $[L+H]^+$: 708.2891; found: 708.2827.

9b:6-butyl-3,5,7-trimethyl-1-[[4-phenyl-3-[2-oxo-2-[4-[4-(methyl)phenyl]piperazin-1-yl] ethyl]sulfanyl-2*H*-1,2,4-triazol-5-yl]methoxy]pyrrolo[3,4-*d*]pyridazin-4-one

Yield: 55.89%; m.p.: 129–131 °C;

FT-IR (selected lines, γ_{max}, cm^{-1}): 2958, 2925, 2870 (C-H aliph.), 1639 (C=O); ^{1}H NMR (300 MHz, $CDCl_3$) δ: 0.94–0.99 (m, 3H, -CH_2-CH_2 CH_2-CH_3), 1.35–1.38 (m, 2H, -CH_2-CH_2 CH_2-CH_3), 1.61 (m, 2H, -CH_2-CH_2 CH_2-CH_3), 2.28 (s, 3H, Ar-CH_3), 2.33 (s, 3H, 7-CH_3), 2.65 (s, 3H, 5-CH_3), 3.11–3.16 (m, 4H, CH_2—piperazine), 3.45 (s, 3H, 3-CH_3), 3.76 (m, 4H, CH_2—piperazine), 3.84–3.89 (m, 2H, -CH_2-CH_2 CH_2-CH_3), 4.41 (s, 2H, *S*-CH_2) 5.31 (s, 2H, *O*-CH_2-); 6.83–6.86 (m, 2H, Ar-H), 7.08–7.11 (m, 2H, Ar-H), 7.33–7.34 (m, 2H, Ar-H), 7.43–7.46 (m, 3H, Ar-H); ^{13}C NMR (75 MHz, $CDCl_3$) δ:10.60, 10.98, 11.19, 13.69, 20.02, 20.43, 32.31, 36.39, 36.94, 42.23, 43.87, 46.17, 49.81, 50.28, 56.94, 108.25, 111.78, 117.111, 122.21, 126.76, 127.16, 128.89, 129.78, 129.90, 130.19, 130.36, 132.61, 133.46, 148.16, 148.65, 152.25, 159.13, 165.49; MS (ESI-MS) (*m*/*z*): calcd. for $C_{35}H_{42}N_8O_3S$ $[L+Na]^+$: 677.2993; found: 677.2945.

7c:6-butyl-3,5,7-trimethyl-1-[[4-(4-methoxy)phenyl-3-[2-oxo-2-(4-phenylpiperazin-1-yl) ethyl]sulfanyl-2*H*-1,2,4-triazol-5-yl]methoxy]pyrrolo[3,4-*d*]pyridazin-4-one

Yield: 59.71%; m.p.: 150–152 °C;

FT-IR (selected lines, γ_{max}, cm^{-1}): 3060, (C-H arom.), 2957, 2929, 2871 (C-H aliph.), 1640 (C=O), 1271 (C=S); ^{1}H NMR (300 MHz, $CDCl_3$) δ: 0.94–0.99 (m, 3H, -CH_2-CH_2 CH_2-CH_3), 1.36–1.39 (m, 2H, -CH_2-CH_2 CH_2-CH_3), 1.61 (m, 2H, -CH_2-CH_2 CH_2-CH_3), 2.36 (s, 3H, 7-CH_3), 2.66 (s, 3H, 5-CH_3), 3.16 (m, 2H, CH_2—piperazine), 3.23 (m, 2H, CH_2—piperazine), 3.47 (s, 3H, 3-CH_3), 3.78 (m, 4H, CH_2—piperazine), 3.81 (s, 3H, *O*-CH_3), 3.84–3.89 (m, 2H, -CH_2-CH_2 CH_2-CH_3), 4.40 (s, 2H, *S*-CH_2) 5.28 (s, 2H, *O*-CH_2-); 6.89–6.94 (m, 5H, Ar-H), 7.21–7.31 (m, 4H, Ar-H); ^{13}C NMR (75 MHz, $CDCl_3$) δ: 10.62, 11.23, 13.71, 20.05, 32.32, 36.22, 36.95, 42.16, 43.89, 46.12, 49.25, 49.72, 55.59, 56.94, 108.29, 111.78, 114.99,

116.75, 120.71, 122.23, 124.91, 127.97, 128.87, 129.28, 148.24, 150.76, 152.55, 153.09, 159,13, 160.71, 165.58; HRMS (ESI-MS) (*m*/*z*): calcd. for $C_{35}H_{42}N_8O_4S$ [L+Na]$^+$: 693.2942; found: 693.2956.

8c:6-butyl-3,5,7-trimethyl-1-[[4-(4-methoxy)phenyl-3-[2-oxo-2-[4-[3-(triflouromethyl) phenyl]piperazin-1-yl]ethyl]sulfanyl-2*H*-1,2,4-triazol-5-yl]methoxy]pyrrolo[3,4-*d*]pyridazin-4-one

Yield: 69.10%; m.p.: 114–117 °C;

FT-IR (selected lines, γ_{max}, cm^{-1}): 2959, 2929, 2871 (C-H aliph.), 1644 (C=O); ^{1}H NMR (300 MHz, $CDCl_3$) δ: 0.94–0.99 (m, 3H, -CH_2-CH_2 CH_2-CH_3), 1.33–1.41 (m, 2H, -CH_2-CH_2 CH_2-CH_3), 1.62 (m, 2H, -CH_2-CH_2 CH_2-CH_3), 2.36 (s, 3H, 7-CH_3), 2.66 (s, 3H, 5-CH_3), 3.22 (m, 2H, CH_2—piperazine), 3.29 (m, 2H, CH_2—piperazine), 3.46 (s, 3H, 3-CH_3), 3.81 (s, 3H, *O*-CH_3), 3.84 (m, 4H, CH_2—piperazine), 3.86–3.89 (m, 2H, -CH_2-CH_2 CH_2-CH_3), 4.37 (s, 2H, *S*-CH_2) 5.28 (s, 2H, *O*-CH_2-); 7.89–6.92 (m, 2H, Ar-H), 7.05–7.14 (m, 3H, Ar-H), 7.21–7.24 (m, 2H, Ar-H), 7.35–7.40 (m, 1H, Ar-H); ^{13}C NMR (75 MHz, $CDCl_3$) δ: 10.59, 11.21, 13.69, 20.03, 32.32, 35.86, 36.94, 41.98, 43.88, 45.92, 48.72, 49.14, 55.57 56.92, 108.30 111.79, 112.88, 114.99, 116.87, 119.39, 122.21, 124.91, 127.97, 128.90, 129.75, 131.42, 131.84, 148.22, 150.89, 152.62, 152.91, 159.12, 160.74, 165.72; HRMS (ESI-MS) (*m*/*z*): calcd. for $C_{36}H_{41}F_3N_8O_4S$ [L+Na]$^+$: 761.2816; found: 761.2812.

9c:6-butyl-3,5,7-trimethyl-1-[[4-(4-methoxy)phenyl-3-[2-oxo-2-[4-[4-(methyl)phenyl] piperazin-1-yl]ethyl]sulfanyl-2*H*-1,2,4-triazol-5-yl]methoxy]pyrrolo[3,4-*d*] pyridazin-4-one

Yield: 67.44%; m.p.: 119–121 °C;

FT-IR (selected lines, γ_{max}, cm^{-1}): 3052, 3002 (C-H arom.), 2957, 2922, 2871 (C-H aliph.), 1643 (C=O); ^{1}H NMR (300 MHz, $CDCl_3$) δ: 0.94–0.99 (m, 3H, -CH_2-CH_2 CH_2-CH_3), 1.34–1.41 (m, 2H, -CH_2-CH_2 CH_2-CH_3), 1.59–1.61 (m, 2H, -CH_2-CH_2 CH_2-CH_3), 2.28 (s, 3H, Ar-CH_3), 2.36 (s, 3H, 7-CH_3), 2.66 (s, 3H, 5-CH_3), 3.10 (m, 2H, CH_2—piperazine), 3.16 (m, 2H, CH_2—piperazine), 3.46 (s, 3H, 3-CH_3), 3.78 (m, 4H, CH_2—piperazine), 3.81 (s, 3H, *O*-CH_3), 3.84–3.89 (m, 2H, -CH_2-CH_2 CH_2-CH_3), 4.40 (s, 2H, *S*-CH_2) 5.28 (s, 2H, *O*-CH_2-); 6.83–6.2 (m, 4H, Ar-H), 7.08–7.11 (m, 2H, Ar-H), 7.21–7.24 (m, 2H, Ar-H); ^{13}C NMR (75 MHz, $CDCl_3$) δ:10.61, 11.22, 13.69, 20.04, 20.44, 32.32, 36.28, 36.95, 42.22, 43.88, 46.18, 49.81, 50.29, 55.58, 56.94, 108.30, 111.79, 114.99, 117.10, 122.22, 124.94, 127.97, 128.87, 129.79, 130.35, 148.24, 148.66, 152.54, 153.11, 159.13, 160.72, 165.54; HRMS (ESI-MS) (*m*/*z*): calcd. for $C_{36}H_{44}N_8O_4S$ [L+H]$^+$: 685.3279; found: 685.3246.

3.2. Biological Evaluation

3.2.1. Cell Line and Conditions

Normal human dermal fibroblasts (NHDF) were purchased from Lonza and used in bioassays between 7–12 passages. The cells were incubated in 5% CO_2, 95% humidity at 37 °C with morphology and confluence assessments twice weekly using EVOS FL microscopy. The cells were passaged with TrypLE solution when the cell confluence was greater than 70%. The cells were transferred to a tube and centrifuged at 1000× *g* for 5 min. Then, the supernatant was removed, and the cells were resuspended in a fresh medium, and the number of cells was counted using the Burcher chamber. Finally, the cells were plated on the assay plates or reduced by about half and placed back in the culture flasks. The NHDF cells were grown in Dulbecco's modified Eagle's medium (DMEM) without phenol red supplemented with 10% fetal bovine serum (FBS), 2 mM ultra-glutamine and 2 μg/mL gentamicin and streptomycin. The medium was stored at 4–8 °C for one month or until used.

3.2.2. Tested Compounds

The tested compounds were dissolved in dimethyl sulfoxide (DMSO) to form 10 mM stock solutions which were stored at −20 °C. These compounds were thawed immediately before the preparation of the bioassay concentrations. The concentration range of 10–100 μM was used, so the DMSO concentration did not exceed 1% at the higher concen-

tration tested. The bioassay concentrations were prepared in DMEM without phenol red, which was supplemented as a medium for traditional cultures, but with a reduced amount of FBS to 5%.

3.2.3. Cyclooxygenase Inhibition Assay

The cyclooxygenase (COX) inhibition was evaluated using a ready-to-used test from the Cayman company. In this study, the only 100 μM concentrations that were tested, each in triplicate, for the obtained results were calculated IC_{50}—concentration, which inhibited activity of COX-1 or COX-2 about 50% compared to 100% activity of these enzymes. In these studies, *Meloxicam*, *Diclofenac* and *Celecoxib* were used as reference compounds.

3.2.4. MTT Assay

The assessment of cell viability after 24-hour incubation with the test compounds was performed according to ISO 10993 Part 5 Appendix C. The cells were seeded at 10,000 cells per well and left in a CO_2 incubator overnight to allow the cells to adhere. Non-adherent cells were removed with the medium, and freshly prepared concentrations of test compounds were added for 24 h. During the last hour of 24-hour incubation, the cells were assessed microscopically according to the ISO 10,993 scale for cytotoxicity. The medium with the compounds was replaced with a 1 mg/mL MTT in phosphate buffered saline (PBS) for 2 h at 37 °C. The solution was then gently removed and the purple crystals dissolved in isopropanol, and the absorbance was measured at 570 nm with a VirusScan microplate reader.

3.2.5. Anti-Inflammatory and Antioxidant Activity

To evaluate the anti-inflammatory and antioxidant activity of the tested compounds, the MTT, DCF-DA and Griess assays were performed. In the first assay, the NHDF cells were seeded at a density of 10,000 cells per well, and in the other assay, 40,000 cells per well. After the cells adhered overnight, the supernatant with the non-adherent cells was replaced with 50 μg/mL lipopolysaccharide (LPS) for 24 h. Next, the cells were washed, and freshly prepared concentrations of the test compounds were added for 24 h. Then, the culture plate was washed for MTT assay, and the procedure described in Section 3.2.4. was used. To evaluate the free radicals scavenging of tested the compounds, the 50 μL supernatant was transferred to a new plate. The rest of the supernatant was removed and 25 μM of DCF-DA solution in MEM without phenol red was added for 1 h at 37 °C to measure the reactive oxygen species (ROS) and into collected supernatant 50 μM mixture reagent A and reagent B in a volume ratio 1:1 for 20 min at RT in the dark to measure the nitric oxide (NO). The ROS was measured at 498 nm excitation and 535 nm emission, and NO at 548 nm using a VirusScan microplate reader.

3.3. Molecular Docking

The structure optimization was performed using the DFT/B3LYP method combined with the 6–311+G (d,p) basis set. From the Protein Data Bank (http://www.rcsb.org, accessed on 1 May 2021), the following crystal structure was selected for the docking studies: 4O1Z, 4M11, 3V03. The ligand and receptor files were prepared using AutoDock 4.2.6 software and AutoDock Tools 1.5.6. All of the ligands and water molecules were removed, and then polar hydrogen atoms and Kollman charges were added to the protein structure. To prepare the ligand molecules, the partial charges were calculated, non-polar hydrogens were merged, and rotatable bonds were assigned. The interactions with COX-1, COX-2 and BSA were performed using AutoDock Script downloaded from The Scripps Research Institute (TSRI). The centers of the grid boxes for COX-1 and COX-2 were set according to the *Meloxicam* binding site in the crystal structure 4O1Z, 4M11. The centers of the grid boxes for BSA were set according to the binding site I phenylbutazone (PDB ID: 2BXC) and site II *Ibuprofen* (PDB ID: 2BXG) on HSA [58]. The Lamarckian genetic algorithm was selected for the conformational search. The running times of the genetic algorithm

and the evaluation times were set to 100 and 2.5million, respectively. After the molecular docking, the ligand–receptor complexes were further analyzed using Discovery Studio software (http://accelrys.com/, accessed on 1 May 2021).

3.4. Spectroscopic Studies

3.4.1. Fluorescence

The spectroscopic fluorescence studies were performed using a Cary Eclipse 500 spectrophotometer (Agilent, Santa Clara, CA, USA). A concentration of BSA was 1.0×10^{-6} mol·dm^{-3}. A solution of BSA was titrated by successive additions of 1.0×10^{-3} mol·dm^{-3} solution of the studied compounds to give a final concentration of 0.2×10^{-6}–2.0×10^{-6} mol·dm^{-3}. Experiments were carried out at three temperatures: 297, 303, and 308 K in pH = 7.4. The quenching spectra were recorded at excitation and an emission wavelength of 280 nm and 300–500 nm. The molar ratio compound/BSA was 0.1–2.0 with 0.2 steps. Binding site identification studies were indicated in the presence of the two site markers, *Phenylbutazone* (PHB) and *Ibuprofen* (IBP), as sites I and II markers, respectively. Concentrations of BSA and site markers were set at 1.0×10^{-6} and 3.0×10^{-6} mol·dm^{-3}, respectively.

3.4.2. Circular Dichroism

Circular dichroism (CD) spectra were measured on the Jasco J-1500 magnetic circular dichroism spectrometer. All of the measurements for the BSA solutions in the absence and presence of the analyzed compounds were made at room temperature under simulated physiological conditions in pH 7.4, in phosphate buffer as a solvent. The CD spectra were collected in the range of 205–250 nm at a scan rate speed of 50 nm min^{-1}, with a response time of 1 s, 10 mm path length, and were baseline corrected. The concentrations of BSA and the analyzed compounds were 1×10^{-6} mol·dm^{-3} and 1×10^{-3} mol·dm^{-3}, respectively. BSA performed experiments on each analyzed compound in molar ratios: 1:0, 1:0.5, 1:1, 1:5 and 1:10.

3.4.3. FT-IR Measurement

Infrared spectra were recorded on the Nicolet iS50 FT-IR (Thermo Fisher Scientific, Waltham, MA, USA) equipped with a deuterated triglycine sulphate (DTGS) detector and KBr beam splitter. The spectra were obtained at room temperature using the attenuated total reflectance (ATR) method. The spectral data were recorded within 4000 to 600 cm^{-1} with resolution 4 cm^{-1} and 100 scans were averaged for each spectrum.

Bovine serum albumin (Sigma Aldrich) was dissolved in an aqueous solution containing phosphate buffer (pH = 7.5) (Sigma Aldrich) to obtain 0.02 mol·dm^{-1} concentration. The concentration of the studied compounds was 0.01 mol·dm^{-1} andsolutions were prepared in methanol (Chempur). The 200 µL solution of BSA was mixed with the appropriate amount of the compounds solution to achieve 0.25, 0.50, 0.75 and 1.0 molar ratio and 10 µL of mixture was dropped on the crystal to register a spectrum.

The analysis of the secondary structure was proceeded by Omnic 9.3.30 (Thermo Fisher Scientific Inc.) software. The analysis of the FT-IR spectra was evaluated by the Byler and Susi procedure [56]. After normalization of each spectrum, the fragment with the peak 1650 cm^{-1} was extracted, and a second derivate was made. The major peaks are characteristic for the α-helix (1660–1650 cm^{-1}), β-sheet (1640–1610 cm^{-1}), β-turn (1691–1680 cm^{-1}), β-antiparallel (1660–1650 cm^{-1}) and random coil (1650–1640 cm^{-1}) [56,62–64]. The self-deconvolution and curve-fitting by Gaussian function allowed for us to determine the intensity and total area under peaks. The calculation of the percentage of area peaks corresponds with the contribution of the type of structure.

3.5. Statistical Analysis

The biological results are shown again as the mean ± SD of the IC_{50} in the cyclooxygenase inhibition assay and the E/E_0 ratio in the remaining assays. E is the mean result for

the compounds tested, and E_0 is the mean result for the controls. For the viability assay, E_0 cells were incubated only with a medium without the test compounds. In assessing the anti-inflammatory activity of the tested compounds, cells treated with only 50 μg/mL LPS were controls. The statistical analyses were performed using the Statistica program. One-way ANOVA and Tukey post-hoc analysis were calculated. The *p*-value was set at 0.05.

4. Conclusions

The present paper describes the design, synthesis and complex biological, computational and also spectroscopic studies of novel, three series of *N*-substituted-1,2,4-triazole-based derivatives of pyrrolo[3,4-*d*]pyridazinone. The structures of the title compounds were inspired by the results of our previous investigations and most recent literature reports. Their formation relied on the molecular hybridization of the biheterocyclic scaffold of pyrrolo[3,4-*d*]pyridazinone, *N*-substituted-1,2,4-triazole moiety and aryl piperazine pharmacophore (Scheme 1, Figure 7). Our goal was to receive potent anti-inflammatory agents with possibly the best affinity towards an inducible COX-2 isoform. The evaluation of the viability revealed that five compounds **8a-c**, **9b**, **9c** cause cell lysis and were excluded from further examination. The results of in vitro COX inhibition assay indicate that molecules **4a-7a**, **9a**, **4b**, **7b** and **4c** have good, comparable to *Meloxicam*, inhibitory activity towards COX-2 isoenzyme and are characterized by a promising COX-2/COX-1 selectivity ratio. Moreover, derivatives **4a**, **6a**, **9a** and **4c** acted as selective COX-2 inhibitors. These findings were supported by the results of the molecular docking studies, according to which, new molecules take position in the active site of COX-2 very similar to *Meloxicam* and did not show an affinity to COX-1 isoform. What is more, the potential good anti-inflammatory and antioxidant activity of the examined derivatives was confirmed in the performed in vitro evaluation within cells. As it has already been stated, all molecules bind and interact with serum albumin, which is the most abundant protein in blood. Some of them, especially those belonging to series **a**, exert promising and beneficial properties in the executed in silico ADME prediction.

Taking the above information into account, we can summarize that title *N*-substituted-1,2,4-triazole-based derivatives of pyrrolo[3,4-*d*]pyridazinone can serve as promising and valuable structures in the development of novel anti-inflammatory agents. Undoubtedly, further, extended investigations, especially in vivo experiments, concerning these compounds are necessary. Moreover, based on the described biological, computational, structure–activity relationship (SAR) and ADME study, we are going to perform rational structural modifications of the reported derivatives in order to receive a new series of potent and effective molecules.

Supplementary Materials: The following are available online at https://www.mdpi.com/article/10.3390/ijms222011235/s1: The structures of all reported compounds **2a-c-9a-c** (Table S1), the ^{1}H and ^{13}C NMR (Table S2), ESI-MS (Table S3), FT-IR (Table S4), spectra of reported derivatives. Molecular formula strings (CSV) (Table S5). BSA binding interactions—CD spectra (Table S6), FT-IR spectra (Tables S7 and S8).

Author Contributions: Conceptualization, Ł.S. and P.Ś.; methodology, Ł.S., P.Ś., E.K., B.W., A.M. and A.K.; software, E.K.; formal analysis, Ł.S., E.K., B.W., A.M. and A.K.; investigation, Ł.S., E.K., B.W., P.J., A.M. and A.K.; resources, P.Ś.; data curation, Ł.S.; writing—original draft preparation, Ł.S., E.K., B.W., A.M., A.K. and P.Ś.; writing—review and editing, Ł.S., E.K., B.W., P.J., A.M., A.K. and P.Ś.; visualization, Ł.S., E.K., B.W., A.M. and A.K.; supervision, Ł.S. and P.Ś.; project administration, Ł.S. and P.Ś.; funding acquisition, P.Ś. All authors have read and agreed to the published version of the manuscript.

Funding: This study was financially supported by the Ministry of Health subvention according to the number SUB.D070.21.094 from the IT Simple system of Wroclaw Medical University.

Institutional Review Board Statement: Not applicable.

Informed Consent Statement: Not applicable.

Data Availability Statement: Calculations have been carried out in Wroclaw Centre for Networking and Supercomputing (http://www.wcss.wroc.pl, accessed on 1 May 2021).

Conflicts of Interest: The authors declare no conflict of interest.

Abbreviations

ADME, Absorption Distribution Metabolism Excretion; Arg, Arginine; ATR, Attenuated Total Reflectance; BBB. Blood Brain Barrier, BSA, Bovine Serum Albumin; CD, Circular Dichroism; COX, Cyclooxygenase; DCF-DA, Dichlorofluorescin Diacetate; DMEM, Dulbecco's Modified Eagle's Medium; DMSO, Dimethyl Sulfoxide; ELISA, Enzyme-Linked Immunosorbent Assay; ESI-MS, Electrospray Ionization Mass Spectrometry; FBS, Fetal Bovine Serum; FT-IR, Fourier Transform Infrared; GI, Gastrointestinal; HSA, Human Serum Albumine; IBP, *Ibuprofen*; IC, Inhibitory Concentration; Leu, Leucine; LPS, Lipopolysaccharide; MPO, Myeloperoxidase; MTT 3-(4,5-dimethylthiazol-2-yl)-2,5-diphenyltetrazolium bromide; MW, Molecular Weight; NA, Not Applicable; NHDF, Normal Human Dermal Fibroblasts; NMR, Nuclear Magnetic Resonance; NO, Nitric Oxide; NSAIDs, Non-Steroidal Anti-Inflammatory Drugs; PBS, Phosphate Buffered Saline; PGE_2, Prostaglandin E_2; PGs, Prostaglandins; PHB, *Phenylbutazone*; RONS, Reactive Oxygene and Nitrogen Species; Ro5, Rule of Five; ROS, Reactive Oxygen Species; RT, Room Temperature; SAR, Structure-Activity Relationship; SD, Standard Deviation; Ser, Serine; TLC, Thin Layer Chromatography; TMS, Tetramethylsilane; TPSA, Topological Polar Surface Area; Trp, Tryptophan; Tyr, Tyrosine.

References

1. Nathan, C. Points of control in inflammation. *Nature* **2002**, *420*, 846–852. [CrossRef] [PubMed]
2. Serhan, C.N.; Savill, J. Resolution of inflammation: The beginning programs the end. *Nat. Immunol.* **2005**, *6*, 1191–1197. [CrossRef] [PubMed]
3. Negus, S.S.; Vanderah, T.W.; Brandt, M.R.; Bilsky, E.J.; Becerra, L.; Borsook, D. Preclinical Assessment of Candidate Analgesic Drugs: Recent Advances and Future Challenges. *J. Pharmacol. Exp. Ther.* **2006**, *319*, 507–514. [CrossRef] [PubMed]
4. Medzhitov, R. Origin and physiological roles of inflammation. *Nature* **2008**, *454*, 428–435. [CrossRef] [PubMed]
5. Leuti, A.; Fazio, D.; Fava, M.; Piccoli, A.; Oddi, S.; Maccarrone, M. Bioactive lipids, inflammation and chronic diseases. *Adv. Drug Deliv. Rev.* **2020**, *159*, 133–169. [CrossRef] [PubMed]
6. Cashman, J.N. The Mechanisms of Action of NSAIDs in Analgesia. *Drugs* **1996**, *52*, 13–23. [CrossRef]
7. Vane, J.R.; Botting, R.M. Mechanism of action of nonsteroidal anti-inflammatory drugs. *Am. J. Med.* **1998**, *104*, 25–85. [CrossRef]
8. Marnett, L.J. Cyclooxygenase mechanisms. *Curr. Opin. Chem. Biol.* **2000**, *4*, 545–552. [CrossRef]
9. Blobaum, A.L.; Marnett, L.J.; Hancock, A.B. PerspectiVe Structural and Functional Basis of Cyclooxygenase Inhibition. *J. Med. Chem.* **2006**, *50*, 1425–1441. [CrossRef]
10. Soliva, R.; Almansa, C.; Kalko, S.G.; Luque, J.; Orozco, M. Theoretical Studies on the Inhibition Mechanism of Cyclooxygenase-2. Is There a Unique Recognition Site? *J. Med. Chem.* **2003**, *46*, 1372–1382. [CrossRef]
11. Sostres, C.; Gargallo, C.J.; Arroyo, M.T.; Lanas, A. Adverse effects of non-steroidal anti-inflammatory drugs (NSAIDs, aspirin and coxibs) on upper gastrointestinal tract. *Best Pract. Res. Clin. Gastroenterol.* **2010**, *24*, 121–132. [CrossRef]
12. Soll, A.H.; McCarthy, D. NSAID-related gastrointestinal complications. *Clin. Cornerstone* **1999**, *1*, 42–56. [CrossRef]
13. Wallace, J.L. NSAID gastropathy and enteropathy: Distinct pathogenesis likely necessitates distinct prevention strategies. *Br. J. Pharmacol.* **2012**, *165*, 67–74. [CrossRef]
14. Laine, L. Gastrointestinal effects of NSAIDs and coxibs. *J. Pain Symptom Manag.* **2003**, *25*, 32–40. [CrossRef]
15. Wallace, J.L.; Devchand, P.R. Emerging roles for cyclooxygenase-2 in gastrointestinal mucosal defense. *Br. J. Pharmacol.* **2005**, *145*, 275–282. [CrossRef]
16. Cannon, C.P.; Cannon, P.J. Physiology. COX-2 inhibitors and cardiovascular risk. *Science* **2012**, *336*, 1386–1387. [CrossRef]
17. Dogné, J.-M.; Supuran, C.T.; Pratico, D. Adverse Cardiovascular Effects of the Coxibs. *J. Med. Chem.* **2005**, *48*, 2251–2257. [CrossRef] [PubMed]
18. Palkar, M.B.; Singhai, A.S.; Ronad, P.M.; Vishwanathswamy, A.H.M.; Boreddy, T.S.; Veerapur, V.P.; Shaikh, M.S.; Rane, R.A.; Karpoormath, R. Synthesis, pharmacological screening and in silico studies of new class of Diclofenac analogues as a promising anti-inflammatory agents. *Bioorganic Med. Chem.* **2014**, *22*, 2855–2866. [CrossRef] [PubMed]
19. Avci, A.; Taşci, H.; Kandemir, Ü.; Can, Ö.D.; Gökhan-Kelekçi, N.; Tozkoparan, B. Synthesis, characterization, and in vivo pharmacological evaluation of novel mannich bases derived from 1,2,4-triazole containing a naproxen moiety. *Bioorg. Chem.* **2020**, *100*, 103892. [CrossRef]
20. Alsayed, S.S.R.; Elshemy, H.A.H.; Abdelgawad, M.A.; Abdel-Latif, M.S.; Abdellatif, K.R.A. Design, synthesis and biological screening of some novel celecoxib and etoricoxib analogs with promising COX-2 selectivity, anti-inflammatory activity and gastric safety profile. *Bioorg. Chem.* **2017**, *70*, 173–183. [CrossRef] [PubMed]

21. Manjunatha, K.; Poojary, B.; Lobo, P.L.; Fernandes, J.; Kumari, N.S. Synthesis and biological evaluation of some 1,3,4-oxadiazole derivatives. *Eur. J. Med. Chem.* **2010**, *45*, 5225–5233. [CrossRef] [PubMed]
22. El-Sayed, N.A.; Nour, M.S.; Salem, M.A.; Arafa, R.K. New oxadiazoles with selective-COX-2 and EGFR dual inhibitory activity: Design, synthesis, cytotoxicity evaluation and in silico studies. *Eur. J. Med. Chem.* **2019**, *183*, 111693. [CrossRef]
23. Sağlık, B.N.; Osmaniye, D.; Levent, S.; Çevik, U.A.; Çavuşoğlu, B.K.; Özkay, Y.; Kaplancıklı, Z.A. Design, synthesis and biological assessment of new selective COX-2 inhibitors including methyl sulfonyl moiety. *Eur. J. Med. Chem.* **2021**, *209*, 112918. [CrossRef]
24. Jacob, P.J.; Manju, S.L. Identification and development of thiazole leads as COX-2/5-LOX inhibitors through in-vitro and in-vivo biological evaluation for anti-inflammatory activity. *Bioorg. Chem.* **2020**, *100*, 103882. [CrossRef] [PubMed]
25. Abdel-Aziz, S.A.; Taher, E.S.; Lan, P.; Asaad, G.F.; Gomaa, H.A.M.; El-Koussi, N.A.; Youssif, B.G.M. Design, synthesis, and biological evaluation of new pyrimidine-5-carbonitrile derivatives bearing 1,3-thiazole moiety as novel anti-inflammatory EGFR inhibitors with cardiac safety profile. *Bioorg. Chem.* **2021**, *111*, 104890. [CrossRef] [PubMed]
26. Abdellatif, K.R.A.; Abdelall, E.K.A.; Lamie, P.F.; Labib, M.B.; El-Nahaas, E.S.; Abdelhakeem, M.M. New pyrazole derivatives possessing amino/methanesulphonyl pharmacophore with good gastric safety profile: Design, synthesis, cyclooxygenase inhibition, anti-inflammatory activity and histopathological studies. *Bioorg. Chem.* **2020**, *95*, 103540. [CrossRef] [PubMed]
27. Abdellatif, K.R.; Abdelall, E.K.; Elshemy, H.A.; Lamie, P.F.; Elnahaas, E.; Amin, D.M. Design, synthesis of new anti-inflammatory agents with a pyrazole core: COX-1/COX-2 inhibition assays, anti-inflammatory, ulcerogenic, histopathological, molecular Modeling, and ADME studies. *J. Mol. Struct.* **2021**, *1240*, 130554. [CrossRef]
28. Abuo-Rahma, G.E.D.A.A.; Abdel-Aziz, M.; Farag, N.A.; Kaoud, T.S. Novel 1-[4-(Aminosulfonyl)phenyl]-1H-1,2,4-triazole derivatives with remarkable selective COX-2 inhibition: Design, synthesis, molecular docking, anti-inflammatory and ulcerogenicity studies. *Eur. J. Med. Chem.* **2014**, *83*, 398–408. [CrossRef]
29. Abdel-Aziz, M.; Beshr, E.A.; Abdel-Rahman, I.M.; Ozadali, K.; Tan, O.U.; Aly, O.M. 1-(4-Methoxyphenyl)-5-(3,4,5-trimethoxyphenyl)-1H-1,2,4-triazole-3-carboxamides: Synthesis, molecular modeling, evaluation of their anti-inflammatory activity and ulcerogenicity. *Eur. J. Med. Chem.* **2014**, *77*, 155–165. [CrossRef]
30. Abdelazeem, A.H.; El-Din, A.G.S.; Arab, H.H.; El-Saadi, M.T.; El-Moghazy, S.M.; Amin, N.H. Design, synthesis and anti-inflammatory/analgesic evaluation of novel di-substituted urea derivatives bearing diaryl-1,2,4-triazole with dual COX-2/sEH inhibitory activities. *J. Mol. Struct.* **2021**, *1240*, 130565. [CrossRef]
31. Abdellatif, K.R.A.; Abdelall, E.K.A.; Elshemy, H.A.H.; Philoppes, J.N.; Hassanein, E.H.M.; Kahk, N.M. Optimization of pyrazole-based compounds with 1,2,4-triazole-3-thiol moiety as selective COX-2 inhibitors cardioprotective drug candidates: Design, synthesis, cyclooxygenase inhibition, anti-inflammatory, ulcerogenicity, cardiovascular evaluation, and molecular modeling studies. *Bioorg. Chem.* **2021**, *114*, 105122.
32. Mohassab, A.M.; Hassan, H.A.; Abdelhamid, D.; Gouda, A.M.; Gomaa, H.A.M.; Youssif, B.G.M.; Radwan, M.O.; Fujita, M.; Otsuka, M.; Abdel-Aziz, M. New quinoline/1,2,4-triazole hybrids as dual inhibitors of COX-2/5-LOX and inflammatory cytokines: Design, synthesis, and docking study. *J. Mol. Struct.* **2021**, *1244*, 130948. [CrossRef]
33. Cai, H.; Huang, X.; Xu, S.; Shen, H.; Zhang, P.; Huang, Y.; Jiang, J.; Sun, Y.; Jiang, B.; Wu, X.; et al. Discovery of novel hybrids of diaryl-1,2,4-triazoles and caffeic acid as dual inhibitors of cyclooxygenase-2 and 5-lipoxygenase for cancer therapy. *Eur. J. Med. Chem.* **2016**, *108*, 89–103. [CrossRef]
34. Szczukowski, Ł.; Redzicka, A.; Wiatrak, B.; Krzyżak, E.; Marciniak, A.; Gębczak, K.; Gębarowski, T.; Świątek, P. Design, synthesis, biological evaluation and in silico studies of novel pyrrolo[3,4-*d*]pyridazinone derivatives with promising anti-inflammatory and antioxidant activity. *Bioorg. Chem.* **2020**, *102*, 104035. [CrossRef]
35. Szczukowski, Ł.; Krzyżak, E.; Zborowska, A.; Zając, P.; Potyrak, K.; Peregrym, K.; Wiatrak, B.; Marciniak, A.; Świątek, P. Design, Synthesis and Comprehensive Investigations of Pyrrolo[3,4-*d*]pyridazinone-Based 1,3,4-Oxadiazole as New Class of Selective COX-2 Inhibitors. *Int. J. Mol. Sci.* **2020**, *21*, 9623. [CrossRef]
36. Szandruk-Bender, M.; Wiatrak, B.; Szczukowski, Ł.; Świątek, P.; Rutkowska, M.; Dzimira, S.; Merwid-Ląd, A.; Danielewski, M.; Szeląg, A. Oxadiazole Derivatives of Pyrrolo[3,4-*d*]pyridazinone Exert Antinociceptive Activity in the Tail-Flick and Formalin Test in Rodents and Reveal Reduced Gastrotoxicity. *Int. J. Mol. Sci.* **2020**, *21*, 9685. [CrossRef] [PubMed]
37. Dogruer, D.S.; Kupeli, E.; Yesilada, E.; Sahin, M.F. Synthesis of New 2-[1(2H)-Phthalazinon-2-yl]acetamide and 3-[1(2H)-Phthalazinon-2-yl]propanamide Derivatives as Antinociceptive and Anti-inflammatory Agents. *Arch. Pharm. (Weinheim)* **2004**, *337*, 303–310. [CrossRef]
38. Gupta, S.; Pandey, D.; Mandalapu, D.; Bala, V.; Sharma, V.; Shukla, M.; Yadav, S.K.; Singh, N.; Jaiswal, S.; Maikhuri, J.P.; et al. Design, synthesis and biological profiling of aryl piperazine based scaffolds for the management of androgen sensitive prostatic disorders. *Medchemcomm* **2016**, *7*, 2111–2121. [CrossRef]
39. McGarry, T.; Biniecka, M.; Veale, D.J.; Fearon, U. Hypoxia, oxidative stress and inflammation. *Free Radic. Biol. Med.* **2018**, *125*, 15–24. [CrossRef]
40. Burdon, C.; Mann, C.; Cindrova-Davies, T.; Ferguson-Smith, A.C.; Burton, G.J. Oxidative Stress and the Induction of Cyclooxygenase Enzymes and Apoptosis in the Murine Placenta. *Placenta* **2007**, *28*, 724–733. [CrossRef] [PubMed]
41. Li, D.; Zhu, M.; Xu, C.; Ji, B. Characterization of the baicalein-bovine serum albumin complex without or with Cu 2+or Fe 3+ by spectroscopic approaches. *Eur. J. Med. Chem.* **2011**, *46*, 588–599. [CrossRef] [PubMed]

42. Shi, J.H.; Pan, D.Q.; Wang, X.X.; Liu, T.T.; Jiang, M.; Wang, Q. Characterizing the binding interaction between antimalarial artemether (AMT) and bovine serum albumin (BSA): Spectroscopic and molecular docking methods. J. Photochem. Photobiol. *B Biol.* **2016**, *162*, 14–23. [CrossRef] [PubMed]
43. Li, Y.; He, W.; Liu, J.; Sheng, F.; Hu, Z.; Chen, X. Binding of the bioactive component Jatrorrhizine to human serum albumin. *Biochim. Biophys. Acta—Gen. Subj.* **2005**, *1722*, 15–21. [CrossRef]
44. Wani, T.A.; Bakheit, A.H.; Zargar, S.; Bhat, M.A.; Al-Majed, A.A. Molecular docking and experimental investigation of new indole derivative cyclooxygenase inhibitor to probe its binding mechanism with bovine serum albumin. *Bioorg. Chem.* **2019**, *89*, 103010. [CrossRef]
45. Lakowicz, J.R. *Principles of Fluorescence Spectroscopy*, 3rd ed.; Springer: Boston, MA, USA, 2006; ISBN 978-0-387-31278-1.
46. Ware, W.R. Oxygen quenching of fluorescence in solution: An experimental study of the diffusion process. *J. Phys. Chem.* **1962**, *66*, 455–458. [CrossRef]
47. Dufour, C.; Dangles, O. Flavonoid-serum albumin complexation: Determination of binding constants and binding sites by fluorescence spectroscopy. *Biochim. Biophys. Acta—Gen. Subj.* **2005**, *1721*, 164–173. [CrossRef]
48. Abdelhameed, A.S.; Bakheit, A.H.; Mohamed, M.S.; Eldehna, W.M.; Abdel-Aziz, H.A.; Attia, M.I. Synthesis and biophysical insights into the binding of a potent anti-proliferative non-symmetric bis-isatin derivative with bovine serum albumin: Spectroscopic and molecular docking approaches. *Appl. Sci.* **2017**, *7*, 617. [CrossRef]
49. Suryawanshi, V.D.; Walekar, L.S.; Gore, A.H.; Anbhule, P.V.; Kolekar, G.B. Spectroscopic analysis on the binding interaction of biologically active pyrimidine derivative with bovine serum albumin. *J. Pharm. Anal.* **2016**, *6*, 56–63. [CrossRef]
50. Wani, T.A.; Bakheit, A.H.; Al-Majed, A.R.A.; Bhat, M.A.; Zargar, S. Study of the interactions of bovine serum albumin with the new anti-inflammatory agent 4-(1,3-dsioxo-1,3-dihydro-2*H*-isoindol-2-yl)-*N*-[(4-ethoxy-phenyl) methylidene]benzohydrazide using a multi-spectroscopic approach and molecular docking. *Molecules* **2017**, *22*, 1258. [CrossRef]
51. Mohammadnia, F.; Fatemi, M.H.; Taghizadeh, S.M. Study on the interaction of anti-inflammatory drugs with human serum albumin using molecular docking, quantitative structure–activity relationship, and fluorescence spectroscopy. *Luminescence* **2020**, *35*, 266–273. [CrossRef] [PubMed]
52. Klotz, I.M.; Urquhart, J.M. The Binding of Organic Ions by Proteins. Effect of Temperature. *J. Am. Chem. Soc.* **1949**, *71*, 847–851. [CrossRef]
53. Kelly, S.M.; Jess, T.J.; Price, N.C. How to study proteins by circular dichroism. Biochim. Biophys. *Acta—Proteins Proteom.* **2005**, *1751*, 119–139. [CrossRef]
54. Kelly, S.; Price, N. The Use of Circular Dichroism in the Investigation of Protein Structure and Function. *Curr. Protein Pept. Sci.* **2005**, *1*, 349–384. [CrossRef]
55. Lu, Z.X.; Cui, T.; Shi, Q.L. *Applications of Circular Dichroism (CD) and Optical Rotatory Dispersion (ORD) in Molecular Biology*, 1st ed.; Science Press: Beijing, China, 1987.
56. Byler, D.M.; Susi, H. Examination of the secondary structure of proteins by deconvolved FTIR spectra. *Biopolymers* **1986**, *25*, 469–487. [CrossRef]
57. Sudlow, G.; Birkett, D.J.; Wade, D.N. The Characterization of Two Specific Drug Binding Sites on Human Serum Albumin. *Mol. Pharmacol.* **1975**, *11*, 824–832.
58. Ghuman, J.; Zunszain, P.A.; Petitpas, I.; Bhattacharya, A.A.; Otagiri, M.; Curry, S. Structural basis of the drug-binding specificity of human serum albumin. *J. Mol. Biol.* **2005**, *353*, 38–52. [CrossRef] [PubMed]
59. Lipinski, C.A.; Lombardo, F.; Dominny, B.W.; Feeney, P.J. Experimental and computational approaches to estimate solubility and permeability in drug discovery and development settings. *Adv. Drug Deliv. Rev.* **2001**, *46*, 3–26. [CrossRef]
60. FVeber, D.F.; Johnson, S.R.; Cheng, H.-Y.; Smith, B.R.; Ward, K.W.; Kopple, K.D. Molecular Properties That Influence the Oral Bioavailability of Drug Candidates. *J. Med. Chem.* **2002**, *45*, 2615–2623.
61. Ertl, P.; Rohde, B.; Selzer, P. Fast calculation of molecular polar surface area as a sum of fragment-based contributions and its application to the prediction of drug transport properties. *J. Med. Chem.* **2000**, *43*, 3714–3717. [CrossRef]
62. Ahmed, A.; Tajmir-Riahi, H.A.; Carpentier, R. A quantitative secondary structure analysis of the 33 kDa extrinsic polypeptide of photosystem II by FTIR spectroscopy. *FEBS Lett.* **1995**, *363*, 65–68. [CrossRef]
63. Liu, Y.; Xie, M.X.; Kang, J.; Zheng, D. Studies on the interaction of total saponins of panax notoginseng and human serum albumin by Fourier transform infrared spectroscopy. Spectrochim. *Acta Part A Mol. Biomol. Spectrosc.* **2003**, *59*, 2747–2758. [CrossRef]
64. Kong, J.; Yu, S. Fourier Transform Infrared Spectroscopic Analysis of Protein Secondary Structures. *Acta Biochim. Biophys. Sin. (Shanghai)* **2007**, *39*, 549–559. [CrossRef] [PubMed]